TRANSACTIONS
OF THE ASME
Series C

Journal of HEAT TRANSFER

August 1960

RADIATION • CONDUCTION • CONVECTION • COMPLEX SYSTEMS • PHASE CHANGES AND MIXTURES • TRANSIENT PHENOMENA • THERMOPHYSICAL PROPERTIES • EXPERIMENTAL TECHNIQUES • THERMOMETRY • ANALOG METHODS • ANALYTICAL AND NUMERICAL METHODS • APPLICATIONS • DESIGN TECHNIQUES • HEAT EXCHANGERS • INSULATION • ECONOMIC FACTORS BIOTECHNOLOGY • ASTRONAUTICS

Published Quarterly by
THE AMERICAN SOCIETY OF MECHANICAL ENGINEERS

TRANSACTIONS
OF THE ASME
Series C

EDITORIAL DEPARTMENT

Editor, J. J. JAKLITSCH, JR.
Consulting Editor, LEO BLODGETT
Production, JEAN NORTH
Production Asst., CARMEN L. CABRANES
Art Editor, HENRY SALFOUR

HEAT TRANSFER DIVISION

Chairman, H. A. JOHNSON
Secretary, S. OSTRACH
Papers Review, J. P. HARTNETT
Consulting Editor, S. P. KEZIOS

OFFICERS OF THE ASME

President, W. L. CISLER
Secretary, O. B. SCHIER, II
Treasurer, E. J. KATES
Assistant Treasurer, H. J. BAUER

PUBLICATIONS COMMITTEE

Chairman, B. G. A. SKROTZKI
HENDLEY N. BLACKMON
R. D. MINDLIN
MARTIN GOLAND
VITO L. SALERNO

Junior Representatives
A. S. GOLDSTEIN
J. W. FOLLANSBEE

REGIONAL ADVISORY BOARD

Region I, H. M. ROGERS, JR.
Region II, GLENN R. FRYLING
Region III, F. J. HEINZE
Region IV, FRANCIS C. SMITH
Region V, H. M. CATHER
Region VI, C. R. EARLE
Region VII, M. S. UMBENHAUER
Region VIII, CARL J. ECKHARDT

Published quarterly by The American Society of Mechanical Engineers. Publication office at 20th and Northampton Streets, Easton, Pa. The editorial department is located at the headquarters of the Society, 29 West Thirty-Ninth Street, New York 18, N. Y. Cable address, "Mechaneer," New York. Price $3.00 a copy, $10.00 annually; to members, $1.50 a copy, $5.00 annually. Add 50 cents for postage to all countries outside the United States and Canada. Changes of address must be received at Society headquarters seven weeks before they are to be effective on the mailing list. Please send old as well as new address. . . . By-Law: The Society shall not be responsible for statements or opinions advanced in papers or . . . printed in its publications (B13, Par. 4). . . . Second-class mail privileges authorized at Easton, Penna. . . . This publication is authorized to be mailed at the special rates of postage prescribed by Section 132.122 . . . © Copyrighted, 1960, by The American Society of Mechanical Engineers. Reprints from this publication may be made on condition that full credit be given the Transactions of the ASME, Series C—Journal of Heat Transfer, and the author, and that date of publication be stated.

TRANSACTIONS OF THE ASME
is indexed by the Engineering Index, Inc.

Journal of
HEAT TRANSFER

VOL. 82 • SERIES C • NO. 3
August 1960

CONTENTS

155 **Rocket Heat-Transfer Literature**

170 **Unsteady Turbulent Heat Transfer in Tubes**
E. M. Sparrow and R. Siegel

181 **Improved Lumped Parameter Method for Transient Heat Conduction Calculations**
H. G. Elrod, Jr.

189 **Local and Average Heat Transfer and Pressure Drop for Refrigerants Evaporating in Horizontal Tubes**
M. Altman, R. H. Norris, and F. W. Staub

199 **Heat-Transfer and Flow-Friction Characteristics of Crossed-Rod Matrices**
A. L. London, J. W. Mitchell, and W. A. Sutherland

214 **Experiments on Heat Transfer From Spheres Including Combined Natural and Forced Convection**
T. Yuge

221 **Heat Transfer to Freon 12 Near the Critical State in a Natural-Circulation Loop**
J. P. Holman and J. H. Boggs

227 **Combined Free and Forced-Convection Heat-Generating Laminar Flow Inside Vertical Pipes With Circular Sector Cross Sections**
Pau-Chang Lu

233 **On Combined Free and Forced Convection in Channels**
L. N. Tao

239 **The Role of the Skin in Heat Transfer**
A. M. Stoll

243 **The Prediction of Human Thermal Tolerance When Using a Ventilating Garment With an Antiexposure Suit**
J. W. McCutchan

TECHNICAL BRIEFS

252 **Heat Transfer by Laminar Flow From a Rotating Cone**
C. L. Tien

253 **Apparent Emissivity and Heat Transfer in a Long Cylindrical Hole**
E. M. Sparrow and L. U. Albers

255 **On the Variable-Density Single-Fluid Model for Two-Phase Flow**
Novak Zuber

258 **Nearly Quasi-Steady Free Convection Heat Transfer in Gases**
E. M. Sparrow and J. L. Gregg

260 **The Effect of Mass Transfer on Free Convection**
R. Eichhorn

263 **An Interferometric Method of Studying Boundary Layer Oscillations**
J. P. Holman, H. E. Gartrell, and E. E. Soehngen

TRANSACTIONS OF THE ASME Series B

Journal of
ENGINEERING FOR INDUSTRY
Volume 82 • Series B • Number 3

CONTENTS FOR AUGUST, 1960

173 Synthesis of Epicyclic Gear Trains Using the Velocity Ratio Spectrum, by R. C. Brewer. (59—A-22)
179 Helixform Bevel and Hypoid Gears, by G. M. Spear, C. B. King, and M. L. Baxter, Jr. (59—A-90)
191 The Twinworm Drive—A Self-Locking Worm-Gear Transmission of High Efficiency, by B. Popper and D. W. Pessen (59—A-75).
200 Determination of Cutter Trajectories for Contoured Turbine Buckets, by R. G. DeBlass. (59—A-111)
205 An Analysis of Factors Used for Strength Rating Helical Gears, by E. J. Wellauer. (59—A-121)
213 Bending Strength of Gear Teeth by Cantilever-Plate Theory, by E. J. Wellauer and A. Seireg. (59—A-50)
223 Rocket Motor Gear Tooth Analysis (Hertzian Contact Stresses and Times), E. K. Gatcombe and R. W. Prowell. (59—A-256)
231 Analysis of Power Spinning of Cones, by B. Avitzur and C. T. Yang. (59—A-173)
246 Some Problems of Press Forging Lead and Aluminum, by A. G. MacDonald, S. Kobayashi, and E. G. Thomsen. (59—A-164)
253 The Deformation Process in Metal-Cutting, by W. J. McDonald and B. F. Murphey. (59—A-165)
259 Influence Coefficients and Pressure Vessel Analysis, by G. D. Gallotly. (59—A-163)
270 Tube Metal Temperatures for Structural Design, by E. E. Ungar and L. A. Mekler. (59—A-166)
277 Supersonic-Wind-Tunnel Air-Drying-System Design, by T. W. Macios. (59—A-161)

TRANSACTIONS OF THE ASME Series A

Journal of
ENGINEERING FOR POWER
Volume 82 • Series A • Number 3

CONTENTS FOR JULY, 1960

169 An Experimental Investigation of Fuel Additives in a Supercharged Boiler, by R. J. Zoschak and R. W. Bryers. (59—A-160)
181 External Corrosion of Superheaters in Boilers Firing High-Alkali Coals, by P. Sedor, E. K. Diehl, and D. H. Barnhart. (59—A-76)
194 Corrosion of Superheaters and Reheaters of Pulverized-Coal-Fired Boilers, by Wharton Nelson and Carl Cain, Jr. (59—A-89)
205 Considerations for the Reduction of Noise in Ship Installations of Gas Turbines, by E. M. Herrmann. (59—A-238)
215 A Torsional Vibration Problem as Associated With Synchronous Motor Driven Machines, by R. N. Brown. (59—A-141)
221 Design Control of Overcompression in Rotary-Vane Compressors, by E. O. Bransford and R. A. Stein. (59—A-109)
227 Operation of Steam Turbines to Minimize Shell Cracking, by S. B. Coulter and R. L. Jackson. (59—Pwr-10)

TRANSACTIONS OF THE ASME Series D

Journal of
BASIC ENGINEERING
Vol. 82 • Series D • No. 2

CONTENTS FOR JUNE, 1960

251 The Fluids Engineering Laboratory at the University of Michigan, by G. V. Edmonson. (59—Hyd-16)
257 Flow Parameters in Hydrostatic Lubrication for Several Bearing Shapes, by S. Raynor and A. Charnes. (59—SA-61)
265 A General Method for Correlating Labyrinth-Seal Leak-Rate Data, by F. E. Heffner. (59—Lub-7)
276 Hydrostatic Gas Bearings, by J. H. Laub. (59—Lub-1)
287 Effect of Hardness, Surface Finish, and Grain Size on Rolling-Contact Fatigue Life of M-50 Bearing Steel, by R. A. Baughman. (59—Lub-11)
295 The Importance of Spinning Friction in Thrust-Carrying Ball Bearings, by G. S. Reichenbach. (59—Lub-9)
302 The Effect of Ball Bearing Steel Structure on Rolling Friction and Contact Plastic Deformation, by R. C. Drutowski and E. B. Mikus. (59—Lub-2)
309 A General Theory for Elastically Constrained Ball and Radial Roller Bearings Under Arbitrary Load and Speed Conditions, by A. B. Jones. (59—Lub-10)
321 A Sommerfeld Solution for Finite Bearings With Circumferential Grooves, by J. V. Fedor. (59—Lub-4)
327 Bearing Oil-Ring Performance, by D. C. Lemman and E. R. Booser. (59—Lub-5)
335 Torque Produced by Misalignment of Hydrodynamic Gas-Lubricated Journal Bearings, by J. S. Ausman (59—Lub-3)
342 Friction Characteristics of Sliding Surfaces Undergoing Subsurface Plastic Flow, by M. C. Shaw, A. Ber, and P. A. Mamin.
347 Machining Characteristics of Leaded Steel, by F. L. Bagley, Jr., and R. Mennell.
360 A General Flow Graph Technique for the Solution of Multiloop Sampled Systems, by R. Ash, W. H. Kim, and G. M. Kranc. (59—NAC-1)
371 Control System Analysis and Design Via the "Second Method" of Lyapunov, Part I, by R. E. Kalman and J. E. Bertram. (59—NAC-2)
394 Control System Analysis and Design Via the "Second Method" of Lyapunov, Part II, by R. E. Kalman and J. E. Bertram. (59—NAC-3)
401 Relations Between the Notch Tensile Strength of Cylindrical and Prismatic Specimens of Titanium Alloys and Heat-Treated Steels, by G. Sachs, J. G. Sessler, R. F. Pray, and T. H. Yeh. (59—Met-2)

Journal of
BASIC ENGINEERING
Vol. 82 • Series D • No. 2

CONTENTS FOR JUNE, 1960
(CONTINUED)

411 Nonmetallic Inclusions and Fracture Behavior of Steels, by S. Yukawa. (59—Met-10)
417 Fracture Mode Transition for a Crack Traversing a Plate, by G. R. Irwin.
426 Use of the Moire Effect to Measure Plastic Strains, by A. Vinckier and R. Dechaene. (59—Met-7)
435 A Generalization of Cumulative Damage, by R. M. Mains. (59—Met-1)
441 Effect of Relaxation on the Behavior of Materials Under Combined Alternating and Static Stress, by F. H. Vitovec. (59—Met-3)
447 Cyclic Operation of Pressure Piping With γ Heating, by K. R. Merckx. (59—Met-4)
453 Creep Rupture Tests for Design of High-Pressure Steam Equipment, by E. A. Davis. (59—Met-14)
462 Steady Creep of a Tube Under Combined Bending and Internal Pressure, by Iain Finnie. (59—Met-5)
465 Effect of Wall Thickness on Stress-Rupture Life of Tubular Specimens, by J. T. Tucker, Jr., E. E. Coulter, and L. F. Kooistra. (59—Met-11)
477 Design of Pressurized Cylinders for High-Temperature Applications, by J. F. Traexler. (59—Met-8)
482 The Response of a Pressure-Sensing System, by R. P. Benedict. (59—A-289)
489 Dynamics of Heat Exchangers and Their Models, by Herman Thal-Larsen. (59—A-117)

TRANSACTIONS
Series E

Journal of
APPLIED MECHANICS
Volume 82 • Series E • No. 2

CONTENTS FOR JUNE, 1960

TECHNICAL PAPERS

223 Note on the Assessment of Flow Disturbances at a Blunt Body Traveling at Supersonic Speeds Owing to Flow Disturbances in Free Stream, M. V. Morkovin. (60—APM-10)
230 Possible Similarity Solutions for Laminar Free Convection on Vertical Plates and Cylinders, Kwang-Tzu Yang. (59—A-86)
237 On the Annular Damper for a Freely Precessing Gyroscope, G. F. Carrier and J. W. Miles. (59—A-44)
241 Heat Transfer for Laminar Flow in Ducts With Arbitrary Time Variations in Wall Temperature, Robert Siegel. (59—APMW-21)
250 A Study of the Stability of Externally Pressurized Gas Bearings, Lazar Licht and Harold Elrod. (60—APM-5)
259 On the Theoretical Analysis of a Dynamic Thermocouple: 2—The Continuous Area Interface, W. F. Hughes and E. W. Gaylord. (60—APM-19)
263 Normal Modes of Nonlinear Dual-Mode Systems, R. M. Rosenberg. (59—A-93)
269 Classical Normal Modes in Damped Linear Dynamic Systems, T. K. Caughey. (59—A-62)
272 The Vibration Response of a Linear Undamped System Resting on a Nonlinear Spring, P. R. Paslay and M. E. Gurtin. (60—APM-6)
275 The Approximate Analysis of Certain Boundary-Value Problems, H. D. Conway. (59—A-80)
278 Stresses in a Slab Having a Spherical Cavity Under Circular Bending, Chih-Bing Ling and Chen-Peng Tsai. (59—A-64)
283 Elastic Equilibrium of a Plate With a Reinforced Elliptical Hole, Eugene Levin. (59—A-45)
289 A Method of Solution for the Elastic Quarter-Plane, M. Hetényi. (59—A-92)
297 Thermal Stress in a Viscoelastic-Plastic Plate With Temperature-Dependent Yield Stress, H. G. Landau, J. H. Weiner, and E. E. Zwicky, Jr. (59—A-33)
303 Prediction of Creep Failure Time for Pressure Vessels, F. P. J. Rimrott, E. J. Mills, and Joseph Marin. (60—APM-7)
309 On the Plastic Behavior of Rotating Cylinders, F. P. J. Rimrott. (59—A-65)
316 On the Optimum Design of Shells, R. T. Shield. (59—A-47)
323 Yield Conditions for Rotationally Symmetric Shells Under Axisymmetric Loading, P. G. Hodge, Jr. (59—A-129)
332 An Approximate Analysis of the Influence of Aerodynamic Heating and Initial Twist on the Torsional Stiffness of Thin Wings, L. S. Han. (60—APM-13)
335 Postbuckling Behavior of Rectangular Plates With Small Initial Curvature Loaded in Edge Compression—(continued), Noboru Yamaki. (59—APMW-22)
343 The Junction Problem of Solid-Slotted Cylindrical Shells, D. H. Cheng and N. A. Weil. (60—APM-2)

BRIEF NOTES

350 Method of Numerical Evaluation of a Large Determinant, F. R. E. Crossley and U. Germen. 352 On the Griffith-Irwin Theory, J. L. Sanders, Jr. 353 On the Flexure of Plastic Plates, S. Lerner and W. Prager. 355 Induced Velocities in Two-Dimensional Cascade Theory, J. Polasek. 356 Relation Between Stress Concentration and Boundary Displacement, J. S. Brock. 357 Bending of an Isotropic Triangular Plate, B. D. Aggarwala. 358 Simplified Analysis of a Thrust-Augmentation System, K. L. Bergman. 359 Stress Concentration in a Rotating Disk, Ta-Cheng Ku.

DISCUSSION

361 Discussion of previously published papers by M. K. Newman; M. V. Morkovin; P. G. Hodge, Jr., and R. Sankaranarayanan; Joseph Marin; R. R. Berlot; Norman Davids; T. Gillespie and A. W. Gunter; J. W. Dally, W. F. Riley, and A. J. Durelli; T. K. Caughey; H. H. Bleich and O. W. Dillon, Jr.; H. D. Conway; P. S. Theocaris; D. S. Johnson; R. P. Kanwal; Yi-Yuan Yu; C. W. Nelson; A. E. Bryson

377 BOOK REVIEWS

A SIX-PART SURVEY

Rocket Heat-Transfer Literature[1]

The survey has been divided into the following parts:

Rocket-Engine Heat Sources
Rocket Cooling Techniques
Nozzle Wall Materials
Variable Fluid-Property Effects
Predictions of Thermal Properties
Flow Separation and Acoustic Effects

Introduction

In recent years the rocket power plant has assumed an increasing importance in our technology. Not only does it represent one of the few schemes for propulsion outside of planetary atmospheres, but the large energy-release rates make it uniquely capable of fulfilling a number of missions such as planetary escape and high-acceleration trajectories.

At the same time it is recognized that the desirable features of rocket power plants are responsible for many design difficulties in their utilization. One of these difficulties which is particularly severe is the problem of thermally isolating the hot propulsive gases from the rocket shell or frame.

It is the purpose of this survey to bring together the information on these heat-transfer problems from a variety of sources, so that present workers in the field may benefit from these many researches. Particular emphasis has been placed on the advances which have been made in the last decade.

Rocket-Engine Heat Sources

By R. W. Graham and G. Morrell[2]

The gas-side heat-transfer process in rocket engines is influenced by the velocity of the combustion products, the geometry of the engine, the heat-release rate of the combustion process, and the transport properties of the combustion products. Only the latter two will be considered in this section.

Specifically, a discussion is presented on space-heating rates or conversion rates in rocket combustors and the influence of combustion instability on the conversion process. Next, the chemical energy per unit mass is considered and is related to gas temperatures. The thermodynamic and transport properties are treated and, finally, approximate methods for calculating heat-transfer rates are outlined.

Volumetric Heat-Release Rates in Rocket Combustion

The last ten years have seen two notable approaches to the problem of describing the processes of heat release in flow combustors and, in particular, rocket combustors. Of course, the ultimate goal of each approach is the a priori prediction of heat-release rates for arbitrary boundary conditions. Some researchers have attempted to treat the process as essentially aerodynamic in nature but modified by consideration of chemical kinetic effects. Others have attempted to study the mechanics of the process by assuming a single rate-controlling step, the assumed step being a function of the initial boundary conditions.

About eight years ago, von Karman [1][3] pointed out that a complete description of the flowing combustion system required a consideration of chemical kinetics as well as aerodynamics and thermodynamics. For this subject he coined the term "aerothermochemistry," and he has recently summarized the equations involved [2]. Actually, this is a special application of the general equations of chemical flow reactors proposed by Damköhler [3] and later by Hulbert [4]. The chief advantage of the aerothermochemical equation is that it permits easy qualitative generalization about parametric effects on heat-release rate. A serious disadvantage is that quantitative solution requires a precise knowledge of the pertinent rate constants which is not now available and is not likely to be available in the foreseeable future. Two notable applications of these equations have been in rocket-engine scaling with similarity parameters by Penner [5], Crocco [6], and Ross [7], among others, and in the characterization of nozzle flow conditions by Penner [8], Krieger [9], and others.

The mechanistic approach, while capable of giving quantitative predictions of heat-release rates, suffers from the rather severe assumptions required to produce a simple model. If one calculates the maximum chemical space-heating rates (Btu/hr-cu ft) in rocket combustors, the values are in the range 10^{14} to 10^{17}, whereas the measured values are of the order of 10^{6}. This indicates that physical processes are probably rate controlling, at least at high pressures. Application of turbulent-duffusion theory to rocket combustors by Bittker [10] indicates that turbulent mixing may not be the slow step in many combustors. A more promising model seems to be that based on droplet evaporation or burning as a slow step in the over-all conversion to hot gas. Extensive studies have been made on the rate of evaporation of single drops and sprays with and without concomitant combustion; for example, Ingebo [11], Spalding [12], and Godsave [13]. Recently, Priem, Heidmann, and others [14] have applied a droplet-evaporation model to rocket combustion and have obtained reasonable agreement between predicted and measured combustor volume required to obtain a given combustion efficiency. The most serious gaps in the procedure lie in assessing the initial drop-size distribution and the influence of liquid-phase heat-release effects.

In the field of solid-propellant combustion, an excellent review by Geckler [15] indicates that the situation is similar to that for liquid propellants. In recent papers [16], the mechanistic approaches based on heat-transfer or evaporation-rate controlling steps seem to be providing more quantitative predictions of conversion rates and erosive burning effects.

Combustion Instability

The term combustion instability is generic for a variety of periodic and aperiodic pressure, velocity, and temperature disturbances which can occur in flow combustors, including rockets.

[1] Prepared by members of the Subcommittee on Rocket Heat Transfer of the Heat Transfer Division of The American Society of Mechanical Engineers. Edited by Thomas F. Irvine, Jr., North Carolina State College, Chairman.

[2] Lewis Research Center, NASA, Cleveland, Ohio.

[3] Numbers in brackets designate References at end of this part.

These range from random pressure peaks to low-frequency oscillations associated with all or part of the feed system to high-frequency oscillations associated with the mass of gas in the combustor and nozzle [17, 18].

Many experimental studies have established that these oscillations consist of large-amplitude pressure waves or shock waves which occur at the natural frequency of part of the feed system or at the resonance frequency of the combustor, e.g. [19–26].

The most complete linear analysis of periodic instability is due to Crocco and Cheng [27]. This is based on a solution of the equations of aerothermochemistry, including a time-lag parameter which is responsible for the periodicity. The analysis has recently been shown to predict the limits of instability for longitudinal waves. A partial analysis of transverse oscillations has been presented by Moore and Maslen [28]. Neither analysis is mechanistic in nature, but combines the driving and damping mechanisms into a time-lag parameter. Current research is directed toward studies on the details of the driving and damping mechanisms in such flow systems. The need for continuing research stems from the abnormal stresses and high heat-transfer rates which these oscillations produce—Male [19], for example, shows pressure ratios as high as 3 and heat-transfer ratios as high as 10—and from the lack of knowledge on periodic combustion.

Heat-Release Rates Per Unit Mass of Rocket Propellants

The models used to predict the spatial heat-release rates in rocket engines are primarily aerodynamic with some modifications for rate-controlling processes. The methods employed in computing energy-release rates per unit mass of propellant reactants involve the chemistry of reactions and thermodynamics. The gas temperature, which is the driving potential of the gas-side heat transfer, and the molar distribution of the combustion-products species can be derived from this type of computation.

The energy release per unit mass of combustion products is identically the heat of reaction of these products. A portion of the energy release is transformed into kinetic energy to produce thrust, while another part is transferred out through the rocket walls as heat. The specific impulse (thrust-per-unit-mass-flow rate) can be related to the heat of reaction through an empirical equation of the form

$$I_{sp} = C\sqrt{Q} \text{ seconds}$$

where Q is the heat of reaction in kilocalories per gram at 0 deg C. From the above relationship, it is apparent that the energy release per unit mass, Q, is the function of the square of the specific impulse. Thus the heat transferred in the rocket engine is also a function of the square of the specific impulse, since the heat transferred is some fraction of the energy release per unit mass.

Table 1 is a compilation of heats of reaction, flame temperatures, and theoretical-specific-impulse values. According to Gordon and McBride [53], the coefficient C of the equation is approximately 205 for the propellant combinations listed in Table 1. This coefficient depends on the propellant combination selected and also on the expansion pressure ratio.

In the actual rocket chamber the comparative heat-release level may be different for these propellant combinations. Equilibrium coefficients and the dissociation and recombination energies will influence the energy release. The listing of the heats of reaction does point out the wide variations possible in heat release as a function of the propellant combination.

The heat of reaction, which is readily computed, is a first-order estimate of the relative magnitude of heat transfer from the combustion products of rocket propellants.

However, the literature contains much information on theoretical thermodynamic and transport properties for most of the liquid propellants and their combustion products, for example [29–53]. These theoretical properties can be used with the analytical techniques for estimating heat-transfer coefficients or rates. Most of these references have presented the thermodynamic and transport properties over a range of combustion and expansion conditions encountered in rocket engines. Special parameters of interest to the rocket designer, such as the characteristic velocity C^* and the thrust coefficient, are also tabulated in these references.

Estimation of Combustion Temperature

In order to estimate gas-side heat-transfer coefficients and heat-transfer rates, the combustion-gas temperature must be estimated. The characteristic velocity C^* is a measure of the effectiveness of the combustion process in converting chemical energy into thermal energy. Consequently, combustion-gas temperature is related to C^*. It can be shown that they are related approximately in the following way

$$C^* = \frac{\sqrt{g\gamma_R \dfrac{T_c}{M}}}{\left(\dfrac{2}{\gamma+1}\right)^{\dfrac{\gamma+1}{2(\gamma-1)}}}$$

where

g = acceleration due to gravity
M = molecular weight, gm/mole
R = universal gas constant
T_c = combustion temperature
γ = ratio of specific heats

If the influences of variable molecular weight and gamma are neglected, C^* is simply proportional to the square root of the temperature. Employing this assumption, the theoretical values of C^* and combustion temperature obtained from [29–53] can be related to the experimental C^* and combustion temperature through the equation

$$\frac{T_{c_{ex}}}{T_{c_{th}}} = \left(\frac{C_{ex}^*}{C_{th}^*}\right)^2$$

The subscripts ex and th stand for experimental and theoretical, respectively. The experimental C^* can be computed from rocket data $\dfrac{\text{chamber pressure} \times \text{throat area}}{\text{propellant flow rate}}$ or may be estimated as being 85 to 99 per cent of the theoretical C^*. The injector type will govern the selection of the percentage.

Table 1

	Propellant	Combustion temperature, T_c, deg F	Heat of reaction, kcal/gm	Estimated specific impulse	Theoretical specific impulse from literature, p_e = 14.7 psi[a] p_c = 300 psi[b]
1	OV Grain solid propellant	...	0.78	182	200[c]
2	$NH_3 + 6HNO_3$	...	1.132	218	225.2
3	$NH_3 + 0.375N_2O_4$	4600	1.300	234	237.2
4	$NH_3 + 1.5H_2O_2$	4100	1.307	234.3	237.9
5	$N_2H_4 + ClF_3$	5840	1.449	246	257.0
6	$N_2H_4 + 0.5N_2O_4$	...	1.591	258	253.7
7	JP-4 + $0.9855O_2$	5700	1.628	260	246.7
8	$NH_3 + 0.75O_2$	4800	1.639	262	255.6
9	$N_2H_4 + 2F_2$	5700	2.431	320	315.7
10	$H_2 + F_2$	8000	3.084	359	342.5

[a] p_e is the nozzle exit pressure.
[b] p_c is combustion pressure.
[c] Evaluated at 1000-psi chamber pressure.

In addition to the mean-gas temperature, the transport properties of the gas mixtures are needed for heat-transfer computations. Estimates of transport properties of gases at high temperatures suffer from a lack of experimental data for each species at these temperatures. The high-temperature transport properties have been extrapolated from low-temperature data. All of the NASA or NACA references use a molar averaging technique to compute the viscosity of the gas mixtures, namely,

$$\mu = \frac{PM}{\sum_i \frac{P_i}{\mu_i/M_i}}$$

where

p = total pressure
M_i = molecular weight of the i^{th} species, gm/mole
P_i = partial pressure of the i^{th} species
μ_i = coefficient of viscosity of the i^{th} species

Thermal conductivity is computed from the Euken equation which relates viscosity and specific heat to thermal conductivity.

$$k = \mu\left(c_p + \frac{5}{4}\frac{R}{M}\right)$$

The Euken equation is an approximate expression which applies to pure polyatomic gases. Reference [54] contains a more exact but more difficult method for computing thermal conductivity in reacting gases involving any number of components. Probably the best general discussion on methods of computing transport properties of gas mixtures is found in [55], but most of the methods in this reference are laborious. For many heat-transfer calculations, the labor involved in the more exact computation of the gas-mixture transport data may not be warranted.

One analytical technique employed by rocket-engine designers in estimating the gas-side heat transfer is to section the engine into axial segments and compute the heat transfer for each segment. The over-all heat-transfer load of the engine is the integrated value. The film coefficient at each axial station in the rocket is computed by treating the axial segment as a piece of pipe and computing the coefficient from the pipe-flow heat-transfer correlations of the literature. From first appearances this approach may seem to be wrong inasmuch as the pipe-flow heat-transfer correlations are based upon fully developed turbulent flow. Intuitively, it does not seem possible to have fully developed turbulent pipe flow in a rocket engine inasmuch as the highly turbulent combustion gases do not have the sufficient flow length nor nonrandom velocity direction to produce a fully developed boundary layer. However, Bartz [56] claims that computations of the turbulent boundary layer show that, under certain circumstances, the mass-flow rate per unit area is the most dominant variable. Variables, such as velocity profile and boundary-layer thickness, are secondary. This conclusion suggests that the heat-transfer coefficient can be computed by a relation which in form is identical to the pipe-flow heat-transfer relation; namely,

$$\mathrm{Nu} = 0.026\mathrm{Re}^{0.8}\mathrm{Pr}^{0.4}$$

where

Nu = Nusselt number
Pr = Prandtl number
Re = Reynolds number

When the above equation is applied to the rocket engine, no assumption concerning fully developed turbulent flow is implied. However, the heat transfer in the chamber cannot be characterized by the convec ive mode only, so the author of [56] suggests that the convective-heat-transfer relationship be applied to the nozzle only.[4]

Similar empirical convective heat-transfer relationships based on pipe-flow experiments with high flux values are available in the literature. For example, the second author has applied the correlation of [57] to rocket-engine heat-transfer computations and found the computed over-all heat flux to agree favorably with the experimental.

References

1 T. von Karman, "Aerothermodynamics and Combustion Theory," Sorbonne lectures 1951–1952, Sorbonne, Paris, *L'Aerotecnica*, 33, 80–86 (1953).

2 T. von Karman, "Fundamental Equations in Aerothermochemistry," pt. 2, AGARD, "Selected Combustion Problems," Butterworths Scientific Publications, London, England, 1956, pp. 167–184.

3 G. Damköhler, "The Influence of Flow, Diffusion, and Heat Transfer on the Performance of Reactors," *Zeitschrift für Elektrochemistrie*, vol. 42, 1936, pp. 846–862.

4 H. M. Hulbert, "Chemical Processes in Continuous Flow Systems," *Ind. and Eng. Chem.*, 36, 1012 (1944); *Ibid.*, 37, 1063 (1945).

5 S. S. Penner, "Similarity Analysis for Chemical Reactors and the Scaling of Liquid-Fuel Rocket Engines," Combustion Research and Reviews, AGARD, Butterworths Scientific Publications, London, England, 1955, pp. 140–162. See also, "Rational Scaling Procedures for Liquid-Fuel Rocket Engines," *Jet Propulsion*, 27, 156 (1957).

6 L. Crocco, Considerations on the Problem of Scaling Rocket Motors," pt. 2, AGARD, "Selected Combustion Problems," Butterworths Scientific Publications, London, England, 1956, pp. 457–468.

7 C. C. Ross, "Scaling of Liquid-Fuel Rocket Combustion Chambers," pt. 2, *Ibid.*, pp. 444–456. (See also, A. E. Weller, *Ibid.*, pp. 371–383.)

8 S. S. Penner, "Thermodynamic and Chemical Kinetics of One-Dimensional Nonviscous Flow Through a Laval Nozzle," *Jour. Chem. Phys.*, 19, 877 (1951).

9 F. J. Krieger, "Chemical Kinetics and Rocket-Nozzle Design," *Journal of the American Rocket Society*, 21, 179 (1951).

10 D. A. Bittker, "An Analytical Study of Turbulent and Molecular Mixing in Rocket Combustion," NACA TN 4321 (1956).

11 R. D. Ingebo, "Atomization, Acceleration, and Vaporization of Liquid Fuels," Sixth Symposium (International) on Combustion, pp. 684–687 (1956). (See also, NACA TN's 4087 and 4222.)

12 D. B. Spalding, "Combustion of Liquid Fuel in a Gas Stream," *Fuel*, 29, 2, 25 (1959); "The Combustion of Liquid Fuels," Fourth Symposium (International) on Combustion, pp. 847–864, The Williams & Wilkins Company, Baltimore, Md., 1953.

13 G. A. E. Godsave, "Studies of the Combustion of Drops in a Fuel Spray—the Burning of Single Drops of Fuel," Fourth Symposium (International) on Combustion, pp. 818–828, The Williams & Wilkins Company, Baltimore, Md., 1953.

14 R. J. Priem and M. F. Heidmann, "The Vaporization of Propellants in Rocket Engines," paper presented at the Thirteenth Annual Meeting, Am. Rocket Soc., November, 1958.

B. J. Clark, M. Hersch, and R. J. Priem, "Propellant Vaporization as a Criterion for Rocket-Engine Design; Experimental Performance, Vaporization, and Heat-Transfer Rates With Various Propellant Combinations," NASA Memo 12-29-58E (1959).

15 R. D. Geckler, "The Mechanism of Combustion of Solid Propellants," AGARD, "Selected Combustion Problems," Butterworths Scientific Publications, London, England, 1954, pp. 289–339.

16 L. Green, Jr., "Erosive Burning of Some Composite Solid Propellants," *Jet Propulsion*, 24, 9 (1954).

E. W. Price, "One-Dimensional, Steady Flow With Mass Addition and the Effect of Combustion-Chamber Flow on Rocket Thrust," *Jet Propulsion*, 28, 386 (1958).

L. Green, Jr., "Some Properties of a Simplified Model of Solid Propellant Burning," *Jet Propulsion*, 28, 386 (1958).

[4] Editor's note: According to Bartz, Ref. [10] in the portion of the paper entitled "Prediction of Thermal Properties," the resulting excellent agreement between heat-transfer coefficients determined from the turbulent-pipe-flow equation and those from calculations based on turbulent-boundary-layer development, Ref. [56] of this portion, is partially due to the fact that the local diameter on which the Reynolds number is based is a very appropriate characteristic dimension for the development of the local turbulent boundary layer in convergent-divergent nozzles (see Fig. 3 of Ref. [7] in the portion on "Variable Fluid-Property Effects)."

R. Friedman, R. G. Nugent, K. E. Rumbel, and A. C. Scurlock, "Deflagration of Ammonium Perchlorate," Sixth Symposium (International) on Combustion, Reinhold Publishing Corporation, New York, N. Y., 1957. p. 612.

R. D. Schultz and A. O. Kekker, "Transition-State Theory of the Linear Rate of Decomposition of Ammonium Perchlorate," *Ibid.*, p. 618.

J. M. Lenoir and G. Robillard, "A Mathematical Method to Predict the Effects of Erosive Burning in Solid-Propellant Rockets," *Ibid.*, p. 663.

17 A. O. Tischler and T. Male, "Oscillatory Combustion in Rocket-Propulsion Engines," Gas Dynamic Symposium, Northwestern University, Evanston, Ill., 1955.

18 C. C. Ross and P. P. Datner, "Combustion Instability in Liquid-Propellant Rocket Motors—A Survey," AGARD "Selected Combustion Problems," Butterworths Scientific Publications, London, England, 1954.

19 L. Berman and S. H. Cheney, Jr., "Combustion Studies in Rocket Motors," *Jour. Am. Rocket Soc.*, 23, 89 (1953).

T. Male, W. R. Kerslake, and A. O. Tischler, "Photographic Study of Rotary Screaming and Other Oscillations in a Rocket Engine," NACA RM E54A29, May 25, 1954.

20 A. O. Tischler and D. R. Bellman, "Combustion Instability in an Acid-Heptane Rocket," NACA TN 2936 (1953).

21 D. R. Bellman, J. C. Humphrey, and T. Male, "Photographic Investigation of Combustion in a Two-Dimensional Transparent Rocket Engine," NACA Rep. 1134 (1953). (Supersedes NACA RM E8F01.)

22 H. Ellis, et al., "Experimental Investigation of Combustion Instability in Rocket Motors," Fourth Symposium (International) on Combustion, p. 880, The Williams & Wilkins Company, Baltimore, Md., 1953.

23 R. P. Smith and D. F. Sprenger, "Combustion Instability in Solid-Propellant Rockets," *Ibid.* (1953), p. 893.

24 M. Barrere and J. J. Bernard, "Influence of the Injector Pressure Drop on Low-Frequency Instability in Liquid-Propellant Rockets," Sixth Symposium (International) on Combustion, p. 487, Reinhold Publishing Corporation, New York, N. Y., 1957.

25 L. Green, Jr., "Some Effects of Oxidiser Concentration and Particle Size on Resonance Burning of Composite Solid Propellants," *Jet Propulsion*, 28, 159 (1958).

26 M. J. Zucrow and J. R. Osborn, "An Experimental Study of High-Frequency Combustion Pressure Oscillations," *Ibid.* (1958), p. 654.

27 L. Crocco and S. I. Cheng, "Theory of Combustion Instability in Liquid Propellant Rocket Motors," AGARDograph No. 8, Butterworths Scientific Publications, London, England, 1956.

28 F. K. Moore and S. H. Maslen, "Transverse Oscillations in a Cylindrical Combustion Chamber," NACA TN 3152 (1954).

29 Cole Elverum and C. Deisher, "The Influence of Chamber Pressure on Theoretical Performance of F_2-N_2H_4, F_2-NH_3, and F_2-H_2 Propellant Systems," Memo 20-130, Jet Prop. Lab., C.I.T. (June, 1956).

30 F. D. Rossini, et al., "Selected Values of Chemical Thermo Properties," *Circular* 500, NBS (February, 1952).

31 Battelle Memorial Institute, "Physical Properties and Thermo Functions," vols. 1, 2, and 3, The Rand Corporation, Santa Monica, Calif., 1949.

32 T. Lesser, "High-Speed Digital Calculation of the Composition and Thermo Properties of Propellant Gases by the Brinkley Method," Rept. No. 1023, Ballistic Res. Lab. (August, 1957).

33 C. B. Henderson, "Theoretical Performance of Selected Propellant Systems," vol. 1, Atlantic Res. Corp. (April, 1958).

34 V. N. Huff and A. Fortini, "Theoretical Performance of JP-4 and Liquid Oxygen as a Rocket Propellant. I—Frozen Composition," NACA RM E56A27 (1956).

35 V. N. Huff, A. Fortini, and S. Gordon, "Theoretical Performance of JP-4 Fuel and Liquid Oxygen as a Rocket Propellant. II—Equilibrium Composition," NACA RM E56D23 (1956).

36 A. Fortini and V. N. Huff, "Theoretical Performance of Liquid Hydrogen and Liquid Fluorine as a Rocket Propellant for a Chamber Pressure of 600 Pounds per Square Inch Absolute," NACA RM E56L10a (1957).

37 V. N. Huff, C. S. Calvert, and V. C. Erdmann, "Theoretical Performance of Diborane as a Rocket Fuel," NACA RM E8117a, 1949.

38 V. N. Huff and S. Gordon, "Theoretical Rocket Performance of JP-4 Fuel With Mixture of Liquid Ozone and Fluorine," NACA RM E56K14 (1957).

39 V. N. Huff, S. Gordon, and V. E. Morrell, "General Method and Thermodynamic Tables for Computation of Equilibrium Composition and Temperature of Chemical Reactions," NACA Rep. 1037. (Supersedes NACA TN's 2113 and 2116.)

40 S. Gordon and V. N. Huff, "Theoretical Performance of Lithium and Fluorine as a Rocket Propellant," NACA RM E51C01 (1951).

41 S. Gordon and V. N. Huff, "Theoretical Performance of Liquid Hydrogen and Liquid Fluorine as a Rocket Propellant," NACA RM E52L11 (1953).

42 S. Gordon and V. N. Huff, "Theoretical Performance of Liquid Ammonia and Liquid Fluorine as a Rocket Propellant," NACA RM E53A26 (1953).

43 S. Gordon and V. N. Huff, "Theoretical Performance of Liquid Hydrazine and Liquid Fluorine as a Rocket Propellant," NACA RM E53E12 (1953).

44 S. Gordon and V. N. Huff, "Theoretical Performance of Mixtures of Liquid Ammonia and Hydrazine as Fuel With Liquid Fluorine as Oxidant for Rocket Engines," NACA RM E53F08 (1953).

45 S. Gordon and R. L. Wilkins, "Theoretical Maximum Performance of Liquid Fluorine-Liquid Oxygen Mixtures With JP-4 Fuel as Rocket Propellant," NACA RM E54H09 (1954).

46 S. Gordon and V. N. Huff, "Theoretical Performance of JP-4 Fuel With a 70 Per Cent Fluorine-30 Per Cent Oxygen Mixture as a Rocket Propellant. I—Frozen Composition," NACA RM E56A13a (1956).

47 S. Gordon and V. N. Huff, "Theoretical Performance of JP-4 Fuel With a 70-30 Mixture of Fluorine and Oxygen as a Rocket Propellant. II—Equilibrium Composition," NACA RM E56F04 (1956).

48 S. Gordon and K. S. Drellishak, "Theoretical Rocket Performance of JP-4 Fuel With Several Fluorine-Oxygen Mixtures Assuming Frozen Composition," NACA RM E57G16a (1957).

49 S. Gordon, "Theoretical Performance of JP-4 Fuel With Several Fluorine-Oxygen Mixtures Assuming Equilibrium Composition," NACA RM E57K22 (1958).

50 S. Gordon and A. R. Glueck, "Theoretical Performance of Liquid Ammonia and Liquid Oxygen as a Rocket Propellant," NACA RM E58A21 (1958).

51 S. Gordon and M. E. Kastner, "Theoretical Rocket Performance of Liquid Methane With Several Fluorine-Oxygen Mixtures Assuming Frozen Composition," NACA RM E58B20 (1958).

52 V. N. Huff and S. Gordon, "Theoretical Performance of Liquid Ammonia, Hydrazine, and Mixtures of Ammonia and Hydrazine as Fuels With Liquid Oxygen Bifluoride as Oxidant for Rocket Engines. I—Mixtures of Liquid Ammonia and Hydrazine," NACA RM E51L11 (1952); "II—Hydrazine," NACA RM E52G09 (1952); "III—Liquid Ammonia," NACA RM E52H14 (1952).

53 S. Gordon and B. McBride, "Theoretical Performance of Liquid Hydrogen With Liquid Oxygen as a Rocket Propellant," NASA MEMO 5-21-59E (1959).

54 J. N. Bittker and R. S. Brokaw, "Thermal Conductivity of Gas Mixtures in Chemical Equilibrium," *Jour. Chem. Phys.* 26 (June, 1957).

55 J. O. Hirschfelder, C. F. Curtiss, and R. B. Bird, "Molecular Theory of Gases and Liquids," John Wiley & Sons, Inc., New York, N. Y., 1954.

56 D. Bartz, "A Simple Equation for Rapid Estimation of Rocket Nozzle Convective Heat-Transfer Coefficients," *Jet Propulsion*, 27, 49–51 (1957).

57 L. V. Humble, W. J. Lowdermilk, and L. C. Desmon, "Measurements of Average Heat Transfer and Friction Coefficients for Subsonic Flow of Air in Smooth Tubes at High Surface and Fluid Temperatures," NACA Report 1020 (1951). (Formerly RM's E7L31, E8103, E50E23, and E50H23.)

Rocket Cooling Techniques

By R. D. Turnacliff[6]

Rocket-engine thrust chambers and nozzles have been cooled principally by regenerative means for liquid-propellant rockets and by use of a simple heat sink for solid-propellant systems. Reliability and weight considerations were of prime importance in determining the type of the cooling methods used. It is likely that these methods will continue to be used in systems of the immediate future with the heat-sink and/or ablation-type cooling becoming more common as material technology advances. The additional complexity and poorer reliability of both transpiration and film cooling will probably limit their applications to special problems as well as to containment and expansion of extremely high energy fluids.

[6] Space Technology Laboratory, Los Angeles, California.

Predictions of convective-heat-transfer rates have been considered by various authors of which [1][6] is one of the more recent and reliable methods. However, considerable uncertainty still exists in prediction of exact local values in actual engines. This is probably due to nonuniform radial temperatures and fluid composition in the gas stream which is strongly influenced by the injector and combustion pattern. The effects upon heat transfer of dissociated combustion products can be approximately taken into consideration in the above equation by using computed enthalpy in place of temperature differences. Experimental evidence of the effects of dissociated combustion products upon the convective-heat-transfer coefficient is discussed in [2].

Regenerative cooling of rocket engines is limited principally to liquid-phase forced-convection and nucleate-boiling heat-transfer processes. One exception to this is forced-convection cooling using gaseous hydrogen [3, 4]. The low thermal conductivity of other gas-phase propellants usually eliminates their use due to the excessively high wall temperatures required for operation and the relatively low temperature limits of most wall materials. In rare instances, cooling has been accomplished through film boiling [12]. The problem of heat transfer in the vicinity of the critical temperature is discussed in [5]. The use of various propellant combinations as regenerative coolants is reviewed in [6] where a criterion for acceptable cooling is established, and the influence of various physical properties of the coolant upon its effectiveness as a regenerative coolant is also discussed. The operating mixture ratio is shown there to be an important system parameter which influences the cooling problem [6]. Data on the nucleate boiling and convective-heat-transfer coefficients for selected regenerative coolants, such as JP fuel, WFNA, UDMH, RFNA, and so forth, may be found in [7–13, 31].

Porous-wall or transpiration cooling of rocket engines was investigated quite extensively in the late 1940's [14–19]. Nonuniformity of injection resulting from fabrication of the porous material gave unpredictable performance. Although some improvement in uniformity of injection has been accomplished, the additional complexity of the system plus poorer reliability has greatly reduced its usefulness in rocket-engine cooling. It has potential application in the containment of very high energy working fluids when other methods fail.

Film cooling or slot injection offers a somewhat more reliable system than transpiration cooling although still relatively complex in comparison with present systems. Recent studies in the use of film cooling in rocket nozzles indicate that it is a useful means of cooling local areas when it cannot be done by conventional means [20–27].

Recent advances in material technology associated with the nose-cone re-entry problem and solid-propellant engine development have opened the field of more advanced heat-sink as well as ablation-cooling methods. Little published literature is available on the problem as directly applied to rocket-engine cooling, although [28] discusses the application of ablation cooling to rocket nozzles and describes calculation methods for predicting ablation rates and internal temperature gradients. Wall-coating techniques for reducing heat transfer to a regeneratively cooled engine are discussed in [29, 30].

References

1 D. R. Bartz, "A Simple Equation for Rapid Estimation of Rocket-Nozzle Convective-Heat-Transfer Coefficients," *Jet Propulsion*, 27(49) (1957).

2 H. Ziebland, "Some Experimental Observations Regarding the Convective Heat Transfer From Highly Dissociated Combustion Gases to Cooled Wall of Rocket Engines," ERDE Tech. Memo No. 13/M156 (July, 1956).

3 NACA 1957 Flight Propulsion Conference.

4 W. B. Powell, "Analysis of Heat Transfer to Hydrogen Gas Flowing Through Tubes Having Constant Wall Temperature," CIT JPL Progress Report No. 1-63 (1948), ASTIA ADR-58-486.

5 W. B. Powell, "Heat Transfer to Fluids in the Region of the Critical Temperature," CIT JPL Progress Report No. 20-285 (April 1, 1956).

6 D. R. Bartz, "Factors Which Influence the Suitability of Liquid Propellants as Rocket-Motor Regenerative Coolants," CIT JPL Memo No. 20-139 (December, 1956), ASTIA-AD-133-919.

7 C. M. Beighley and L. E. Dean, "Study of Heat Transfer to JP-4 Jet Fuel," *Jet Propulsion*, 24(3) (1954).

8 E. Ashley, "Heat-Transfer Measurements for White Fuming Nitric Acid," Bell Aircraft Corp. Report 56-982-016 (1953).

9 Banchero, Baner, and Ball, "Heat-Transfer Characteristics of Boiling Oxygen, Fluorine, and Hydrazine," Univ. of Michigan Eng. Res. Inst. Report 51-11, ASTIA ADR-58-3030.

10 F. Kreith and M. Summerfield, "Heat Transfer From an Electrically Heated Tube in Aniline at High Heat Flux," CIT JPL Progress Report No. 4-88 (1948).

11 H. Wolf and F. L. Gray, "Experimental Investigation of the Heat Transfer and Fluid Friction Characteristics of White Fuming and Red Fuming Nitric Acid at High Heat Flux Densities," NACA Contract NAW-6286 (Loan from Washington, D. C.).

12 L. E. Dean, "Heat-Transfer Characteristics of UDMH," Aerojet Report TRC-142 (Dec., 1958).

13 J. N. Barger, "Application of Alkylhydrazines to Rocket Power Plant," Aerojet Report 1293 (1957).

14 W. D. Rannie, "A Simplified Theory of Porous-Wall Cooling," JPL Progress Report No. 4-50 (Nov., 1957).

15 H. L. Wheeler, Jr., and Pol Duwez, "Heat Transfer Through Sweat-Cooled Porous Tubes," *Jet Propulsion*, 25(10), 519–542 (Oct., 1955).

16 J. Friedman, "A Theoretical and Experimental Investigation of Rocket-Motor Sweat Cooling," *J. Am. Rocket Society*, 79, 147–154 (Dec., 1949).

17 E. Mayer and J. G. Bartas, "Transpiration Cooling in Porous Metal Walls," *Jet Propulsion*, 24(6), 366–368 (Nov.-Dec., 1954).

18 S. Weibaum and H. L. Wheeler, Jr., "Heat Transfer in Sweat-Cooled Porous Metals," *J. Appl. Phys.*, 20, 113–122 (Jan., 1949).

19 H. L. Wheeler, Jr., "Heat Transfer in Nitrogen and Hydrogen Sweat-Cooled Tubes," CIT JPL Progress Report 20-160 (Jan., 1952).

20 M. J. Zucrow and A. R. Graham, "Some Considerations of Film Cooling for Rocket Motors," *Jet Propulsion*, 27(6), 650–656 (June, 1957).

21 C. F. Warner and B. A. Reese, "Investigation of Factors Affecting Attachment of Liquid Film to Solid Surface," *Jet Propulsion*, 27(8), 877–881 (August, 1957).

22 Glenn A. Schurman, "An Investigation of Film Cooling in Flame Tube," CIT JPL Progress Report 1-74 (June, 1948).

23 G. R. Kinney, A. E. Abramson, and J. L. Sloop, "Internal Liquid Film-Cooling Experiments With Air-Stream Temperatures to 2000 F in 2 and 4-inch Diameter Horizontal Tubes," NACA Report 1087 (1952).

24 A. R. Graham and J. J. Zucrow, "Film Cooling, Its Theory and Application," Jet Propulsion Center Tech. Memo 57-3, Purdue Universtity (1957).

25 A. R. Graham, "An Experimental and Theoretical Investigation of Film Cooling of Rocket Motors," *Ibid.* (1957).

26 Z. A. Typaldos and R. B. Canright, "An Experimental Evaluation of Transpiration Cooling in a Rocket-Motor Chamber," CIT JPL Report No. 135 (1952).

27 R. H. Boden, "Heat Transfer in Rocket Motors and the Application of Film and Sweat Cooling," TRANS. ASME 73(4), 385–390 (May, 1951).

28 D. Baer and A. Ambrosio, "Heat Conduction in a Semi-infinite Slab With Sublimation at the Surface," Space Tech. Lab. TR-0000-00610 (February, 1959).

29 D. D. Thomas and L. G. Cole, "The Reduction of Heat Transfer to Rocket Motors by Motor-Wall-Coating Techniques," CIT JPL Progress Report No. 9-50 (1950).

30 L. C. Land, "A Study of Ceramic Liners for Uncooled Rocket-Motor Chambers," CIT JPL Memo 4-26 (1948).

31 J. J. Jicha and E. J. Lemanski, "Nucleate Boiling Literature Search," AEC-MND-1062-1, April, 1957. (Supplement to MND-1062.)

[6] Numbers in brackets designate References at end of this part.

Nozzle Wall Materials

By J. H. Robinson and K. G. Englar[7]

For uncooled rocket nozzles, such as are customarily used with

[7] Douglas Aircraft Company, Inc., El Segundo, Calif.

solid-propellant rocket motors, the heat transferred to the walls from the hot gases passing through the nozzle must be absorbed by the materials comprising the nozzle. If this heat is absorbed by the nozzle walls acting as a heat sink, the nozzle walls are necessarily heavy in order to absorb the large quantity of heat transferred from the burning gases. In addition, metals with a melting point high enough (4000 F and above) to withstand the effects of high-energy propellant combustion are very dense. Some of the metals which have been used as heat-sink material for rocket nozzles are molybdenum, tungsten, tantalum, and columbium. Graphite has been extensively used, but erodes badly. Cermets show promise as heat-sink materials for rocket nozzles, being less dense than metals, although some have poor thermal shock characteristics. Among the cermets being used, or being considered, are aluminum oxide, boron nitride, and the carbides of tungsten, silicon, tantalum, and hafnium.

The chemical composition of an exhaust flame at high temperature often acts either as a reducing or an oxidizing agent upon metal and cermet nozzle materials. Therefore, in cases of severe reaction, it is necessary to apply a protective coating of a material compatible to nozzle materials and resistant to reaction with the exhaust flames. Experience shows that ceramic materials are well suited to this function, but must be selected to be chemically compatible with the propellant used. A similar problem occurs in nozzles constructed of steel alloys with low melting points, where a protective coating of compatible ceramic is applied to resist erosion.

One way of reducing the mass of the nozzle walls is to place an insulating material on the inner surface of the nozzle. The insulating material should have much the same properties as a "heat-sink material"; i.e., physical strength at elevated temperatures, resistance to erosion and thermal shock, high melting point, and compatibility with the chemical properties of the exhaust gases. Most insulators either ablate or sublime. It is often desirable to choose a material with a relatively low melting point, or one which sublimes so the material leaves the nozzle walls as a liquid or a gas. If a material with a high melting point is used, the nozzle material which is eroded by the gases passing through the nozzle would be carried as solid particles by the gas stream, adding to the erosiveness of the exhaust gases. In addition, it is necessary that the erosion of the insulator be predictable with respect to change in throat area. Preferably, the amount of material eroded away should be small, and erosion should be uniform around the periphery of the nozzle and take place at a constant rate. Some of the insulating materials which have been used are Refrasil, asbestos, fiberglass, and zirconium oxide.

In selecting a rocket-nozzle material for a given application, the temperature distribution through the nozzle walls must be known as a function of time in order to determine surface temperatures, thermal stress, and so forth. Unfortunately, the differential equations describing this transient heat transfer within the nozzle walls do not lend themselves readily to solution in closed form, due to the transient character of the conditions at the boundary between the hot gases and the nozzle wall. Heat transfer within homogeneous or composite nozzle walls can be analytically determined by expressing the differential equations describing heat flow as finite-difference equations. Solution of these equations by numerical methods is discussed in detail by Dusinberre [1],[8] who has enlarged considerably on the method originally used by Schmidt [2].

The finite-difference equations for most one and two-dimensional heat-transfer problems are readily solvable by hand calculations, which Dusinberre [1] covers well. The thermal field gets quite complicated for most two and three-dimensional cases, leading to the use of digital computers for their solution. These, as well as many other aspects of transient and steady-state conduction heat transfer, are discussed in Schneider's excellent treatise [3]. Many of the digital-computing programs are set up, however, to treat specific thermal networks and are not readily adapted to changes in the thermal network. Programs have been established for the digital computer so that changes in the thermal network can be easily accomplished [4].

Ease of altering the network is one of the prime advantages of electrical analogs. One such analog developed by Liebmann [5, 6] solves the finite-difference equations in space and time by an electrical-resistance network, with both thermal resistance and thermal capacitance analogized by electrical resistances. Transient temperatures at discrete spatial points in the thermal network are computed at discrete time intervals.

A more common analog [7] replaces the thermal resistances and capacitances with electrical resistances and capacitances, respectively. This R-C network uses voltage and current as analogized temperature and heat flux, respectively. Here the space variable is retained in derivative form. Temperatures at discrete points are then obtained as a continuous function of time.

References

1 G. M. Dusinberre, "Numerical Analysis of Heat Flow," 1 ed., McGraw-Hill Book Company, Inc., New York, N. Y., 1949.

2 E. Schmidt, "Foppls Festschrift," pp. 179–198, Julius Springer Verlag, Berlin, Germany, 1924; abstracted by T. K. Sherwood and C. E. Reed, "Applied Mathematics in Chemical Engineering," McGraw-Hill Book Company, Inc., New York, N. Y., 1939, p. 211.

3 P. J. Schneider, "Conduction Heat Transfer, "Addison-Wesley Publishing Company, Cambridge, Mass., 1955.

4 K. G. Englar and W. H. Mead, "Use of the IBM 701 to Solve Complex Heat-Transfer Problems of a General Nature," Engineering Department Report No. SM-22742, Douglas Aircraft Company, Inc., Santa Monica, Calif., March 5, 1957.

5 G. Liebmann, "A New Electrical Analog Method for the Solution of Transient Heat Conduction Problems," TRANS. ASME, vol. 78, 1956, p. 655.

6 G. Liebmann, "Solution of Transient Heat-Transfer Problems by the Resistance-Network Analog Method," TRANS. ASME, vol. 78, 1956, p. 1267.

7 V. Pasckis and H. D. Baker, "A Method for Determining Unsteady-State Heat Transfer by Means of an Electric Analogy," TRANS. ASME, vol. 64, 1942, p. 105.

Variable Fluid-Property Effects

By R. G. Deissler,[9] Mem. ASME

Because of the high heat fluxes occurring between the walls and fluid streams in rocket engines, the temperature variations across the streams are large. Thus the variations of fluid properties with distance from the wall are in general large, and the heat-transfer and fluid-flow processes are affected. In the chemical rocket, variable fluid properties can occur, for instance, in the boundary layer of the nozzle, in the coolant passages, and in the combustor. In the nuclear rocket, heat is usually transferred at high rates directly from the reactor walls to the propellant, so that the effect of variable properties on the heat transfer in the reactor can be important. At high temperatures the fluid may dissociate. Heat transfer with dissociation or chemical reaction can often be treated as a variable fluid-property problem, at least for the case where the properties are in chemical equilibrium.

In approaching the problem of variable properties, the results of essentially constant property experiments or analyses have often been adapted to the case of high heat fluxes by evaluating the properties in the equations at an appropriate reference temperature. However, in order to determine the correct reference temperature, experiments or analyses (preferably both) must be

[8] Numbers in brackets designate References at end of this part.

[9] Lewis Research Center, NASA, Cleveland, Ohio.

carried out for variable properties. An essential difficulty in variable-property heat transfer is that, strictly speaking, each fluid should be treated separately, because its property variations with temperature are different. In spite of this difficulty it has been found possible in many cases to correlate results by using a reference temperature close to the average of the wall and bulk (or free-stream) temperatures [1–6].[10] This reference temperature should be used with some caution for new cases, however, especially when the property variations with temperature are unusual.

Inasmuch as the flow in rocket engines is generally turbulent, only turbulent flow will be considered in the present section. An analysis of the heat transfer in the turbulent boundary layer in a nozzle, which is in agreement with data for actual rocket engines, is given in [7]. The results are simplified in [3] by showing that they can be represented by an equation of the type used for pipe flow. Although the effect of compressibility on the development of the boundary layer was considered in this study, it is not strictly a variable-property analysis inasmuch as the reference temperature was assumed rather than calculated. Most of the variable-property analyses have been carried out for the simpler cases of turbulent flow through circular tubes or over flat plates. Thus most of the remainder of this section will consider the work done for these cases; this work should give some insight into the more complicated flows sometimes encountered in rocket engines.

An extensive experimental investigation of average heat-transfer and friction coefficients for flow of air in smooth electrically heated tubes is summarized in [1]. Surface temperatures on the order of 2500 F were reached. The surface-to-air temperature ratio varied from about 0.46 to 3.5, with heat fluxes up to 10^6 Btu/hr-ft^2. The effect of surface-to-air temperature ratio was eliminated by evaluating the properties of the air, including density, in the Nusselt number, Reynolds number, and friction coefficient at a temperature halfway between the average wall and bulk temperatures. Recently the work was extended to helium at surface temperatures up to 5500 F [8]. Essentially the same type of correlation was obtained as was found to apply for air.

A variable-property analysis for turbulent flow of air in a tube with high rates of heat transfer is presented in [9]. In order to check the analysis experimentally, local heat-transfer coefficients were measured for air flowing in an electrically heated tube at high heat fluxes. The agreement between predicted and measured heat-transfer coefficients was good. Both indicated that the effects of variable properties could be eliminated by evaluating the properties at a reference temperature about halfway between the wall and bulk temperatures. In using this result for calculating heat-transfer coefficients, the same assumptions concerning the variation of properties as were used in the analysis should be made; that is, constant specific heat, and viscosities and thermal conductivities both proportional to the 0.68 power of the absolute temperature should be used. If other property variations are used a different reference temperature may be obtained. The analysis is extended to liquids with variable viscosity in [10] and to entrance regions in [6]. In both cases, the reference temperatures for evaluating the properties were found to be near the average of the wall and bulk temperatures, as before. An alternate approach for heat transfer in liquids with variable properties is given in [14], and some additional work for entrance regions is given in [26].

A variable-property analysis for supercritical water is given also in [9]. In this case the reference temperature varied between the wall and the bulk temperatures because of the unusual variation of properties of supercritical fluids with temperature. An analysis for supercritical water using a somewhat different approach is given in [27] and gives results in reasonable agreement with those in [9]. In [11] the analytical method of [9] is used for calculating heat transfer to supercritical carbon dioxide, and experiments were run for the conditions of the analysis. A comparison between theory and experiment for one wall temperature is given in Fig. 1, where good agreement is indicated. (The quantity β is a heat-flux parameter and subscripts 0 indicate properties evaluated at the wall.) Similar agreement was obtained for other wall temperatures near the critical temperature. Some experimental results for supercritical oxygen and for supercritical water are given in [12] and [13]. It would be of interest to compare these results with an analysis similar to that given in [9] or [11], but using the properties for the appropriate fluids and the conditions in the experiments. Uncertainty in the property values of the fluids might, however, make the comparison difficult. Under certain conditions a boiling-like phenomenon (which would not be predictable by the analysis) may occur in supercritical fluids ([9], discussion by Goldman). Many of the foregoing analyses and experiments are summarized in [15] and [16].

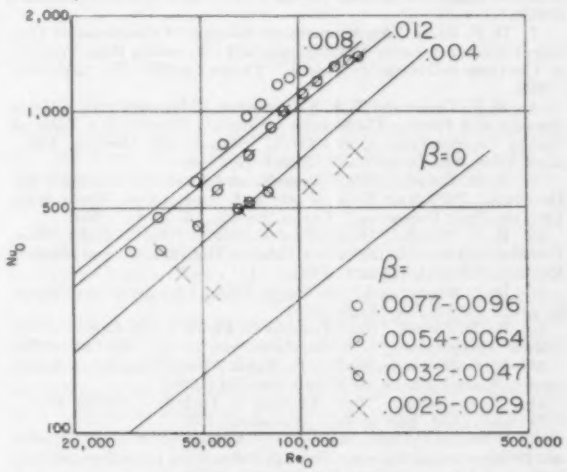

Fig. 1 Experimental and theoretical results for heat transfer to carbon dioxide in the critical region. Pressure = 1200 psia; t_b = 130 F. Ref. [11].

A large number of analyses for flow over flat plates at high velocities, which include the effects of variable fluid properties in varying degrees, have been carried out. Some of these are reported in [5, 17–23]. It is difficult to compare the analyses because of the many different assumptions used by the various authors. The analysis in [5] uses the assumptions that were used for flow in tubes [2, 6, 9], and gives heat-transfer and friction coefficients in good agreement with available experimental data (which extend to Mach 9). The results are also in agreement with the reference temperatures recommended in [24], except at low Reynolds numbers. The analysis was recently extended to sublimation mass transfer at supersonic speeds [25], where good agreement with experimental data was again obtained.

In conclusion, it appears that sufficient analytical information is available so that the determination of heat transfer at high fluxes for various fluids need not be entirely an empirical process. A reasonable procedure might be to run experiments using several fluids of interest in rocket applications and to compute analytical results using the properties of those fluids. If agreement between theory and experiment is obtained, the analysis could then be used to obtain results for other fluids. Such calculations are not particularly difficult with the computing equipment now available (at least not for the simpler flows discussed here). The utility of

[10] Numbers in brackets designate References at end of this part.

the method would, of course, depend on the availability of property values for the fluids of interest.

References

1 L. V. Humble, W. H. Lowdermilk, and L. G. Desmon, "Measurement of Average Heat-Transfer and Friction Coefficients for Subsonic Flow of Air in Smooth Tubes at High Surface and Fluid Temperatures," NACA Report 1020 (1951). (Formerly RM's E7L31, E8L03, E50E23, and E50H23.)

2 R. G. Deissler and C. S. Eian, "Analytical and Experimental Investigation of Fully Developed Turbulent Flow of Air in a Smooth Tube With Heat Transfer With Variable Fluid Properties," NACA TN 2629 (1952).

3 D. R. Bartz, "A Simple Equation for Rapid Estimation of Rocket-Nozzle Convective-Heat-Transfer Coefficients," *Jet Propulsion*, pp. 49–51 (January, 1957).

4 E. R. G. Eckert, "Survey on Heat Transfer at High Speeds," WADC Tech. Rpt. 54-70 (April, 1954).

5 R. G. Deissler and A. L. Loeffler, Jr., "Turbulent Flow and Heat Transfer on a Flat Plate at High Mach Numbers With Variable Fluid Properties," NASA TR R-17 (1959). (Supersedes NACA TN 4262, 1958.)

6 R. G. Deissler, "Turbulent Heat Transfer and Friction in the Entrance Regions of Smooth Passages," TRANS. ASME 77, 1221–1233 (1955).

7 D. R. Bartz, "An Approximate Solution of Compressible Turbulent Boundary-Layer Development and Convective Heat Transfer in Convergent-Divergent Nozzles," TRANS. ASME, 77, 1235–1245 (1955).

8 M. F. Taylor and T. A. Kirchgessner, "Measurements of Heat-Transfer and Friction Coefficients for Helium Flowing in a Tube at Surface Temperatures up to 5900 R," Semi-Annual Meeting, Amer. Rocket Soc., San Diego, Calif. (June 8–11, 1959).

9 R. G. Deissler, "Heat Transfer and Fluid Friction for Fully Developed Turbulent Flow of Air and Supercritical Water With Variable Fluid Properties," TRANS. ASME, 76, 73–85 (1954).

10 R. G. Deissler, "Analysis of Turbulent Heat Transfer, Mass Transfer, and Friction in Smooth Tubes at High Prandtl and Schmidt Numbers," NACA TR 1210 (1955).

11 R. P. Bringer and J. M. Smith, "Heat Transfer in the Critical Region," *AIChE Jour.* 3, 49 (1957).

12 W. B. Powell, "Heat Transfer to Fluids in the Region of the Critical Temperature," *Jet Propulsion*, vol. 27, pp. 776–783 (1957).

13 N. L. Dickinson and C. P. Welsh, "Heat Transfer to Supercritical Water," TRANS. ASME 80, 746–752 (1958).

14 W. D. Rannie, "Heat Transfer in Turbulent Stream Flow," PhD thesis, Calif. Inst. of Tech., Pasadena (1951).

15 B. Pinkel, "A Summary of NACA Research on Heat Transfer and Friction for Air Flowing Through Tubes With Large Temperature Difference," TRANS. ASME, 76, 305–317 (1954).

16 R. G. Deissler, "Turbulent Heat Transfer and Friction in Smooth Passages," section in vol. V, "High Speed Aerodynamics and Jet Propulsion," Princeton, 1959, pp. 288–313.

17 W. F. Cope, "The Turbulent Boundary Layer in Compressible Flow," ARC R&M 2840 (1953).

18 M. W. Rubesin, "A Modified Reynolds, Analogy for the Compressible Turbulent Boundary Layer on a Flat Plate," NACA TN 2917 (1953).

19 M. Tucker, "Approximate Calculation of Turbulent-Boundary-Layer Development in Compressible Flows," NACA TN 2337, 1951.

20 Coleman duP. Donaldson, "On Form of Turbulent Skin-friction Law and Its Extension to Compressible Flows," NACA TN 2692 (May, 1952).

21 E. R. Van Driest, "The Turbulent Boundary Layer for Compressible Fluids on a Flat Plate With Heat Transfer," North American Aviation Rept. AL-1006 (Feb. 20, 1950).

22 E. R. Van Driest, "The Turbulent Boundary Layer With Variable Prandtl Number," North American Aviation Aerophysics Department AL-1914, (April 2, 1954).

23 F. Frankl and V. Voishel, "Turbulent Friction in the Boundary Layer of a Flat Plate in a Two-dimensional Compressible Flow at High Speeds," NACA TM 1053 (1943).

24 E. R. G. Eckert, "Survey on Heat Transfer at High Speeds," WADC Tech. Rept. 54-70 (April, 1954).

25 O. Trass, "Sublimation Mass Transfer Through Compressible Boundary Layers on a Flat Plate," DSc Thesis, Mass. Inst. of Tech. (September, 1958).

26 H. Wolf, "The Experimental and Analytical Determination of the Heat-Transfer Characteristics of Air and Carbon Dioxide in the Thermal Entrance Region of a Smooth Tube With Large Temperature Differences Between the Gas and the Tube Wall," PhD thesis, Purdue University (March, 1958).

27 K. Goldman, "Heat Transfer to Supercritical Water and Other Fluids With Temperature-Dependent Properties," "Nuclear Engineering—Part I," "Chemical Engineering Progress Symposium Series," 50(11), Amer. Inst. of Chem. Engineers.

Predictions of Thermal Properties

By D. R. Bartz, Mem. ASME[11]

The range of pressures over which thermal properties of gases are required for rocket-motor calculations extends from 2000-psi chamber pressures of some solid-propellant rockets down to a small fraction of a pound per square inch at the nozzle exit of low-chamber-pressure rocket motors. The range of temperatures of interest extends from about 8500 R in the combustion chamber of an F_2-H_2 engine, at which temperature substantial dissociation is anticipated, down to about 1000 R, which is typical of cooled motor walls and of conditions in the free stream at the exit of highly expanded nozzles. The species of most importance to rocket-motor-combustion gas flows are N_2, CO_2, H_2O, HF CO, HCl, H_2, O_2, F_2, N, O, H, F, and OH in about that order. In addition, the presence of some light-metal oxides and certain boron compounds may become important as a consequence of new high-energy propellants under consideration.

Despite the broad range of pressures, temperatures, and species for which thermal properties are required in analyzing rocket-motor heat-transfer problems the required thermodynamic properties are generally adequately supplied from standard works such as [1][12] and compilations in more convenient form such as [2] and [3]. Partial voids do exist in the area of the light-metal oxides and some of the boron compounds at high temperatures. These voids will probably be filled in the next few years as a result of active research in these areas. Even though the maximum temperatures are high, they are still sufficiently low in chemical rockets so that there is little likelihood of any important consequences of ionization or the excitation of any of the still higher energy modes. Furthermore, the deviations from the perfect-gas law (that is, compressibility) are generally so low that treating the gases as perfect in this sense leads to negligible error. Thus the only thermal properties that may require special consideration for the problems of rocket-motor heat transfer are the transport properties which will be the principal subject of the remainder of this section.

Properties Required

Because of the high mass-flow rates per unit area, high free-stream turbulence levels, short flow lengths compared with flow diameters, and strong axial-pressure gradients characteristic of rocket-motor-combustion gas flow, the predictions of convective-heat-transfer coefficients usually involve analysis of the turbulent-boundary-layer flow. Whether the analyses have been based on empirical correlations such as the Blasius fricton equation coupled to modified Reynolds analogies [4, 5, 6], or have been based on the eddy-diffusivity and mixing-length concepts coupled with the Prandtl boundary-layer equations [7, 8], the same transport properties, μ and Pr, are involved. Although these transport properties appear in the two different types of analyses in different form, their influence is essentially the same in both types (i.e., exponential)—μ to about the 1/4 or 1/5 power, and Pr to about the 0.6 or 0.7 power. In the strict sense, of course, Pr is not a transport property, but a ratio of two transport properties, μ and k, multiplied by the thermodynamic property C_p. However, because of the simple relationships for Pr derivable from the statistical mechanical theory [9] and its first-order temperature

[11] Jet Propulsion Laboratory, Pasadena, Calif.

[12] Numbers in brackets designate References at end of this part.

independence, it is convenient to treat Pr as a transport property. In addition, the thermodynamic quantity C_p is usually involved to about the first power, but is generally known quite precisely from thermochemical calculations. Based on an arbitrary assumption that the maximum acceptable uncertainty in the heat-transfer coefficient due to uncertainties in the transport properties was about 10 per cent, it was shown in [10] that the viscosity should be known to within about 25 per cent and the Prandtl number within about 8 per cent.

Sources and Methods

Undoubtedly, the most complete compilation of experimental transport-property data for gases is contained in the NBS-NACA Tables [11]. In addition, correlation equations generally based on the statistical-mechanics theory are fitted to what are considered to be the "most probable" values. Individual papers on significant advances since the publication of [11] are contained in [12] and [13].

Studying the "departure" plots of [11] (i.e., percentage departure of experimental data from values calculated from the correlation equations), two things become apparent. First, the experimental data barely extend into the temperature range of interest for most species of interest. Highest temperature-viscosity data extend to only about 2500 R and highest temperature thermal-conductivity and Prandtl-number data extend to only about 1500 R. Second, for most gases the experimental transport properties are already showing systematic departures from the calculated values over even this limited temperature range. The calculated values for most nonpolar gases have been determined from statistical-mechanical methods [9, 14, 15] based on the two force constants r_0 and ϵ/k, determined from room-temperature experimental values. While the predicted temperature dependence of the transport properties for nonpolar gases appears to be on solid theoretical ground as a result of the statistical-mechanical approach, unfortunately there is insufficient experimental data to anchor the values at the high-temperature end which is of the most interest. From a theoretical standpoint the high-temperature region is most easily handled, since the required collision integrals begin to take on asymptotic values and therefore become more easily determined. With such a lack of high-temperature experimental data it is not clear whether the trends in the departure plots indicate that the theory is inadequate or whether there is a systematic error in the experimental measurements at the higher temperatures. If the former is the case, and the trends established over the limited temperature range are extrapolated linearly out to 8500 R, the departures and hence perhaps the uncertainties in the viscosity values approach the 25 per cent suggested as a tolerable uncertainty for rocket-motor heat-transfer calculations [10, Fig. 2]. Nevertheless, for the want of anything more certain, the statistical-mechanical methods have been used to extend calculation of the transport properties of air and its constituents out to temperatures in excess of 15,000 R [16, 17, 18]. Until some means of obtaining high-temperature experimental data is developed, it appears that the only course open is to use such extrapolation techniques as the statistical-mechanics theory affords, or the even more empirical equations such as are necessary for polar gases [11, Tables 1-B and 1-C], with the realization that there may be sizable errors in the values so determined. The high-temperature experimental viscosity data for water, which is the most strongly polar molecule of those normally present in rocket exhausts, are not correlated by the statistical-mechanics theory but rather by an empirical modification of the Sutherland formula developed by Bonilla [19]. Although CO, HF, and HCl are slightly polar, their deviations from nonpolar behavior are only minor so that their viscosity data have been correlated reasonably well by statistical-mechanical methods. Of the undissociated species listed earlier, the least amount of high-temperature viscosity data exists for HF, HCl, and F_2, which is understandable because of their high reactivity. Nevertheless, values of the force constants have been suggested in [14] from which at least approximate values can be calculated. There are no experimental data on which to establish statistical-mechanical correlation equations for the dissociated species N, O, H, F, and OH. Furthermore, calculations made on the rigid-sphere model for such species by Baulknight [16] suggest that use of such a model may lead to substantial error at high temperature. Fortunately, however, it is believed that due to rapid recombination reactions these species may not be present in important proportions near highly cooled walls [10, 20, 21, 22]. It is also fortunate that the effect of pressure on viscosity is apparently negligible over the range of pressures and species of interest [11].

In view of the potential for significant uncertainties in the viscosity values, it would appear justifiable in most calculations to use the very simple expression for Prandtl number derivable in terms only of the ratio of specific heats, by use of the Euken approximation [10].

$$\mathrm{Pr} = \frac{\gamma}{1.94\gamma - 0.74}$$

A further refined treatment given in [17] predicts variations in Prandtl number due to dissociation which are not predicted by this simple equation. The influence on the value for air was as high as 25 per cent under conditions of maximum influence of the dissociation of nitrogen.

The computation of transport properties of mixtures seems to be possible by any of three general methods. One method, based on rigorous kinetic theory [14], requires knowledge of the molecular-collision characteristics of each of the species with each of the other species, and then requires the solution of a determinant of one order larger than the number of species. Another method, Buddenberg and Wilke [23], based on the Sutherland-type correlation equation, eliminates the determinant but still retains the need for nonlike molecular-diffusion coefficients. A further development along the lines of the latter method [24] eliminates the need for even the various nonlike molecular-diffusion coefficients and becomes quite simple. It appears that the real need to be filled at this time is to measure transport properties of mixtures at high temperature in order that the accuracy of the values computed from each of these methods can be compared against the varying effort required. Furthermore, it is necessary to determine the importance of trace concentrations (less than 10 per cent) of species to resulting values of the transport properties of mixtures. If it develops that in order to obtain values consistent with the accuracy requirements discussed it is necessary to both consider the trace constituents, and to make use of the rigorous kinetic-theory method, such computations should be programmed at a central high-speed, computing facility.

For approximate calculations, use can be made of the fact that the high-temperature viscosity values of most monatomic, diatomic, and some triatomic molecules are within a few per cent of each other and of the values for the air mixture. To show the relatively small deviations that exist as far as turbulent-boundary-layer heat-transfer calculations are concerned, values of the fifth root of the viscosity have been plotted versus temperature for a number of species in Fig. 2. Note that the only species having values more than 5 per cent different from those of air are water and H_2. Thus it is possible to determine a mixture value within about 10 per cent, merely by computing (or even estimating by eye) a mole fraction-weighted value for the major species involved in the mixture of interest, using Fig. 2. In this connection, it is interesting to compare the viscosity value computed by Gin [25]

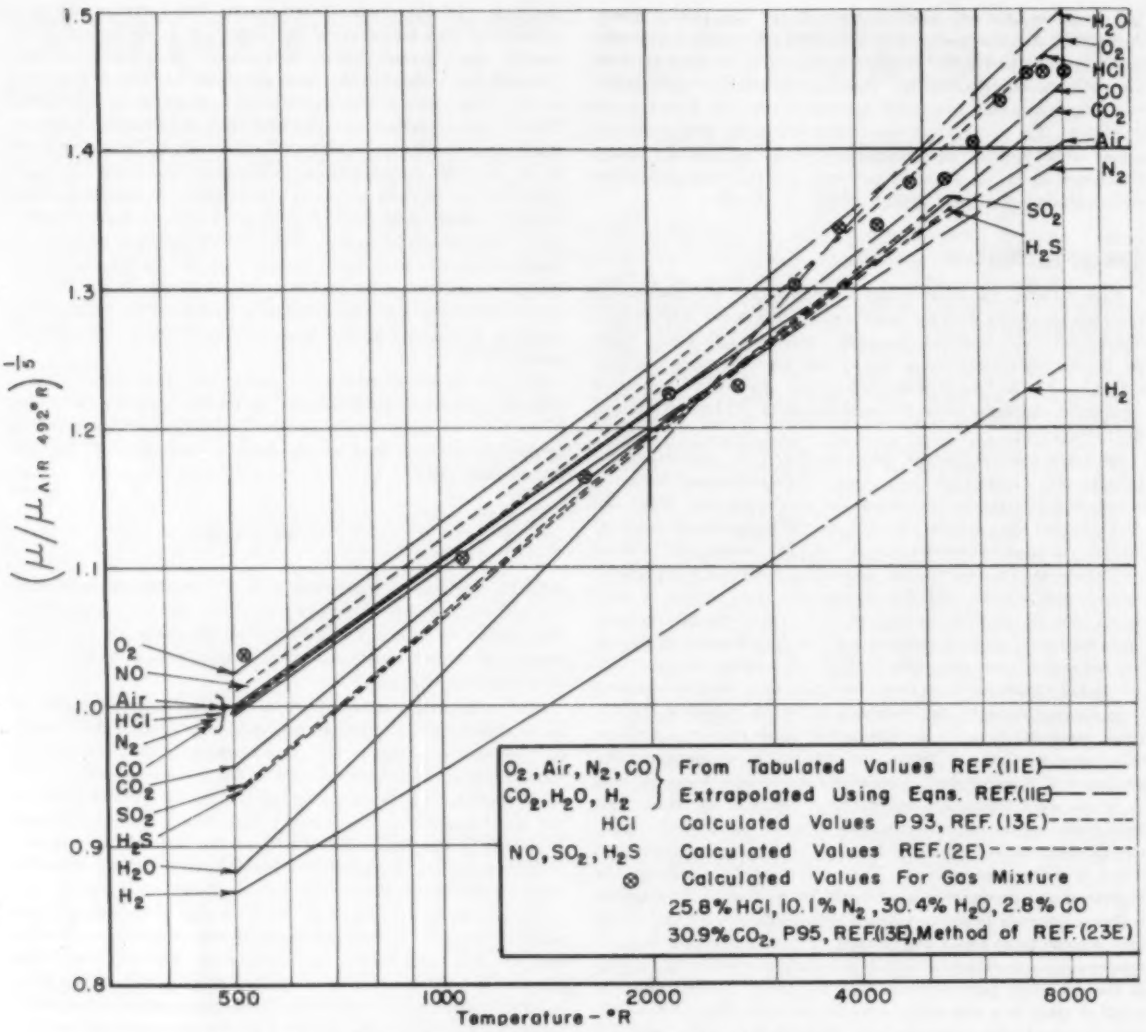

Fig. 2 Fifth root of viscosity versus temperature for various rocket exhaust gas constituents

for a particular multicomponent rocket-combustion-gas mixture using the exact methods of [14] with the value for air at the same temperature. The difference was only 1 per cent.

Influence of Chemical Reaction

The calculation of heat transfer in a boundary-layer flow is usually accomplished with the use of the equation

$$q = k\left(\frac{dT}{dy}\right)_w = \left[k\frac{d}{dy}\left(\frac{T - T_w}{T_e - T_w}\right)\right]_w (T_e - T_w) \quad (1)$$

where q is heat flux; k is thermal conductivity; T is temperature; w is wall; and e is edge of boundary layer. The magnitude of the gradient is established by a combination of the temperature difference between free stream and wall and the nondimensional temperature gradient which is determined by solution of the equations of motion of the flow in the layer nearest the wall. For a laminar boundary layer the equations assume the form

$$\frac{\partial}{\partial x}(\rho u) + \frac{\partial}{\partial y}(\rho v) = 0 \quad (2)$$

$$\rho\left(u\frac{\partial u}{\partial x} + v\frac{\partial u}{\partial y}\right) = -\frac{\partial p}{\partial x} + \frac{\partial}{\partial y}\left(\mu\frac{\partial u}{\partial y}\right) \quad (3)$$

$$\rho\left(u\frac{\partial h}{\partial x} + v\frac{\partial h}{\partial y}\right) = u\frac{\partial p}{\partial x} + \frac{\partial}{\partial y}\frac{\bar{\mu}}{\overline{\Pr}}\frac{\partial h}{\partial y} + \phi + \frac{\partial}{\partial y}\frac{\bar{\mu}}{\overline{\Pr}}\sum_i (\mathrm{Le}_i - 1)\frac{\partial C_i}{\partial y}h_i \quad (4)$$

$$\rho u\frac{\partial C_i}{\partial x} + \rho v\frac{\partial C_i}{\partial y} = W_i + \frac{\partial}{\partial y}\left(\rho D_{i2}\frac{\partial C_i}{\partial y}\right) \quad (5)$$

where ρ is density; u and v are velocity components; p is pressure; μ is viscosity; h is static enthalpy; $\overline{\Pr}$ is mixture Prandtl number; ϕ, dissipation; Le_i is Lewis number of i^{th} specie; C_i is concentration by weight of i^{th} specie; W_i is net rate of production of i^{th} species; and D_{i2} is coefficient of diffusion of specie 1 into 2. In laminar flows, the gradient can be predicted from straightforward theoretical considerations. In the case of chemically reacting systems, Butler and Brokaw [22] have suggested the use of an effective thermal conductivity consisting of two parts—that

due to molecular collisions and that due to chemical reaction. They have successfully predicted values of this combined thermal conductivity, using statistical mechanics techniques [14], which are in excellent agreement with measurements with the $N_2O_4 \rightarrow NO_2$ reaction at one atomsphere and the $6HF \rightarrow (HF)_6$ reaction at pressures from $^1/_{22}$ to 1 atm. In general, in order to evaluate the nondimensional temperature-gradient factor, it is necessary to solve both the momentum and energy equations as well as the chemical-diffusion equations. In doing so, the influence of the chemical reaction on the viscosity, Prandtl-number, density, thermal-conductivity, specific-heat, and diffusion coefficients as used in the continuity, momentum, energy, and diffusion equations must, in principal, be evaluated.

Lees [21], however, has recognized the simplifications possible due to the fact that the form of the energy equation for a reacting laminar-boundary-layer flow is the same as that for a nonreacting flow when the Lewis number is unity. Under these circumstances the surface-heat-transfer rate is independent of the mechanism of heat transfer (molecular conduction or molecular diffusion) at all free-stream velocities. Further, Lees showed that the heat-transfer rate is the same as it would be for the special case in which the recombination reaction rates are very fast with respect to diffusion rates. Under this condition, local equilibrium concentration of each specie is established in unique relationship to local pressure and temperature distributions across the boundary layer, and the diffusion equation, equation (5), becomes superfluous.

In considering reactive flows under these "restrictive" conditions, it should be possible to make extensive use of existing solutions and empirical correlations for nonreactive flow, since the equations in the appropriate form (for Le = 1) contain only the thermal properties viscosity and Prandtl number which are to a first order essentially independent of dissociation or recombination [17]. While these results apply strictly only to laminar-boundary-layer flows with Lewis-number unity, it should be mentioned with regard to application to turbulent boundary-layer flow of the type in rocket motors that: (*a*) Principles relative to the effects of property variations across boundary layers established by laminar boundary-layer theory (e.g., Young and Janssen [26]) have been found to be substantiated by empirical correlations of turbulent-boundary-layer heat transfer [27]; (*b*) there is no real knowledge of the proper values of the thermal properties which constitute the Lewis number for turbulent boundary layers—the effective physical value could be near unity even though there is some experimental basis [28] for suggesting that it might be as high as 1.4; and (*c*) the rates of recombination in rocket-motor boundary layers are generally believed to be so high that it is likely that equilibrium is maintained [20]. Thus it may well be possible to make use of correlations of nonreactive turbulent-boundary-layer heat transfer for calculations in rocket motors, with perhaps only a minor correction for Lewis-number deviations from unity which may be established later by experiment.

In treating nonreacting turbulent-boundary-layer heat-transfer problems, it is found useful to lump the factors in the bracket in equation (1) and call it the heat-transfer coefficient, which can usually be correlated in terms of the dimensionless parameters Nusselt number, Reynolds number, and Prandtl number. The second factor, the temperature difference, is the driving potential for the heat-transfer process. Note that the general form of the energy equation, equation (4), is written in terms of enthalpy gradients, and that it is only possible to write it in terms of temperature gradients in the special case of constant-property flow when the specific heat can be factored out as a constant. In the case of a reacting boundary layer, it is not possible to factor out the specific heat so it is found to be convenient to make use of the enthalpy gradient at the wall, resulting from solution of the energy equation; e.g.,

$$q = \frac{k}{\bar{C}_p}\left(\frac{\partial h}{\partial y}\right)_w = \left[\frac{k}{\bar{C}_p}\frac{d}{dy}\frac{(h - h_w)}{(h_s - h_w)}\right](h_s - h_w) \quad (6)$$

where $\bar{C}_p$ is mixture specific heat at constant pressure. But by definition for the nonreacting boundary layer,

$$\left[\frac{k}{\bar{C}_p}\frac{d}{dy}\frac{(h - h_w)}{(h_s - h_w)}\right] = C_h(\rho u)_s \quad (7)$$

where C_h is the Stanton number as defined for nonreactive flow. Thus if, as suggested above, it is possible to make use of results of solutions of the equations-of-motion and empirical correlations for nonreactive flows in treating heat transfer in reactive flows, then the appropriate form of the equation turns out to be

$$q_{\text{reactive flow}} = C_{h\ \text{nonreactive}}(\rho u)_s(h_s - h_w)_{\text{reactive flow}} \quad (8)$$

(See further discussion on the basis for this equation in [21, 29, and 30].) The value of C_h determined from the nonreactive-flow correlation of the form

$$\text{Nu} = a\ \text{Re}^b\ \text{Pr}^c \quad (9)$$

turns out to be

$$C_h = a\{d(\rho u)_s\}^{b-1}\left[\frac{u^{b-1}}{\text{Pr}^{1-c}}\right] \quad (10)$$

where Nu is Nusselt number; Re is Reynolds number; a, b, c are constants; and d is the linear dimension appropriate to the particular problem (e.g., [31]). Note that the value of C_h does not depend on thermal properties strongly affected by energy release in the boundary layer due to reaction and can be treated by usual methods for variation of properties across the boundary layer.

The approach suggested by equation (8) has been found to correlate hypersonic flow with dissociation and recombination [28] and low-speed turbulent pipe flow with chemical reaction [32, 33]. Whether or not it will be successful for reactive turbulent boundary layers in rocket motors is yet to be determined by experimental measurements of heat-flux distribution in rockets burning very-high-energy propellants. It appears at present to represent at least an upper limit to reactive-flow heat fluxes with perhaps one exception, that being wall-surface-catalyzed recombination, which may or may not be important to rocket-motor heat transfer [20].

References

1 F. D. Rossini, D. D. Wagman, W. H. Evans, S. Levine, and I. Jaffe, "Selected Values of Chemical Thermodynamic Properties," Natl. Bur. Standards Circ. 500, U.S. Government Printing Office (1952).

2 "Liquid Propellants Handbook, vol. 2," prepared by Division of Chemical Engineering, Battelle Memorial Institute with Department of the Navy Bureau of Aeronautics (p. 731), Washington, D. C. (September, 1957) (Confidential).

3 J. S. Martinez, G. W. Elverum, Jr., "A Method of Calculating the Performance of Liquid-Propellant Systems Containing the Species C, H, O, N, F, and One Other Halogen—With Tables of Required Thermochemical Properties to 6000 K," Memorandum No. 20-121, Jet Propulsion Laboratory, Pasadena (December 6, 1955).

4 Jerome Persh, "An Analytical Investigation of Turbulent-Boundary-Layer Heat-Transfer Coefficients for Supersonic and Hypersonic Flow," NAVORD Report 4099, U. S. Naval Ordnance Laboratory, White Oak, Md. (October 31, 1955).

5 Merwin Sibulkin, "Heat Transfer to An Incompressible Turbulent Boundary Layer and Estimation of Heat-Transfer Coefficients at Supersonic Nozzle Throats," *Journal of the Aeronautical Sciences*, 23(2), 162–172 (February, 1956).

6 D. R. Bartz, "An Approximate Solution of Compressible Turbulent-Boundary Layer Development and Convective Heat Transfer in Convergent-Divergent Nozzles," TRANS. ASME, 77(8), 1235–1245 (November, 1955).

7 R. G. Deissler, "Heat Transfer and Fluid Friction for Fully Developed Turbulent Flow of Air and Supercritical Water With Variable Fluid Properties," TRANS. ASME, 76, 73–85 (1954).

8 E. R. Van Driest, "Turbulent Boundary Layer in Compressible Fluids," *Journal of the Aeronautical Sciences*, 18(3), 145–160 (March, 1951).

9 S. Chapman and T. G. Cowling, "The Mathematical Theory of Non-Uniform Gases," Cambridge University Press (1939, 1952).

10 D. R. Bartz, "The Role of Transport Properties in the Problems of Jet Engines and Rockets, Transport Properties in Gases," Proceedings of the Second Biennal Gas Dynamics Symposium, Northwestern University Press, Evanston, Ill., 1958, pp. 105–118.

11 Joseph Hilsenrath, Charles W. Beckett, William S. Benedict, Lilla Fano, Harold J. Hoge, Joseph F. Masi, Ralph L. Nuttall, Yeram S. Touloukian, and H. W. Woolley, "Tables of Thermal Properties of Gases," U. S. Department of Commerce, National Bureau of Standards, Circular 564 (November 1, 1955).

12 Ali Bulent Cambel and John B. Fenn, editors, "Transport Properties in Gases," Proceedings of the Second Biennial Gas Dynamics Symposium, Northwestern University Press, Evanston, Ill., 1958.

13 "Thermodynamic and Transport Properties of Gases, Liquids and Solids," papers presented at the Symposium on Thermal Properties, Purdue University, Lafayette, Ind., sponsored by Standing Committee on Thermophysical Properties Heat Transfer Division, The American Society of Mechanical Engineers, McGraw-Hill Book Company, Inc., New York, N. Y., 1959.

14 J. O. Hirschfelder, C. F. Curtiss, and R. B. Bird, "The Molecular Theory of Gases and Liquids," John Wiley & Sons, New York, N. Y., 1954.

15 J. O. Hirschfelder, C. F. Curtiss, R. B. Bird, and E. L. Spotz, "The Transport Properties of Gases and Gaseous Mixtures, High Speed Aerodynamics and Jet Propulsion," vol. I, "Thermodynamics and Physics of Matter," Princeton University Press, Princeton, N. J., 1955.

16 C. W. Baulknight, "The Calculation of Transport Properties at Elevated Temperatures, Transport Properties in Gases," Proceedings of the Second Biennial Gas Dynamics Symposium, Northwestern Universty Press, Evanston, Ill., 1958, pp. 89–95.

17 C. F. Hansen, "Approximations for the Thermodynamic and Transport Properties of High-Temperature Air," NACA Technical Note 4150, National Advisory Committee for Aeronautics, Washington, D. C. (March, 1958).

18 E. Bauer and M. Zlotnick, "Transport Coefficients of Air to 8000 K," an AVCO Report, Wilmington, Mass. (September, 1958).

19 C. F. Bonilla, R. D. Brooks, and P. L. Walker, "The Viscosity of Steam and Nitrogen at Atmospheric Pressure and High Temperature," Proceedings of the General Discussion on Heat Transfer, The Institution of Mechanical Engineers (London), 1951, pp. 167–173.

20 D. Altman and H. Wise, "Effect of Chemical Reactions in the Boundary Layer on Convective Heat Transfer," *Jet Propulsion*, 26(4), 256–259 (April, 1956).

21 Lester Lees, "Laminar Heat Transfer Over Blunt-Nosed Bodies at Hypersonic Flight Speeds," *Ibid.*, pp. 259–269 (April, 1956).

22 James N. Butler and Richard S. Brokaw, "Thermal Conductivity of Gas Mixtures in Chemical Equilibrium," *The Journal of Chemical Physics*, 26(6), 1636–1643 (June, 1957).

23 J. W. Buddenberg and C. R. Wilke, "Calculation of Gas-Mixture Viscosities," *Industrial and Engineering Chemistry*, 41, 1345–1347 (1949).

24 C. Wilke, "A Viscosity Equation for Gas Mixtures," *Journal of Chemistry and Physics*, 18, 517–519 (1950).

25 W. Gin, "Calculated Viscosity of a Solid-Propellant Rocket Exhaust-Gas Mixture," *Jet Propulsion*, 26(2), 127–128 (February, 1958).

26 G. B. W. Young and Earl Janssen, "The Compressible Boundary Layer," *Journal of the Aeronautical Sciences*, 19(4), 229–236, 288 (1952).

27 Ernst R. G. Eckert, "Survey on Heat Transfer at High Speeds," WADC Technical Report 54-70 and ASTIA Document No. 38093, University of Minnesota (April, 1954).

28 P. H. Rose, R. F. Proestein, and M. C. Adams, "Turbulent Heat Transfer Through a Highly Cooled, Partially Disassociated Boundary Layer," *Journal of the Aero/Space Sciences*, 25(12), 751–760 (December, 1958).

29 R. Bromberg and R. P. Lipkis, "Heat Transfer in Boundary Layers With Chemical Reactions Due to Mass Addition," *Jet Propulsion*, 26, 669–674 (October, 1958).

30 D. E. Rosner, "Recent Advances in Convective Heat Transfer with Dissociation and Atom Recombination," *Jet Propulsion*, 27(1), 49–51 (January, 1957).

31 D. R. Bartz, "A Simple Equation for Rapid Estimation of Rocket-Nozzle Convective-Heat Transfer Coefficients," *Ibid.* (January, 1957).

32 J. L. Beal and R. L. Lyerly, "The Influence of Gas Dissociation on Heat Transfer," WADC Technical Report 56-494 and ASTIA Document No. AD 118074, Cornell Aero Lab. Report (September, 1956).

33 W. F. Krieve, "Heat Transfer in Reacting Systems: Heat Transfer to N_2O_4 Gas Under Turbulent-Pipe-Flow Conditions," Progress Report 20-366, Jet Propulsion Laboratory, Pasadena, Calif. (November 3, 1958).

Flow Separation and Acoustic Effects

By H. N. McManus, Jr.,[13] and Erich E. Soehngen[14]

Effect of Separation on Heat Transfer

The work on systems undergoing separated flow due to pressure gradients divides into two groups—that on cylinders or spheres in crossflow and that on packed beds. The latter, because of their geometry and consequent difficulty of supplying heat, are normally studied by transient methods, and for them only over-all values of the convection coefficient are available. The former have been studied fairly extensively and local transfer values indicate the effect of separation.

The low Reynolds-number range ($20 < Re < 500$) for cylinders in crossflow has been studied by Eckert and Soehngen [3].[15] These investigators determined both over-all and local heat-transfer coefficients. The range of Reynolds numbers greater than 1000 has been studied by Comings, Clapp, and Taylor [2]; Giedt [4, 5]; Schmidt and Wenner [7]; and Zapp [8]. These investigators found a severe dependence of the heat transfer in the separated region upon the Reynolds number. The local Nusselt number exhibited in all cases a minimum value at the point of separation and an increasing value in the separated region. In many cases the local Nusselt value exceeds the value at the forward stagnation point. At very high Reynolds numbers the curves exhibit two minima [7, 8]—the first attributed to boundary-layer transition, the second to separation.

The local-heat-transfer coefficient has been studied on spheres by Carey [1]. It was found that a minimum value existed at the separation point, and in the separated zone the transfer value rose sharply at first and then at decreasing rate. The values attained in the separated region again equaled or exceeded those at the forward stagnation point.

The effect of turbulence of the approach stream has been found to affect heat transfer on cylinders both in the unseparated and separated regions [6, 8]. In general, the unseparated coefficient is increased with increasing turbulence level, while the values in the separated region are relatively unaffected and with extreme turbulence actually depressed because of delayed separation.

The work which exists for heat transfer in separated flow is confined almost exclusively to cylinders or spheres in crossflow. This restricts severely the geometries which can be analyzed even approximately. No work appears to have been published on flat plates undergoing separation, or heat transfer on areas of separation caused by abrupt enlargements or contractions.

Acoustics and Vibrational Effects on Heat Transfer

The phenomenon of streaming induced by sound fields has been studied since the late nineteenth century as a fluid-flow phenomenon in isothermal systems. The first work involving vibrational effect upon heat transfer was published by Martinelli and Boelter [16] in 1938. These investigators found that at low-vibrational Reynolds numbers no effect upon heat transfer was

[13] Cornell University, Ithaca, N. Y. Assoc. Mem. ASME.

[14] Aeronautical Research Laboratory, WADC, Dayton, Ohio.

[15] Numbers in brackets designate References at end of this part.

evidenced; at high vibration intensities, the heat-transfer coefficient showed increases of up to 400 per cent. Boelter later reported that the results of this work could not be reproduced.

Kubanskii [11, 12] has performed extensive investigations upon the influence of a steady-sound field upon the free convection from a heated horizontal cylinder in the air. Shadowgraph techniques indicated that circulation cells near the hot surface were produced with outward flow at the nodes and inward flow at the antinodes. The sound field was found to increase free-convection heat transfer by 75 per cent. In later works [13], this investigator studied a standing sound field's effect on cylinders with horizontal crossflow. Heat-transfer rates increased up to 50 per cent, but only when the average vibrational velocity was equal to or greater than crossflow velocity.

Lemlich [14] studied the effect of vibrations upon free-convection heat transfer from horizontal heated wires to air. The frequency range was low. Heat transfer increased with increases of frequency and/or amplitude. Anantanarayanan and Ramachandran [9] observed increases of up to 130 per cent from a heated wire in forced parallel flow. Their results showed that the ratio of mean vibrational velocity to air velocity was a controlling factor.

Tsui [19] has demonstrated that the general equations relating vibrations and heat transfer are presently not solvable. This investigator studied vibrational effects upon a vertical heated plate. Shine [18] showed heat-transfer increases of up to 50 per cent when a vertical plate was vibrated normal to itself. A critical vibration intensity was shown to exist. Harrison, et al. [10], studied the effect of a sound field upon transfer in a vertical tube undergoing free and forced convection.

Lighthill [15] and Nickerson [17] have analytically studied the effect of fluctuations upon the heat transfer from systems with laminar boundary layers. Generally, studies of heat-transfer phenomena in pulsating-flow systems have shown increased rates of heat transfer, but data have also been reported which show no effect or even a decrease of the rate of heat transfer. This apparent conflict is due to the fact that the reported data were obtained at different frequencies, amplitudes, wave forms, Reynolds and Prandtl numbers, and so forth, and no theory was available for a rational interpretation of these experimental findings. However, as it is shown in [26] part of these apparent discrepancies may be explained by theoretical considerations. Richardson [20] showed that in the laminar region of a pulsating flow the velocity profile at the wall has a steeper gradient than in a similar steady flow. Therefore if similarity considerations would be valid, increased heat transfer may be expected. Linke [22] measured such an increase by a factor of 4 for laminar flow of oil in tubes. In the turbulent regime an increase of only 35 per cent was obtained. However, for turbulent flow of water West and Taylor [21] reported increased heat transfer by about 70 per cent. Havemann and Narayan Rao [23] investigated the heat transfer from a heated tube to pulsating air at Reynolds numbers between 5000 and 35,000 and frequencies between 5 and 33 cycles per second. It was found that in general for turbulent flow the heat transfer may increase by about 30 per cent, depending on frequency, amplitude, Reynolds number, and wave form. As a specifically interesting result it was found that below a certain "critical frequency" the heat transfer showed no effect or decreased below the value of the equivalent steady-state flow. Above the critical frequency which depends on wave form and Reynolds number the heat transfer increases steadily but in a "wavy" fashion as is shown in [24]. For the investigated conditions (1-in. pipe diameter, airflow chopped by internal-combustion-engine valve system) this critical frequency was about 18 cps at Re = 15,000 and 28 cps at Re = 20,000. Finally, Romie [25] showed a theoretical and experimental study with pulsating air in a tube of almost 1-in. diameter at frequencies between 3 and 133 cps that for laminar flow at least some of the apparent discrepancies of the various reported data may be analytically explained. On the basis of the laminar-flow theory also the experimentally measured general behavior of the turbulent pulsating flow which was in good agreement with the data reported in [24] could be explained. In essence, the following results were obtained: (*a*) The phase difference between temperature of the surface and the temperature gradient of the fluid exerts a large influence on the heat transfer; time-invariant wall temperatures show the largest effect, in phase-fluctuating wall temperatures, i.e., constant-heat-flux conditions, considerably less; (*b*) velocity pulsations, as such, in laminar flow decrease the heat-transfer coefficient below the steady-state value; in turbulent flow increasing heat transfer may be obtained by a pulsation-affected increase in turbulence; (*c*) the amplitude of the fluctuation exerts a major influence on the heat transfer only if the ratio of the pulsative velocity increment to the mean velocity is larger than unity, i.e., if the local velocity at the wall reverses direction during the pulsation cycle. The difference of the reciprocal heat-transfer coefficients was found to be proportional to the square of the mentioned velocity ratio. A similar result was experimentally found by [22]. This effect increases with increasing frequency. Although Ref. [25] improved the state of the art by a considerable step, more systematic analytical and experimental work is needed to find the general solution for predicting the heat-transfer effects in fluctuating-flow systems. A similar condition exists with respect to the effects of sound waves on the heat transfer. Sufficient experimental evidence has been presented by recent investigations that sound waves affect the boundary layers on heat-exchanging surfaces, resulting in increased rates of heat transfer. Since the convective heat transfer is primarily determined by the local mass flow along the heat-exchanging surface the effects of sound phenomena on the heat transfer may very likely be traced to the effects due to interactions of the sound field with the local flow field on the heat-exchanging surface. For about 70 years considerable effort has been spent on analyzing and measuring the interaction phenomena of sound waves with solid bodies. Fand and Kaye [28] present a very complete survey of the past and current efforts determining such interaction phenomena on bodies of simple geometry, mainly spheres or cylinders. Raney [26] and others have analyzed and experimentally measured such sound-induced flow fields, called "acoustical streaming" in the vicinity of cylinders. It was shown that a rather complex vortex system is generated whose profile depends on sound frequency, wave lengths, body dimension, viscosity, and so forth. Unfortunately, no analysis has been reported yet describing the mechanism of the interaction of the acoustical streaming field with the flow field in the boundary layer along the body. All experimental data reported so far deal with the gross effects on the heat transfer. Holman and Mott-Smith [27] investigated the over-all free-convection heat transfer from horizontal cylinders in constant-pressure sound fields. Increase of the heat transfer by more than 100 per cent over the no-sound value was observed at sound-pressure levels up to 150 db within the frequency range from 2780 to 4710 cps. Little effect was observed below a "critical sound-pressure level" of 134 db. The influence of the frequency on the heat transfer diminished at the higher sound-pressure levels, and it was only slight at the lower levels. Fand and Kaye [28] studied systematically the free convection on horizontal cylinders in standing sound waves in the frequency range of 1100 to 6120 cps at sound intensities of up to 151 db. They also found a "critical sound-pressure level" between 136 and 140 db beyond which the heat-transfer rate considerably increased, up to three times that of the no-sound value under otherwise equal thermal conditions. A flow-visualization study by means of smoke streams revealed the generation of large vortices near the rear stagnation point of the cylinder, which may be explained as a flow-separation effect. The authors could represent their findings by the empirical correlation

$h = 0.722[(t_w - t_0)(y \cdot f)_{av}^2]^{1/3}$ for cylinder of $^3/_4$ in. diameter

where

h = heat-transfer coefficient (Btu/hr, ft², deg F)
t_w = temperature of the cylinder surface
t_0 = temperature of the air
y = harmonic displacement amplitude, ft
f = sound frequency, cps

Tests were also conducted in traveling waves which showed at the lower frequency regime about the same increase as the standing-wave experiments, but somewhat less increase at the higher frequencies. In order to gain more insight into the mechanism involved, Sprott and Holman [29] repeated their earlier tests [27] in traveling sound waves over the frequency range from approximately 1000 to 5000 cps at similar sound intensities as before. At the lower frequencies increases of the heat transfer by about 185 per cent were observed. Flow-visualization tests by means of motion-picture shadowgraphs revealed that the sound did not affect the boundary layer in vicinity of the stagnation point but had considerable affect on the formation of the wake. It appears from the shadowgraphs, shown in Fig. 3 from [29] that the sound causes an upstream shift of the separation point with a subsequent random turbulent motion in the very much enlarged separation zone, which may be responsible for the observed increase in the heat transfer rate. (See attached photographs.) Jackson, et al. [30] studied the effects of standing sound waves on the combined free and forced-convection heat transfer in a vertical tube. Increase in heat transfer by about 50 per cent was obtained beyond a critical sound-pressure level of 118 db. This increase was attributed to secondary flow phenomena caused by acoustic streaming from the nodes to the antinodes of the sound waves in the tube. Similar data observed at higher velocities in horizontal

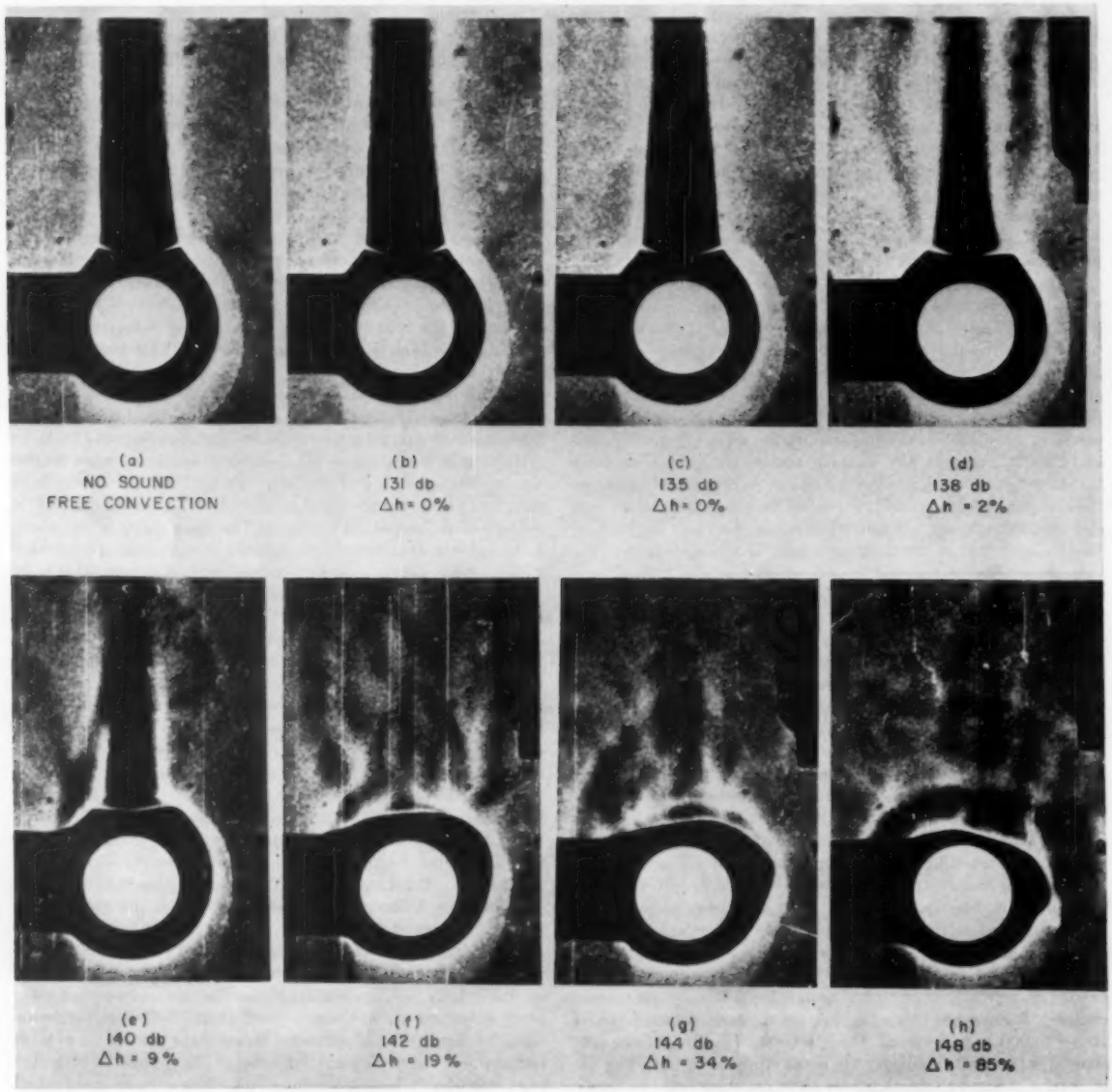

Fig. 3 Effect of sound pressure level on free convection boundary layer at 1660 cycles per second

tubes were reported by Spurlock, Jackson, Purdy [31]. A critical or threshold sound-pressure level of 141 db was found, below which little effect on the heat transfer could be observed. At about 151 db increases of the local-heat-transfer coefficients by 75 per cent were measured in the frequency range from 217 to 500 cps. Although the data could be represented by an empirical correlation, no analysis was reported.

Acknowledgment

The assistance of the Department of Engineering Research, North Carolina State College, in the preparation of the manuscript is gratefully acknowledged.

References

1 J. R. Carey, "The Determination of Local Forced-Convection Coefficients for Spheres," TRANS. ASME, 75, 483 (1953).

2 E. W. Comings, J. T. Clapp, and J. F. Taylor, "Air Turbulence and Transfer Processes—Flow Normal to Cylinders," *Ind. & Eng. Chem.*, 40, 1076 (1948).

3 E. R. G. Eckert and E. Soehngen, "Distribution of Heat-Transfer Coefficients Around Circular Cylinders in Cross Flow at Reynolds Numbers From 20 to 500," TRANS. ASME, 74, 343 (1952).

4 W. H. Giedt, "Investigation of Variation of Point Unit Heat-Transfer Coefficient Around a Cylinder Normal to an Air Stream," TRANS. ASME, 71, 375 (1949).

5 W. H. Giedt, "Effect of Turbulence Level of Incident Air Stream on Local Heat Transfer and Skin Friction on a Cylinder," *J. Aero. Sci.*, 18, 725 (1951).

6 J. Kestin and P. F. Maeder, "Influence of Turbulence on Transfer of Heat From Cylinders," NACA TN 3018 (1957).

7 E. Schmidt and K. Wenner, "Heat Transfer Over the Circumference of a Heated Cylinder in Transverse Flow," NACA TM 1050 (1943).

8 G. M. Zapp, "The Effect of Turbulence on Local Heat Transfer Coefficients Around a Cylinder Normal to an Air Stream," MS thesis, Oregon State College (1950).

9 R. Anantanarayanan and A. Ramachandran, "Effect of Vibration on Heat Transfer From a Wire to Air in Parallel Flow," TRANS. ASME 80, 1426 (1958).

10 W. B. Harrison, W. C. Bolter, T. W. Jackson, A. Lowi, and F. A. Thomas, "Heat Transfer to Vibrating Air Columns," Final Report, Project No. A-183, Engineering Experiment Station, Georgia Inst. of Tech., NACA N-39857 (December, 1955).

11 P. N. Kubanskii, "Currents Around a Heated Solid in a Standing Acoustic Wave," *Trans. USSR Academy Sci.*, 82, 585 (1952).

12 P. N. Kubanskii, "Techeniz u nagretaovo tverdovo tela v stoiachei akusticheskoi volne," *Zhurnal Tekhnicheskoi Fiziki*, 22, 585 (1953). (Available in English translation as: "Flow Near a Heated Solid Body in a Standing Acoustic Wave," LAL, NACA (October, 1955).)

13 P. N. Kubanskii, "Vliiani akusticheskikh kolebanii konechnoi emplitudi na progranichnii sloi," *Zhurnal Tekhnicheskoi Fiziki*, 22, 593 (1952). (Available in English translation as: "Effect of Acoustical Vibrations of Finite Amplitude on the Boundary Layer," LAL, NACA (October, 1955).)

14 R. Lemlich, "Effect of Vibration on Natural Convection Heat Transfer, Symposium on Pulsatory and Vibrational Phenomena," *Industrial and Eng. Chem.*, 47, 1125 (1955).

15 M. J. Lighthill, "The Response of Laminar Skin Friction and Heat Transfer to Fluctuations in the Stream Velocity," *Proc. Roy. Soc. Lond.*, A224, 1 (1954).

16 R. C. Martinelli, and L. M. K. Boelter, "The Effect of Vibration Upon the Free Convection From a Horizontal Tube," Proc. 5th Inter. Congr. Appl. Mech. 578 (1938).

17 R. J. Nickerson, "The Effect of Free-Stream Oscillations on the Laminar Boundary of a Flat Plate," ScD thesis, M.I.T., Department of Mechanical Engineering (1957).

18 A. J. Shine, "The Effect of Transverse Vibrations on the Heat-Transfer Rate From a Heated Vertical Plate," MS thesis, Air Inst. of Tech., Wright-Patterson Air Force Base, Ohio (1957).

19 Y. T. Tsui, "The Effect of Vibration on Heat-Transfer Coefficients," PhD Thesis, Ohio State University (1953).

20 E. G. Richardson, "Dynamics of Real Fluids," London, England, 1950, pp. 39–44.

21 F. B. West and A. T. Taylor, "The Effect of Pulsations on Heat Transfer," *Chem. Eng. Progress*, vol. 48, pp. 39–43 (1952).

22 W. Linke, "Waermeübergang bei pulsierender Strömung," *Zeitschrift d. Vereins Deutscher Ingenieure (VDI)*, vol. 95, p. 1179 (1953).

23 H. A. Havemann and N. N. Narayan Rao, "Waermeübertragung bei pulsierender Strömung," *Forschung Ing. Wes.*, vol. 20, 1954, p. 58.

24 H. A. Havemann and N. N. Narayan Rao, and P. Jaychandra, "Studies for a New Hot Air Engine," *Journal Indian Inst. of Science*, vol. 38, pp. 172–201 (1956).

25 F. E. Romie, "Heat Transfer to Fluids Flowing With Velocity Pulsations in a Pipe," PhD thesis University of Calif., Los Angeles, 1956.

26 W. P. Raney, W. C. Corelli, and P. J. Westerfeld, "Acoustical Streaming in the Vicinity of a Cylinder," *Journal Acoust. Soc. Am.*, vol. 27, pp. 1006-14 (1954).

27 J. P. Holman and T. P. Mott-Smith, "The Effect of High Constant-Pressure Sound Fields on Free-Convection Heat Transfer From a Horizontal Cylinder," WADC TN 58-352 and *Journ. Aero/Space Sci.*, vol. 26, p. 188 (1959).

28 R. M. Fand and J. Kaye, "The Effect of High-Intensity Stationary and Progressive Sound Fields on Free Convection From a Horizontal Cylinder," U. S. Air Force, WADC TN 59-18 (1959).

29 A. L. Sprott, J. P. Holman, and F. L. Durand, "An Experimental Study of the Interaction of Strong Sound Fields With Free-Convection Boundary Layers," U. S. Air Force, WADC TN (to be published) 1959.

30 T. W. Jackson, W. B. Harrison, and W. C. Boteler, "Free Convection, Forced Convection, and Acoustic Vibrations in a Constant-Temperature Vertical Tube," JOURNAL OF HEAT TRANSFER—TRANS. ASME, series C, vol. 81, 1959, p. 68.

31 J. M. Spurlock, T. W. Jackson, K. R. Purdy, "The Effects of Resonant Acoustic Vibrations on Heat Transfer," U. S. Air Force, TN 59-330 (1959).

Unsteady Turbulent Heat Transfer in Tubes

E. M. SPARROW[1]
R. SIEGEL

NASA, Lewis Research Center, Cleveland, Ohio. Assoc. Mem. ASME

An analysis is made of the unsteady turbulent heat transfer in a circular tube whose wall temperature varies arbitrarily with time. The flow is steady and fully developed. The formulation permits the heat-transfer coefficient to vary with time and position in accordance with the energy conservation principle. This is in contrast to previous transient analyses where it has been standard to use steady-state, fully developed coefficients. The first step in the analysis yields the heat-transfer response to a step jump in wall temperature, and this is then generalized by a superposition technique to apply to arbitrary time variations. Use of the generalized results is illustrated by application to the case where the wall temperature varies linearly with time. Comparison is made between the unsteady heat-transfer results of the present theory and those computed using steady-state heat-transfer coefficients.

Introduction

CONSIDERABLE PRACTICAL INTEREST in the unsteady heat-transfer characteristics of flow systems has been stimulated by the needs of modern technology, especially in relation to the use of automatic control equipment. To gain insight into the transient behavior of heat exchange devices, it has been common to study a typical element of the apparatus; namely, a single passage and its bounding walls. The flow in such a passage will almost always be turbulent.

In previous analyses of unsteady turbulent heat transfer, some assumptions have been introduced to make the problem more tractable. First of all, the heat-transfer coefficient used for the unsteady situation has been evaluated from *steady-state* relationships. This assumption sets aside any consideration of the actual transient temperature and energy transfer processes at each point in the cross section. Instead, the thermal state of the fluid is represented by a single bulk temperature at each cross section, and energy conservation is then written on a one-dimensional basis. A second simplifying assumption which is generally invoked in the unsteady analysis is that the heat-transfer coefficient is uniform along the length of the passage. In short passages or in the thermal entrance regions of longer ones, steady-state turbulent heat-transfer theory has shown this assumption to be inadequate.

In the analysis to be reported here, an altogether different approach is taken toward the problem of unsteady turbulent heat transfer in passages. Instead of assuming heat-transfer coefficients which are steady with both time and position, the heat-transfer coefficient will now be permitted to vary as it wishes in accordance with the energy conservation principle.

The system selected for study, as pictured in Fig. 1, is a circular tube whose wall temperature may vary with time. Through the tube there passes a steady, fully developed turbulent flow which is unchanging along the length. At the entrance section

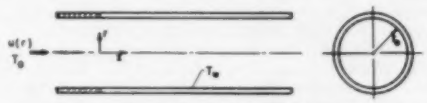

Fig. 1 Physical model and co-ordinates

[1] Dr. Sparrow is now Professor of Mechanical Engineering, University of Minnesota, Minneapolis, Minn.

Contributed by the Heat Transfer Division of THE AMERICAN SOCIETY OF MECHANICAL ENGINEERS and presented at the ASME-AIChE Heat Transfer Conference, Storrs, Conn., August 9–12, 1959.
Manuscript received at ASME Headquarters, May 18, 1959. Paper No. 59—HT-16.

Nomenclature

A = coefficient in linearly varying wall temperature, see equation (33)
a_n = coefficient defined in equation (19)
C_n = coefficients in series expansion of temperature distribution
c_p = specific heat at constant pressure
D_n = coefficients in series expansion of temperature distribution for pure diffusion
d = tube diameter, $2r_0$
F_n = function of x and t in transient solution, see equation (20)
h = local heat-transfer coefficient, $q/(T_w - T_b)$
J_n = quantity defined in equation (30)
k = thermal conductivity
N = index determined from equation (31)
Nu = local Nusselt number, hd/k
Pr = Prandtl number, ν/α
q = local heat-transfer rate per unit area at tube wall
r = radial co-ordinate measured from tube center line; r_0, tube radius
r^+ = dimensionless radial co-ordinate, $r\sqrt{\tau_0/\rho}/\nu$; r_0^+, dimensionless tube radius, $r_0\sqrt{\tau_0/\rho}/\nu$
Re = Reynolds number, $\bar{u}d/\nu$
T = temperature; T_b, bulk fluid temperature; T_0, temperature of fluid entering tube (a constant); T_w, tube wall temperature
t = time; t_{ss}, refers to time required to reach steady state
t^+ = dimensionless time, $t\nu/r_0^2$
u = fluid velocity in the x-direction; $\bar{u}$, mean fluid velocity
u^+ = dimensionless velocity in the x-direction, $u/\sqrt{\tau_0/\rho}$
x = axial co-ordinate measuring distance from tube entrance
x^+ = dimensionless axial co-ordinate, x/d
y^+ = dimensionless co-ordinate, $r_0^+ - r^+$
α = molecular diffusivity for heat, $k/\rho c_p$
β_n^2 = eigenvalues of equation (6)
γ = dimensionless total thermal diffusivity, $(\alpha + \epsilon_h)/\nu$
ϵ_h = eddy diffusivity for heat
θ = dimensionless temperature, $(T - T_w)/(T_0 - T_w)$
μ = absolute viscosity
ν = kinematic viscosity
λ = dummy integration variable
λ_n^2 = eigenvalues of equation (23)
ρ = fluid density
τ_0 = wall shear stress
ϕ_n = eigenfunctions of equation (6)
Ω_n = eigenfunctions of equation (23)

($x = 0$), the temperature distribution within the fluid is uniform at T_0. Prior to the transient period, either of two possible initial conditions may prevail: (1) The tube walls may also be at T_0, with no heat being transferred to or from the fluid; or (2) the tube walls may be at some uniform value different from T_0, resulting in a steady-state turbulent heat transfer to or from the fluid. At $t = 0$, a heating or cooling process begins in which the wall temperature changes with time (but is spatially uniform at any instant). In response to the prescribed change in wall temperature, there will be a corresponding variation of the heat-transfer rate as a function both of time and of position along the tube. Our goal is to formulate a predictive theory for the heat transfer which sets aside the previously standard assumption that the heat-transfer coefficient is constant.

The first step in the study is to determine the heat-transfer response to a sudden change (step function) in wall temperature, starting from an initial condition of no heat transfer (i.e., initially, $T_w \equiv T_0$). To illustrate the method and show trends with the Reynolds and Prandtl numbers, numerical computations are carried out for the following Reynolds-Prandtl combinations: Pr = 0.7, 10, and 100 for Re = 100,000; and Pr = 0.7 for Re = 500,000. The step function formulation serves as a fundamental solution, since by a superposition technique it is generalized to apply for arbitrary time-variations in wall temperature. A further generalization is made to permit the transient to start from an already-established steady-state heat-transfer situation (initially $T_w \neq T_0$). To show the use of the generalized results, an example is carried out for the situation where the wall temperature increases in a linear fashion with time, i.e., a ramp function.

The heat-transfer results for the step function and for the ramp function are compared with those computed using the approximation that the heat-transfer coefficient is steady. From this, it will be possible to gain insight into the errors associated with this simplifying assumption.

A method similar to that used here was devised by Siegel [1][2] in connection with unsteady laminar heat transfer in tubes and channels.

Step Change in Wall Temperature

The starting point for our study of the transient response to a step change in wall temperature is the conservation of energy principle. The mathematical statement of this law appropriate to fully developed hydrodynamic conditions may be expressed in cylindrical co-ordinates as

$$\frac{\partial T}{\partial t} + u\frac{\partial T}{\partial x} = \frac{1}{r}\frac{\partial}{\partial r}\left[r(\alpha + \epsilon_h)\frac{\partial T}{\partial r}\right] \tag{1}$$

where α and ϵ_h, respectively, denote the molecular and eddy diffusivities for heat. In writing equation (1), the axial diffusion of heat and the viscous dissipation have been neglected relative to the radial diffusion. In addition, the variation of the fluid properties has not been considered.

Before approaching the formidable task of solving equation (1), it is useful to note some of the physical characteristics of the problem which will be useful in constructing and verifying the solution. First of all, for a period of time immediately following the step change in wall temperature, the heat transfer at each axial position is due to diffusion alone. The effects of axial convection do not manifest themselves at a given position x until fluid which was situated at the entrance section at $t = 0$ has traveled down to position x. Hence the duration of this period of pure diffusion increases with distance from the entrance. Any solution which is proposed for equation (1) will have to be compared with that for purely diffusional heat transfer. Second, for large values of time, the transient effects should die away and the heat-transfer characteristics should approach those of the steady state. Since the steady-state solution will be used in constructing a solution for equation (1), a brief review of the steady-state formulation appears worth while.

Review of Steady-State Solution. For steady state, equation (1) may be applied once the energy storage term $\partial T/\partial t$ has been deleted. A dimensionless form of this equation may be written as

$$\frac{u^+}{2}\frac{\partial \theta}{\partial x^+} = \frac{r_0^+}{r^+}\frac{\partial}{\partial r^+}\left(r^+\gamma\frac{\partial \theta}{\partial r^+}\right) \tag{2}$$

where u^+, r^+, x^+, and θ are the dimensionless counterparts of u, r, x, and T as defined in the symbol list, while γ is a dimensionless diffusivity. The boundary conditions which must be satisfied by the temperature are

$$T(0, r) = T_0, \qquad T(x, r_0) = T_w, \qquad \frac{\partial T}{\partial r}(x, 0) = 0 \tag{3}$$

The first two of these represent the imposed temperatures at the entrance section and at the tube wall, while the third condition is the symmetry requirement at the center line. In terms of the new variables, the boundary conditions (3) become

$$\theta(0, r^+) = 1, \qquad \theta(x^+, r_0^+) = 0, \qquad \frac{\partial \theta}{\partial r^+}(x^+, 0) = 0 \tag{4}$$

The solution to the boundary value problem represented by equations (2) and (4) may be written in the form (refs. [2, 3])

$$\theta = \sum_{n=1}^{\infty} C_n\phi_n(r^+)e^{-4\beta_n^2 x^+/\mathrm{Re}} \tag{5}$$

where β_n and ϕ_n are the eigenvalues and eigenfunctions of the following Sturm-Liouville problem[3]

$$\left.\begin{aligned} &\frac{d}{dr^+}\left[r^+\gamma\frac{d\phi_n}{dr^+}\right] + \left[\frac{2\beta_n^2}{\mathrm{Re}}\frac{r^+}{r_0^+}u^+\right]\phi_n = 0 \\ &\phi_n(r_0^+) = 0, \qquad d\phi_n/dr^+|_0 = 0 \end{aligned}\right\} \tag{6}$$

Once the eigenfunctions have been found, the set of constants C_n may be determined in accordance with Sturm-Liouville theory from the quotient:

$$C_n = \frac{\int_0^{r_0^+} r^+u^+\phi_n\,dr^+}{\int_0^{r_0^+} r^+u^+\phi_n^2\,dr^+} \tag{7}$$

and this assures that

$$\sum_{n=1}^{\infty} C_n\phi_n = 1 \tag{7a}$$

to satisfy the condition that $\theta = 1$ at $x = 0$.

From the temperature distribution, equation (5), various quantities of engineering interest can be determined. For example, the local wall heat transfer, heat-transfer coefficient, and Nusselt number may be computed from their definitions

$$q = k\left(\frac{\partial T}{\partial r}\right)_{r_0}, \qquad h \equiv \frac{q}{T_w - T_b}, \qquad \mathrm{Nu} = \frac{hd}{k} \tag{8a}$$

where the bulk temperature T_b is given by

[2] Numbers in brackets designate References at end of paper.

[3] Solutions of equation (6) are possible only for a discrete, though infinite, set of values of β_n.

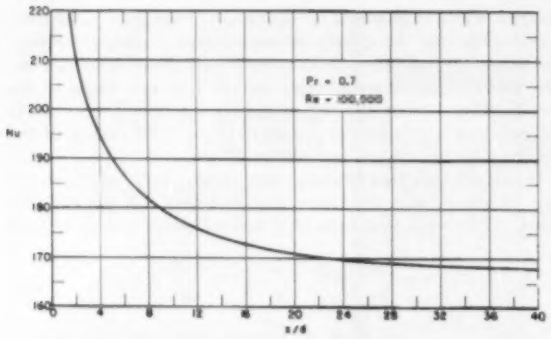

Fig. 2 Representative steady-state Nusselt number curve

$$T_b = \frac{\int_0^{r_0} T\,u\,2\pi r\,dr}{\int_0^{r_0} u\,2\pi r\,dr} \tag{8b}$$

A typical steady-state Nusselt number curve (Pr = 0.7, Re = 100,000) is shown in Fig. 2. The plot illustrates the manner in which the high entrance region Nusselt numbers decrease steadily toward the fully developed value as x/d increases. The thermal entrance length is defined as that portion of the tube in which the Nusselt number deviates significantly (e.g., by 5 per cent or more) from the fully developed value. For fluids in the range $\mathrm{Pr} \geq 0.7$, the extent of the thermal entrance length decreases appreciably with increasing Prandtl number, while the Reynolds number has only a small influence.

The steady-state analysis depends upon obtaining solutions of the eigenvalue problem (6). Since both the Reynolds and Prandtl[4] numbers enter the equation, it is clear that there will be a different set of eigenvalues for each pair of these parameters. It is also necessary to specify the velocity distribution u^+ and the dimensionless diffusivity γ, and this information is given in Appendix A. Although knowledge of the eddy diffusivity is still in a state of uncertainty, the application of the expressions used here in previous analyses has led to excellent heat-transfer predictions for the Prandtl number range of present interest, $\mathrm{Pr} \geq 0.7$.

Utilizing the Kutta-Runge method of numerical integration in conjunction with an IBM 653 electronic computer, seven eigenvalues and the corresponding eigenfunctions have been determined for each of the Reynolds-Prandtl combinations which have been mentioned in the Introduction. Some of the prime results are listed in Appendix B, Table 2, and this information will be directly applicable to the transient solution.

A final relationship needed in carrying out the transient analysis may be found by integrating equation (6) from $r^+ = 0$ to r_0^+, giving

$$\beta_n^2 = -\frac{r_0^{+2}\,\mathrm{Re}(d\phi_n/dr^+)_{r_0^+}}{2\mathrm{Pr}\int_0^{r_0^+} r^+u^+\phi_n\,dr^+} \tag{9}$$

Complete Solution for Transient and Steady States. We now return to the time-dependent energy equation (1) to seek a solution which will apply during both the transient and steady states and which is valid in both the entrance and fully developed regions. To facilitate the solution, equation (1) is integrated across the section from $r = 0$ to r_0, giving

$$\frac{1}{r_0^{+2}}\frac{\partial}{\partial t^+}\left[\int_0^{r_0^+} r^+\theta\,dr^+\right] + \frac{1}{2r_0^+}\frac{\partial}{\partial x^+}\left[\int_0^{r_0^+} r^+u^+\theta\,dr^+\right] = \frac{r_0^+}{\mathrm{Pr}}\left(\frac{d\theta}{dr^+}\right)_{r_0^+} \tag{10}$$

where dimensionless variables have been introduced. The temperature must obey the same boundary conditions as stated in equations (3) or (4), plus the initial condition that

$$T(x, r) = T_0 \quad \text{at} \quad t = 0, \quad \text{or} \quad \theta(x^+, r^+) = 1 \quad \text{at} \quad t^+ = 0 \tag{11}$$

The form of the steady-state solution, equation (5), plus previous experience with the laminar flow problem prompts us to now propose a solution of the form

$$\theta = \sum_{n=1}^{\infty} C_n F_n(x^+, t^+)\phi_n(r^+) \tag{12}$$

where the C_n and ϕ_n are the values from the steady-state solution, and the F_n are a set of functions which depend only on x and t. The F_n are found by applying the integral conservation of energy principle (10). Introducing (12) into (10) and rearranging gives

$$\frac{1}{r_0^{+2}}\sum_{n=1}^{\infty} C_n\left[\int_0^{r_0^+} r^+\phi_n\,dr^+\right]\frac{\partial F_n}{\partial t^+} + \frac{1}{2r_0^+}\sum_{n=1}^{\infty} C_n\left[\int_0^{r_0^+} r^+u^+\phi_n\,dr^+\right]\frac{\partial F_n}{\partial x^+} = \sum_{n=1}^{\infty} C_n\frac{r_0^+}{\mathrm{Pr}}\left[\frac{d\phi_n}{dr^+}\right]_{r_0^+}F_n \tag{13a}$$

or

$$\frac{1}{r_0^{+2}}\left[\int_0^{r_0^+} r^+\phi_n\,dr^+\right]\frac{\partial F_n}{\partial t^+} + \frac{1}{2r_0^+}\left[\int_0^{r_0^+} r^+u^+\phi_n\,dr^+\right]\frac{\partial F_n}{\partial x^+} = \frac{r_0^+}{\mathrm{Pr}}\left[\frac{d\phi_n}{dr^+}\right]_{r_0^+}F_n \tag{13b}$$

Equation (13b) is a partial differential equation for determining the F_n as a function of x^+ and t^+. An equation of this form is ideally suited for solution by the method of characteristics. As is indicated in reference [4], the solution of the partial differential equation (13b) is equivalent to the solution of the following pair of ordinary differential equations

$$\frac{dt^+}{\frac{1}{r_0^{+2}}\left[\int_0^{r_0^+} r^+\phi_n\,dr^+\right]} = \frac{dx^+}{\frac{1}{2r_0^+}\left[\int_0^{r_0^+} r^+u^+\phi_n\,dr^+\right]} = \frac{dF_n}{F_n\frac{r_0^+}{\mathrm{Pr}}\left[\frac{d\phi_n}{dr^+}\right]_{r_0^+}} \tag{14}$$

On the $x^+ - t^+$ plane (Fig. 3), there is a family of straight characteristic lines whose slope is found by using the first equality of (14):

$$\frac{dt^+}{dx^+} = \frac{2\int_0^{r_0^+} r^+\phi_n\,dr^+}{r_0^+\int_0^{r_0^+} r^+u^+\phi_n\,dr^+} = -\frac{4\beta_n^2\mathrm{Pr}\int_0^{r_0^+} r^+\phi_n\,dr^+}{r_0^{+3}\mathrm{Re}(d\phi_n/dr^+)_{r_0^+}} \tag{15}$$

[4] See the definition of γ in Appendix A.

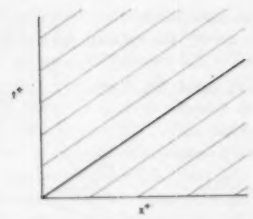

Fig. 3 Representation of characteristic lines on $x^+ - t^+$ plane

where equation (9) has been introduced to obtain the last term of (15). The variation of F_n with x^+ and t^+ along the characteristic lines is also found from equation (14). Along those characteristics which intersect the x^+ axis, we find from the first and last members of (14) that

$$F_n = \exp\left\{\frac{r_0^{+2}(d\phi_n/dr^+)_{r_0^+}}{\mathrm{Pr}\int_0^{r_0^+} r^+\phi_n\,dr^+}\,t^+\right\} \tag{16}$$

It is noted that $F_n = 1$ when $t^+ = 0$. With this, and making use of equations (12) and (7a), it is seen that the initial condition $\theta = 1$ is satisfied. Along the characteristics which intersect the t^+ axis, the second and third members of equation (14) give

$$F_n = \exp\left\{\frac{2r_0^{+2}(d\phi_n/dr^+)_{r_0^+}}{\mathrm{Pr}\int_0^{r_0^+} r^+u^+\phi_n\,dr^+}\,x^+\right\} \tag{17}$$

or by using equation (9)

$$F_n = \exp\left\{-\frac{4\beta_n^2}{\mathrm{Re}}\,x^+\right\} \tag{18}$$

For $x^+ = 0$, $F_n = 1$, and hence from equations (12) and (7a) it is seen that the entrance condition that $\theta = 1$ at $x = 0$ is also satisfied.

So far, we have succeeded in finding a solution for F_n in two parts, one to be applied on the characteristics intersecting the x^+ axis and the second on the characteristics intersecting the t^+ axis. Thus the characteristic passing through the origin becomes the dividing line to delineate when we use one expression or the other. Now, from equation (15), the equation of this limiting characteristic is

$$t^+ = \left\{-\frac{4\beta_n^2}{r_0^{+3}\mathrm{Re}}\,\frac{\mathrm{Pr}\int_0^{r_0^+} r^+\phi_n\,dr^+}{(d\phi_n/dr^+)_{r_0^+}}\right\} x^+ \tag{19a}$$

$$= a_n x^+ \tag{19b}$$

where a_n is an abbreviation of the quantity in braces. Then it follows that, if $t^+ \leq a_n x^+$, we use equation (16) for F_n; while, if $t^+ \geq a_n x^+$, equation (18) is used.

With this, we can restate our general temperature solution as

$$\theta = \sum_{n=1}^{\infty} C_n F_n(x^+, t^+)\phi_n(r^+)$$

$$F_n = \begin{cases} \exp\left\{\dfrac{r_0^{+3}(d\phi_n/dr^+)_{r_0^+}}{\mathrm{Pr}\int_0^{r_0^+} r^+\phi_n\,dr^+}\,t^+\right\}, & t^+ \leq a_n x^+ \\ \exp\left\{-\dfrac{4\beta_n^2}{\mathrm{Re}}\,x^+\right\}, & t^+ \geq a_n x^+ \end{cases} \tag{20}$$

This solution satisfies all boundary conditions and the initial condition. Also, it is clear that as $t^+ \to \infty$, the correct steady-state solution is approached [see equation (5)]. So, equation (20) provides a means for calculating the temperature distribution (and hence the heat transfer) throughout the entire transient period provided only that steady-state solutions are available.

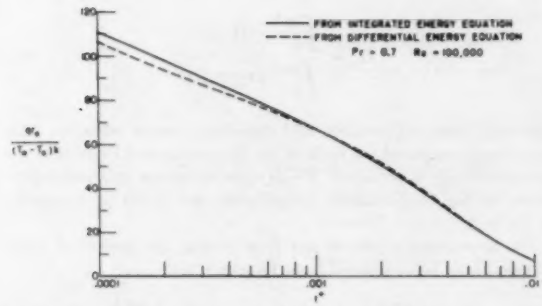

Fig. 4 Representative comparison of heat-transfer predictions for period of pure diffusion

Before turning to the heat-transfer computation, there is a final aspect of the general temperature solution which requires discussion. It should be noted that this solution satisfies an integrated energy equation (10) rather than the corresponding differential equation, and it is desirable to inquire as to whether important errors are introduced. One source of confidence in our solution is that, for large times, it approaches the correct steady-state solution. A second support for the solution would be a close agreement at small times with the results for purely diffusional heat transfer. Such a comparison is made in the next section.

Verifying the Solution at Early Times. It has already been pointed out that for a period of time immediately following the step jump, convection has no influence, and all of the heat transfer is due to one-dimensional diffusion. This diffusion is made up of both molecular conductivity and eddy diffusivity. For this period of pure diffusion, we now proceed to find a temperature solution which satisfies the differential form of the conservation of energy equation. These results will be compared with those from equation (20), which satisfy an integrated form of energy conservation.

For the period of pure diffusion, equation (1) may be applied once the convection term $u\,\partial T/\partial x$ has been deleted. Introducing dimensionless variables, the equation becomes

$$\frac{\partial\theta}{\partial t^+} = \frac{r_0^{+2}}{r^+}\,\frac{\partial}{\partial r^+}\left(r^+\gamma\,\frac{\partial\theta}{\partial r^+}\right) \tag{21}$$

A solution may be written in the form

$$\theta = \sum_{n=1}^{\infty} D_n\Omega_n(r^+)e^{-\lambda_n^2 t^+} \tag{22}$$

where Ω_n and λ_n^2 are the eigenvalues and eigenfunctions of the following Sturm-Liouville problem

$$\left.\begin{aligned} &\frac{d}{dr^+}\left[r^+\gamma\,\frac{d\Omega_n}{dr^+}\right] + \left(\frac{r^+}{r_0^{+2}}\,\lambda_n^2\right)\Omega_n = 0 \\ &\Omega_n(r_0^+) = 0, \qquad d\Omega_n/dr^+\big|_0 = 0 \end{aligned}\right\} \tag{23}$$

The constants D_n are found by imposing the (initial) condition that at $t^+ = 0$

$$\theta = 1 = \sum_{n=1}^{\infty} D_n\Omega_n(r^+)$$

Using the property that the eigenfunctions Ω_n are orthogonal with respect to the weighting function r^+, it immediately follows that

$$D_n = \frac{\int_0^{r_0^+} r^+ \Omega_n \, dr^+}{\int_0^{r_0^+} r^+ \Omega_n^2 \, dr^+} \tag{24}$$

The first seven eigenvalues and eigenfunctions of equation (23) have been computed for each of the Reynolds and Prandtl numbers previously mentioned. From these solutions, quantities pertinent to the heat-transfer computation are listed in Appendix B, Table 3.

The heat-transfer rate at any time during the period of pure diffusion may be computed from Fourier's law

$$q = k\left(\frac{\partial T}{\partial r}\right)_{r_0} = -\frac{k}{r_0}(T_w - T_0) r_0^+ \left(\frac{\partial \theta}{\partial r^+}\right)_{r_0^+} \tag{25}$$

For the temperature solution (22) which corresponds to the differential form of the energy equation, the heat transfer is

$$\frac{qr_0}{k(T_w - T_0)} = -r_0^+ \sum_{n=1}^{\infty} D_n e^{-\lambda_n^2 t^+} \left(\frac{d\Omega_n}{dr^+}\right)_{r_0^+} \tag{26}$$

Numerical values needed to evaluate the series (26) are given in Appendix B, Table 3.

For comparison with equation (26), an alternate heat-transfer prediction for the period of pure diffusion can be made from the general temperature solution (20), which satisfies an integral form of the energy equation. Applying Fourier's law (25) to equation (20), it is found that

$$\frac{qr_0}{(T_w - T_0)k} = -r_0^+ \sum_{n=1}^{\infty} C_n \left(\frac{d\phi_n}{dr^+}\right)_{r_0^+} \exp\left\{\frac{r_0^{+2}(d\phi_n/dr^+)_{r_0^+}}{\Pr \int_0^{r_0^+} r^+ \phi_n \, dr^+} t^+\right\} \tag{27}$$

where numerical values needed to compute the series are found in Appendix B, Table 2.

The heat-transfer results from equations (27) and (26) have been compared over a large span of time for each of the cases tabulated in Appendix B. The comparisons for all of the cases were so similar that only the results for a typical case (Pr = 0.7, Re = 100,000) need be shown. Referring to Fig. 4, it is seen that the heat-transfer predictions from these two equations are very close, the greatest deviation being about 4 per cent. So, this demonstration of accuracy for the period of pure diffusion lends further support to the over-all temperature solution (20).

Heat-Transfer Results. Having established the validity of the over-all temperature solution (20) for small as well as for large times, we now proceed to use it in deriving heat-transfer predictions for the *entire transient period*. Applying Fourier's law (25) to equation (20), there is obtained

$$\frac{qr_0}{(T_w - T_0)k} = -r_0^+ \sum_{n=1}^{\infty} C_n F_n(x^+, t^+) \left(\frac{d\phi_n}{dr^+}\right)_{r_0^+} \tag{28}$$

where the F_n are as defined in (20). Equation (28) has been evaluated for the several Reynolds-Prandtl combinations for which steady-state information is listed in Appendix B, Table 2. The heat-transfer results corresponding to each case are plotted as a function of time as solid lines in Figs. 5 through 8. In each figure, curves are given which show the heat-transfer response at positions ranging from $x/d = 2$ to $x/d = 100$. Discussion of the dotted and the dashed lines, which correspond to predictions based on steady-state heat-transfer coefficients, will be deferred until a later section.

Aside from scale changes, the manner in which the heat transfer varies with time is generally the same in all the figures. Turning to Fig. 5 for purposes of discussion, suppose we focus our attention on some position along the tube, say $x/d = 20$. At very small times, the heat transfer is only by pure diffusion and follows along the envelope curve, decreasing with increasing time. Then, at $t^+ = 0.00078$, convection begins to act and the curve breaks away from the pure diffusion envelope, with the heat transfer continuing to decrease until the horizontal steady-state line is reached. If, as an approximation, the steady-state line were extended to the left to intersect the pure diffusion curve, the heat transfer thus predicted would be lower than that given by equation (28), but not by a practically significant amount. However, such an approximation does not provide any labor-saving aspects, since it requires the computation of the curve for pure diffusion, a task which is no easier for turbulent flow than the computation of the steady-state functions needed for equation (28).

It is observed from the figures that the curves computed from equation (28) do not have continuous curvature during the transient convection period. This arises because of the approximations of the theory; namely, that an integrated energy equation has been satisfied rather than a differential energy equation. At the larger x/d, fewer terms contribute to the solution (because the exponential factors are small), so the curves appear less continuous. In evaluating equation (28), cognizance was taken of the fact that the series was truncated after seven terms. The practical effect of this truncation was that the curves of Figs. 5 through 8 could not be extended all the way back to $t^+ = 0$; but rather, had to begin from some later time (which varied with the Reynolds and Prandtl numbers).

The results of Figs. 5 through 8 serve to illustrate the analytical method as well as to supply heat-transfer information for specific Reynolds and Prandtl numbers. Corresponding results for any Reynolds-Prandtl combination can be determined by duplicating the procedure followed here. The required solutions of the steady-state equation (6) can be expeditiously obtained by high-speed electronic computing equipment.

A result of practical interest which may be obtained from the figures is the duration of the transient period, and this will be discussed in the following section.

Time to Reach Steady State After a Step Jump. Since the approach to steady state is actually an asymptotic process, we will define a steady-state time as that required for the heat transfer to come to within 5 per cent of the steady-state value. Such times have been found from Figs. 5 through 8 and plotted as a function of position x/d as solid curves in Fig. 9. Also appearing in this figure are straight lines (dotted) corresponding to the time $x/\bar{u}$, which approximately represents the time at which the heat-transfer process at any position x is influenced by the convection of fluid from the tube entrance. In dimensionless variables, $t_{ss} = x/\bar{u}$ becomes $t_{ss}^+ = 4(x/d)/\mathrm{Re}$.

The upper grouping of three solid curves are all for a Reynolds number of 100,000 with the Prandtl number varying from 0.7 to 100.[5] As the Prandtl number increases, there is a decrease in the time required to attain steady state, but by no more than a factor of three for this Prandtl number range. The Reynolds number has a significant effect on the steady-state time; with the time going approximately in inverse proportion to the Reynolds number. The simple relation $t_{ss} = x/\bar{u}$ gives a fairly good estimate for a Prandtl number around unity, but tends to overestimate the time as Prandtl number increases. However, for the purpose of providing an order of magnitude estimate (which is sometimes all that is required), $x/\bar{u}$ appears to be useful.

[5] The curves of Fig. 8 do not extend back to sufficiently short times to permit computation of the complete Pr = 100 curve.

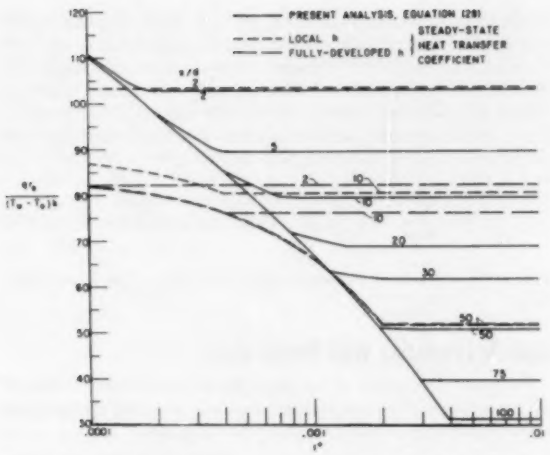

Fig. 5 Heat-transfer response to a step jump in wall temperature; Pr = 0.7, Re = 100,000

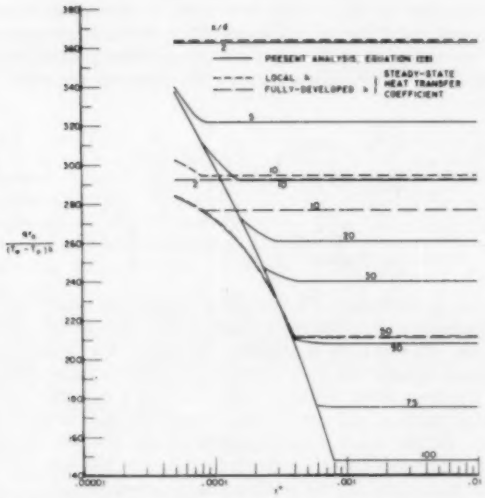

Fig. 6 Heat-transfer response to a step jump in wall temperature; Pr = 0.7, Re = 500,000

Arbitrary Time-Dependent Wall Temperature

The linearity of the energy equation permits us to use a superposition technique to generalize the step-function results. Consider a process in which there is no heat transfer (i.e., $T_w = T_0$) for $t < \lambda$; and then, at $t = \lambda$, a step change in wall temperature of magnitude dT_w is applied. The heat-transfer response to such a process may be computed from equation (28) to be

$$\frac{qr_0}{k} = dT_w \left\{ -r_0{}^+ \sum_{n=1}^{\infty} C_n F_n(x^+, t^+) \left(\frac{d\phi_n}{dr^+}\right)_{r_0{}^+} \right\} \quad (29)$$

But, as may be seen by referring to Fig. 10, this small step may be considered as an elementary part of an arbitrarily variable wall temperature. The heat transfer corresponding to such a time-dependent wall temperature is found by integrating equation (29). After introducing the definitions of the F_n from equation (20) and rearranging, there results

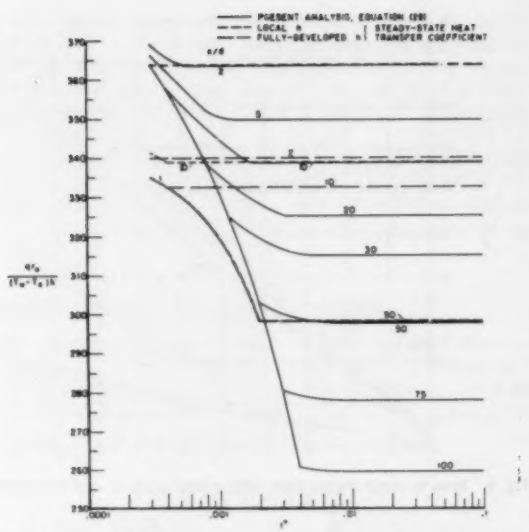

Fig. 7 Heat-transfer response to a step jump in wall temperature; Pr = 10, Re = 100,000

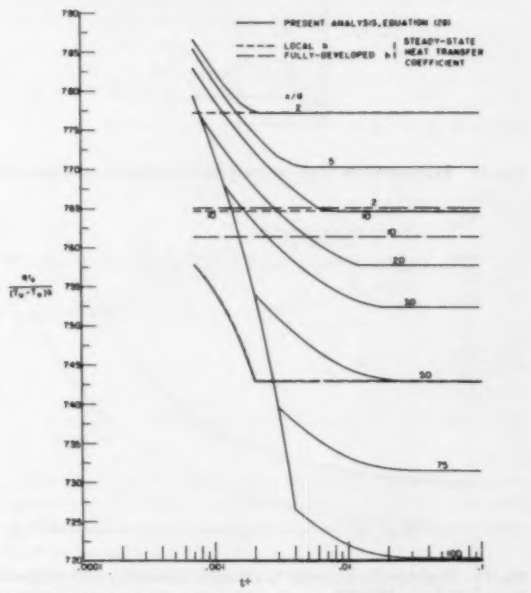

Fig. 8 Heat-transfer response to a step jump in wall temperature; Pr = 100, Re = 100,000

$$-\frac{qr_0}{k} = r_0{}^+ \sum_{n=1}^{N-1} C_n \left(\frac{d\phi_n}{dr^+}\right)_{r_0{}^+} \left\{ e^{J_n a_n x^+} (T_w - T_0)_{t^+ - a_n x^+} + \int_{t^+ - a_n x^+}^{t^+} e^{J_n (t^+ - \lambda)} \, dT_w(\lambda) \right\}$$

$$+ r_0{}^+ \sum_{n=N}^{\infty} C_n \left(\frac{d\phi_n}{dr^+}\right)_{r_0{}^+} \left[\int_0^{t^+} e^{J_n (t^+ - \lambda)} \, dT_w(\lambda) \right] \quad (30)$$

where

$$J_n = r_0{}^{+2} (d\phi_n/dr^+)_{r_0{}^+} / \mathrm{Pr} \int_0^{r_0{}^+} r^+ \phi_n \, dr^+$$

and for a given t^+ and x^+, N is found from

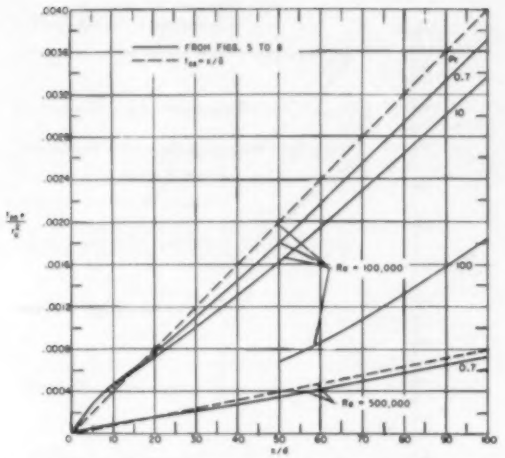

Fig. 9 Time to reach steady state after a step jump in wall temperature

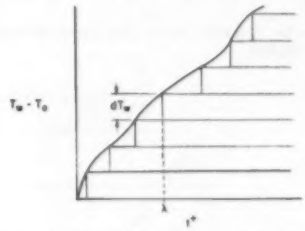

Fig. 10 Representation of an arbitrary time variation in wall temperature

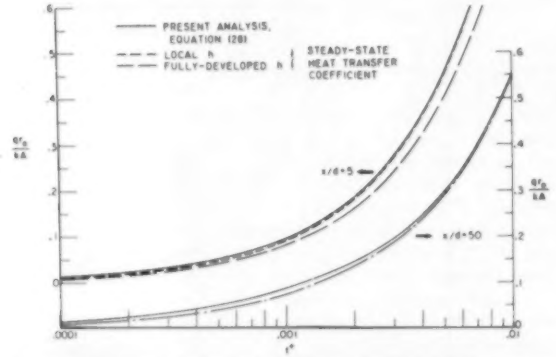

Fig. 11 Heat-transfer response to a linearly increasing wall temperature; Pr = 0.7, Re = 100,000

$$a_{N-1} < \frac{t^+}{x^+} \leq a_N \tag{31}$$

and $\sum_1^0 \equiv 0$, $a_0 \equiv 0$. The integrals appearing in equation (30) are Stiljes integrals, so that step jumps as well as smoothly varying wall temperatures are included. Once T_w has been prescribed, the computation of q essentially amounts to the adding up of the several terms[6] of the series for each t^+ and x^+ of interest. The use of equation (30) will be illustrated in a later section.

Generalization to $T_w \neq T_0$ initially. The preceding discussion has been confined to the situation where the transient started from a condition of zero heat transfer ($T_w \equiv T_0$). Now, we consider the case where there initially exits a steady-state heat transfer with $T_w \neq T_0$. To facilitate the derivation, we imagine that the steady state at $t = 0$ was achieved after an earlier imaginary transient process in which the initial conditions for equation (30) were fulfilled. Following through on this basis, it is found that equation (30) will apply if the following term is added:

$$r_0^+ \sum_N^\infty C_n \left(\frac{d\phi_n}{dr^+}\right)_{r_0^+} e^{J_n a_n x^+} (T_w - T_0)_{t=0} \tag{32}$$

where the value of N corresponding to t^+ and x^+ is found from (31).

Linearly Increasing Wall Temperature

To illustrate the use of the generalized heat-transfer results of the preceding section, we consider the case of a wall temperature which increases in a linear fashion with time, i.e.,

$$T_w - T_0 = At^+ \tag{33}$$

The findings thus obtained will be later compared with an alternate heat-transfer prediction using the previously standard assumption that the heat-transfer coefficient is constant with time.

Introducing the linear wall temperature variation into equation (30) and noting that $dT_w(\lambda) = Ad\lambda$, we are able to carry out the integration. After rearrangement, the heat-transfer result becomes

$$-\frac{qr_0}{kA} = r_0^+ \sum_{n=1}^{N-1} C_n \left(\frac{d\phi_n}{dr^+}\right)_{r_0^+} \left\{ e^{J_n a_n x^+} \left[t^+ - a_n x^+ + \frac{1}{J_n} \right] - \frac{1}{J_n} \right\} + \frac{\Pr}{r_0^{+2}} \sum_{n=N}^{\infty} C_n \left[\int_0^{r_0^+} r^+ \phi_n \, dr^+ \right] [e^{J_n t^+} - 1] \tag{34}$$

where N is determined from equation (31) for a given t^+ and x^+. For purposes of illustration, we have evaluated equation (34) for the case: Pr = 0.7, Re = 100,000. In Fig. 11, the dimensionless wall heat transfer has been plotted (solid lines) against time for two positions along the tube: $x/d = 5$ and $x/d = 50$. Curves at other values of x/d are omitted to preserve the clarity of the figure. At the larger times appearing on the abscissa, the heat transfer increases *linearly* with time; but unfortunately, this behavior is obscured by the semilogarithmic co-ordinates.

Comparison With Results for Constant h

We now proceed to compute for comparison purposes, the heat-transfer response to a prescribed time-dependent wall temperature, under the assumption that the heat-transfer coefficient h is constant with both time and position. For such an analysis, the state of the fluid at any cross section may be represented by a single bulk temperature. Then a one-dimensional energy balance on a cross section yields

$$\rho\pi r_0^2 c_p \frac{\partial T_b}{\partial t} dx + \rho\pi r_0^2 \bar{u} c_p \frac{\partial T_b}{\partial x} dx = h 2\pi r_0 \, dx (T_w - T_b) \tag{35}$$

where the left-hand side represents the stored and convected energy, while the right-hand side is the heat transfer at the wall. In terms of the dimensionless variables of the analysis, equation (35) can be rephrased as

$$\frac{4}{\mathrm{Re}} \frac{\partial T_b}{\partial t^+} + \frac{\partial T_b}{\partial x^+} = \frac{4\mathrm{Nu}}{\mathrm{RePr}} (T_w - T_b) \tag{36}$$

Using the method of characteristics, an equivalent statement of this partial differential equation is

[6] The information of Appendix B permits the use of the first seven terms.

$$\frac{dt^+}{4/\mathrm{Re}} = dx^+ = \frac{dT_b}{\frac{4\mathrm{Nu}}{\mathrm{RePr}}(T_w - T_b)} \tag{37}$$

This equation has the same form as equation (14), and so the description of the solution given there in terms of the characteristics diagram applies here as well.

Corresponding to a step change in wall temperature, a solution for the bulk temperature may be found from equation (37) and the local heat-transfer rate may be computed from: $q = h(T_w - T_b)$. The final result is

$$\frac{qr_0}{k(T_w - T_0)} = \frac{\mathrm{Nu}}{2} e^{-\mathrm{Nu}t^+/\mathrm{Pr}}, \qquad t^+ \leq \frac{4}{\mathrm{Re}} x^+ \tag{38a}$$

$$\frac{qr_0}{k(T_w - T_0)} = \frac{\mathrm{Nu}}{2} e^{-4\mathrm{Nu}x^+/\mathrm{RePr}}, \qquad t^+ \geq \frac{4}{\mathrm{Re}} x^+ \tag{38b}$$

The first of these represents a purely diffusional heat transfer, while the second provides the steady-state result.

For the linearly increasing wall temperature: $T_w - T_0 = At^+$, the solution of (37) yields:

$$\frac{qr_0}{Ak} = \frac{\mathrm{Pr}}{2}(1 - e^{-\mathrm{Nu}t^+/\mathrm{Pr}}), \qquad t^+ \leq \frac{4}{\mathrm{Re}} x^+ \tag{39a}$$

$$\frac{qr_0}{Ak} = \frac{\mathrm{Pr}}{2}\left[1 + e^{-4\mathrm{Nu}x^+/\mathrm{RePr}}\left(\frac{\mathrm{Nu}}{\mathrm{Pr}} t^+ - \frac{4\mathrm{Nu}}{\mathrm{RePr}} x^+ - 1\right)\right], \qquad t^+ \geq \frac{4}{\mathrm{Re}} x^+ \tag{39b}$$

We now compare equations (38) and (39) with the results of the general analysis given in the preceding sections of the paper.

Comparison for Step Function. The solid lines of Figs. 5 through 8 represent the heat-transfer response to a step jump in wall temperature as computed from the temperature solution (20). Equations (38) offer an alternate prediction for the heat-transfer response. These equations are based on a steady-state heat-transfer coefficient which is uniform with position. In reality, the steady-state coefficient varies with x/d in the thermal entrance region of a tube. Hence there is an uncertainty as to how to select the Nusselt number. With this in mind, equations (38) have been evaluated using two different Nusselt numbers at each x/d; namely, the local value corresponding to the particular x/d, and the fully developed value. The results thus obtained have been plotted in Figs. 5 through 8 as dotted lines (local Nu) and dashed lines (fully developed Nu). The distinction between the dotted and dashed lines exists in the entrance region, while as x/d increases they tend to fall on top of one another. To keep the figures fairly simple, equation (38) has been plotted for only three values of x/d on each.

The figures show that regardless of which steady-state Nusselt number is used, equation (38) gives a poor prediction of the transient heat-transfer response to a step jump. This type of temperature change is the most severe test of the application of the steady-state coefficients, and the resulting poor performance is not surprising. It is clear, however, that the use of local Nusselt numbers (rather than fully developed values) gives better heat-transfer predictions.

Comparison for Ramp Function. The heat-transfer results derived from the new formulation of this paper have already been presented in Fig. 11. In this figure, there have also been plotted the predictions of equations (39) based on the use of steady-state heat-transfer coefficients. The distinction between local[7] and fully developed Nusselt numbers is again made. From the figure, it is seen that except at early values of time, the approximate method of equation (39) yields very good heat-transfer predictions, provided that the local heat-transfer coefficient is used. This implies that the heat transfer is essentially quasi-steady after an initial period.

Comparing the findings for the step jump with those for the ramp function, we are led to conclude that the accuracy of the predictions computed using steady-state heat-transfer coefficients depends strongly on the type of wall temperature change being considered.

[7] A further computation of the heat transfer at $x/d = 5$ was made which included the variation of the steady-state h between $x/d = 0$ and $x/d = 5$. These results agreed closely with those using the local coefficient at 5.

Concluding Remark: Variation of T_w With x

In the analysis presented here, it has been assumed that the wall temperature is uniform along the tube at any instant of time. Extension to the situation where the wall temperature varies with x can be achieved by using a superposition technique similar to that carried out in deriving equation (30).

APPENDIX A

Relations for u^+ and γ

The turbulent velocity distribution used in the analysis is given as a function of r^+ by the following relations (ref. [5]):

$$\frac{du^+}{dy^+} = \frac{1}{1 + (0.124)^2 u^+ y^+ [1 - e^{-(0.124)^2 u^+ y^+}]}, \qquad 0 \leq y^+ \leq 26 \tag{40}$$

$$u^+ = \frac{1}{0.36} \ln\left(\frac{y^+}{26}\right) + 12.8493, \qquad 26 \leq y^+ \tag{41}$$

where $y^+ = r_0^+ - r^+$.

The total thermal diffusivity is evaluated from (ref. [6])

$$\gamma = \frac{1}{\mathrm{Pr}} + (0.124)^2 u^+ y^+ [1 - e^{-(0.124)^2 u^+ y^+}], \qquad 0 \leq y^+ < 26 \tag{42}$$

$$\gamma = \frac{1}{\mathrm{Pr}} + 0.36 y^+ (1 - y^+/r_0^+) - 1, \qquad y^+ > 26 \tag{43}$$

The value of γ at $y^+ = 26$ is taken as the average of equations (42) and (43). The minus one term appearing on the right side of equation (43) is retained for $26 < y^+ < r_0^+/2$ and is deleted for larger values of y^+.

References

1 R. Siegel, "Heat Transfer for Laminar Flow in Ducts With Arbitrary Time Variations in Wall Temperature," to be published in the *Journal of Applied Mechanics*. Paper No. 59—APMW-21.

2 V. J. Berry, Jr., "Nonuniform Heat Transfer to Fluids Flowing in Conduits," *Applied Scientific Research*, vol. 4, sec. A, 1953, pp. 61–75.

3 C. A. Sleicher, Jr., and M. Tribus, "Heat Transfer in a Pipe With Turbulent Flow and Arbitrary Wall-Temperature Distribution," TRANS. ASME, vol. 79, 1957, pp. 789–797.

4 F. B. Hildebrand, "Advanced Calculus for Engineers," Prentice-Hall, Inc.; New York, N. Y., 1949, p. 368.

5 R. G. Deissler, "Analysis of Turbulent Heat Transfer, Mass Transfer, and Friction in Smooth Tubes at High Prandtl and Schmidt Numbers," NACA Rep. 1210, 1955. (Supersedes NACA TN 3145.)

6 E. M. Sparrow, T. M. Hallman, and R. Siegel, "Turbulent Heat Transfer in the Thermal Entrance Region of a Pipe With Uniform Heat Flux," *Applied Scientific Research*, vol. 7, sec. A, 1957, pp. 37–52.

APPENDIX B

Numerical Coefficients

Table 1

Re	r_0^+
100,000	2360
500,000	9940

Table 2

(a) Re = 100,000; Pr = 0.7

n	β_n^2	$(d\phi_n/dr^+)_{r_0^+}$	C_n	$\int_0^{r_0^+} r^+\phi_n\,dr^+$	a_n
1	239.7	−0.02865	1.211	0.2182×10^7	0.3891×10^{-4}
2	3036	0.01641	−0.3961	-0.1793×10^6	0.7071×10^{-4}
3	7594	−0.01216	0.3671	0.6105×10^5	0.8130×10^{-4}
4	13920	0.01000	−0.3623	-0.2988×10^5	0.8865×10^{-4}
5	22030	−0.008648	0.3606	0.1742×10^5	0.9461×10^{-4}
6	31940	0.007775	−0.3588	-0.1140×10^5	0.9983×10^{-4}
7	43630	−0.007138	0.3563	0.8025×10^4	0.1046×10^{-3}

(b) Re = 100,000; Pr = 10

n	β_n^2	$(d\phi_n/dr^+)_{r_0^+}$	C_n	$\int_0^{r_0^+} r^+\phi_n\,dr^+$	a_n
1	68.39	−0.1363	1.061	0.2593×10^7	0.3964×10^{-4}
2	2652	0.06555	−0.1111	-0.1319×10^6	0.1625×10^{-3}
3	6937	−0.04423	0.09728	0.4299×10^5	0.2053×10^{-3}
4	12930	0.03409	−0.09473	-0.2052×10^5	0.2370×10^{-3}
5	20630	−0.02808	0.09505	0.1178×10^5	0.2635×10^{-3}
6	30030	0.02440	−0.09690	-0.7651×10^4	0.2867×10^{-3}
7	41140	−0.02189	0.09987	0.5375×10^4	0.3076×10^{-3}

(c) Re = 100,000; Pr = 100

n	β_n^2	$(d\phi_n/dr^+)_{r_0^+}$	C_n	$\int_0^{r_0^+} r^+\phi_n\,dr^+$	a_n
1	15.32	−0.3201	1.014	0.2738×10^7	0.3990×10^{-4}
2	2551	0.1461	−0.02467	-0.1144×10^6	0.6081×10^{-3}
3	6780	−0.09735	0.02137	0.3798×10^5	0.8055×10^{-3}
4	12700	0.07524	−0.02099	-0.1848×10^5	0.9504×10^{-3}
5	20330	−0.06284	0.02147	0.1083×10^5	0.1067×10^{-2}
6	29630	0.05589	−0.02253	-0.7200×10^4	0.1163×10^{-2}
7	40620	−0.05176	0.02415	0.5191×10^4	0.1240×10^{-2}

(d) Re = 500,000; Pr = 0.7

n	β_n^2	$(d\phi_n/dr^+)_{r_0^+}$	C_n	$\int_0^{r_0^+} r^+\phi_n\,dr^+$	a_n
1	846.9	−0.02487	1.179	0.4043×10^8	0.7838×10^{-5}
2	12420	0.01388	−0.3356	-0.2832×10^7	0.1443×10^{-4}
3	31260	−0.01008	0.3128	0.9266×10^6	0.1635×10^{-4}
4	57370	0.008110	−0.3133	-0.4376×10^6	0.1762×10^{-4}
5	90760	−0.006875	0.3176	0.2478×10^6	0.1862×10^{-4}
6	131400	0.006035	−0.3223	-0.1570×10^6	0.1946×10^{-4}
7	179400	−0.005416	0.3263	0.1072×10^6	0.2021×10^{-4}

Table 3

(a) Re = 100,000; Pr = 0.7

n	λ_n^2	$(d\Omega_n/dr^+)_{r_0^+}$	D_n
1	250.8	−0.02967	1.214
2	3158	0.01886	−0.4069
3	7868	−0.01455	0.3871
4	14380	0.01230	−0.3922
5	22720	−0.01092	0.4015
6	32890	0.01009	−0.4124
7	44890	−0.009568	0.4249

(b) Re = 100,000; Pr = 10

n	λ_n^2	$(d\Omega_n/dr^+)_{r_0^+}$	D_n
1	69.53	−0.1381	1.062
2	2702	0.07720	−0.1153
3	7052	−0.05693	0.1077
4	13100	0.04845	−0.1146
5	20840	−0.04534	0.1292
6	30180	0.04600	−0.1520
7	41050	−0.04971	0.1849

(c) Re = 100,000; Pr = 100

n	λ_n^2	$(d\Omega_n/dr^+)_{r_0^+}$	D_n
1	15.40	−0.3213	1.014
2	2577	0.1856	−0.02746
3	6827	−0.1555	0.02900
4	12700	0.1654	−0.03832
5	20080	−0.2191	0.05963
6	28490	0.3684	−0.1061
7	36780	−0.6407	0.1685

(d) Re = 500,000; Pr = 0.7

n	λ_n^2	$(d\Omega_n/dr^+)_{r_0^+}$	D_n
1	874.2	−0.02553	1.180
2	12770	0.01565	−0.3418
3	32020	−0.01176	0.3241
4	58630	0.009652	−0.3296
5	92600	−0.008308	0.3387
6	133900	0.007384	−0.3481
7	182600	−0.006702	0.3569

DISCUSSION

Kwang-tzu Yang[6]

The authors are to be complimented for another significant contribution to the literature of forced convection inside ducts. Their continued interest in unsteady heat-transfer problems will undoubtedly stimulate future works which would eventually enable us to better understand the mechanism of unsteady energy transfer.

The authors' solution in utilizing the energy-integral equation to their basic problem of step change in tube-wall temperature is indeed very interesting. In order to appreciate this, the following may be considered: When the assumed form of solution, equation (12), is substituted into the energy equation (1), there results a differential equation for $F_n(x^+, t^+)$:

$$\frac{\partial F_n}{\partial t^+} + f_{1n}(r^+)\frac{\partial F_n}{\partial x^+} = f_{2n}(r^+)F_n \tag{44}$$

where

$$f_{1n}(r^+) = \frac{r_0{}^+}{2}u^+$$

$$f_{2n}(r^+) = \frac{r_0{}^{+2}}{r^+\phi_n}\frac{d}{dr^+}\left(r^+\gamma\frac{d\phi_n}{dr^+}\right)$$

which are both known functions of r^+. To solve for $F_n(x^+, t^+)$, these functions f_{1n} and f_{2n} must be constants. A natural answer is to have these functions assume average values for the variation of r^+ between zero and $r_0{}^+$. The authors' technique, which is very adequate, of using the energy-integral equation corresponds obviously to employing a weighted mean. Another advantage of their solution is that for long times the exact steady solution is automatically obtained. Nevertheless, equation (44) points out the fact that the authors' solution is not unique in the sense that other mean values for f_{1n} and f_{2n} could also be used to arrive at solutions to this basic problem.

Furthermore, the accuracy of the authors' solution can actually be significantly improved without carrying out further numerical calculations. In view of Fig. 4, the maximum error of about 4 per cent as mentioned in the paper apparently occurs in the time interval when the exact solution of the corresponding pure-diffusion problem is valid. This observation immediately suggests a similar solution to be based on the exact result of the pure-diffusion problem as follows: Let

$$\theta = \sum_{n=1}^{\infty} D_n\Omega_n(r^+)G_n(x^+, t^+) \tag{45}$$

By following the same procedure of solution of obtaining $F_n(x^+, t^+)$, it may be readily shown that

$$G = \begin{cases} \exp\left\{\dfrac{2r_0{}^{+2}}{\Pr}\dfrac{\left[\dfrac{d\Omega_n}{dr^+}\right]_{r_0{}^+}}{\displaystyle\int_0^{r_0{}^+} r^+u^+\Omega_n dr^+}x^+\right\} & t^+ \geq b_n x^+ \\ \exp\{-\lambda_n{}^2 t^+\} & t^+ \leq b_n x^+ \end{cases} \tag{46}$$

where

$$b_n = \frac{2\displaystyle\int_0^{r_0{}^+} r^+\Omega_n dr^+}{r_0{}^+\displaystyle\int_0^{r_0{}^+} r^+u^+\Omega_n dr^+}$$

It is obvious that evaluation of G_n is elementary in view of the numerical results already obtained by the authors. Thus the complete solution to the basic problem of step change in wall temperatures is now given by equations (45) and (46) in this discussion and equations (12) and (20) in the paper. Advantages of this composite solution are (1) that the less accurate portion of the authors' result is now replaced by an exact solution, and (2) that the time period for which pure diffusion prevails is now well defined by $0 \leqslant t^+ \leqslant b_n x^+$.

The authors have also mentioned that discontinuities in curvature as shown in Figs. 5, 6, 7, and 8 are due to approximations arising from using the energy-integral equation. This, however, is not correct, since these discontinuities are inherent in the original differential equation in conjunction with the following conditions:

$$\theta(x^+, r^+, 0) = 1 \qquad \theta(0, r^+, t^+) = 1$$

This is in close analogy with the unsteady problem of a semi-infinite plate moving in the direction of its own surface from rest with a step change in velocity or a constant acceleration.

From a practical point of view, the application of the quantitative results obtained by the authors is somewhat limited because of the few Reynolds number and Prandtl number values chosen. Extension of these calculations to cover reasonable ranges of Re and Pr probably would not be justifiable, even with computers. A possible alternative may lie in the utilization of the usual integral procedure, especially in view of its success in the corresponding laminar-flow cases as dealt with by the same authors recently. Because of its relative simplicity, the integral procedure could even possibly be used to treat more realistic unsteady problems of variable properties, simultaneous hydrodynamic and thermal entrance to ducts, or low Prandtl number fluids.

[6] Associate Professor, Department of Mechanical Engineering, University of Notre Dame, Notre Dame, Ind. Assoc. Mem. ASME.

Authors' Closure

The authors wish to extend their thanks to Professor Yang for his interest and comments on this problem.

In connection with the use of the integrated form of the energy equation, we feel that this is a logical approach to follow when seeking an approximate solution of the problem. However, we agree with Professor Yang that there does exist a variety of other approximate procedures.

As has been noted in the paper, the deviations between the complete temperature solution, equation (20), and the exact solution for the period of pure diffusion are quite small. So any attempt to refine the solution during this initial period is primarily of theoretical interest. The alternate temperature solution embodied in equations (45) and (46) serves well for the period of pure diffusion, but is in error for the steady state. In recognition of this, there is proposed in the Discussion a composite solution composed of equations (45) and (46) for short times, and equation (20) of the paper for long times. But the difficulty which then arises is that it is not known at what time the two solutions are to be joined. In any event, from the practical standpoint, it is unlikely that the small improvement in accuracy for short times, relative to equation (20), would warrant the use of a more complex solution. It is mentioned in the Discussion that the period of pure diffusion in the composite solution is $0 \leq t^+ \leq b_n$. This is probably a misprint and is likely intended to read $0 \leq t^+ \leq b_1$.

With regard to the discontinuities of the curves of Figs. 5 through 8, we continue to feel that they are due to the form of the solution. On any curve of heat transfer against time for a fixed x/d, there is a small discontinuity at each $t^+ = a_n(x/d)$. Most of these breaks are not clearly visible in the figures because they are of such small extent.

Although only a limited number of Reynolds-Prandtl combinations have been considered in the paper, the extension to other operating conditions is straightforward. With modern electronic computers, the computation of the steady-state eigenvalues and related parameters needed in equation (20) proceeds very rapidly. The authors assume that the statements in the last paragraph of the Discussion regarding the "usual integral procedure" refer to a boundary-layer-type computation for an entrance region. This type of approach is limited to the initial portion of the tube before the boundary layers meet and fill the cross section. The present method is, in fact, an integral procedure which applies over the entire length of the tube.

Improved Lumped Parameter Method for Transient Heat Conduction Calculations

H. G. ELROD, JR.
Technical Adviser, Nuclear Development Corporation; Professor, Mechanical Engineering Department, Columbia University, New York, N. Y. Assoc. Mem. ASME

A general mathematical method is presented suitable for the "lumping" of many damped linear systems when the response function and the forcing function can be related by a convolution integral. The method is illustrated by application to transient heat conduction in slabs and cylindrical rods. An ordinary differential equation (equation 26) relating the mean temperature of these bodies to their surface temperature is derived, and then applied to the solution of several problems. Agreement with exact results is found to be excellent except for very rapid transients. Means for estimating error are provided in the paper.

Introduction

With system analysis becoming increasingly important in today's engineering applications, the need for simple, though accurate, mathematical models for subsystems and components has increased. This paper illustrates a method for the accurate representation of many heat-transfer subsystems, and it is believed that the method may actually have usefulness in numerous fields other than heat transfer.

Development of the method was motivated by the necessity of performing transient calculations of the temperatures in reactor fuel elements. Because of the interaction of the nuclear and thermal phenomena, these calculations must often be performed simultaneously with calculations of the entire reactor system. As a consequence, detailed numerical treatment of the partial differential equations is not feasible, even on modern computing machinery. Nuclear engineers have therefore been forced to adopt various "lumped parameter" techniques for transient heat-conduction analyses, often with some misgivings concerning the accuracy attainable with the approximations adopted.

In this paper the mathematical basis of the new "lumping" procedure is first given, and then the method is used to derive simple first-order differential equations for the mean temperature during thermal transients for flat-slab and cylindrical-rod fuel elements. Formulas for finding the difference between the mean and surface temperatures in terms of the mean-temperature history are also given. These two temperatures are the most important for heat-balance and thermal-stress purposes. The new relations are shown to yield a high order of accuracy by comparing their results with those of precise analytical theory.

Contributed by the Heat Transfer Division of The American Society of Mechanical Engineers and presented at the ASME-AIChE Heat Transfer Conference, Storrs, Conn., August 9–12, 1959.
Note: Statements and opinions advanced in papers are to be understood as individual expressions of their authors and not those of the Society. Manuscript received at ASME Headquarters, June 29, 1959. Paper No. 59—HT-28.

Basis of Lumping Method

Let an initially "dead" linear system be stimulated by some forcing function, $G(t)$. Let the observed response to this stimulation be designated at $Y(t)$. Then $Y(t)$ and $G(t)$ are related through Duhamel's formula [1].[1] Thus:

$$Y(t) = G(+0)H(t) + \int_0^t H(t-u)G'(u)du \qquad (1)$$

where $H(t)$ is the special form which the response $Y(t)$ assumes

[1] Numbers in brackets designate References at end of paper.

Nomenclature

a = subscript for ambient property
A = constant in dominating function defined by equation (56)
B = constant in dominating function by equation (58)
c = specific heat of conducting medium
$\mathcal{E}(t)$ = residual term, defined by equation (20)
$f(s)$ = Laplace transform of $H'(t)$
$G(t)$ = forcing function
h = surface heat transfer coefficient
$H(t)$ = response of system to unit-step forcing function
$\mathcal{I}(t)$ = function defined by equation (9)
j = dummy summation variable
k = thermal conductivity of medium
l = volume of slab or cylindrical rod per unit surface area
L = half-thickness of symmetrically heat slab; radius of cylindrical rod
m = subscript for mass-mean property
n = constant in dominating function defined by equation (56)
N = dimensionless ratio, $(hL^2)/(kl)$
q = heat generation in energy per unit volume per unit time
r = root of equation (34)
s = subscript for surface; Laplace transform parameter
t = time
T = temperature
u = dummy variable corresponding to time
V = specified surface temperature
x = distance normal to face of slab
$Y(t)$ = response function, given by equation (1)
α = constant defined by equation (26)
β = constant defined by equation (26)
γ = abbreviation for $H(\infty) - \lambda \int_0^\infty H'(u)\,udu$
ζ = dummy variable corresponding to u
κ = thermal diffusivity of the medium
λ = special decay constant, defined by equation (8)
μ = dimensionless ratio, $(L^2\nu)/\kappa$
ν = exponent in exponential rise of surface temperature
ξ = dummy variable corresponding to τ
ρ = mass density of conducting medium
τ = dimensionless time, $(\kappa t)/L^2$

An overhead bar is used to denote the Laplace transform of a quantity.

when the linear system is forced by the unit step function, $G(t) = 0,\ t < 0;\ G(t) = 1,\ t \geq 0$. A simple change of variable within the convolution integral, plus one integration by parts, yield the following equivalent expression:

$$Y(t) = G(t)H(0) + \int_0^t H'(u)G(t-u)du \tag{2}$$

These expressions for $Y(t)$ at the time t involve a knowledge of the entire prior history of the forcing function.

Now in a damped linear system it is reasonable to assume that the past-history effects of $G(t)$ tend to fade away, leaving present, and recent, values of $G(t)$ to produce the dominant effect on $Y(t)$. To capitalize on this supposition, we expand $G(t-u)$ in a Taylor series. Thus:

$$G(t-u) = G(t) - uG'(t) + \frac{u^2}{2}G''(t) - \ldots. \tag{3}$$

Substitution of this series into equation (2) gives:

$$Y(t) = H(t)G(t) - G'(t)\int_0^t H'(u)\,udu + G''(t)\int_0^t H'(u)\frac{u^2}{2}du - \ldots. \tag{4}$$

However, the damped linear system, when jarred by a unit step function, will acquire asymptotically a steady value of response, $H(\infty)$, and the derivative of this response will attenuate exponentially. Therefore the integrals in equation (4) will converge, and asymptotically we can write:

$$Y(t) = H(\infty)G(t) - G'(t)\int_0^\infty H'(u)udu + G''(t)\int_0^\infty H'(u)\frac{u^2}{2}du - \ldots. \tag{5}$$

Correspondingly, we have:

$$Y'(t) = H(\infty)G'(t) - G''(t)\int_0^\infty H'(u)\,udu + \ldots. \tag{6}$$

By taking the proper linear combination of equations (5) and (6) we obtain a first-order differential equation for $Y(t)$ which contains as its inhomogeneous part all the derivatives of $G(t)$, save the second. Thus:

$$Y'(t) + \lambda Y(t) = \lambda H(\infty)G(t) + \left\{H(\infty) - \lambda\int_0^\infty H'(u)udu\right\}G'(t) + \ldots \tag{7}$$

where

$$\lambda = \frac{2\int_0^\infty H'(u)udu}{\int_0^\infty H'(u)u^2du} \tag{8}$$

If we clip equation (7) so that it contains only the terms actually shown, our choice of λ has given us, in one sense, the best possible first-order differential equation for $Y(t)$ since it is the only one of so few terms which is exact for forcing functions which are second-degree polynomials in time.

The heuristic derivation of equation (7) just given is supplemented by a more convincing mathematical development in Appendix 1. There it is shown that solutions for $Y(t)$ obtained through the use of the terms shown in equation (7) will not differ from the exact solutions obtained from equation (1) by an amount exceeding in absolute value the quantity $|G'''|_{\max}\frac{B}{\lambda n}$, as $t \to \infty$. In this error term $|G'''|_{\max}$ denotes the maximum absolute value achieved by the third derivative of $G(t)$ in the time period $0 \to t$. The constants B and n are positive numbers chosen so that the function Be^{-nt} dominates for all t the function

$$g(t) = \int_0^\infty H'(t+u)\left(u - \frac{\lambda}{2}u^2\right)du \tag{9}$$

The manner of obtaining the constants B and n is demonstrated in Appendix 2 for certain types of $H'(t)$.

When $H(0) = 0$, the Laplace transform of equation (2) gives:

$$\overline{Y(s)} = f(s)\,\overline{G(s)} \tag{10}$$

where

$$f(s) = \int_0^\infty e^{-st}H'(t)\,dt \tag{11}$$

Evidently, when the integrals in equation (5) converge, the following relations hold:

$$(0) = H(\infty); \qquad \lambda = -\frac{2f'(0)}{f''(0)}; \qquad \int_0^\infty H'(u)udu = -f'(0) \tag{12}$$

The required constants in equation (7) are then simply obtained.

A relation between transforms like that given in equation (10) often appears in heat-transfer analyses involving extension in space as well as time. In these cases, the principal features of the extended system are lumped in the several well-chosen constants obtained from equations (12). It should be observed that these constants need not be analytically determined. The response $H(t)$ to unit-step excitation can be found by digital computation or by experiment and the requisite integrals involving $H'(t)$ evaluated numerically.

Differential Equations for Flat Slabs and Cylindrical Rods

Consider a flat slab of infinite extent in the y-z plane, lying in the region $0 < x < L$. The slab material has constant thermal properties. The face at $x = 0$ is insulated. At $t = 0$ the temperature of the slab is uniformly zero. It is then subjected to uniform volumetric heat generation $q(t)$ and arbitrary temperature variation on its surface at $x = L$. The well-known differential equation for the temperature $T(x, t)$ is:

$$\frac{\partial T}{\partial t} = \kappa\frac{\partial^2 T}{\partial x^2} + \frac{q(t)}{\rho c} \tag{13}$$

where κ is the thermal diffusivity of the medium, ρ its density, and c its specific heat. The boundary conditions are:

$$T(x, 0) = 0;\ 0 \leq x < L: \quad \frac{\partial T}{\partial x}(0, t) = 0; \quad T(L, t) = T_s(t) \tag{14}$$

The differential equation for the Laplace transform of the temperature $\overline{T(x, s)}$ is:

$$\frac{d^2\bar{T}}{dx^2} - \frac{s}{\kappa}\bar{T} = -\frac{\overline{q(s)}}{\rho\kappa} \tag{15}$$

Its appropriate solution is:

$$\bar{T} - \frac{\bar{q}}{\rho cs} = \left\{\bar{T}_s - \frac{\bar{q}}{\rho cs}\right\}\frac{\cosh\left(x\sqrt{\frac{s}{\kappa}}\right)}{\cosh\left(L\sqrt{\frac{s}{\kappa}}\right)} \tag{16}$$

This last equation is in the same form as equation (10) if we take

$$Y(t) = T(x, t) - \int_0^t \frac{q(u)}{\rho c}\, du \tag{17}$$

$$G(t) = T_s(t) - \int_0^t \frac{q(u)}{\rho c}\, du \tag{18}$$

Accordingly, we might apply the approximation method to find a differential equation for $T(x, t)$. Instead, we shall find such a relation for the mean slab temperature. The transform of this mean temperature $T_m(t)$ is given by the following equation:

$$T_m - \frac{\bar{q}}{\rho c s} = \left\{ T_s - \frac{\bar{q}}{\rho c s} \right\} \frac{\tanh\left(L\sqrt{\frac{s}{\kappa}}\right)}{L\sqrt{\frac{s}{\kappa}}} \tag{19}$$

where

$$f(s) \equiv \frac{\tanh\left(L\sqrt{\frac{s}{\kappa}}\right)}{L\sqrt{\frac{s}{\kappa}}} = 1 - \frac{1}{3}\frac{s}{\kappa}L^2 + \frac{2}{15}\frac{s^2}{\kappa^2}L^4 + \cdots \tag{20}$$

$$= f(0) + f'(0)s + f''(0)\frac{s^2}{2} + \cdots \tag{21}$$

$$\therefore f(0) = 1; \qquad f'(0) = -\frac{1}{3}\frac{L^2}{\kappa}; \qquad f''(0) = \frac{4}{15}\frac{L^4}{\kappa^2} \tag{22}$$

and

$$\lambda = \frac{5}{2}\frac{\kappa}{L^2} \tag{23}$$

The differential equation for $T_m(t)$ can now be obtained from equations (7) and (12) using the values given for the derivatives of $f(s)$ and the value of λ. Thus

$$T_m'(t) - \frac{q(t)}{\rho c} + \lambda\left[T_m(t) - \int_0^t \frac{q(u)}{\rho c}\, du\right] = \lambda\left[T_s(t) - \int_0^t \frac{q(u)}{\rho c}\, du\right] + [1 + \lambda f'(0)]\left[T_s'(t) - \frac{q(t)}{\rho c}\right] \tag{24}$$

or

$$T_m'(t) + \frac{5}{2}\frac{\kappa}{L^2}T_m(t) = \frac{5}{2}\frac{\kappa}{L^2}T_s(t) + \frac{1}{6}T_s'(t) + \frac{5}{6}\frac{q(t)}{\rho c} \tag{25}$$

This last differential equation can also be considered to apply to the case of symmetrical heating or cooling of a flat slab of thickness $2L$.

An analysis very similar to that just given can be performed for the infinite solid cylinder. The resulting differential equations for the mean temperature in both slabs and cylinders can be written in the single form:

$$T_m'(\tau) + \alpha T_m(\tau) = \alpha T_s(\tau) + \beta T_s'(\tau) + (1 - \beta)\frac{q(\tau)L^2}{k} \tag{26}$$

where L now denotes the distance from center to surface, and $\tau = \frac{\kappa t}{L^2}$. The constants α and β are as follows:

	α	β
Symmetrically heated slab	5/2	1/6
Cylindrical rod	6	1/4

Equation (26) can be coupled with other differential equations involving T_m and T_s. It is anticipated that this will be its principal use. Here let us consider its combination with the equation for Newtonian cooling through a heat-transfer coefficient. In order that the analysis may apply equally well to both slab and cylinder, let us take l as the volume of solid per unit of exposed surface area. Then

$$\rho c l\, T_m'(t) = h(T_a - T_s) \tag{27}$$

where T_a is the ambient temperature. Elimination of T_s between equations (26) and (27) gives:

$$\frac{\beta}{N}T_m''(\tau) + \left(1 + \frac{\alpha}{N}\right)T_m'(\tau) + \alpha T_m(\tau) = \alpha T_a + \beta T_a'(\tau) + (1 - \beta)\frac{q(\tau)L^2}{k} \tag{28}$$

where $N = \frac{hL^2}{kl}$.

Comparisons of Approximate and Exact Mean Temperatures

As a first empirical test of the accuracy of equation (26), let us take the simple case of a flat slab or a solid rod initially at a uniform temperature V. At time zero let the surface temperature be suddenly reduced to zero and maintained there. No internal heat generation is present. The mean-temperature history is desired.

With $q(\tau) = 0$, the general solution of equation (26) is:

$$T_m(\tau) = e^{-\alpha\tau}\left[\text{constant} + \int_0^\tau e^{\alpha\xi}\{\alpha T_s(\xi) + \beta T_s'(\xi)\}\, d\xi\right] \tag{29}$$

Now the use of a Taylor series in equation (3) involved the assumption of a forcing function continuous in time, with a continuous first derivative. Hence as the initial value for T_s in equation (29) we take V and not zero. Then we let the derivative of T_s become strongly negative for a very short time as T_s drops to zero. During this very short time interval $e^{\alpha\xi} \cong 1$. As a consequence

$$\int_0^\tau e^{\alpha\xi}\{\alpha T_s(\xi) + \beta T_s'(\xi)\}\, d\xi \cong -\beta V \tag{30}$$

The final expression for $T_m(\tau)$ is

$$T_m(0) = V; \qquad T_m(\tau) = (1 - \beta)Ve^{-\alpha\tau} \tag{31}$$

Thus the approximate analysis substitutes an oblique "corner" for the rapid transition period preceding the exponential decay. For times greater than zero, we get the following approximate results:

$$\text{Slab: } T_m = 0.833\, e^{-2.5\tau} \qquad \text{Rod: } T_m = 0.75\, e^{-6\tau} \tag{32}$$

In Table 1 the results from these formulas are compared with the exact analytical results of Groeber (as read from figures in ref. [2]). Except for very small $\kappa t/L^2$, the agreement is excellent.

If the cooling in this problem is accomplished with a finite, rather than infinite, heat-transfer coefficient, equation (28) may be used, with the result:

Table 1 Approximate and exact mean-temperature ratios, T_m/V, for sudden surface-temperature reduction to zero

$\frac{\kappa t}{L^2}$	Slab		Rod	
	Exact	Approximate	Exact	Approximate
0.01			0.775	0.706
0.02	0.86	0.790		
0.05	0.75	0.735	0.55	0.545
0.10	0.64	0.653	0.40	0.412
0.30	0.39	0.393	0.12	0.124
0.50	0.24	0.238	0.04	0.040
0.70	0.15	0.145		

$$T_m = -V\frac{[(N+r_2)e^{r_1\tau} - (N+r_1)e^{r_2\tau}]}{\frac{N}{\beta}\sqrt{\left(1+\frac{\alpha}{N}\right)^2 - \frac{4\alpha\beta}{N}}} \tag{33}$$

where r_2 is the more negative or the two roots r_1, r_2, given by:

$$r = \frac{-\left(1+\frac{\alpha}{N}\right) \pm \sqrt{\left(1+\frac{\alpha}{N}\right)^2 - \frac{4\alpha\beta}{N}}}{\left(\frac{2\beta}{N}\right)} \tag{34}$$

Except for very small τ the first exponential in equation (33) dominates the second. Neglecting the second exponential, we get:

$$T_m = V\left[\frac{1}{2} + \frac{\beta\left(\frac{1}{2\beta} - 1 + \frac{\alpha}{2\beta N}\right)}{\sqrt{\left(1+\frac{\alpha}{N}\right)^2 - \frac{4\alpha\beta}{N}}}\right]e^{r_1\tau} \tag{35}$$

When $N \to \infty$ in equation (35), the solution given by equation (31) is recovered, whose accuracy has been shown to be good. When $N \to 0$ the exact result is obtained. For intermediate values of N the difference between the exact and approximate results is scarcely perceptible on the standard Gurney-Lurie charts so that equation (35) may be said to summarize adequately the entire exponential decay portion of these charts.

As a further, rather severe test of equation (26), let us apply it to the symmetrical heating of a slab of thickness $2L$ when the surface temperature is given by:

$$T_s(t) = 0,\ t < 0; \qquad T_s(t) = Ve^{\nu t},\ t \geq 0 \tag{36}$$

The exact solution for the temperature at a distance x from the slab center-plane is given in ref. [3] as:

$$T(x,t) = Ve^{\nu t}\frac{\cosh\left(x\sqrt{\frac{\nu}{\kappa}}\right)}{\cosh\left(L\sqrt{\frac{\nu}{\kappa}}\right)} + 0\left(e^{-\frac{\pi^2\tau}{4}}\right) \tag{37}$$

Asymptotically, the exact answer for T_m is:

$$T_m(t) = Ve^{\nu t}\frac{\tanh\left(L\sqrt{\frac{\nu}{\kappa}}\right)}{L\sqrt{\frac{\nu}{\kappa}}}; \qquad t \to \infty \tag{38}$$

$$= Ve^{\nu t}\left[1 - \frac{1}{3}\mu + \frac{2}{15}\mu^2 - 0.0540\,\mu^3 + \ldots\right] \tag{39}$$

where $\mu = \dfrac{L^2\nu}{\kappa}$.

Applying equation (26) to this case, we get:

$$T_m(\text{approx.}) = Ve^{\nu t}\frac{1+\frac{1}{15}\mu}{1+\frac{2}{5}\mu}; \qquad t \to \infty \tag{40}$$

$$= Ve^{\nu t}\left[1 - \frac{1}{3}\mu + \frac{2}{15}\mu^2 - 0.0533\,\mu^3 + \ldots\right] \tag{41}$$

The agreement between the exact and approximate results given by equations (38) and (40), respectively, is very good for small μ, as evidenced by the close agreement of the series expansions in equations (39) and (41). However, for large μ, errors of importance can arise. For example, as $\mu \to \infty$:

$$\frac{T_m(\text{exact})}{T_s} \to \frac{1}{\sqrt{\mu}} \to 0; \quad \text{whereas:} \quad \frac{T_m(\text{approx.})}{T_s} \to \frac{1}{6} \tag{42}$$

Table 2 presents a comparison of exact and approximate temperature ratios over the entire range of μ. Throughout the range the difference between the exact and approximate values of temperature ratio is less in absolute value than the error term derivable from the results of Appendix 2; viz.,

$$|\text{Error}| \leq |T_s'''(t)|_{\max}\frac{B}{\lambda n} \leq Ve^{\nu t}(p^3)(0.00143)\left(\frac{L^2}{\kappa}\right)^3$$
$$\leq 0.00143\mu^3 Ve^{\nu t} \tag{43}$$

Table 2 Approximate and exact mean-temperature ratios, T_m/T_s, for exponential rise in surface temperature of slab

$\mu = \frac{L^2\nu}{\kappa}$	$T_s = Ve^{\nu t}$ T_m/T_s (exact)	T_m/T_s (approx.)
0	1.000	1.000
1	0.761	0.761
4	0.482	0.487
9	0.331	0.348
16	0.250	0.279
25	0.200	0.242
∞	$\sqrt{1/\mu}$	0.167

Computation of Surface Temperatures From Mean-Temperature History

It may very well be that when equation (26) is coupled with other simultaneous differential equations, certain temperatures of interest are not "carried" in the computer solution. In such cases, if the desired unknown $Y(t)$ can be related by equation (1) to some temperature or function $G(t)$ which has been carried in the computer solution, then the expansion of equation (4) can be used to estimate $Y(t)$.

In the previous example of Newtonian cooling, a solution for the mean temperature was obtained from equation (28) without ever finding the surface temperature $T_s(t)$. Suppose now we wish to find this quantity from the asymptotic solutions given by equation (35). Since equation (26), a specialized form of equation (7), was actually used in the derivation of equation (28), we first solve equation (7) for $G(t)$ in terms of $Y(t)$. The result is readily found to be:

$$G(t) = \frac{1}{\gamma}Y(t) + \frac{\lambda\left(1 - \frac{H(\infty)}{\gamma}\right)}{\gamma}\int_0^t e^{-\frac{\lambda H(\infty)}{\gamma}(t-u)}Y(u)\,du$$
$$+ \left\{G(+0) - \frac{Y(+0)}{\gamma}\right\}e^{-\frac{\lambda H(\infty)}{\gamma}t} \tag{44}$$

where $\gamma = H(\infty) - \lambda\int_0^\infty H'(u)\,u\,du$

If $\frac{\lambda H(\infty)}{\gamma} > 0$, we can successively integrate by parts in equation (44) to obtain the following expression valid for large time, provided the series converges.

$$G(t) = \frac{Y(t)}{\gamma} + \left(\frac{1}{H(\infty)} - \frac{1}{\gamma}\right) \sum_{j=0}^{\infty} (-1)^j \left(\frac{\gamma}{\lambda H(\infty)}\right)^j Y^j(t) \tag{45}$$

Specializing equation (45) for Newtonian cooling of the solid rod, we have:

$$G(t) = T_s(t); \qquad Y(t) = T_m(t)$$

$$H(\infty) = 1; \qquad \gamma = \beta = \frac{1}{4}; \quad \lambda = \frac{\kappa}{L^2}\alpha = 6\frac{\kappa}{L^2}$$

with $T_m(t)$ given by equation (35), we obtain:

$$T_s(t) = Ve^{r_1 t}\left[\frac{1}{2} + \frac{\frac{1}{4}\left(1 + \frac{12}{N}\right)}{\sqrt{\left(1 + \frac{6}{N}\right)^2 - \frac{6}{N}}}\right]\left(\frac{1 + \frac{r_1}{6}}{1 + \frac{r_1}{24}}\right) \tag{46}$$

In Table 3 the results of this formula are compared with those of precise analysis. Again, the agreement is excellent.

Table 3 Approximate and exact surface-temperature ratios, T_s/V, for Newtonian cooling of solid rod

	$\tau = 2$	
$hL/k = N/2$	T_s/V (exact)	T_s/V (approx.)
0.5	0.154	0.152
1.0	0.0334	0.0329
2.0	0.00367	0.00368

APPENDIX 1

The approximating differential equation for $Y(t)$ will here be derived. The response function $Y(t)$ is defined to be related to the forcing function $G(t)$ as follows:

Definition 1

$$Y(t) = \int_0^t H(t-u)G'(u)du + G(0)H(t) \tag{47}$$

where both H and G are known functions. Concerning them we make the following assumptions:

Assumption 1. For $t \geq 0$, $G(t)$ is continuous, with continuous first and second derivatives. Its third derivative is sectionally continuous.

Assumption 2. For $t > 0$, $H(t)$ is continuous, with a sectionally continuous first derivative. The integral

$$\int_0^\infty |H'(u)|u^n du$$

exists for $n = 0$, 1, and 2.

By differentiation of equation (47) and a change of variable in the convolution integral, we obtain:

$$Y'(t) = H(0)G'(t) + G(0)H'(t) + \int_0^t H'(t-u)G'(u)du \tag{48}$$

Combination of equations (47) and (48) then readily gives:

$$Y'(t) + \lambda Y(t) = H(0)G'(t) + G(0)H'(t) + \lambda G(0)H(t) + \int_0^t \{H'(u) + \lambda H(u)\} G'(t-u)du \tag{49}$$

where λ may be, so far, any arbitrary constant.

To permit a compact representation of results, we now introduce an auxiliary function $g(t)$. Thus:

Definition 2

$$g(t) = \int_0^\infty H'(t+u)\left(u - \frac{\lambda}{2}u^2\right)du \tag{50}$$

with λ chosen so that $g(0) = 0$. Alternatively, equation (50) can be written as:

$$g(t) = \int_t^\infty H'(u)\left\{(u-t) - \frac{\lambda}{2}(u-t)^2\right\}du \tag{51}$$

Differentiation then gives successively:

$$g'(t) = \int_t^\infty H'(u)\{-1 + \lambda(u-t)\}du \tag{52}$$

$$g''(t) = H'(t) - \lambda\int_t^\infty H'(u)du \tag{53}$$

$$= H'(t) - \lambda\{H(\infty) - H(t)\} \tag{54}$$

Or

$$H'(t) + \lambda H(t) = g''(t) + \lambda H(\infty) \tag{55}$$

With the use of equation (55), the last integral in equation (49) can be integrated successively by parts. Thus:

$$\int_0^t \{H'(u) + \lambda H(u)\} G'(t-u)du$$

$$= \int_0^t \{g''(u) + \lambda H(\infty)\}G'(t-u)du$$

$$= \lambda H(\infty)[G(t) - G(0)] + G'(0)g'(t) - G'(t)g'(0) + G''(0)g(t) + \int_0^t G'''(t-u)g(u)du \tag{56}$$

Hence:

$$Y'(t) + \lambda Y(t) = G(0)[H'(t) + \lambda H(t) - \lambda H(\infty)] + G'(0)g'(t) + G''(0)g(t) + \lambda H(\infty)G(t) + \{H(0) - g'(0)\}G'(t) + \int_0^t g(t-u)G'''(u)du \tag{57}$$

$$\therefore Y'(t) + \lambda Y(t) = \lambda H(\infty)G(t) + \{H(0) - g'(0)\}G'(t) + G(0)g''(t) + G'(0)g'(t) + G''(0)g(t) + \int_0^t g(t-u)G'''(u)du \tag{58}$$

Assumption 3

$$|H'(u)| \leq Ae^{-nu}; \qquad \begin{matrix} u \geq u_0 \\ n > 0 \end{matrix} \tag{59}$$

For $t \geq u_0$ we can use inequality (59) in equation (50) to get:

$$|g(t)| \leq Ae^{-nt}\int_0^\infty e^{-nu}\left[u + \frac{|\lambda|}{2}u^2\right]du \leq \frac{A}{n^2}\left(1 + \frac{|\lambda|}{n}\right)e^{-nt} \tag{60}$$

Furthermore, because $g(0) = 0$ and $g(t)$ exists for all t by virtue of the properties of H given under assumption 2, there exists a constant B, dependent on the properties of H, such that:

$$|g(t)| \leq Be^{-nt}; \qquad t \geq 0 \tag{61}$$

In a similar manner, using equations (52), (53), and inequality (59), we can prove that, for $t \geq u_0$:

$$|g'(t)| \leq \frac{A}{n}\left(1 + \frac{|\lambda|}{n}\right) e^{-nt} \tag{62}$$

$$|g''(t)| \leq A\left(1 + \frac{|\lambda|}{n}\right) e^{-nt} \tag{63}$$

The inequalities (60), (62), and (63), when used in equation (58), show how the influence of the initial derivatives of the forcing function fades away.

An upper bound can be established for the convolution integral in equation (58). Thus

$$\left|\int_0^t g(t-u)G'''(u)du\right| = \left|\int_0^t G'''(t-u)g(u)du\right|$$

$$\leq |G'''|_{\max}\int_0^t Be^{-nu}du \tag{64}$$

$$\therefore \left|\int_0^t g(t-u)G'''(u)du\right| \leq |G'''|_{\max}\frac{B}{n}\,1 - e^{-nt}) \tag{65}$$

We are thus led to considering equation (58) as an approximating differential equation, written in the form:

$$Y'(t) + \lambda Y(t) = \lambda H(\infty)G(t) + \{H(0) - g'(0)\}G'(t) + \mathcal{E}(t) \tag{66}$$

where the residual term $\mathcal{E}(t)$ is generally small, and for $t \geq u_0$ satisfies the inequality:

$$|\mathcal{E}(t)| \leq A\left(1 + \frac{|\lambda|}{n}\right)\left[\frac{|G''(0)|}{n^2} + \frac{|G'(0)|}{n} + |G(0)|\right] e^{-nt} + |G'''|_{\max}\frac{B}{n}\,(1 - e^{-nt}) \tag{67}$$

Consequently, the residual term has an asymptotic value not greater than $|G'''|_{\max}\left(\frac{B}{n}\right)$.

To evaluate the error in $Y(t)$ incurred through the neglect of $\mathcal{E}(t)$, we first examine the exact solution of equation (66). Thus:

$$Y(t) = Y(0)e^{-\lambda t} + e^{-\lambda t}\int_0^t e^{\lambda u}[\lambda H(\infty)G(u) + \{H(0) - g'(0)\}\,G'(u)]du + e^{-\lambda t}\int_0^t e^{\lambda u}\mathcal{E}(u)du \tag{68}$$

Portions of the last integral in equation (68) can be integrated by parts to obtain this error term in more convenient form.

$$e^{-\lambda t}\int_0^t e^{\lambda u}\mathcal{E}(u)du = e^{-\lambda t}\int_0^t e^{\lambda u}\{G(0)g''(u) + G'(0)g'(u) + G''(0)g(u)\}\,du + e^{-\lambda t}\int_0^t e^{\lambda u}\left\{\int_0^u g(u-\xi)G'''(\xi)d\xi\right\}du \tag{69}$$

$$= G(0)g'(t) + G'(0)g(t) - \lambda G(0)g(t) - e^{-\lambda t}G(0)g'(0) + \{\lambda^2 G(0) - \lambda G'(0) + G''(0)\}e^{-\lambda t}\int_0^t e^{\lambda u}g(u)du + e^{-\lambda t}\int_0^t\left\{\int_0^u g(u-\xi)G'''(\xi)d\xi\right\}e^{\lambda u}du \tag{70}$$

Using the inequalities (61), (62), (63), and (65) we can now write:

$$\left|e^{-\lambda t}\int_0^t e^{\lambda u}\mathcal{E}(u)du\right| \leq \frac{A}{n}\left(1 + \frac{|\lambda|}{n}\right)e^{-nt}$$

for $t \geq u_0$

$$\left[|G(0)| + \frac{|G'(0)|}{n} + \frac{|\lambda|}{n}|G(0)|\right] + e^{-\lambda t}|G(0)|\,|g'(0)| + \{\lambda^2|G(0)| + |\lambda|\,|G'(0)| + |G''(0)|\} \times Be^{-\lambda t}\int_0^t e^{(\lambda-n)u}du + |G'''|_{\max}\left[\frac{B}{n}\int_0^t e^{\lambda u}(1 - e^{-nu})du\right]e^{-\lambda t} \tag{71}$$

Assumption 4

$$\lambda \equiv \frac{2\int_0^\infty H'(u)udu}{\int_0^\infty H'(u)u^2du} > 0 \tag{72}$$

It follows from assumption (50) that the *asymptotic* inequality corresponding to equation (71) is:

$$\left|e^{-\lambda t}\int_0^t e^{\lambda u}\mathcal{E}(u)du\right| \leq |G'''|_{\max}\frac{B}{\lambda n}. \tag{73}$$

In view of the preceding analysis, we can make, then, the following statement. Providing assumptions (47) to (50) are applicable, the function $Y(t)$ defined by equation (47) can be found as a solution of the approximating differential equation

$$Y'(t) + \lambda Y(t) = \lambda H(\infty)G(t) + \{H(0) - g'(0)\}G'(t) \tag{74}$$

with the initial condition: $Y(0) = G(0)\,H(0)$.

The approximate $Y(t)$ so-obtained differs from the exact $Y(t)$ by an amount not exceeding in absolute value $|G'''|_{\max}(B/\lambda n)$ as $t \to \infty$.

APPENDIX 2

Assumption 1

$$H(t) = H(\infty) - \sum_{j=0}^{\infty} a_j e^{-\lambda_j t}; \qquad \begin{matrix} a_j > 0 \\ 0 \leq \lambda_0 < \lambda_1 < \lambda_2 \ldots \end{matrix} \tag{75}$$

$$\therefore H'(t) = \sum_{j=0}^{\infty} a_j\lambda_j e^{-\lambda_j t} \tag{76}$$

From equation (50):

$$g(t) = \int_0^\infty \sum_{j=0}^{\infty} a_j\lambda_j e^{-\lambda_j t}e^{-\lambda_j u}\left(u - \frac{\lambda}{2}\,u^2\right)du \tag{77}$$

$$= \sum_{j=0}^{\infty} a_j\lambda_j e^{-\lambda_j t}\left(\frac{1}{\lambda_j^2} - \frac{\lambda}{\lambda_j^3}\right) \tag{78}$$

Since:

$$g(0) = 0 = \sum a_j\left(\frac{1}{\lambda_j} - \frac{\lambda}{\lambda_j^2}\right) \tag{79}$$

$$\therefore \lambda = \frac{\sum_{j=0}^{\infty}\frac{a_j}{\lambda_j}}{\sum_{j=0}^{\infty}\frac{a_j}{\lambda_j^2}} = \lambda_0\frac{\left[1 + \frac{1}{a_0}\sum_{j=1}^{\infty}a_j\frac{\lambda_0}{\lambda_j}\right]}{\left[1 + \frac{1}{a_0}\sum_{j=1}^{\infty}a_j\left(\frac{\lambda_0}{\lambda_j}\right)^2\right]} \tag{80}$$

The summation in the numerator of the last ratio in equation (80) exceeds the summation in the denominator by the amount:

$$\frac{1}{a_0}\sum_{j=1}^{\infty}a_j\frac{\lambda_0}{\lambda_j} - \frac{1}{a_0}\sum_{j=1}^{\infty}a_j\left(\frac{\lambda_0}{\lambda_j}\right)^2$$

$$= \frac{1}{a_0} \sum_{j=1}^{\infty} a_j \frac{\lambda_0}{\lambda_j} \left(1 - \frac{\lambda_0}{\lambda_j}\right) > 0 \quad (81)$$

since every term in the last summation is positive.

$$\therefore \lambda > \lambda_0 \quad (82)$$

Assumption 2

$$\lambda < \lambda_1 \quad (83)$$

Using equations (78), (80), and (83), we can write the following inequality:

$$|g(t)| \leq a_0 \left(\frac{\lambda}{\lambda_0^2} - \frac{1}{\lambda_0}\right) e^{-\lambda_0 t} + \sum_{j=1}^{\infty} a_j \left(\frac{1}{\lambda_j} - \frac{\lambda}{\lambda_j^2}\right) e^{-\lambda_j t} \quad (84)$$

$$< a_0 \left(\frac{\lambda}{\lambda_0^2} - \frac{1}{\lambda_0}\right) e^{-\lambda_0 t} + \left\{\sum_{j=1}^{\infty} a_j \left(\frac{1}{\lambda_j} - \frac{\lambda}{\lambda_j^2}\right)\right\} e^{-\lambda_0 t} \quad (85)$$

However, from equation (79) we obtain the following equality:

$$\sum_{j=1}^{\infty} a_j \left(\frac{1}{\lambda_j} - \frac{\lambda}{\lambda_j^2}\right) = a_0 \left(\frac{\lambda}{\lambda_0^2} - \frac{1}{\lambda_0}\right) \quad (86)$$

Hence we have:

$$\therefore |g(t)| \leq \frac{2a_0}{\lambda_0} \left(\frac{\lambda}{\lambda_0} - 1\right) e^{-\lambda_0 t}$$

The constants of the dominating function of equation (61) are then identified as:

$$B = \frac{2a_0}{\lambda_0} \left(\frac{\lambda}{\lambda_0} - 1\right); \qquad n = \lambda_0 \quad (87)$$

The values listed below are readily derived from formulas in reference [3] (p. 97, equation (10), for the slab; and p. 199, equation (6), for the cylindrical rod).

	B	n
Symmetrically heated slab	$0.0087 \frac{L^2}{\kappa}$	$2.47 \frac{\kappa}{L^2}$
Cylindrical rod	$0.0087 \frac{L^2}{\kappa}$	$5.80 \frac{\kappa}{L^2}$

References

1 R. V. Churchill, "Modern Operational Mathematics in Engineering," McGraw-Hill Book Company, Inc., New York, N. Y., 1944, p. 193.

2 M. Jakob, "Heat Transfer," John Wiley & Sons, Inc., New York, N. Y., 1949, pp. 274, 278.

3 H. S. Carslaw and J. C. Jaeger, "Conduction of Heat in Solids," Oxford University Press, London, England, 1959, p. 105.

DISCUSSION

John S. Thomsen[2]

The author has presented an interesting and useful approach for simplifying many complicated heat transfer calculations. However, it seems worth while to emphasize certain limitations of this technique.

First, it should be stressed that this method is derived only for the case where the initial temperature is zero throughout the solid. In his first example the author successfully applies the differential equation to a slab at constant initial temperature V; but this problem may be restated with zero initial temperature by a rather trivial change of variable. However, with more complicated initial conditions (e.g., $V \cos 3\pi x/2L$), the lumped parameter solution may be in error by an order of magnitude.

Second, it should be emphasized that the error criterion involving $|G'''|_{max}$ is applicable only to the asymptotic solution, as indicated in connection with equation (73), Appendix 1. This implies that $\tau \gg 1$. In many cases the asymptotic solution is known by inspection; for instance, in the first example treated by the author, the asymptotic solution is identically zero. In other cases, where the asymptotic solution is not so trivial, the chief interest may lie in the solution for moderate values of τ. Hence, even when $|G'''|_{max}$ exists, the error criterion must be applied with caution and may be of limited value.

It is interesting to consider under what circumstances the lumped parameter method can give a good approximation to the transient. The transient portion of the temperature solution for a slab of thickness $2L$ ($0 \leq x \leq 2L$) with temperature prescribed at the two faces is of the form[3]

$$\sum_n a_n e^{-n^2\pi^2\tau/4} \sin(n\pi x/2L) \quad (88)$$

(Note that the origin is at the left, rather than the center.) The mean temperature is found by integrating over the entire slab and dividing by the thickness $2L$, giving

$$\sum_{\text{odd } n} \frac{2a_n}{n\pi} e^{-n^2\pi^2\tau/4} \quad (89)$$

Since the even harmonic terms have vanished and the remaining odd amplitudes have been divided by n, the series for the mean temperature converges much more rapidly than that for temperature at a fixed point. Noting the effect of the exponential terms, one sees that the first term will usually provide a good approximation to the sum for very moderate values of τ.

Now the lumped parameter method gives a first-order ordinary differential equation, which permits only a single exponential term in the transient solution. Obviously, a single exponential cannot represent precisely the infinite sum in equation (89). However, a good approximation may be possible when the first term in the sum is sufficiently large compared to all the others. Clearly, this condition is satisfied much better for mean temperature than for temperature at a fixed point. In the case of temperature at a fixed point, equation (88) shows that the condition holds better for points near the center of the slab than for those close to one face.

Numerical examples computed by the writer tend to confirm the above considerations. For example, the exact and approximate temperature solutions were computed at a point a distance $L/3$ from the face of the slab in the first example considered by the author. The error is defined as $(T_m/V)_{approx} - (T_m/V)_{exact}$. A comparison of temperature error at this fixed point and mean temperature error (from Table 1 of the paper) is shown:

τ	Error at fixed point	Error in mean temperature
0.02	−0.20	−0.07
0.05	−0.056	−0.015
0.1	0.027	0.013
0.3	0.026	0.003

It may be noted that the lumped parameter technique can easily be extended by treating a number of simple examples and

[2] Assistant Professor, Department of Mechanical Engineering, Johns Hopkins University, Baltimore, Md.

[3] H. S. Carslaw and J. C. Jaeger, "Conduction of Heat in Solids," Oxford University Press, London, England, second edition, 1958, chap. 3.

using the principle of superposition, as is done in obtaining exact solutions. For example, one can thus show that equation (25) applies to a slab with asymmetrical boundary conditions provided that T_s is taken as the mean temperature of the two faces. As stated by the author, the lumped parameter method may well be useful in fields other than heat transfer. It can be applied not only to reduce distributed parameter systems to lumped parameter ones, but also to reduce complex cases with lumped parameters to much simpler models.

Author's Closure

The author appreciates the interest and comments of Professor Thomsen, but believes that his interpretations of the method presented in the author's paper are in certain respects incorrect and overrestrictive.

As Professor Thomsen states, the differential equations for flat slabs and cylindrical rods are, indeed, derived for the case of zero initial temperature. This case subsidiarily includes all initial distributions which might be attained by various applications of surface temperature and uniformly distributed heat generation, since the system can always be "prepared" by applications of the forcing functions prior to the times of special interest for the investigation. In the use of such a simple artifice, the $|G'''_{max}|$ of the error term must cover the behavior of the forcing function during the preparation time, as well as during the time of special interest. Preparatory temperature distributions corresponding to second-degree time behavior of the surface temperature can be attained with vanishingly small error.

Despite the generality so simply attained from a solution which is apparently restricted, by no means all conceivable cases are included by the generalization. Professor Thomsen has cited such an exceptional case. Such exceptional cases would involve the action of agencies other than the specified forcing functions at times close to the times of interest, or perhaps even construction of the system immediately prior to the process being investigated. For example, the initial temperature distribution adduced by Professor Thomsen [i.e., $T = V \cos(3\pi x/2L)$] is incompatible with symmetry or insulation at $x = L$. How is such an "initial" temperature distribution to be brought about? Ways can be named, but they often become pathological, rather than practical, in character. It is actually the exceptional, rather than the usual case where an engineer starts to analyze a system "on the fly," instead of beginning from some simple, or equilibrium condition.

The second point raised by Professor Thomsen is that "the error criterion involving $|G'''_{max}|$ is applicable only to the asymptotic solution . . ." This quoted statement is definitely incorrect. The formula for the error term becomes asymptotically correct for large time, but there is no necessity for the solution of the problem to be asymptotic as well. For example, equation (26) might, during the initial moments of a reactor's operation, yield an error (for the mean fuel temperature) greater than the asymptotic error. However, thereafter the asymptotic error formula would apply despite noncyclic or varied operation of the reactor. Application of the error formula to the problem stated in equation (36), with its attendant asymptotic solution, came about because of the author's need for a simple analytical solution, and not because the error formula is inherently limited to such comparisons. Like any error formula, it does, of course, overestimate the actual error once time enough has elapsed for it to be applicable.

The third point raised by Professor Thomsen concerns the accuracy of the lumping method for prediction of local temperatures as contrasted with mean temperatures. He shows that in the slab problem treated by the author the temperature at a position one third of the way from the exposed to the insulated face is predicted with less accuracy than is the mean slab temperature. The author is inclined to agree with Professor Thomsen that this feature may often be present. But it would certainly be possible to cite counterexamples. In the course of developing this portion of the discussion, Professor Thomsen states that "the lumped parameter method gives a first order ordinary differential equation, which permits only a single exponential term in the transient solution." Presumably, this statement is intended to apply only to the special example under discussion, since an *inhomogeneous* first order differential equation with constant coefficients for its homogeneous part need not possess such character in general.

Professor Thomsen's mention of additional uses of the lumping method is appreciated. It is the author's belief that the basic lumping technique has utility well beyond the special heat-conduction examples contained in the paper.

M. ALTMAN
Missile and Space Vehicle Department,
General Electric Company,
Philadelphia, Pa.

R. H. NORRIS
General Engineering Laboratory,
General Electric Company,
Schenectady, N. Y.
Mem. ASME

F. W. STAUB
General Engineering Laboratory,
General Electric Company,
Schenectady, N. Y.
Assoc. Mem. ASME

Local and Average Heat Transfer and Pressure Drop for Refrigerants Evaporating in Horizontal Tubes

A test facility is described that has been constructed to investigate local heat transfer and pressure drop for evaporating or condensing refrigerants. The empirical method of B. Pierre [1][1] for correlating the average heat-transfer coefficients of refrigerants evaporating in horizontal tubes is presented in conjunction with the data of several authors [3–6]. Data on local heat-transfer coefficients and pressure drop are presented for Refrigerant-22 evaporating in two 4-ft-long, 0.343-in-ID straight horizontal tubes, and are correlated by a refinement of the curve proposed in [1]. The procedure of Martinelli-Nelson [9] correlated the data for local pressure drop within 15 per cent.

Introduction

Increasing emphasis is being placed on the optimization of evaporators. Airborne refrigerant evaporators in particular have placed a premium on minimum size and weight. An improved knowledge of the local evaporating heat transfer and pressure drop is therefore mandatory before true optimization can be accomplished.

The correlations of heat transfer for evaporating refrigerants of widest established scope seem to be the two developed by Pierre [1]. These correlations apply to several different refrigerants, namely, Refrigerant-11, 12, and 22 and to CH_3Cl, and are summarized in references [1] and [2]. They appear reasonably consistent with all the test results published by other authors, references [3], [4], [5], and [6], for the rather wide range of variables considered by Pierre.

The major objection to Pierre's correlations is that they consider only the average, not the local, heat-transfer coefficient and that the outlet conditions are either at 11 deg F superheat or well below 90 per cent vapor quality. The nature of any dependence of the heat transfer on local quality is therefore not considered in Pierre's work.

For pressure drop, no general correlation empirically confirmed for conventional refrigerants seems to be available.

To determine the local heat transfer and pressure drop for evaporating (or condensing) refrigerants, an experimental facility was designed and constructed at the General Engineering Laboratory of the General Electric Company. This equipment is briefly described and preliminary data on the local heat transfer and pressure drop for Refrigerant-22 evaporating in a 0.343-in-ID, 4-ft-long horizontal tube are presented. The data of Pierre are also given in this paper since the available published form of his results are to be found only in Swedish periodicals.

The Martinelli-Nelson method of calculating two-phase pressure drop inside pipes was extended for use with Refrigerant-22 and was then employed to correlate the pressure-drop data in this investigation.

The Refrigerant-22 flow rate was varied from 38 lb per hr to

[1] Numbers in brackets designate References at end of paper.

Contributed by the Heat Transfer Division and presented at the Annual Meeting, Atlantic City, N. J., November 29–December 4, 1959, of The American Society of Mechanical Engineers.

Manuscript received at ASME Headquarters, September 28, 1959. Paper No. 59—A-278.

Nomenclature

c = specific heat at constant pressure, Btu/lb deg F
D = inside tube diameter, ft
g_0 = conversion factor = 4.18×10^8, $\frac{\text{lb mass ft}}{\text{lb force hr}^2}$
G = mass velocity, lb/hr sq ft
h = local heat-transfer coefficient, Btu/hr sq ft deg F
h_{AVE} = average heat-transfer coefficient, Btu/hr sq ft deg F
J = mechanical equivalent of heat 778.26 ft-lb/Btu
k = thermal conductivity, Btu/hr ft deg F
K_f = load factor = $\frac{J\Delta x\lambda}{L}$, dimensionless
L = tube length, ft
N_{Nu} = Nusselt number = hD/k, dimensionless
N_{Pr} = Prandtl number = $c\mu/k$, dimensionless
N_{Re} = Reynolds number = GD/μ, dimensionless
ΔP_0 = pressure drop due to friction assuming all of the Refrigerant-22 flow is in the liquid phase
ΔP_{TPF} = pressure drop due to friction during two-phase (annular) flow at the same total flow rate as ΔP_0
r_2 = multiplier as defined in Fig. 9, cu ft per lb
T = temperature, deg F
x_{in} = inlet-vapor quality to test section (per cent/100 unless otherwise specified)
x_m = arithmetic mean vapor quality in test section (per cent/100 unless otherwise specified)
x_{out} = outlet-vapor quality from test section (per cent/100 unless otherwise specified)
Δx = vapor quality change (per cent/100 unless otherwise specified)
λ = latent heat of vaporization (Btu/lb)
μ = dynamic viscosity, lb/hr ft
ρ = density, pcf

Subscripts

L = pertaining to liquid phase
V = pertaining to vapor phase

300 lb per hr at saturation temperatures of 75 and 40 F. Inlet conditions to the test section were varied from 20 to 99 per cent by weight of vapor and outlet conditions ranged from 40 per cent by weight of vapor to 25 deg F superheat.

Apparatus and Test Procedure

Apparatus. The basic schematic of the associated apparatus is shown in Fig. 1. The system consists of three circuits, a refrigerant circuit, a refrigerant condenser coolant (water-alcohol solution) circuit, and a test section heating (water) circuit. The refrigerant is pumped through its circuit by a liquid-refrigerant, canned-rotor pump. A float-type flow meter, whose float is magnetically coupled to the indicating scale, measures the liquid flow rate. Heater (A) is a 14-kw, 15,000-Btu/hr per sq ft heating surface boiler designed to raise the refrigerant to a maximum vapor quality of 90 per cent. Heater (B) is a 1-kw superheater and the refrigerant condenser is a concentric double-tube counterflow unit. The pressurizer is supplied with a heater to provide the desired saturation temperature in the test section. The sealed refrigerant circuit maintained the Refrigerant-22 ($CHClF_2$, Allied Chemical and Dye Corporation) at an oil content that changed from 0.007 to 0.019 per cent by weight in a four-month period and an air content that changed from 0.18 to 0.23 mole per cent in the same time interval.

When the liquid refrigerant already contains enough air to provide a saturated solution, the data of reference [1] indicate that addition of more air has a negligible effect. Furthermore, oil content in amounts less than 10 per cent by volume appears to have a negligible effect on heat transfer judging from Pierre's results [2]. Since these conclusions only apply to the medium and low-vapor-quality region, however, their effect not being investigated at higher qualities by reference [1] or [2], both the air and oil content were kept low and constant in this investigation to eliminate any effect that they may have on the transfer of heat.

The refrigerant condenser coolant is also pumped through a closed loop as shown in Fig. 1 so that a constant coolant-inlet temperature and temperature difference is maintained across the condenser. The latter is achieved by using a false (heating) load and bypass in the chiller circuit so that "on-off" type operation is avoided. A precision flow meter and Beckman differential thermometers (see Test Section) are employed to obtain an accurate measure of the heat removed from the refrigerant. The closed-loop comprising the test section heating circuit uses an electrical heater and measured heat rejection to a drain to give a constant coolant-inlet temperature to the test section. This naturally implies that the minimum heat addition to the test section is limited by the heat gain of the water from the pump and the environment. With the exception of the bronze water pumps, the only construction materials employed in the system were copper, stainless steel, and plastic foam insulation.

Test Section. The test section, shown schematically in Fig. 1, consisted of two 4-ft long sections of 0.343-in-ID straight, smooth copper tubing connected by a $4^1/_2$-in-radius U-bend, through which the refrigerant was circulated. The two 4-ft-long sections are enclosed by two 0.666-in-ID copper tubes to provide an annulus through which the heating water was passed. The height of this annulus was kept large enough to yield a reasonable pressure drop when sufficient water is circulated to restrict the water-temperature drop to 1 deg F and 3.5 deg F at heat-flux values of 2000 Btu/hr sq ft and 20,000 Btu/hr sq ft, respectively. These bulk water temperature changes were necessitated by the requirement that the local heat-flux variation, outside of the entrance region, be no more than ±10 per cent from the average heat flux for the total 4-ft length. The maximum height of the annulus was limited by the requirement that the length to equivalent diameter had to be greater than 150 to minimize the entrance effects.

To admit the heating medium to the annulus uniformly around the circumference of the inner tube, rectangular holes were cut in the outer jacket which, in turn, was surrounded at each end by a $2^3/_8$-in-OD inlet chamber, Fig. 2. When the effective total inlet-hole area was 1.2 times the annulus area, the velocity

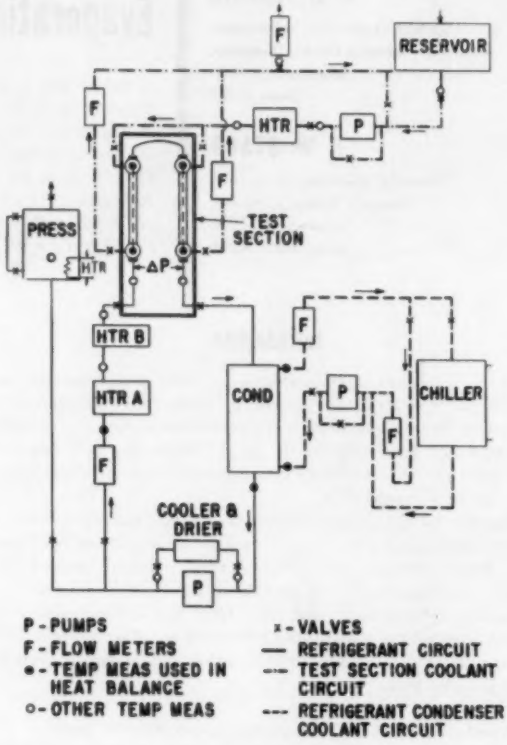

Fig. 1 Schematic of apparatus

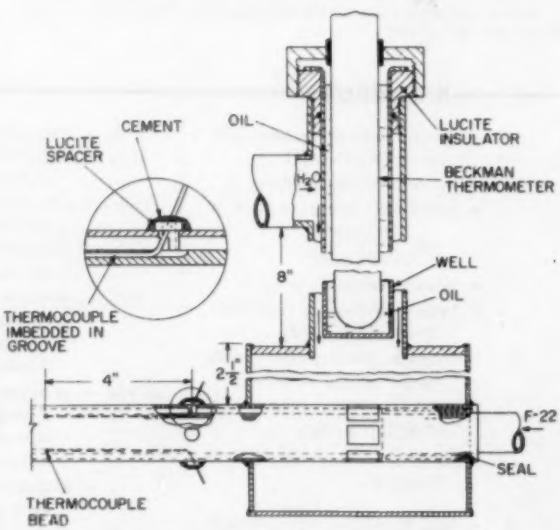

Fig. 2 Schematic of test-section inlet

through the inlet parts was about 12 times greater than the distribution velocity in the inlet chamber around the outside of the jacket.

The absolute and differential temperatures of the heating medium were measured across each 4-ft section. While calibrated immersion thermocouples were suitable for the measurement of the absolute temperature, Beckman differential thermometers were used to measure the water-temperature change to ±0.01 deg F. Although these units may be obtained with a Bureau of Standards corrections to 0.002 deg F, the maximum calculated conduction error in the well assembly shown in Fig. 2 was 0.006 deg F. This rather low error was obtained by immersing 10 in. of thermometer length in an oil-filled well with about a $^1/_{16}$-in. radial clearance and by inserting this well in an insulated pipe with a $^1/_8$-in. radial clearance through which the circulating water passed at high velocity. The well was attached to the enclosing pipe through a lucite section which served as a thermal insulator. An error of as much as 0.1 deg F would have resulted if the Beckman thermometers had been directly exposed to the water due to the compression of the mercury bulb by the pressure differential between the inlet and outlet.

Each of the two 4-ft sections was separately and identically instrumented to yield basic data on the evaporating refrigerant. Six 0.019-in-OD concentric sheathed copper-constantan thermocouples were imbedded in grooves cut into the inner tube of each section and subsequently filled with soft solder. Two thermocouples were placed 180 deg apart on the tube, 6 in. in from each end of the 4-ft section, to avoid the thermal entrance region, and two were placed in the center of the 4-ft section. Each thermocouple was imbedded for a length of 4 in. in the tube to avoid the local turbulence created by plastic supports which led the thermocouples out of the test section through the outer tube, Fig. 2. Calculations indicated that, when about 0.010-in. of insulating cement was placed over the thermocouple bead, the difference between the read temperature and the actual inside wall temperature next to the refrigerant is about 0.1 deg F when the refrigerant film temperature difference is 10.0 deg F.

To limit the instrumental error to a minimum, the differential temperature between the refrigerant and the tube wall was measured directly using a differential thermocouple circuit between the refrigerant inlet and discharge temperatures and the tube-wall temperatures. The inlet and discharge thermocouples were inserted in 9-in-long, $^3/_{16}$-in-OD stainless-steel wells (maximum conduction error 0.01 deg F) which were placed axially into $1^1/_4$-in-ID, 11-in-long mixing chambers attached to the inner tube outside of the water-jacketed test section. All thermocouples on the test section, as well as those used to obtain a heat balance, were initially calibrated and were read with a precision potentiometer, and light-beam galvanometer to an accuracy of ±0.1 deg F.

Test-section pressure drop was recorded with a differential pressure transmitter which was operated at a point where its accuracy was about ±3 per cent of the reading. A pneumatic diaphragm-type transmitter was used to prevent diffusion of air into the refrigerant.

Test Procedure. After steady-state conditions were attained in the system, all measurements were obtained every 20 min over a minimum 2-hr period. The heat flux to the refrigerant was obtained from the water flow and temperature change.

There are two Beckman thermometer wells at the water inlet of each side of the test section and one well at the discharge side. Two thermometers were inserted at the inlet until equilibrium was obtained, at which point one of the thermometers was transferred to the discharge side while the first unit provided the reference temperature.

When the water-temperature drop varied by no more than ±3 per cent for a 1-hr period, equilibrium was assumed. The local heat-transfer coefficient was then determined by dividing the heat flux by the measured refrigerant-to-wall temperature difference. This temperature difference did not vary by more than 12 per cent of its value at the test-section inlet along the length of each 4-ft section. Inlet-vapor quality was calculated from the measured inlet-liquid enthalpy to heater (A) and the electrical heat input to the heaters. The average vapor-quality change in each of the 4-ft sections was about 15 per cent (Table 1).

To achieve a heat balance, the discharge enthalpy from the test section, as determined by the measured net heat input from the heaters (A) and (B) and the test-section coolant, was compared to the test-section discharge enthalpy as determined by the measured heat removal in the refrigerant condenser. The measured liquid enthalpies at the entrance to heater (A) and the exit of the refrigerant condenser were used as the base points in the computation of the heat balance. After correcting for the calibrated heat loss to the environment, the mean calculated heat balance was ±5 per cent. In a series of four identical runs performed over a 4-month interval, the repeatability of the heat-transfer coefficient was well within ±10 per cent of the experimental correlation.

Results

Correlations of B. Pierre. In references [1] and [2] B. Pierre of the Royal Institute of Technology (Stockholm) describes his investigation of boiling heat transfer with Refrigerant-12 and 22, in horizontal test sections. These sections consisted of tubes 12 mm and 18 mm diam and from 4.08 m to 9.5 m long.

The most significant empirical correlations deduced by Pierre were two dimensionless relations, one for outlet-vapor qualities well below 90 per cent, and one for complete evaporation where the outlet condition was 11 deg F superheat. The results of Pierre, as well as the ranges of saturation temperature and quality change, are reproduced in Figs. 3 and 4 for incomplete and complete evaporation, respectively.

The correlation for incomplete evaporation is:

$$h_{avg}D/k_L = 0.0009[(GD/\mu_L)^2(J\Delta x\lambda/L)]^{0.5} \qquad (1)$$

for

$$10^9 < N^2_{Re}K_f < 0.7 \times 10^{12}$$

and for complete evaporation

$$h_{avg}D/k_L = 0.0082[(GD/\mu_L)^2(J\Delta x\lambda/L)]^{0.4} \qquad (2)$$

for

$$10^9 < N^2_{Re}K_f < 0.7 \times 10^{12}$$

It is emphasized that the large quality change in the experiments of B. Pierre implies that the heat-transfer coefficients in (1) and (2) are average values over the quality changes given in Figs. 3 and 4. Data of other authors, references [3], [4], [5], and [6], for incomplete evaporation of Refrigerants-11, 12, and CH_2Cl have been plotted using Relation (1) and are shown in Fig. 5. Correlation equivalent to that with the data of Pierre is achieved. Again the data of these authors are average rather than local.

Without boiling, the heat-transfer coefficient for turbulent forced convection is proportional to $N_{Re}^{0.8}$ and independent of the wall-to-refrigerant ΔT. In the region of strong nucleate boiling the heat-transfer coefficient is proportional to ΔT^n, where n varies from 2 to 3 and is a much weaker function of mass-flow rate. In discussing the data of Dengler, McAdams [8] states that . . . . "the local heat-transfer coefficient (for water vaporized in a 1-in. vertical tube under forced flow) was controlled by the combined influence of boiling and forced convection. At low flow rates and weight fractions of vapor the coefficient increased with increase in ΔT . . . . . At high mass-flow rates the coefficient

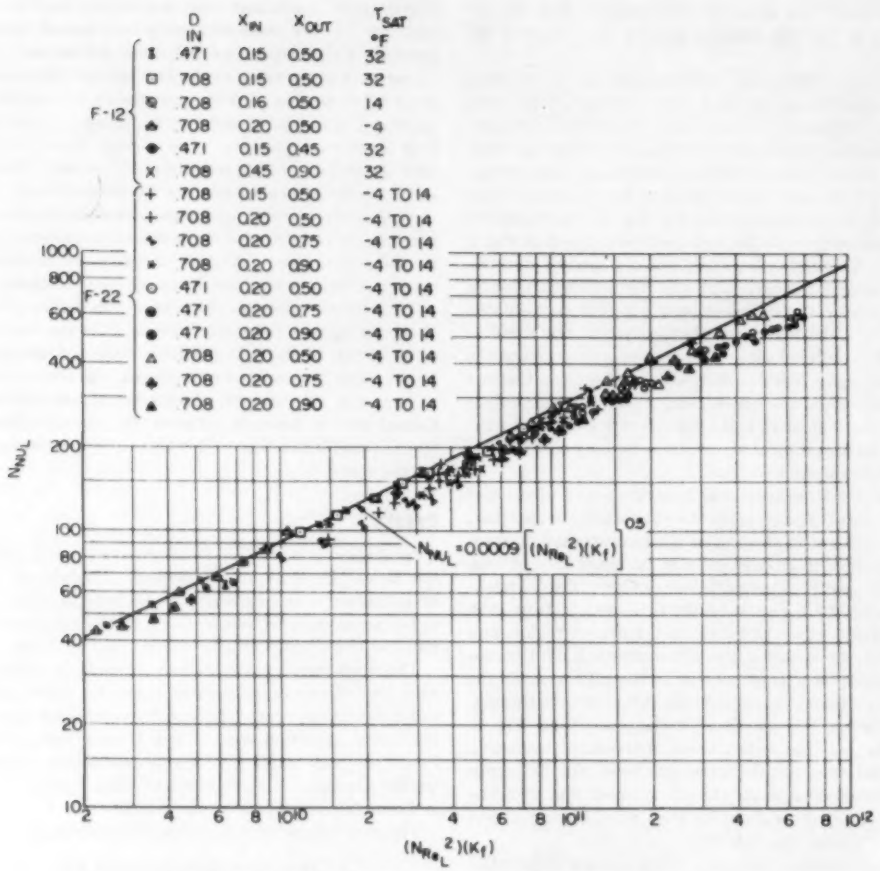

Fig. 3 Data of B. Pierre for exit-vapor qualities below 90 per cent

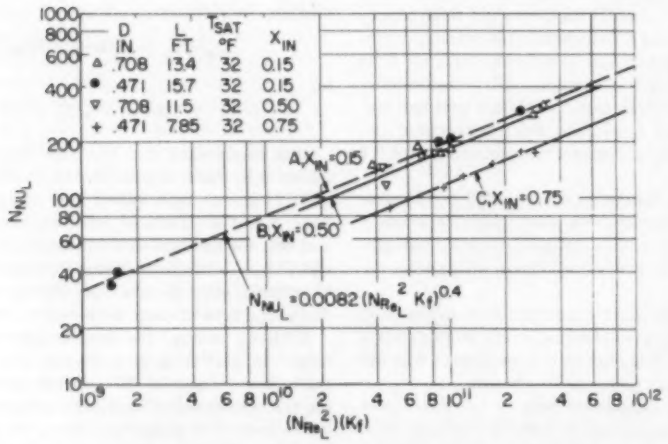

Fig. 4 Data of B. Pierre for evaporation of F-12 to an exit condition of 11 deg F superheat

Table 1 Test data

Symbol	Run No.	Refrigerant Temperature $T_{in,sat}$ °F	Refrigerant Temperature T_{out} °F	Refrig. Flow Lb/Hr	Heat Balance %	Vapor Quality In x_{in} %	Vapor Quality Out x_{out} %	Vapor Quality Mean x_m %	Test Section Pressure Drop Meas. Δp psi	Test Section Pressure Drop Calc. Δp psi	Deviation of (h_{TP}) on Water Side from Relation [3] %	Experimental Refrigerant $\frac{h_{TP}}{h_L}$
○	1A	78.8	—	270	+ 2.93	22.8	39.8	31	2.9	3.4	+ 4	750
♀	1B	—	77.4	270		39.8	59.1	49			+ 9	860
●	2A	77.8	—	297	- 9.49	60.0	77.7	69	4.3	5.1	- 6	725
●	2B	—	75.2	297		77.7	93.0	85			-10	430
□	3A	77.1	—	197	+ 3.88	57.7	76.0	67	2.3	2.4	+12	565
■	3B	—	75.8	197		76	89.6	83			+19	312
◑	4	76.2	74.8	297	- 1.58	85.7	94.1	90	5.1	5.7	- 6	473
▽	5A	76.3	—	134	- 9.16	26.5	36.7	32	0.58	0.72	- 5	370
▽	5B	—	75.8	134		36.7	48.6	43			+ 3	447
▷	6A	77.3	—	292	+10.78	68.9	88.6	79	3.75	5.2	0	154
△	6B	—	79.0	292		88.6	100 sat.	95			0	72
◎	7A	78.1	—	264	+ 6.13	22.9	40.7	32	2.28	3.4	+ 5	725
◎	7B	—	76.7	264		40.7	60.2	50			+ 1	680
◎	7A'	76.9	—	265	+ 1.91	24.5	42.8	34	2.7	3.4	+ 7	739
◎	7B'	—	75.6	265	—	42.8	61.4	52			+ 3	744
◑	8A	79.0	—	153	+ 2.10	73.4	99	86	1.63	1.64	+10	445
▲	8B	—	100.0	153	—	99	25% sat. Sup. Vap.				+10	52
◎	36A	39.8	39.6	69	—	19.8	48.4	34.1	0.56	0.60	—	268
◎	36B	39.6	39.4	69	—	48.4	81.8	65.1			—	352
◑	37B	41.2	41.4	70	—	81.5	100	91	0.61	0.74	—	223
◠	38A	80.6	80.6	37.6	—	56.9	78.4	65.1	Neg.		—	194
◠	38B	80.6	81.2	37.6	—	78.4	100	89.2			—	208

* The A and B series refer to the inlet and outlet 4' test section lengths respectively

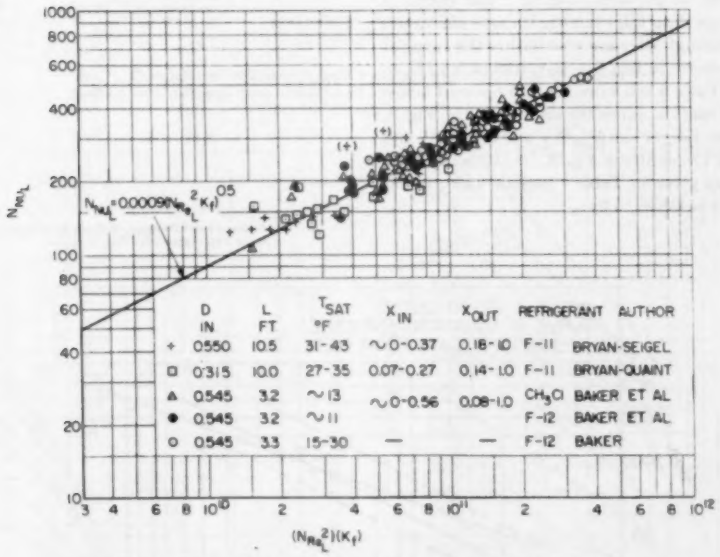

Fig. 5 Degree of correlation obtained with empirical relation (1) of B. Pierre

became independent of ΔT . . . ." Inspection of Relations (1) and (2) and the proportionality $h\Delta T \propto \Delta x$ indicate that h is proportional to $N_{Re}(\Delta T)$ for incomplete evaporation and $N_{Re}^{0.8}(\Delta T)^{0.67}$ for complete evaporation. The low value of the exponent of ΔT and its decreasing value at high vapor qualities point out the somewhat suppressed "turbulence" effect due to nucleate boiling as well as the decreasing effect due to boiling at high vapor qualities (where the thin liquid layer begins to "dry up").

Results of Present Investigation

(a) Heat Transfer—Tube Wall Below Saturation Temperature. The first test run performed on the equipment was entirely in the subcooled region. This provided a brief check on the validity of the data taken. On the refrigerant side, the experimental forced-convection coefficient is within 11 per cent of the value determined by Relation (3),

$$N_{Nu} = 0.027(N_{Re})^{0.8}(N_{Pr})^{1/3}(\mu_b/\mu_w)^{0.14} \tag{3}$$

the familiar correlation of Sieder and Tate. When the (L/D) ratio of the tube is taken into account, the deviation from the expression of Hausen [7] given by Relation (4) is only 7 per cent:

$$N_{Nu} = 0.116[(N_{Re})^{2/3} - 125]N_{Pr}^{1/3} \cdot [1 + (D/L)^{2/3}](\mu_b/\mu_w)^{0.14} \tag{4}$$

On the water side the experiment coefficient was within (−8 per cent) of the values determined by Relation (3). The hydraulic diameter of the annulus was used in (3) for all subsequent data points and the resulting degree of correlation on the water side is shown in Table 1. A heat balance of 2.5 per cent was obtained in the first run, all subsequent heat-balance values are also given in Table 1.

(b) Heat Transfer—Tube Wall Above Saturation Temperature. The test results of this investigation for exit test-section vapor qualities below 80 per cent are correlated by Pierre's Relation (1) for outlet qualities well below 90 per cent (Fig. 6). For values of $N_{Re}^2K_f < 0.6 \times 10^{11}$, these data fall somewhat above the values given by Relation (1), although they are well within the range of data of other authors, as shown in Fig. 6. At values of $N_{Re}^2K_f > 0.6 \times 10^{12}$ the data from Table 1 fall more than 15 per cent below the values given by Relation (1). Since the data of Pierre, Fig. 3, also tend to fall below Relation (1) at $N_{Re}^2K_f > 0.5 \times 10^{12}$, and since no data are given by Pierre above $N_{Re}^2K_f = 0.7 \times 10^{12}$, the best correlation of the data given in Table 1 for exit-vapor qualities less than 80 per cent was taken to be:

For $2.5 \times 10^{10} < N_{Re}^2K_f < 1.5 \times 10^{12}$

$$hD/k_L = 0.0225(GD/\mu_L)^{0.8}(J\Delta x\lambda/L)^{0.4} \tag{5}$$

The pertinent refrigerant properties employed in this investigation are given in Table 2.

Two test runs (6B and 8B in Table 1) were made with inlet qualities 90 per cent or greater. The results of these runs agreed with the conventional forced convection relation for a dry gas (6) within 5 per cent and 19 per cent, respectively.

$$hD/k_V = 0.021(GD/\mu_V)^{0.8}(c_p\mu/k)_V^{0.4} \tag{6}$$

Six data points ranging in average vapor quality from 69 to 90 per cent were not correlated by either Relation (2) or (5). It is expected that the heat-transfer coefficient for vapor qualities above 68 per cent will behave much like that shown in Fig. 14-26, page 398 of reference [8], that is, a nonlinear decrease in h with increasing vapor quality down to the dry-gas value at 100 per cent vapor quality. Insufficient data have been taken so far in this region to warrant any recommended correlation for this investigation.

The dashed lines in Fig. 7 give the data of Pierre also shown in Fig. 4. The plotted values in Fig. 7 were values calculated by integration from the results of this investigation; i.e., Relation (5) and the best approximation from the data of run Nos. 2, 3B, 4, 6, 8, and 37B in Table 1. Although the agreement between our local and Pierre's average results is within 10 per cent, a practical correlation of local data above 68 per cent vapor quality must await additional data.

(c) Pressure Drop. The pressure drop from the inlet to the discharge of the test section was measured for each run, Table 1. This measured pressure drop consists of the sum of the friction drop and the pressure drop due to the momentum change of the accelerating vapor since the gravity effect is absent in a horizontal

Table 2 Liquid Refrigerant-22 properties

Temperature °F	Dynamic Viscosity lb/ft hr μ_L	Density lb/ft³ ρ_L	Specific Heat BTU/lb °F c_L	Thermal Conductivity* BTU/hr ft °F k_L
75	0.57	74.8	0.325	0.052
40	0.62	79.2	0.300	0.059

*Markwood and Benning, DuPont Kinetic Chemical Division, 1942. About 25% higher than data of Riedel.

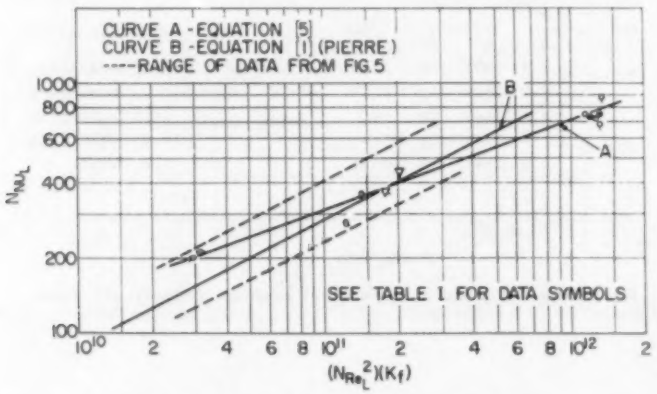

Fig. 6 Correlation of data from Table 1 for exit-vapor qualities below 80 per cent

tube. Martinelli-Nelson [9], in their method of predicting pressure drop during forced-circulation boiling, use the annular-flow model in a tube where the measured pressure drop is taken as the sum of the friction and momentum losses.

The method of reference [9] was used to calculate the pressure drop in the test section since it correlated extensive data, in the case of isothermal two-phase pressure drop for liquids whose Prandtl number range include that of Refrigerant-22, within ±30 per cent [9]. Figs. 8 and 9 were prepared using reference [9] for Refrigerant-22 to permit the evaluation of the friction pressure drop (ΔP_{TPF}) from the pressure drop when only liquid fills the tube at the same mass velocity (ΔP_0) and to allow the determination of the pressure drop due to the increase in vapor momentum. The standard method for calculating single-phase pressure drop in smooth tubes was used to obtain ΔP_0. The pressure drop due to the acceleration of the vapor was computed using the relationship $\Delta P = (r_2)(G^2/g_0)$, Fig. 9.

When the inlet-vapor quality to the test section was other than zero per cent the pressure drop in the test section was calculated by subtracting the pressure drop between zero per cent and the inlet-vapor quality from the pressure drop between zero per cent and the outlet-vapor quality using Figs. 8 and 9. Since uniform heat removal was assumed in this method, the test-section heat flux was employed to determine the "imaginary" tube length between zero per cent and test-section, inlet-vapor quality. The small quality change actually encountered in the test section made this assumption a fairly reasonable one. The pressure drop in the return bend was evaluated using the data of reference [10] for single-phase fluids in conjunction with the actual specific volume of the two-phase mixture existing in the return bend.

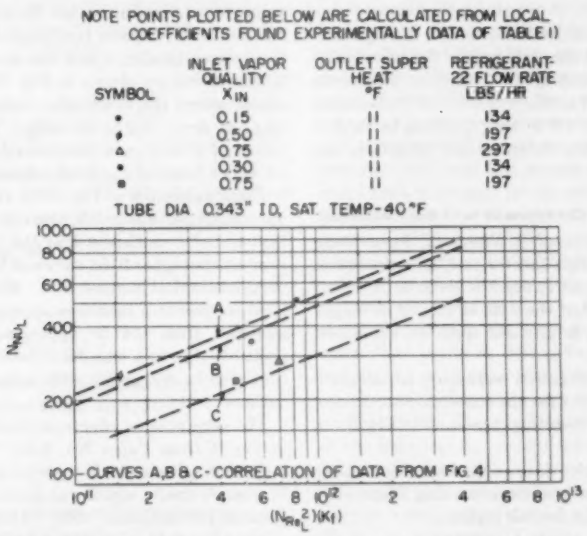
NOTE POINTS PLOTTED BELOW ARE CALCULATED FROM LOCAL COEFFICIENTS FOUND EXPERIMENTALLY (DATA OF TABLE I)
SYMBOL
INLET VAPOR QUALITY X_{IN}
OUTLET SUPER HEAT °F
REFRIGERANT-22 FLOW RATE LBS/HR
• 0.15 11 134
0.50 11 197
△ 0.75 11 297
• 0.30 11 134
■ 0.75 11 197
TUBE DIA 0.343" I.D. SAT. TEMP-40°F
CURVES A,B & C - CORRELATION OF DATA FROM FIG. 4
N_{Nu_L}
$(N_{Re_L}^2)(K_1)$

Fig. 7 Comparison of average heat transfer calculated from local data in Table 1 with average data of reference [2]

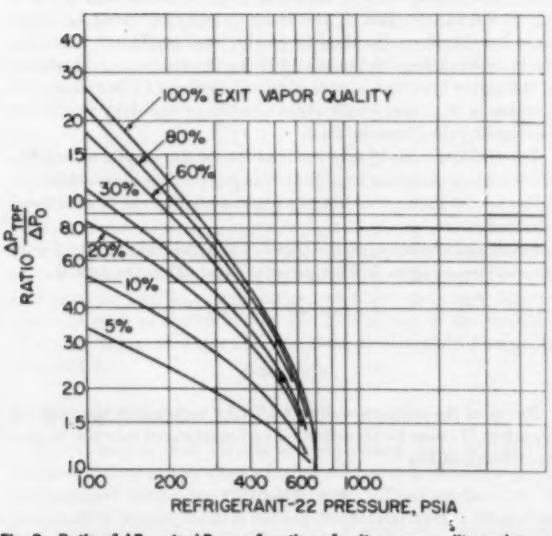

Fig. 8 Ratio of ΔP_{TPF} to ΔP_0 as a function of exit-vapor quality and pressure for zero per cent inlet quality. (Derived from reference [9].)

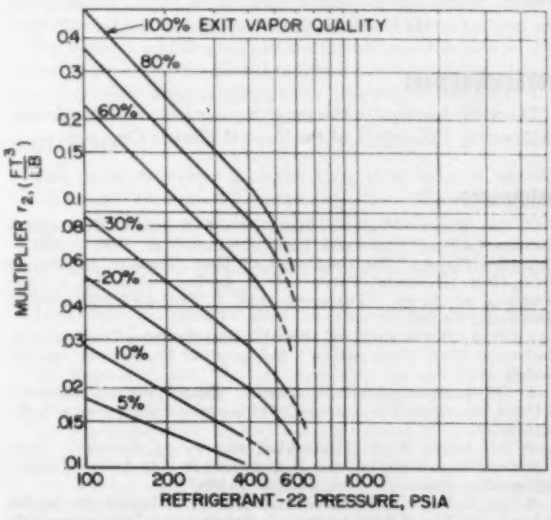

Fig. 9 Multiplier (r_2) versus pressure and exit-vapor quality for zero per cent inlet quality. Pressure drop due to acceleration of fluid during evaporation equals (r_2) (G^2/g_0). (Derived from reference [9].)

As shown in Table 1, of the pressure drop determined for eleven runs, representative of the entire range of conditions investigated, five runs correlated within +5 per cent −10 per cent and nines runs correlated within +5 per cent −20 per cent of the pressure drop as calculated by the method of reference [9].

Summary

Heat Transfer—Evaporation at Exit-Vapor Quantities Below 90 Per Cent.

1 Relation (1) of B. Pierre [1], for exit-vapor qualities well below 90 per cent, correlates his average heat-transfer data for Refrigerants-12 and 22, Fig. 3, within +10 and −20 per cent. Average evaporating heat-transfer coefficients determined by several investigators [3], [4], [5], and [6], for the refrigerants listed in Fig. 5 are correlated with +35 and −20 per cent by the empirical Relation (1) of Pierre.

2 The data in Table 1, on local heat transfer for Refrigerant-22 evaporating in a horizontal tube, fall within the correlation range of Relation (1) as determined by the data from references [1] to [6], Fig. 6, for values of $N_{Re}{}^2K_f < 0.6 \times 10^{12}$. Between values of $0.6 \times 10^{12} < N_{Re}{}^2K_f < 1.5 \times 10^{12}$, the data in Table 1 are correlated by Relation (5) when the exit-vapor quality is less than 80 per cent.

Heat Transfer—Evaporation at Exit Conditions up to 11 deg F Superheat

1 The recommended correlation of B. Pierre [2] for average heat-transfer coefficients for Refrigerants-12 and 22 evaporating in tubes with exit superheat of about 11 deg F is given by Relation (2). Fig. 4 indicates, however, that the data of [2] are no longer correlated by Relation (2) when inlet-vapor qualities exceed 50 per cent.

2 The local data of this investigation were used to calculate the average heat-transfer coefficient for the cases covered by the data of Pierre in Fig. 4. The resulting agreement, Fig. 7, is within 10 per cent.

3 Insufficient local heat-transfer data so far have been taken by the investigators at local vapor qualities exceeding 75 per cent to allow a recommended correlation for this region.

Pressure Drop

Eighty per cent of the data on local pressure drop correlate within +5 and −20 per cent of the pressure drop as calculated by the method of Martinelli-Nelson [9] applied to Refrigerant-22.

Acknowledgment

The work described in this paper was carried out at the General Engineering Laboratory of the General Electric Company.

References

1 Bo Pierre, "Varmeovergangen vid Kokande Koldmedier; Horisontella Ror," *Kylteknisk Tidskrift*, no. 3, May, 1957, p. 129.

2 Bo Pierre, "The Coefficient of Heat Transfer for Boiling Freon-12 in Horizontal Tubes," *S. P. Review*, vol. 2, no. 1, 1955 (English), pp. 55–68. (Published by A. B. Svenska Flaktfabriken, Stockholm, Sweden.)

3 W. L. Bryan and L. G. Siegel, "Heat-Transfer Coefficients in Horizontal Tube Evaporators," *Refrigerating Engineering*, vol. 63, 1955, p. 36.

4 W. L. Bryan and G. W. Quaint, "Heat-Transfer Coefficients in Horizontal Tube Evaporators," *Refrigerating Engineering*, vol. 59, 1951, p. 67.

5 M. Baker, Y. S. Touloukian, and G. A. Hawkins, "Heat Transfer Film Coefficients for Refrigerants Boiling Inside Tubes," *Refrigerating Engineering*, vol. 61, 1953, p. 986.

6 M. Baker, "Heat-Transfer Rates From Heated Horizontal Tubes to Dichlorodifluoromethane," *Refrigerating Engineering*, vol. 64, 1956, p. 35.

7 E. R. G. Eckert, "Introduction to the Transfer of Heat and Mass," McGraw-Hill Book Company, Inc., 1950, p. 115.

8 McAdams, "Heat Transmission," third edition, McGraw-Hill Book Company, Inc., 1954, p. 401.

9 R. C. Martinelli and D. B. Nelson, "Prediction of Pressure Drop During Forced-Circulation Boiling of Water," TRANS. ASME, vol. 70, 1948, pp. 695–702.

10 O. Fritsche and H. Richter, "Flow Resistance in Curved Rough Pipe Lines," *Forschung auf dem Gebiete des Ingenieurwesens*, November-December, 1933, vol. 4, pp. 307–314.

DISCUSSION

S. W. Anderson[2]

The authors are to be commended for a well-presented paper on a subject of particular importance in determining the performance and design of direct expansion type evaporators.

Based on some experimental results we have obtained with a prime tube operating within the region of incomplete evaporation, the local heat-transfer coefficient h is a complex function of both local vapor quality x and the total refrigerant mass velocity G. These effects are shown in Fig. 10 where the vapor fraction increase across the evaporator tube was held approximately constant at $\Delta x = 0.2$ in all cases. The curves shown for constant values of G were each determined by arbitrarily varying the outlet vapor fraction x_{out} from approximately 0.4 to 1.0.

From inspection of Fig. 10 it will be noted that, for x_{out} below approximately 0.8 to 0.9, there is little effect of x_{out} on the local heat-transfer coefficient h at the lower fixed values of G. However, at the higher fixed values of G, an increase in x_{out} results in a very substantial increase in h. For example, at $G = 225{,}000$, the local coefficient h increases approximately 45 per cent when x_{out} increases from 0.4 to approximately 0.9. These effects are probably due to a transition from pool boiling to forced convection type heat transfer with increasing load as discussed in the authors' text.

The same general effects, as shown in Fig. 10, are also indicated in Fig. 4 from Paper No. 2-46, "On Heat Transfer and Flow Pattern for Freon-12 Evaporating in Horizontal Tubes," by P. Worsøe-Schmidt, which was presented at the International Congress of Refrigeration, 1959, Copenhagen, Denmark.

The $(N_{Re})^2(K_f)$ parameter, used in the Pierre correlation, contains only the single vapor quality term Δx and at a given value of G is independent of any change in the outlet vapor fraction x_{out}. For results such as shown in Fig. 10, in the region where $x_{out} < 0.8$ to 0.9, data at the lower values of G could be correlated by the Pierre method since the local coefficient h is relatively independent of the outlet vapor fraction x_{out}. However, at the higher fixed values of G, the local coefficient h increases with increase in x_{out}, and under these conditions the data would not correlate by the Pierre method.

For these reasons it appears that use of the empirical relation of Pierre in correlating local heat-transfer coefficients is subject to rather severe limitations unless supplemented by use of additional parameters.

Using nomenclature of the paper, a general form for the Pierre correlations as given in Equations (1) and (2) of the text is

$$N_{Nu_L} = a[(N_{Re})^2(K_f)]^n \qquad (7)$$

where:

$$a = \text{const}$$

By use of the proportionality, $h\Delta T \alpha \Delta x$, as listed by the authors, Equation (7) may be transformed and rearranged into the dimensional relationship

$$h = B[G\Delta T]^m$$

where

[2] Senior Research Engineer, Carrier Corporation, Syracuse, N. Y.

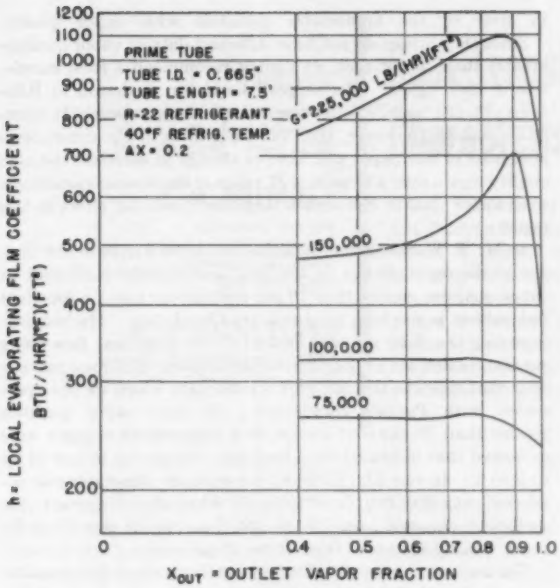

Fig. 10

$$B = \left[\frac{ak_L}{D}\right]^{\frac{1}{1-n}} \left[\frac{AD^3J}{A_s L \mu_L^2}\right]^m \tag{8}$$

A = heat-transfer surface area, ft²
A_s = tube cross-sectional area, ft²

$$m = \frac{n}{1-n}$$

For a particular model, refrigerant and refrigerant temperature, B is constant, and under these conditions from (8)

$$h \alpha [G \Delta T]^m \tag{9}$$

Using the experimental data for the model whose performance is shown in Fig. 10, plots of h versus $G\Delta T$ were made for various values of x_{out} with $\Delta x = 0.2$ to determine the approximate values of m in each case. Results are tabulated below.

x_{out}	Δx	m	n
0.4	0.2	1.0	0.5
0.6	0.2	1.23	0.55
0.8	0.2	1.5	0.6
1.0	0.2	1.5	0.6

From these results it appears that if the performance of a complete evaporator were accurately evaluated from a summation of individual sections, each with say $\Delta x = 0.2$, a set of curves, including an additional parameter, would be necessary for correlations such as shown in Fig. 6. This is due to the variation of n with change in vapor fraction along the length of a complete evaporator.

P. Worsoe-Schmidt[3]

By increasing our knowledge concerning heat transfer in horizontal-tube evaporators which is still most unsatisfactory, the authors have taken up a very useful task. Their approach to the problems is logical as it is indeed from local rather than from average values of the heat transfer that a better understanding shall arise. It is, however, a question whether true, local values may be obtained as an average for a 4-ft section especially at high vapor qualities. Although no details are given in the paper concerning the heat transfer on the water side, it seems probable to assume that the greater resistance to the heat flow is found on the refrigerant side. In this case, rather large variations of the heat flux and, consequently, of the refrigerant film coefficients may occur without corresponding variations in wall-to-refrigerant temperature difference.

At high mass velocities and vapor qualities exceeding 60 to 80 per cent, depending on the flow rate, the present writer has found very abrupt changes of the local heat-transfer coefficients of evaporating Refrigerant-12.[4,5] Contrary to the data shown in Fig. 14-26 of the authors' reference [8], a marked maximum is found for vapor qualities between 80 and 90 per cent. This behavior is explained as the result of a film formation on the tube wall, actually observed as annular or semiannular flow in a glass-tube evaporator. With the rather small inside diameter of the test tubes, the writer would expect an even more pronounced film formation in the present investigation.

If the afore-mentioned assumption is correct, the statement that the local heat flux should not deviate more than ±10 per cent from the average for the test section seems rather questionable. This does not, however, detract from the use of the data obtained, as the test conditions are indeed close to the actual operating conditions for most refrigerating evaporators.

It is true that Professor Bo Pierre's data indicate that even rather heavy contents of oil in Refrigerant-12 does not have any significant effect on the average heat transfer. However, in tests with oil contents in Refrigerant-12 from 1 to 15 per cent by weight, the writer has found that even 1 to 2 per cent oil has a considerable influence on both flow pattern and local heat-transfer coefficients.[4,5] The effect of the oil was an unexpected increase of the heat transfer except for the last part of the evaporator. Due to the fact that electrical heating was applied in these experiments, it is not possible to make a direct comparison of the average values with those obtained by Bo Pierre. Professor Bo Pierre, in reference [1] of the authors, mentions that in a few tests with 4 to 8 per cent oil in Refrigerant-22, the effect of the oil was a lowering of the average heat-transfer coefficient of about 10 per cent. This result may possibly be due to the limited solubility of oil in Refrigerant-22 on the low side.

The writer would like to draw the attention of the authors to a paper by Professor Bo Pierre[6] in which a semiempirical correlation of pressure drop in refrigerating evaporators is presented.

Merl Baker[7]

This paper represents a contribution to an area of research which has not been given adequate attention. The experimental apparatus and test procedure seem quite satisfactory to obtain reliable data. A repeatability of the heat-transfer coefficient over the four-month period within a plus or minus 10 per cent seems reasonably satisfactory.

Admittedly, the authors' data plus data of previous investigators are correlated reasonably well by the Pierre equation, yet

[3] The Danish Refrigeration Research Institute, Copenhagen K, Denmark.

[4] P. Worsøe-Schmidt, "On the Heat Transfer and Flow Pattern for Freon-12 Evaporating in Horizontal Tubes," Paper No. 2-46, 10th International Congress of Refrigeration, Copenhagen, 1959.

[5] P. Worsøe-Schmidt, "Some Characteristics of Flow Pattern and Heat Transfer of Freon-12 Evaporating in Horizontal Tubes," *Ingeniøren*, Int. Ed., vol. 3, no. 3, September, 1959, p. 98.

[6] Bo Pierre, "Strömningsmotstand vid kokande köldmedier" "Flow Resistance of Boiling Refrigerants," in Swedish, *Kylteknisk Tidskrift*, vol. 16, no. 6, December, 1957, p. 225.

[7] Executive Director, Professor, Mechanical Engineering, The Kentucky Research Foundation, University Station, Lexington, Kentucky.

many parameters known to be pertinent to heat transfer in a nucleate boiling system are absent. The absence of the surface tension in this equation may prove serious if it were extended to different ranges or different fluids. The absence of the temperature differential between the evaporating fluid and the heating surface is believed to be a weakness of this equation.

I am of the opinion that the rate of heat transfer between a heated tube surface and a simultaneously flowing and evaporating refrigerant is governed by all of the laws of the nucleate boiling superimposed upon the laws governing forced convection. The degree of tube surface wetting is also a major factor. With the pressure drops reported in the test data of this paper it is reasonable to expect that the tube was completely wet. This may not always be the case.

I am hopeful that the authors will continue research in this field and expand their scope of investigation over the wider range of variables. I believe that this paper does make an important contribution to the knowledge in the field of boiling heat transfer.

Authors' Closure

The authors are grateful for the data provided by Mr. S. W. Anderson and hope that he will publish in the near future additional information on his experimental work. As pointed out in our paper, Mr. B. Pierre's correlations (1) and (2) are for the average evaporating heat-transfer coefficient within the quality and $(N_{Re}{}^{3}K)$ parameter ranges indicated. The authors point out that the initial data in Table 1 for the local heat-transfer coefficient at quality changes in the order of 20 per cent, fall within about +10 and −20 per cent of Relation (1), while our data above vapor qualities of 70 per cent do not correlate using Pierre's correlations. It is of interest that Relation (1) predicts a local coefficient of 950 Btu/(hr ft² deg F) at 225,000 lb/hr ft² using the information given by Mr. Anderson in Fig. 10. The experimental results, shown between 30 and 75 per cent average vapor qualities, respectively, in Fig. 10, indicate coefficients that fall between −25 per cent and +16 per cent of the value calculated using Relation (1). The value of 950 Btu/(hr ft² deg F) from equation (1) represents about the right-average value. Pierre's correlations thus appear applicable to Mr. Anderson's results as practical approximations within the limited ranges given in the text, in spite of the appreciable variation with vapor quality.

Since the authors do not have sufficient data at vapor qualities greater than 70 per cent, we cannot recommend a local correlation in this region. The suggestions of Mr. Anderson in Relations (7), (8), and (9) offer one reasonable approach. It seems quite possible, however, that the basic form of the correlations presented in this paper will have to change to correlate the high quality region over a large enough range of the various parameters since vapor quality has such a large and nonlinear effect in this region.

As Mr. P. Worsøe-Schmidt points out, there is little doubt that, due to the rapid change of the local heat-transfer coefficient at vapor qualities greater than 70 per cent (in our case), a four-foot test section is too long to obtain true local data. His remarks regarding the ±10 per cent change of the local heat flow along our test section are very understandable since we did not make it clear that this was the case only for the data which we have presented with Pierre's correlations. At local vapor qualities greater than 70 per cent abrupt wall temperature changes were measured that indicated local heat flux changes by factors of up to 5 to 1. In run 6A (Table 1), for example, the water-side coefficient was 800 Btu/(hr ft² deg F) while the refrigerant side coefficient changed from 750 to 150 Btu/(hr ft² deg F) as its vapor quality increased from 76 to 92 per cent.

The authors concur with Professor Baker's statement that the absence of such fluid properties as the surface tension restricts the extent to which Pierre's correlations can be extended to other media. The empirical nature of this correlation does, in fact, limit it to only those ranges of variables for which it has been experimentally verified. The temperature differential between the refrigerant and the tube wall is not, however, left out of Pierre's correlation. The implicit proportionality to this temperature difference, raised to some power, is explained in equation (9) of Mr. Anderson's discussion and is also pointed out in the text of the paper.

Professor Baker points out that the tube surface may not necessarily be completely wetted for conditions beyond the range covered by the pressure drop results here reported. This is a rather important point. Both our pressure-drop results and most of our heat-transfer results are admittedly limited to conditions where complete wetting was likely.

A. L. LONDON
Professor of Mechanical Engineering, Stanford University, Stanford, Calif. Mem. ASME

J. W. MITCHELL
Graduate Student, Mechanical Engineering, Stanford University, Stanford, Calif.

W. A. SUTHERLAND
Engineer, General Electric APED, San Jose, Calif. Assoc. Mem. ASME

Heat-Transfer and Flow-Friction Characteristics of Crossed-Rod Matrices

The paper presents a continuation of the program on porous media heat-transfer and flow-friction behavior previously covered in References [2b] and [3b].[1] *All the previous results of interest to the designer on woven-screen matrices and crossed-rod matrices of a random configuration are summarized here. In addition, new design results for the regular in-line and regular staggered crossed-rod-matrix configurations are reported. Matrices of the type considered here may find application as heat-transfer surface geometries for nuclear-reactor fuel elements, for electrical resistance heaters and for periodic-flow-type heat exchangers used for gas-turbine regenerators, and some air-conditioning applications.*

This study follows TR-Nos. 10, 16, and 28 [1, 2a, 3a] in presenting design results for the convective heat-transfer and flow-friction behavior for flow through porous media.

Locke [1] developed a transient test technique for establishing the low Reynolds-number heat-transfer characteristics. Coppage [2a] then utilized this technique in establishing the characteristics for porous solid bodies or matrices formed from stacked woven-wire screens. These results, ranging from $5 < N_R < 1000$, were extended up to $N_R = 10^5$ by Tong [3a] using a different transient technique together with matrices of crossed rods to simulate woven screens. Summaries of the design information so obtained were published in references [2b] and [3b].

The reason for limiting the work mainly to porous bodies formed from stacked woven-wire screens is that these geometries are capable of a fairly clear-cut description. Information now covers the ranges of Reynolds numbers of 5 to 10^5 and porosity of 0.60 to 0.83. In obtaining these characteristics the behavior of what is termed a random stacking of crossed-rod matrices was also established experimentally as a step incidental to the main purpose of simulating the woven-wire matrices for the high N_R range. This simulation involved adjustments of the crossed-rod results to account for the lack of complete geometrical similarity associated with the wire inclination introduced by weaving. These adjustments are described in reference [3b].

Also, in reference [3b] the random stacking, crossed-rod results are reported as such for the ranges $500 < N_R < 10^5$ and $0.60 < \text{porosity } p < 0.83$. This is the same porosity range as for the woven screens because each crossed-rod matrix geometry was designed with a transverse pitch x_t to match the porosity p of a particular screen matrix.

In addition to the random stacking, regular in-line and regular staggered stackings are also of technical interest. These arrangements are described in Fig. 1. For all three arrangements each of the rod rows is paired with one adjacent row crossed at 90 deg. The transverse spacing of the rods is a constant for the matrix and is described by the transverse pitch-diameter product x_t/d. As the crossed-rod pairs contact each other at the crossing points the longitudinal spacing pitch x_l is identically unity. In the random orientation each of the 90-deg crossed pairs is oriented at 45 deg with the neighboring pairs. In the in-line orientation each of the crossed pairs is oriented so that the rods in every other row line up. For the staggered orientation the rods in every fourth row, for instance 1, 5, 9, etc., line up with each other, and so do the rods in rows 2, 6, 10, 14, etc., 3, 7, 11, 15, etc., and 4, 8, 12, 16, etc.

It is the objective of this paper to present the convective heat-transfer and flow-friction characteristics of the in-line and staggered configurations. For completeness and for the purposes of comparison the random stacking configuration as well as the woven-screen characteristics will also be presented. The ranges covered for the crossed-rod configurations are from about 8×10^2

[1] Numbers in brackets designate References at end of paper.

Contributed by the Heat Transfer Division and presented at the Annual Meeting, Atlantic City, N. J., November 29–December 4, 1959, of The American Society of Mechanical Engineers.

Note: Statements and opinions advanced in papers are to be understood as individual expressions of their authors and not those of the Society. Manuscript received at ASME Headquarters, September 3, 1959. Paper No. 59—A-168.

Nomenclature

A = heat-transfer area, sq ft

A_{flow} = matrix average flow area, $A_{flow} = pA_{frontal}$, sq ft

$A_{frontal}$ = matrix frontal area, sq ft

c_p = fluid specific heat at constant pressure, Btu/(lb deg F)

C = thermal capacity of copper cylinder, Btu per deg F

d = diameter of rod and wire, in., ft

e = base of natural logarithms, 2.718...

g_c = reciprocal of proportionality factor in Newton's second law 32.2 (lb/#)(ft/sec^2)

G = average mass velocity in matrix, based on A_{flow}, lb/(hr sq ft)

G_{max} = maximum mass velocity in matrix, based on minimum free-flow area, $\sigma A_{frontal}$, lb/(hr sq ft)

h = unit conductance for thermal convection heat transfer, Btu/(hr sq ft deg F)

k = fluid unit thermal conductivity, Btu/(hr sq ft deg F/ft)

l = length of matrix in the flow direction, ft

p = porosity of matrix, (vol. of voids)/(vol. of matrix), dimensionless

P = pressure, #/sq ft, or in. H_2O

ΔP = pressure differential, #/sq ft, or in. H_2O

r_h = hydraulic radius, Equations (1) and (4), ft

(*Continued on next page*)

to 10^6 for Reynolds number and 0.50 to 0.83 for porosity. The coverage down to a porosity of 0.5 represents an extension of the 0.6 limit for the previously reported random-stacking configurations.

The convective heat-transfer and flow-friction behavior of crossed-rod and woven-screen matrices is of technical interest because of the possible application of these geometries in fuel elements for gas-cooled or diphenyl-cooled nuclear reactors [4, 5]. Matousek [5] summarizes recommended thermal-design data for crossed-rod matrices based on the Stanford heat-transfer and flow-friction results for the random stacking together with some flow-friction results from Argonne for the regular and staggered stacking configurations. The results reported here provide an extension of this summary.

In the automotive-type gas-turbine plant a regenerator is a virtual requirement to realize a competitive specific fuel consumption at light loads. One such regenerator of the periodic-flow type incorporates a screen matrix [6].

Area "densities" of the order of 1000 sq ft transfer area per cubic foot of volume can be realized with 24-mesh screen, and this is of the order of 4 times greater than can be realized with very compact plate-fin surfaces [7] and 25 times greater than that provided by 1-in-diameter tubes in a tube bundle, a geometry typical of many industrial shell-and-tube-type exchangers. A clear advantage in compactness is evidenced for the matrix-type surface. However, its use as a heat-exchanger surface is restricted to either periodic-flow-type exchangers in contrast to the direct-transfer type, or to heat-transfer applications where the solid material of the matrix is the "source" of the thermal energy as by nuclear fission, chemical reaction, or electrical I^2R heating.

Geometrical Parameters

The description of either the woven-screen or crossed-rod matrices is provided by the geometric parameters in Table 1.

Table 1 Geometric parameters

Dimensional	Nondimensional
Flow hydraulic radius, r_h, ft	Porosity, p
Heat-transfer area density, α sq ft/cu ft	Transverse pitch, x_t
Rod or wire diameter, d, ft	Longitudinal pitch, x_l
	Minimum flow area to frontal area ratio, σ

For the crossed-rod matrices x_l is unity; for woven-screen matrices x_l may be slightly less or greater than unity because of flattening or crimping of the wire during the weaving process. While generally two transverse pitches are needed, for present purposes only square-mesh geometries will be considered so that one will suffice.

The general definition of the hydraulic radius is

$$r_h \triangleq lA_{flow}/A \tag{1}$$

where the average flow area A_{flow} in distinction to the minimum flow area $\sigma A_{frontal}$ is defined by

$$A_{flow} \triangleq pA_{frontal} \tag{2}$$

The area density is defined as the transfer area per unit matrix volume

$$\alpha \triangleq A/lA_{frontal} \tag{3}$$

The definitions (1), (2), and (3) combine to yield

$$r_h = p/\alpha \tag{4}$$

These relations are generally applicable to any porous solid or matrix providing all the voids are connected to permit through flow. Moreover, with suitable definition of the void volume, they will apply to either side of any heat exchanger surface.

For the *crossed-rod matrices* of square mesh using circular cylinder rods the following simple relations may be readily derived:

$$p = 1 - \pi/(4x_t) \tag{5}$$

$$\sigma = (x_t - 1)^2/x_t^2 \tag{6}$$

$$\alpha d = \pi/x_t \tag{7}$$

$$r_h/d = \left(\frac{x_t}{\pi} - \frac{1}{4}\right) \tag{8}$$

It is evident that x_t and d describe the matrix with respect to p, σ, α, and r_h. Additionally, the character of the stacking, Fig. 1, is required to complete the description.

Woven-screen matrices are not so simply specified because of the wire inclination which results from weaving and the previously

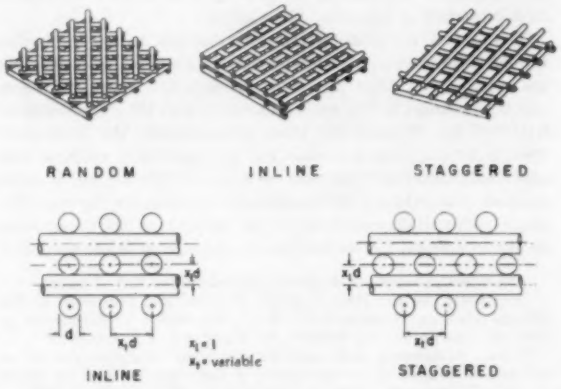

Fig. 1 Configuration geometries; comparison of random, in-line, and staggered crossed-rod matrices

Nomenclature

W = mass-flow rate, lb per hr
α = heat-transfer area per unit volume of matrix, or "area density" Equation (3), sq ft/cu ft
θ = time, hr
μ = fluid viscosity, lb/(hr ft)
ρ = fluid density, lb/cu ft
σ = ratio of minimum free flow to frontal area, dimensionless
τ = matrix friction drag force per unit of matrix surface area, $\#$/sq ft

Dimensionless Groups

C_D = aerodynamic drag coefficient, Equations (16) and (19)
C_P = pressure coefficient, Equations (15) and (18)
f = Fanning friction factor, Equations (14) and (17)
N_{Pr} = Prandtl number, $N_{Pr} = \mu c_p/k$
N_R = Reynolds number for tubelike flow or interior flow, $N_R = 4r_hG/\mu$
$N_{R(d)}$ = Reynolds number for flow over a body, $N_{R(d)} = dG_{max}/\mu$
N_{St} = Stanton number, $N_{St} = h/Gc_p$
x_l = longitudinal pitch, ratio of longitudinal spacing to wire or rod diameter
x_t = transverse pitch, ratio of transverse spacing to wire or rod diameter
$\#$ = denotes pounds force in distinction to lb for pounds mass
$\triangleq$ = denotes defining equation

mentioned possibility of flattening or crimping effects. The definitions Equations (1), (2), and (3) still apply as does the related Equation (4). Also Equation (6) applies for square-mesh screens.

Correlating Parameters

Two Reynolds numbers will be used for correlating the flow-friction and heat-transfer characteristics

$$N_R \triangleq 4r_h G/\mu \tag{9}$$

$$N_{R(d)} \triangleq dG_{max}/\mu \tag{10}$$

where $G \triangleq W/(pA_{frontal})$, $G_{max} \triangleq W/(\sigma A_{frontal})$. It follows directly that

$$N_R/N_{R(d)} = 4r_h\sigma/(pd)$$

Then from Equation (4)

$$N_R/N_{R(d)} = 4\sigma/(\alpha d) \tag{11}$$

and this relationship is valid for both the crossed-rod and woven-wire matrices. Specifically for the crossed-rod matrices, Equations (6) and (7) may be introduced to yield

$$N_R/N_{R(d)} = 4(x_l - 1)^2/(\pi x_l) \tag{12}$$

Equation (12) is graphed in Fig. 2.

The heat-transfer parameter that will be used is the conventional Stanton number in preference to the equally conventional Nusselt number

$$N_{St} \triangleq h/(Gc_p) \tag{13}$$

Three flow-friction parameters are employed in this presentation: (*a*) A Fanning-type friction factor, f, conventionally found useful for internal flow situations (such as for longitudinal flow in a cylindrical tube); (*b*) a pressure coefficient, C_P; and (*c*) an aerodynamic drag coefficient, C_D, useful for external flow situations (like flow over a circular cylinder). The f-factor is more useful in design applications; C_P and C_D are of value in interpretation and discussion of the flow-friction behavior, particularly for large magnitudes of x_l such that the porosity approaches unity. Their definitions follow:

$$f \triangleq p\tau \Big/ \left\{\rho \frac{G^2/\rho^2}{2g_c}\right\} \tag{14}$$

$$C_P \triangleq \frac{2x_l d}{r_h} p\tau \Big/ \left\{\rho \frac{G_{max}^2/\rho^2}{2g_c}\right\} \tag{15}$$[2]

$$C_D \triangleq C_P/(1 - \sigma) \tag{16}$$

For essentially constant-density flow, the drag force per unit surface area τ is related to the matrix pressure drop ΔP, by

$$\tau A = A_{frontal}\Delta P$$

Then Equations (14), (15), and (16) together with the defining Equations (1) and (2) for r_h and A_{flow}, yield

$$\frac{\Delta P}{\rho} = f\frac{l}{r_h}\left(\frac{G^2/\rho^2}{2g_c}\right) \tag{17}$$

$$\frac{\Delta P}{\rho} = C_P\left(\frac{l}{2x_l d}\right)\left(\frac{G_{max}^2/\rho^2}{2g_c}\right) \tag{18}$$

$$\tau A = C_D\left(\frac{l}{2x_l d}\right)(A_{frontal})(1 - \sigma)\left(\frac{G_{max}^2/\rho^2}{2g_c}\right)\rho \tag{19}$$

It is seen from Equation (17) that f incorporates the flow losses at the entrance and exit sections of the matrix while usually for tube-type flow these losses are accounted for by separate additive terms in an equation like (17) involving empirically established loss coefficients [7]. In the usual tube-type definition for f the p in Equation (14) is omitted [7]. The reason for including it for the matrix is that by doing so f does combine the entrance and exit effects with the core friction, since these losses are not amenable to separation as in the case of tube-type flow.

When the flow density cannot be treated as a constant, a flow acceleration term also comes into the pressure-drop evaluation and this consideration is treated in reference [7].

From Equation (18), since $(l/2x_l d)$ is the number of pairs of crossed-rod rows or the number of woven screens in the matrix, C_P is effectively a pressure coefficient for one pair of crossed-rod rows or for one screen. Since the hydraulic radius goes to infinity as the porosity approaches unity it is evident from the defining Equation (15) that $C_P = 0$ for $p = 1$. Note, however, that the factor f does not behave this way and is finite for $p = 1$.

The relationship between f and C_P is provided by the defining Equations (14) and (15) as

$$\frac{C_P}{f} = \left(\frac{2x_l d}{r_h}\right)\left(\frac{\sigma}{p}\right)^2 \tag{20}$$

For the crossed-rod-matrix geometry, since $x_l = 1$, Equations (4), (5), (6), (7), and (20) combine to yield

$$\frac{C_P}{f} = \frac{2d\alpha\sigma^2}{p^2} = \frac{[2\pi(x_l - 1)^4/x_l^5]}{[1 - \pi/4x_l]^2} \tag{21}$$

It is clear here too that for $p = 1$, since $x_l = \infty$, C_P/f is zero and so C_P must be zero.

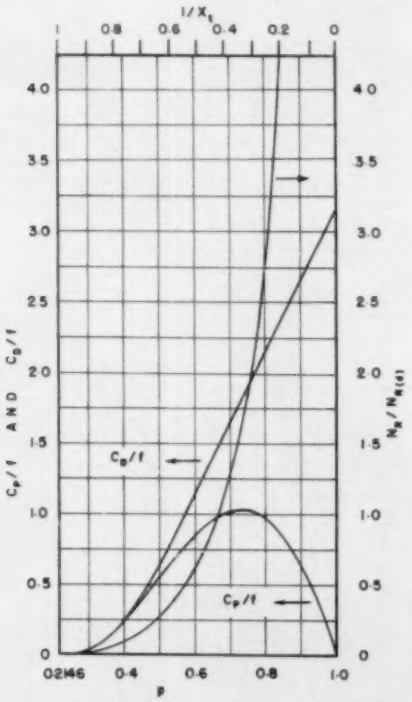

Fig. 2 Ratios of Reynolds numbers and friction parameters as a function of porosity for crossed-rod matrices

[2] In the references [3a] and [3b] C_P is called a drag coefficient for a screen. It differs from what is conventionally called a drag coefficient as indicated by Equation (16).

Equation (21) is graphed in Fig. 2 for crossed-rod matrices. Either porosity p or the transverse pitch x_t will suffice as an abscissa since p is uniquely related to x_t in accordance with Equation (5).

From Equation (19) it is evident that C_D is the drag force (τA) per pair of crossed-rod rows per unit of projected area of one crossed-rod pair, $(1 - \sigma)A_{frontal}$, divided by the velocity-head-density product term. Thus C_D matches the conventional definition of a drag coefficient. Unlike C_P which goes to zero as porosity approaches unity, C_D tends to a finite value. This fact is not fully evident from the defining Equation (16) because as C_P approaches zero, the solidity $(1 - \sigma)$ also approaches zero and the ratio is indeterminate. If Equations (15) and (16) are combined, using Equation (4), it is seen that

$$C_D = \frac{2x_t \alpha d\tau}{(1 - \sigma)} \Big/ \left\{\rho \frac{G_{max}^2/\rho^2}{2g_c}\right\}$$

Now for crossed-rod matrices, with $x_t = 1$, using Equations (6) and (7) for (αd) and σ in terms of x_t and then letting x_t go to ∞, as is the case for $p = 1$, results in

$$C_{D,p=1} = \pi\tau \Big/ \left\{\rho \frac{G_{max}^2/\rho^2}{2g_c}\right\}$$

or the drag force

$$A\tau = C_{D,p=1} \frac{A}{\pi} \left\{\rho \frac{G_{max}^2/\rho^2}{2g_c}\right\}$$

But A/π is equal to the number of crossed-rod row pairs times the projected area of one pair, which is also, the number of single rows times the projected area of one row. Thus $C_{D,p=1}$ is the drag coefficient for either an in-line series of cylinders or for crossed cylinders in line as indicated in Fig. 3. A point of interest is that the in-line cylinders corresponding to the in-line and staggered matrices are spaced 2 and 4 diameters apart, respectively.

The ratio C_D/f can be formed readily from C_P/f as given by Equation (21) and C_D/C_P from Equation (16). This result, as a function of x_t or porosity, is graphed, Fig. 2. For a porosity of unity x_t goes to infinity and C_D/f approaches π.

The following points summarize the reasons for using three different friction coefficients in this presentation:

1 The Fanning-type friction factor f is the most convenient one to use in heat-transfer flow-friction design calculations.

2 The pressure coefficient C_P is useful in interpreting the variation of matrix-friction behavior with porosity, particularly at high porosities since C_P approaches zero as p approaches unity. Moreover, it was discovered in earlier work on this program [3a, 3b] that C_P versus $N_{R(d)}$ served to correlate very well the friction behavior of the woven-screen matrices with that of the crossed-rod matrices.

3 The drag coefficient C_D is also useful in interpreting the variation of matrix-friction behavior with porosity. As p approaches unity, the matrix C_D will approach that of the in-line isolated cylinders described in Fig. 3. C_P would not permit a comparison of this type.

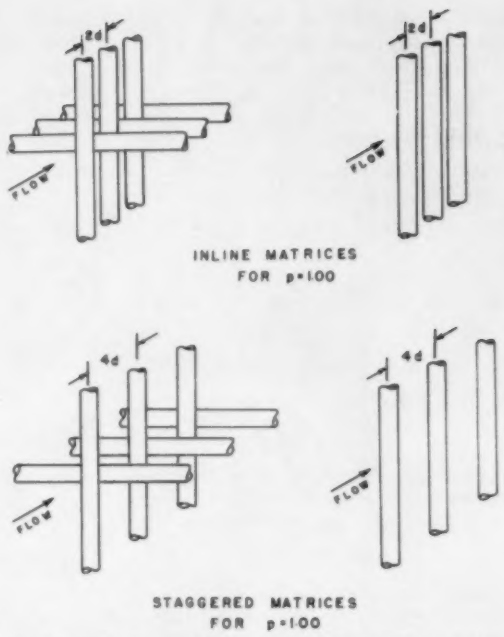

Fig. 3 Approach of crossed-rod matrix to in-line cylinder geometry as porosity goes to unity

Description of Matrices and Tests

The crossed-rod matrices tested are described in detail in Table 2. All of the matrices were formed from $^1/_8$-in-diameter plastic rods.

The 0.725 porosity matrix, No. IV, is pictured in Fig. 4. Each row of rods was pinned into its own plastic ring having an ID of 10.00 in. and a length of 0.375 in. Longitudinal keyways on the outside ring periphery allowed accurate alignment of the rows. Matrices Nos. I, II, and III contained six crossed-rod pairs while Nos. IV, V, VI, and VII contained five pairs. The porosity range covered was from 0.832 for matrix No. I to 0.500 for matrix No. VII.

As indicated in Fig. 4, one rod element of the assembly was made of a 0.375-in-diameter solid copper cylinder with plastic-rod end pieces. This cylinder, located in the seventh row in the air-flow direction (the front row of the fourth crossed-rod pair) was designed to be withdrawn from the matrix or inserted through the hole in the duct pictured in Fig. 4.

The test procedure to establish the heat-transfer coefficient in-

Table 2 Specifications for crossed-rod matrices

Matrix no.	I	II	III	IV	V	VI	VII
Porosity, p	0.832	0.817	0.766	0.725	0.675	0.602	0.500
Rod diameter, d, in.	0.375	0.375	0.375	0.375	0.375	0.375	0.375
Transverse pitch, x_t	4.675	4.292	3.356	2.856	2.417	1.974	1.571
Hydraulic radius, r_h, ft	0.0387	0.0349	0.0256	0.0206	0.0162	0.0118	0.00781
Area density, a, sq ft/cu ft	21.5	23.4	30.0	35.2	41.6	50.9	64.0
Free flow/frontal area, σ	0.618	0.588	0.493	0.422	0.344	0.243	0.132
Capacitor length, in.	8.56	8.56	5.00	5.00	4.44	4.44	8.56
C/A, Btu/(sq ft deg F)	0.391	0.391	0.396	0.396	0.395	0.395	0.391
$N_R/N_{R(d)}$	3.68	3.21	2.11	1.536	1.058	0.612	0.264
C_P/f	0.891	0.929	1.012	1.030	0.998	0.864	0.558
C_P/C_D	0.382	0.412	0.507	0.578	0.656	0.757	0.868
C_D/f	2.33	2.26	1.995	1.782	1.521	1.142	0.643

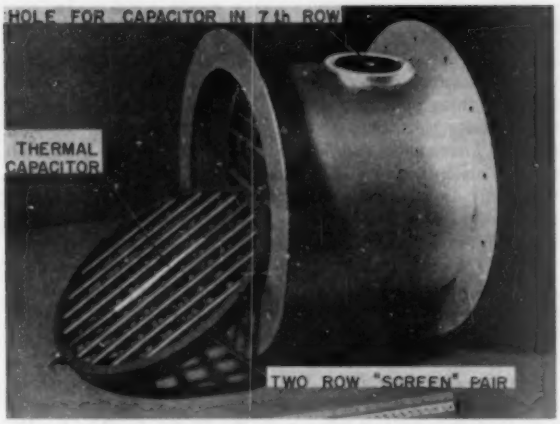

Fig. 4 Crossed-rod matrix test core; porosity of 0.725, matrix No. IV, Table 2. Thermal-capacitor element is located in first row of fourth crossed-rod pair of flow direction.

volves the measurement of the temperature-time history of the copper-rod element as it cools in place in the matrix. The rod can be treated as a lumped thermal capacitor with negligible internal resistance. This technique was used in 1940 for both heat and mass-transfer investigations [8] and more recently in its application to tube-bank heat transfer [9, 10].

The seventh-row location for the copper element was established, by tests reported in reference [3*a*], as that providing the convective heat-transfer coefficient representative of a matrix with many rows on the order of 50 or more (25 or more crossed-rod pairs). The first row had a coefficient only about 65 per cent of the seventh row. The variation of the average matrix coefficient with the number of pairs of crossed-rod rows could be obtained by integration of the row-to-row local coefficient variation. Further discussion on this point will be given later.

Fig. 5 shows the duct containing the test matrix. The removable thermal capacitor has installed in it an iron-constantan thermocouple. With the air flow established at a desired rate, the capacitor element was withdrawn from the matrix and heated in a small electric oven 50 to 60 deg F above the duct air-flow temperature. The element was then reinserted in position in the test matrix and its temperature-time history measured. For the slower cooling rates a Brown Electronik indicator (25-in. scale, 5-millivolt range, 0.5-sec full-scale response) was used with a stop watch to note the times at 1.0, 0.9, 0.8, 0.7, 0.6, and 0.5 millivolt above the reference junction in the air stream. The test cooling range was thus about 15 deg F starting about 30 deg F above the air-flow temperature. For the faster cooling rates a Brown Electronik recorder was used. This instrument has a full-scale response of less than 0.5 sec. An optional range selector was set to 2 millivolts full scale on a 10-in. scale.

The temperature-time behavior of a thermal capacitor of capacitance C Btu per deg F, cooling in an air stream with a pure convection resistance at the surface of $1/(hA)$ hr deg F/Btu, is given by the relationship [3*a*, 8, 9]

$$\frac{t}{t_{\theta=0}} = e^{-\frac{h}{C/A}\theta} \tag{22}$$

where the temperatures are referred to an air-stream datum and A is the cylindrical surface area of the capacitor. For the small cooling range considered, the thermocouple emf response is linear with temperature so that the minus logarithm of the emf ratio plotted versus time yields a straight line of slope $h/(C/A)$. The convective heat-transfer coefficient was evaluated from this slope and the (C/A) magnitudes of Table 2.

C/A is of the order of 0.40 Btu/(deg F sq ft) and the test h magnitudes ranged from 3 to 100 Btu/(hr deg F sq ft). Thus the "time constant," $(C/A)/h$, for the thermal resistance-capacitance circuit ranged from 0.133 to 0.004 hr ($\approx$15 sec). From this last magnitude it becomes clear why a recording potentiometer was required for the faster cooling runs.

The friction-factor coefficient determination was made from the measured matrix pressure drop. Since essentially constant-density flow conditions obtained, Equation (17) was used. Because of the wide flow range, it was necessary to measure ΔP with either compound vertical-and-inclined draft gages or with a 2-in-range micromanometer which had a sensitivity of 2×10^{-4} in. of water. The test ΔP range was from 10 to 0.01 in. of water.

Air flow was induced from the laboratory room through a smoothly convergent inlet, then through the straightener, the matrix, the metering orifices, and the blower in series. Air-flow metering was accomplished by a set of four ASME standard orifices to cover the test range. Uniformity of flow upstream of the test matrix was obtained by adjustment of trim tabs on an egg-crate flow straightener.

The estimated uncertainty intervals associated with the test measurements are as follows [3*a*]:

$N_{St} \pm 3$ per cent $f \pm 5$ per cent

$N_R \pm 2$ per cent $N_{Pr} \pm 2$ per cent

From the test results presented graphically, Figs. 6 to 13, it is clear that the experimental scatter on f and N_{St} is generally well within these limits.

A more detailed description of the test equipment is contained in reference [3*a*].

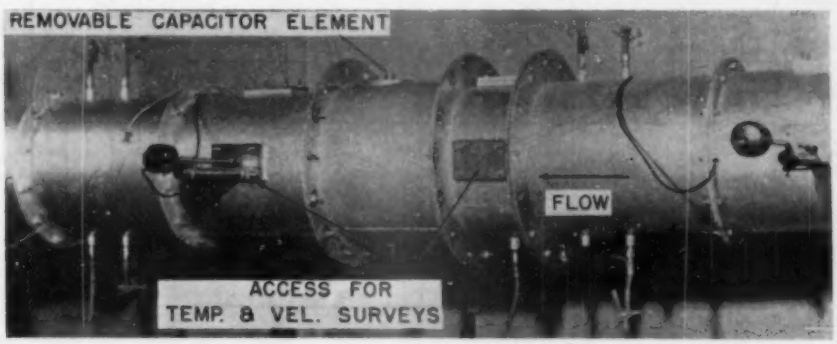

Fig. 5 Test duct with matrix installed

Results

Previously reported results [3*a*, 3*b*] included only the random stacking configuration for matrices I, II, III, IV, V, and VI described in Table 2. The new results reported here include the regular staggered and regular in-line configurations for matrices I, III, V, VI, and VII as well as the random configuration for matrix VII. Matrix VII was introduced to extend the porosity range down to 0.50. Matrices II and IV were omitted from this test sequence in that they represented intermediate values of porosity already adequately covered by the others.

Figs. 6 to 10 provide the basic heat-transfer and flow-friction characteristics for the random, the staggered, and the in-line configurations in the form of $N_{St}N_{Pr}^{2/3}$ and f versus the Reynolds number, N_R, based on hydraulic radius. The N_R range is from about 800 to 10^5 and the porosity range from 0.50 to 0.83.

As can be seen, there are no striking differences in the heat-transfer behavior until the porosity exceeds 80 per cent. However, the friction behavior is substantially different with the staggered arrangement, providing the lowest f at $p = 0.500$ by 10 to 20 per cent and the highest f at $p = 0.832$ by 30 to 40 per cent relative to the random configuration. The in-line configuration has about the same f as the random configuration for the porosity range 0.500 to 0.675, but for $p = 0.766$ and 0.832 it is substantially lower. The two-to-one ratio of f (staggered) to f (in-line) at $p = 0.832$ was quite unexpected, but can be explained in a satisfactory manner as will be shown in the discussion to follow.

Figs. 11, 12, and 13 show the influence of porosity separately for each of the three crossed-rod configurations while Figs. 14 and 15 provide the same comparison for the woven-screen matrices.

Discussion

All of the foregoing results are for the behavior of a representative single screen or a crossed-rod pair in a many row matrix. The first three pairs of rows will have progressively increasing heat-transfer coefficients. The coefficient is then constant for the fourth row and beyond. In Fig. 16 the integrated average matrix heat-transfer coefficient, h_{avg}, is compared to h_∞, the coefficient of a rod element located in the fourth or higher crossed-rod pair. Also shown is the comparable tube-bank behavior from reference [9], and it substantiates the behavior of the matrices. Clearly for less than 10 screens or 10 crossed-rod pairs of 20 rows in a tube bank, the lower heat-transfer performance of the first few rows has sufficiently large influence so that it should be taken into account by the designer. Fig. 16 will be useful for this purpose.

The three configurations, random, in-line, and staggered, all exhibit about the same heat-transfer behavior at a given porosity and Reynolds number, Figs. 6 to 10, except possibly for the higher porosities, p greater than 0.80. The woven-screen matrices also closely match the crossed-rod matrix heat-transfer behavior at the same porosity and N_R; since the woven-screen information covers a wider range of N_R, 10^5 down to about 5, it may be used as a guide to extrapolate the crossed-rod matrix characteristic to lower values of N_R than the test limit of about 10^3.

The friction-factor f versus N_R characteristics for the three crossed-rod configurations are reasonably close to each other at a given porosity for p less than 0.70. However, while the differences are small at the lower porosities, very substantial differences in f exist at the higher porosities. This behavior is il-

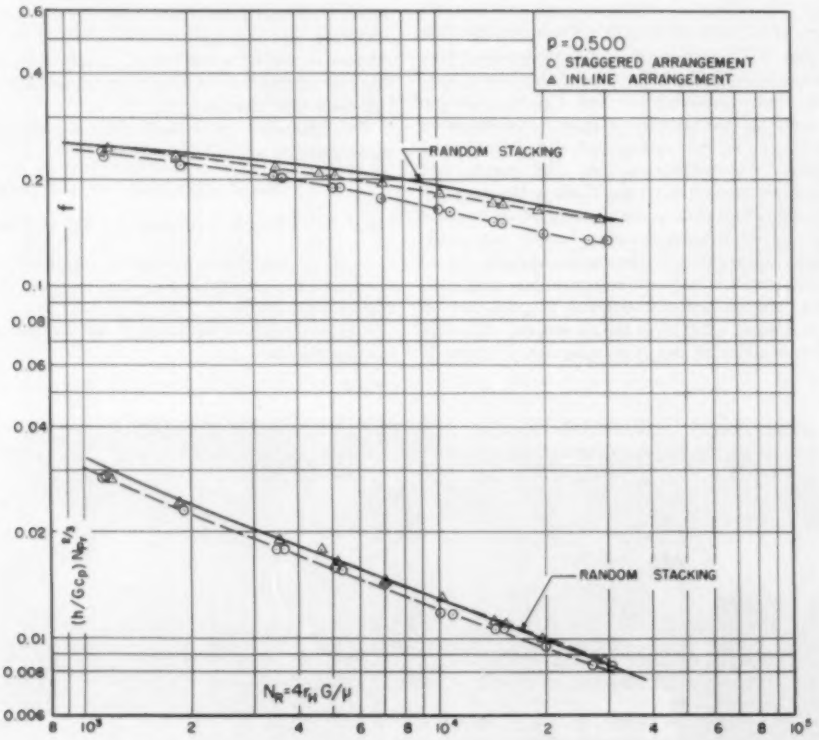

Fig. 6 Effect of configuration on heat transfer and flow friction; porosity = 0.500; matrix VII, Table 2

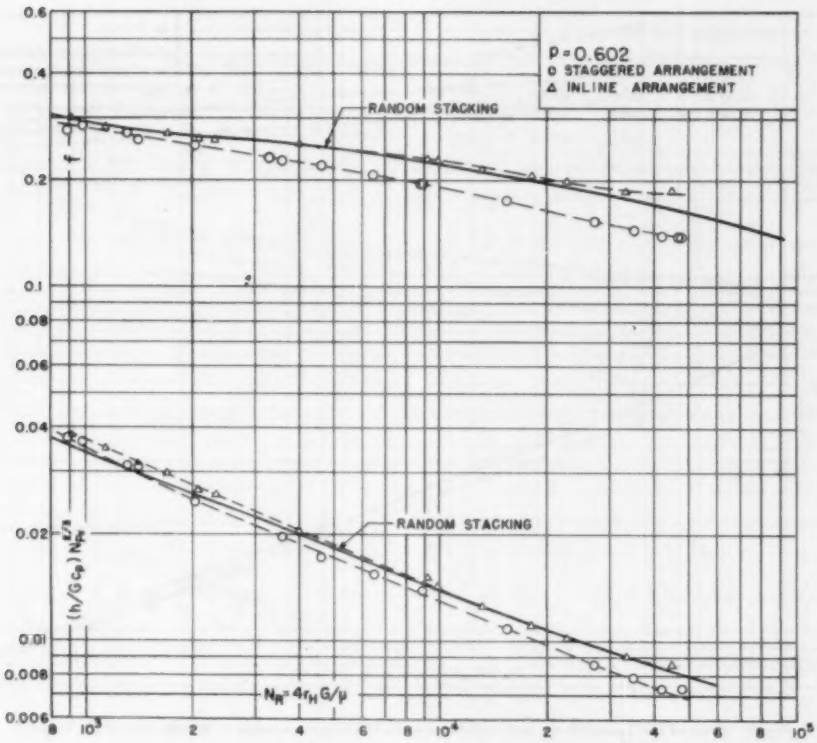

Fig. 7 Effect of configuration on heat transfer and flow friction; porosity = 0.602; matrix VI, Table 2

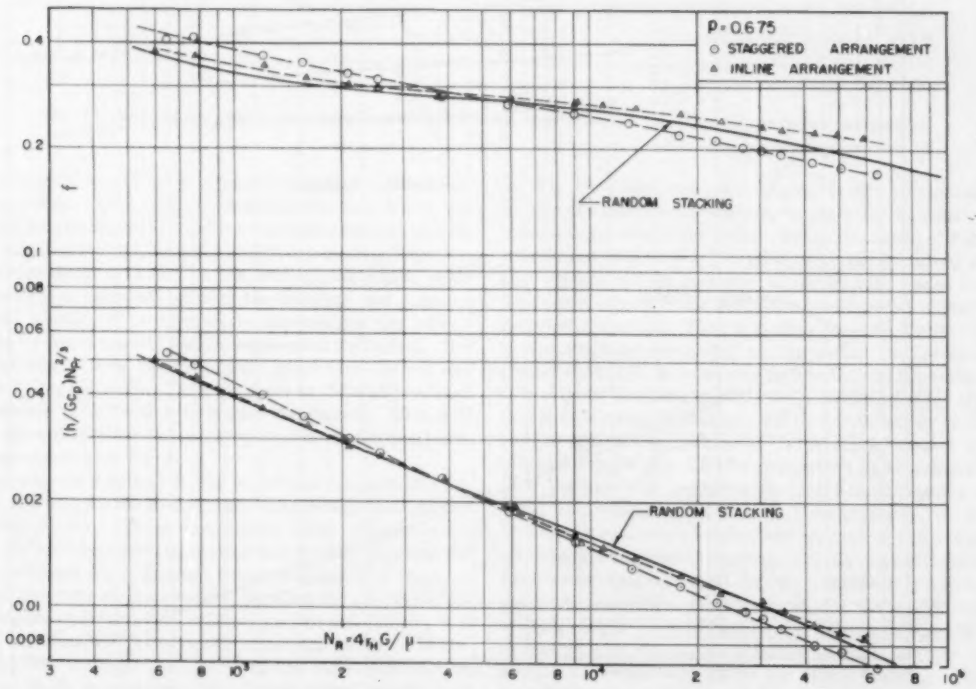

Fig. 8 Effect of configuration on heat transfer and flow friction; porosity = 0.675; matrix V, Table 2

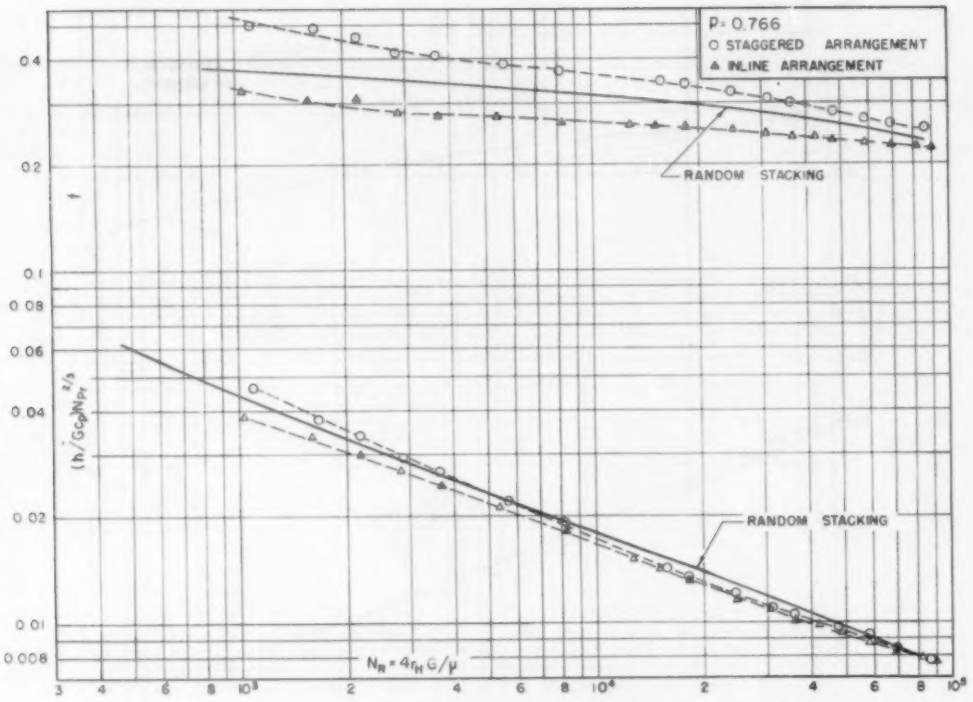

Fig. 9 Effect of configuration on heat transfer and flow friction; porosity = 0.766; matrix III, Table 2

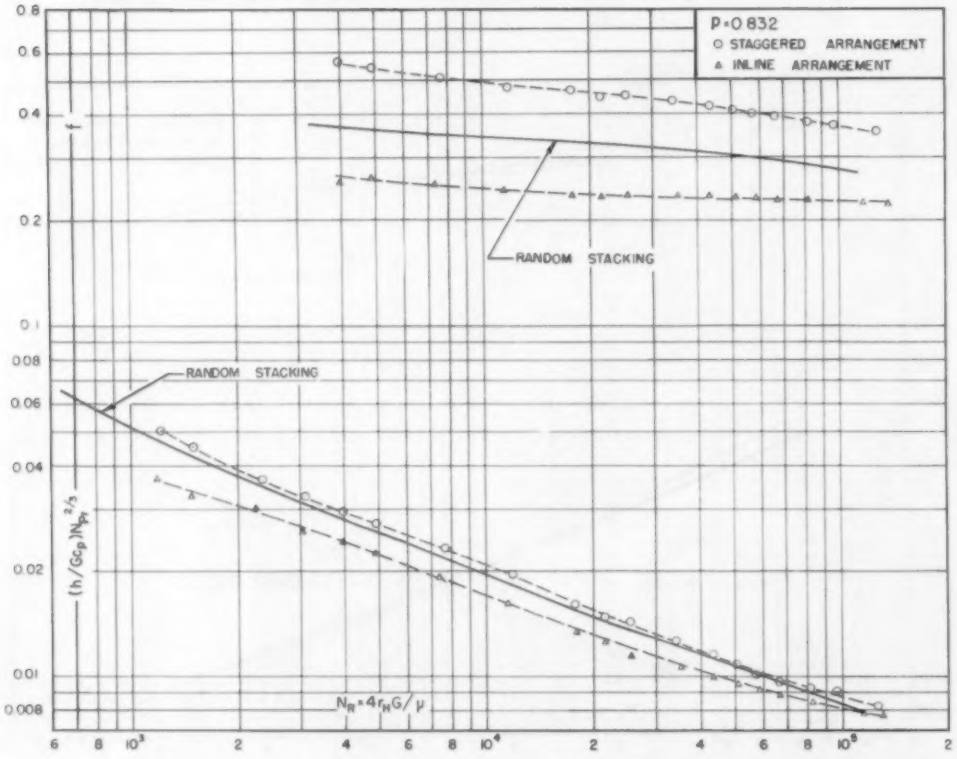

Fig. 10 Effect of configuration on heat transfer and flow friction; porosity = 0.832; matrix I, Table 2

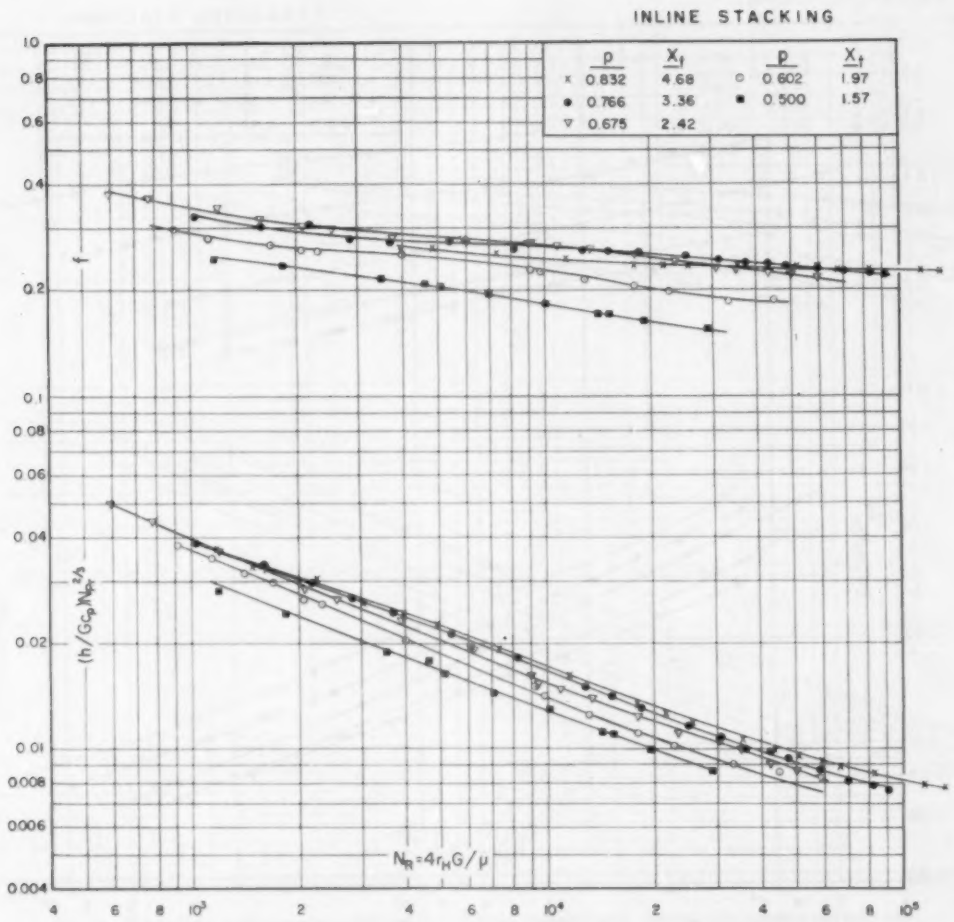

Fig. 11 Crossed-rod matrix heat-transfer and flow-friction characteristics; summary for the in-line configuration

ustrated in Figs. 17 and 18 by cross plots from the $f - N_R$ characteristics of Figs. 11, 12, and 13. Additionally, at a $N_R = 10^4$ some results by Matousek [5] obtained with water flow over small-diameter rods (0.080 to 0.125 in. diam) are presented to extend the porosity range down to 0.37. In the overlapping region quite good agreement is obtained between the Stanford and Argonne (Matousek) results. This agreement substantiates the corrections made by Matousek [5] for the test-section wall effect. His rectangular test sections were relatively small with the rod elements paralleling the walls. Thus the space at the wall produced a low-resistance path for flow to bypass the matrix. This wall condition did not exist for the matrices used in the Stanford program, as is evident from Fig. 4.

At a porosity of 0.80 and a $N_R = 10^4$ the f-magnitudes are 0.26, 0.33, and 0.41 for the in-line, random, and staggered arrangements, respectively. These unexpected large differences at high porosity are also shown in another way by Fig. 19 where the pressure coefficient C_P is graphed versus porosity at a $N_{R(d)} = 10^4$. With this type of presentation, recalling the discussion accompanying the definition of C_P, Equations (15) and (18), $C_P = 0$ at $p = 1$, and thus the characteristic must extrapolate as shown beyond the test limit of 0.83. Some in-line tube-bank friction data are available in reference [11]. These Cornell results, presented in a C_P versus $N_{R(d)}$ form, extrapolate to $C_P = 0$ at $p = 1$ in., Fig. 19. Moreover, the tube bank with a longitudinal tube spacing of 4 diameters has a larger C_P than the 2-diameter spacing tube bank for p less than unity. In the discussion of Fig. 3 it was pointed out that as p approached unity the staggered configuration approached the geometry of in-line tube banks having the 4-diameter spacing while the in-line configuration approached the 2-diameter spacing. Thus it is clear that the higher C_P (and f) of the staggered compared to the in-line configuration, for p greater than 0.70, is supported by the Cornell tube-bank results.

In Fig. 20 the drag coefficient C_D versus porosity representation is used to again compare the friction behavior of the in-line and staggered configurations. This representation allows an extrapolation to $p = 1.00$ for comparison of the matrix behavior with the available aerodynamic-drag information for cylinders either as a single cylinder in an infinite stream, or two cylinders with a 2-diameter longitudinal spacing, or two cylinders with a 4-diameter longitudinal spacing [12]. Because of the wake effect, the average drag coefficient for two cylinders is less than that for the single cylinder. Moreover, C_D for the 4-diameter-spacing cylinders is greater than that for the 2-diameter spacing, and this result supports the matrix behavior at high porosity where the staggered configuration shows the higher friction. The Cornell tube-bank results also extrapolate very well to the $p = 1$ limit to agree with the aerodynamic-drag behavior of cylinders.

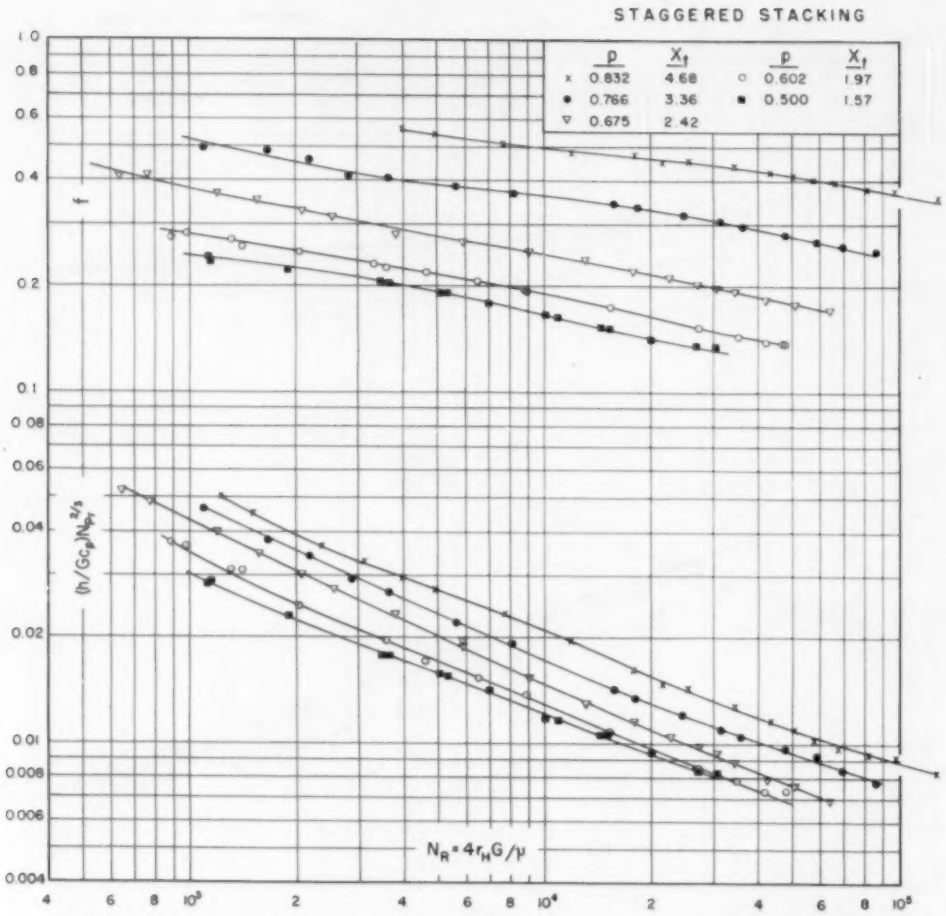

Fig. 12 Crossed-rod matrix heat-transfer and flow-friction characteristics; summary for staggered configuration

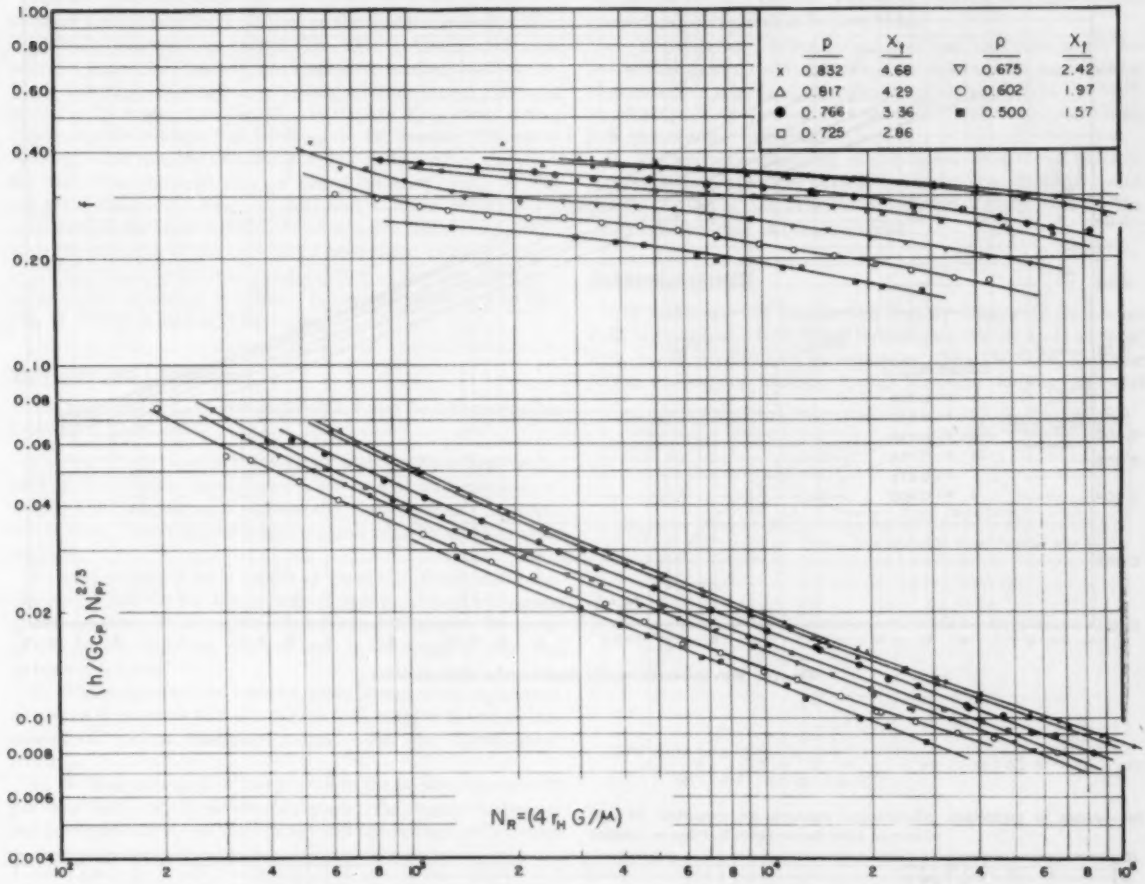

Fig. 13 Crossed-rod matrix heat-transfer and flow-friction characteristics; summary for random configuration

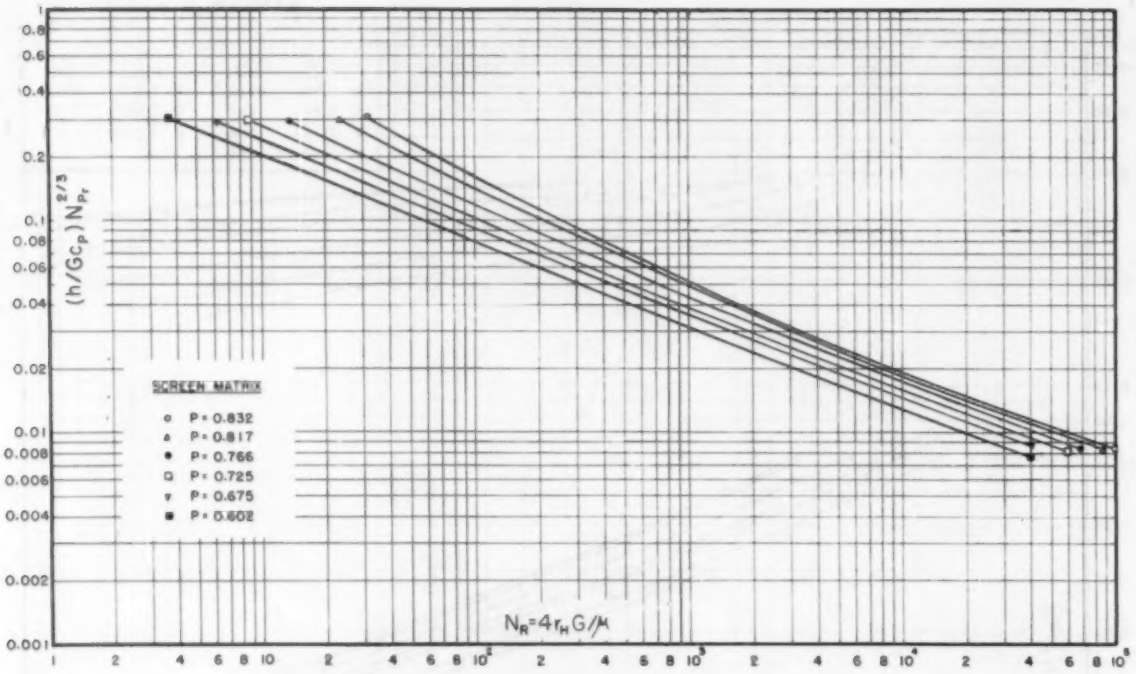

Fig. 14 Woven-screen matrix heat-transfer characteristics

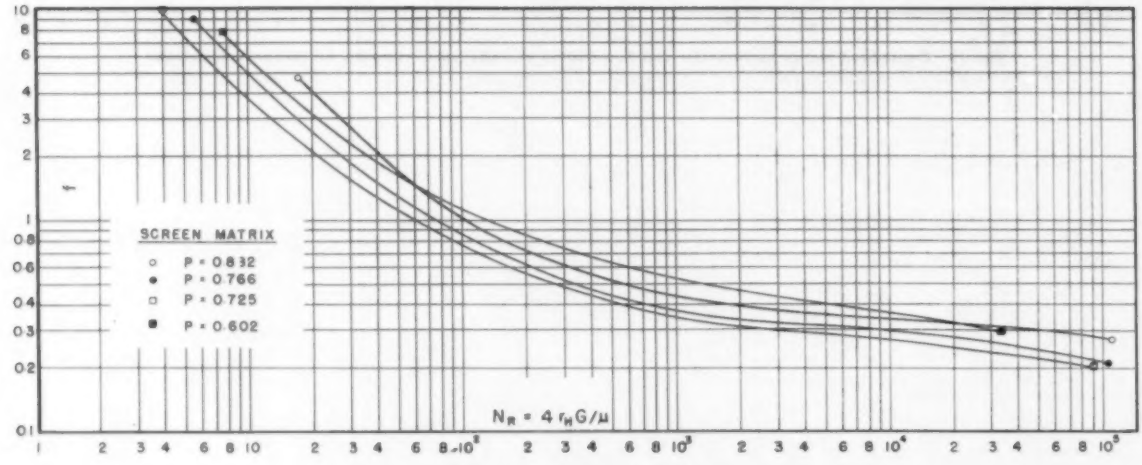

Fig. 15 Woven-screen matrix flow-friction characteristics

This extrapolation of the C_P and C_D curves to the $p = 1$ limit parallels a discussion by T. T. Siao of the single-screen, flow-friction results presented by Baines [13]. W. G. Cornell [14] also provides some information on single-screen drag coefficients. The comparison of single-screen with multiple-screen matrices, from Fig. 15, is shown in Fig. 21. In the low $N_{R(d)}$ range strong similarities are evident, but for $N_{R(d)} > 100$ marked differences develop. The number of screens in the matrix when there are less than three apparently has a strong influence ($N_{R(d)} > 100$) for porosities on the order of 0.60 and a lesser influence for porosities on the order of 0.80. Thus from the designer's point of view the influence of the number of crossed-rod pairs or screens on friction behavior for matrices consisting of less than four rows is not clearly evident at this time. In the meanwhile he may find Fig. 21 of help in making judgments.

Summary and Conclusions

The major features of this presentation may be summarized as follows:

1 Figs. 11–16 provide the designer with the basic heat-transfer and flow-friction characteristics for several configurations of crossed-rod matrices and, additionally, for previously reported woven-screen matrices over a wide range of porosity and Reynolds number.

2 Applications of such results as these are illustrated in references [6] and [7] for the periodic-flow type of heat exchanger and in reference [4] for nuclear-reactor fuel elements. Matrices of this general type also may be used in the design of electrical resistance heaters.

3 With respect to heat transfer, there is apparently no marked difference in behavior between the random, staggered, and in-line crossed-rod matrix configuration and even the woven-screen matrices.

4 With respect to flow friction, when the porosity exceeds 70 per cent there are significant differences; the staggered crossed-rod configuration shows the highest and the in-line configuration the lowest friction factor. The woven-screen and the random crossed-rod configuration behave alike.

5 The different friction behavior at high porosities of the in-line and staggered configurations is consistent with the behavior of comparable tube-bank geometries and extrapolate in the limit, as porosity approaches unity, to agree with the aerodynamic-drag behavior of single cylinders.

6 For matrices consisting of only a few crossed-rod pairs or screens, the designer will have to use judgments developed with the aid of Figs. 16 and 21 to modify the basic design data for the many row matrices as presented here.

Acknowledgments

The previous work done in this area by Messrs. G. L. Locke, J. E. Coppage, and L. S. Tong, former graduate students at Stanford, made possible this presentation. The Harrison Radiator Division of General Motors, through Mr. John Godfrey, provided

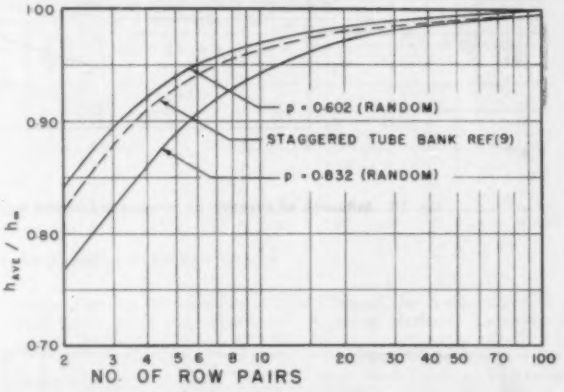

Fig. 16 Influence on average heat-transfer coefficient of number of screens or pairs of crossed-rod rows in matrix

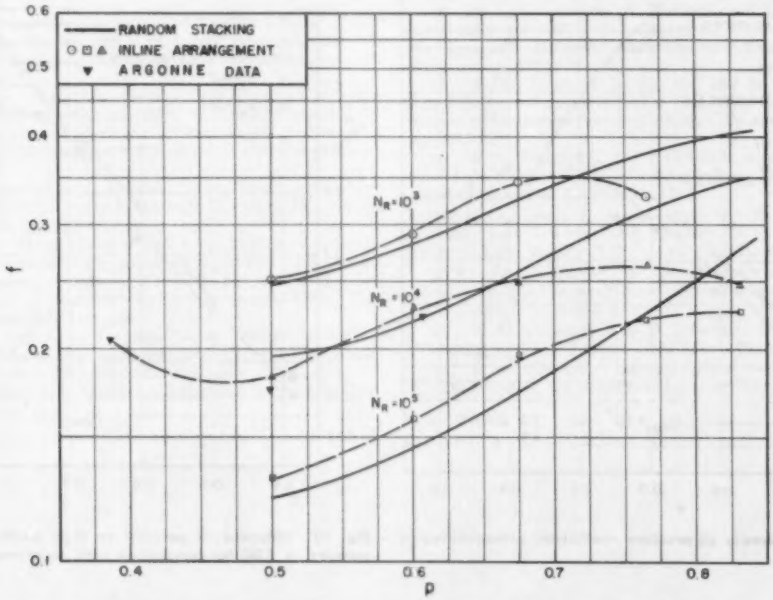

Fig. 17 Influence of porosity on crossed-rod-matrix friction factor, f_f in-line and random configurations compared

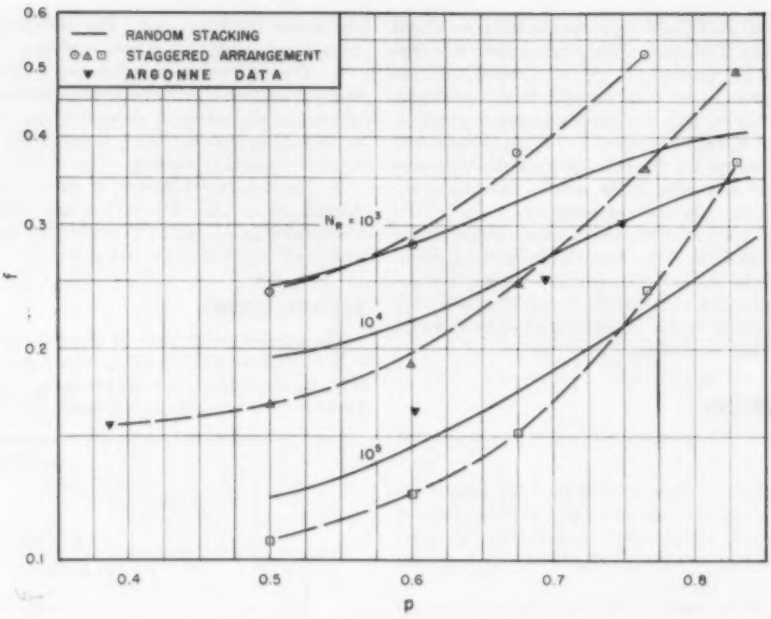

Fig. 18 Influence of porosity on crossed-rod-matrix friction factor, f_f staggered and random configurations compared

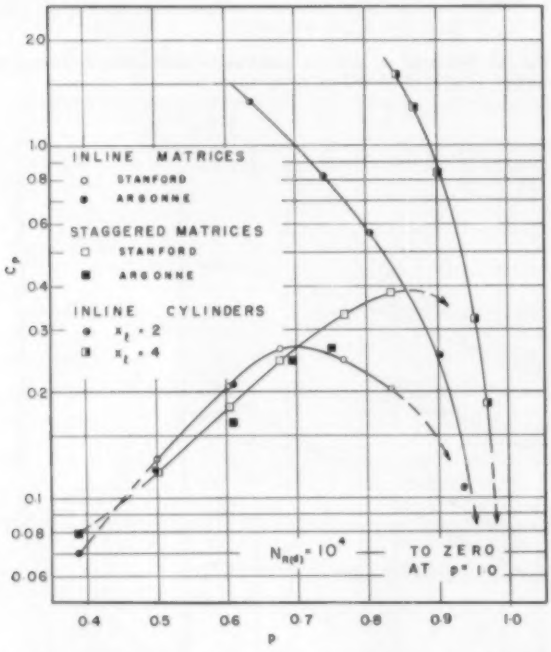

Fig. 19 Influence of porosity on pressure coefficient; extrapolation to porosity = 1.00

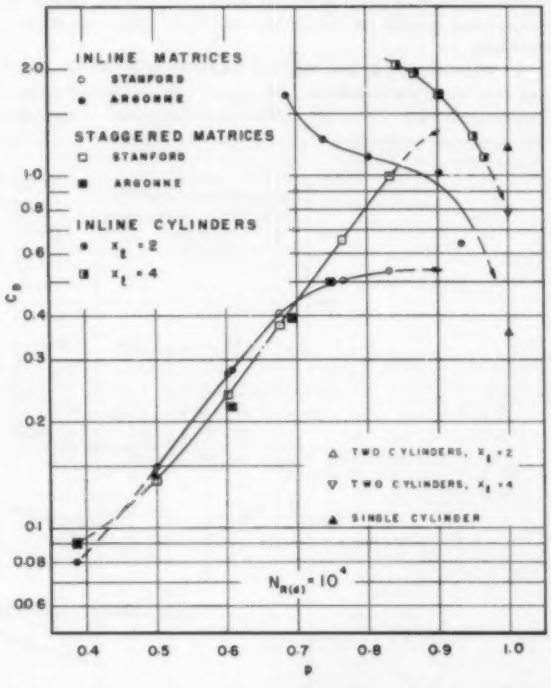

Fig. 20 Influence of porosity on drag coefficient; extrapolation of porosity = 1.00 for comparison with aerodynamic-drag information

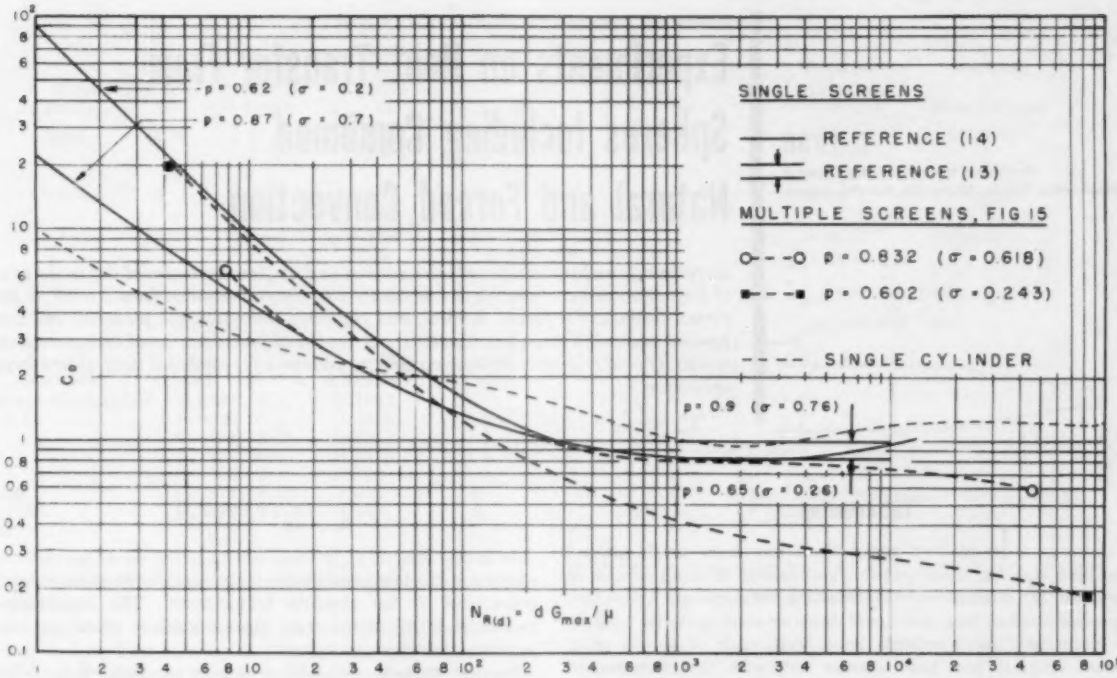
p = 0.62 (σ = 0.2)
p = 0.87 (σ = 0.7)
SINGLE SCREENS
REFERENCE (14)
REFERENCE (13)
MULTIPLE SCREENS, FIG 15
p = 0.832 (σ = 0.618)
p = 0.602 (σ = 0.243)
SINGLE CYLINDER
p = 0.9 (σ = 0.76)
p = 0.65 (σ = 0.26)
C*
N_R(d) = d G_max / μ

Fig. 21 Comparison of friction behavior of single and multiple screens

the very excellent micromanometer used for the small pressure-drop measurements that established the friction behavior at the lower test Reynolds numbers. This work is part of a heat-transfer and thermodynamics research program at Stanford University sponsored by the Office of Naval Research, Contract Nonr 225(23).

References

1 G. L. Locke, "Heat Transfer and Flow Friction Characteristics of Porous Solids," TR-No. 10, Office of Naval Research Contract N6onr 251 Task 6, Department of Mechanical Engineering, Stanford University, June, 1950.

2(*a*) J. E. Coppage, "Heat Transfer and Flow Friction Characteristics of Porous Media," TR-No. 16, Office of Naval Research Contract N6onr 251 Task 6, Department of Mechanical Engineering, Stanford University, December, 1952. Reference 2(*b*) is a summary of this report.

2(*b*) J. E. Coppage and A. L. London, "Heat Transfer and Flow Friction Characteristics of Porous Media," *Chemical Engineering Progress*, vol. 52, 1956, pp. 57F–63F.

3(*a*) L. S. Tong, "Heat Transfer and Flow Friction Characteristics of Screen Matrices at High Reynolds Numbers," TR-No. 28, Office of Naval Research Contract Nonr 225(23), Department of Mechanical Engineering, Stanford University, April, 1956. Reference 3(*b*) is a summary of this report

3(*b*) L. S. Tong and A. L. London, "Heat-Transfer and Flow-Friction Characteristics of Woven-Screen and Crossed-Rod Matrices," TRANS. ASME, vol. 79, 1957, pp. 1558–1570.

4 G. A. Freund and A. L. London, "A General Method for Comparing Thermal Performance of Fuel Element Geometries and Coolants for Non-Boiling Reactors," Argonne National Laboratory Report ANL-5589, January, 1957.

5 J. F. Matousek, "Cross-Rod Matrices—Flow Friction Behavior and Recommended Thermal Design Data," Argonne National Laboratory Report ANL-5590, April, 1957.

6 P. T. Vickers, "Rotary Regenerators for the Whirlfire Vehicular Turbines," ASME Paper No. 59—GTP-12, 1959.

7 W. M. Kays and A. L. London, "Compact Heat Exchangers," McGraw-Hill Book Company, Inc., New York, N. Y., 1959.

8 A. L. London, H. B. Nottage, and L. M. K. Boelter, "Determination of Unit Conductances for Heat and Mass Transfer by the Transient Method," *Industrial and Engineering Chemistry*, vol. 33, 1941, pp. 467–473.

9 W. M. Kays, A. L. London, and R. K. Lo, "Heat Transfer and Friction Characteristics for Gas Flow Normal to Tube Banks—Use of a Transient-Test Technique," TRANS. ASME, vol. 76, 1954, pp. 387–396.

10 R. A. DeBortoli, R. E. Grimble, and J. E. Zerbe, "Average and Local Heat Transfer for Crossflow Through a Tube Bank," ASME Paper No. 55—SA-51, 1955.

11 A. J. Gram, C. O. Mackey, and E. S. Monroe, Jr., "Convection Heat Transfer and Pressure Drop of Air Flowing Across In-Line Tube Banks, II," TRANS. ASME, vol. 80, 1958, pp. 25–33.

12 J. K. Salisbury, editor, "Kent's Mechanical Engineers' Handbook—12 Edition Power," John Wiley & Sons, Inc., New York, N. Y., section 15, 1950, p. 16.

13 W. D. Baines and E. G. Peterson, "An Investigation of Flow Through Screens," TRANS. ASME, vol. 73, 1951, pp. 467–480.

14 W. G. Cornell, "Losses in Flow Normal to Plane Screens," TRANS. ASME, vol. 80, 1958, pp. 791–799.

Experiments on Heat Transfer From Spheres Including Combined Natural and Forced Convection

T. YUGE
Professor, Institute of High Speed Mechanics, Tōhoku University, Sendai, Japan

Experiments on heat transfer between spheres and air flow were carried out in the range of Reynolds numbers from 3.5 to 1.44 × 10^5 and Grashof numbers from 1 to 10^8. Empirical formulas for forced, natural, and combined convection are presented and comparison made with other investigations. A graphical procedure, based on experimental results, is used to predict the heat-transfer performance for combined natural and forced convection.

Introduction

In recent times there has been much interest in heat transfer, mass transfer, and motion of small spheres in studies of combustion, condensation, absorption, and other processes where there are liquid drops or small particles. Many experimental measurements have been made of sphere drag, mass transfer, and heat transfer but, with the exception of sphere drag, the range of Reynolds number was limited.

Previously the author [1][1] had published experimental heat-transfer data for the Reynolds number range from 1.3 × 10^5 to 650. In the present second investigation presented here which is considered to be of greater accuracy than the afore-mentioned, the experimental range of Reynolds number was extended from 1.44 × 10^5 to 3.5 which was extended further by theory to Reynolds numbers near zero. A further extension of the investigation included here are experimental results for natural convection in the Grashof modulus range from 1 to 10^8 and combined natural and forced convection for cross, opposed, and parallel air flows at Reynolds number below 2535. The results of these experiments were reported but the details of the investigations at Reynolds numbers above 5.9 × 10^3 are not included as it is a current study of the influence of turbulence on heat transfer to spheres to be reported later.

Experimental Methods

Measurements were made by two different methods—steady and transient similar to that used in the previous investigation [1].

Steady-State Method. Denoting the heat-transfer coefficients for convection and radiation by h and h_r, respectively, for steady-heat flow,

$$h + h_r = \frac{Q}{A(t_s - t_a)} \tag{1}$$

where Q is the heat-transfer rate, A the surface area, t_s and t_a the temperature of the sphere surface and the surrounding air. The heat-transfer coefficient for radiation is defined as

$$h_r = \epsilon\sigma \frac{(T_s^4 - T_a^4)}{t_s - t_a} \tag{2}$$

where ϵ is the total emissivity, σ the black-body radiation constant, and T the absolute temperature. The heat-transfer coefficient is calculated from these equations when all other quantities have been measured.

Transient Method. Consider a sphere of high thermal-conductivity material at temperature t, specific heat c, and weight w exposed to an air flow at constant colder temperature t_a. Then in the time interval $d\theta$,

$$wcdt = (h + h_r)(t - t_a)Ad\theta.$$

For the small time interval $\Delta\theta$, obtain by integration

$$h + h_r = \frac{wc}{A}\frac{1}{\Delta\theta}\ln\frac{t_1 - t_a}{t_2 - t_a} \tag{3}$$

where t_1 and t_2 are the temperatures of the sphere at the beginning and end of the time interval.

The mean temperature difference for the time interval is then

$$\Delta t_m = (t_1 - t_2)\Big/\ln\frac{t_1 - t_a}{t_2 - t_a} \tag{4}$$

The heat-transfer coefficient is calculated by using equations (2) and (3) and measuring all other quantities.

Equipment

The specifications for the wind tunnels, sizes of test spheres, type of combined convection, Reynolds number, and Grashof number ranges are summarized in Table 1. The three types of combined convection were obtained by setting the wind tunnel in horizontal, upright, and upset positions.

Wind Tunnels. Fig. 1 shows the scheme of the two interchangeable wind tunnels used, which are both suction free jet type.

The smaller (first) wind tunnel is connected on the downstream end, in order, to an air cooler, an anemometer, an air-speed regulator, air dampers, and finally to vacuum pumps. It was observed that the flow was laminar and without pulsations.

The larger (second) wind tunnel was operated by a centrifugal fan driven by a 1/2-hp d-c motor and regulation of wind velocity was done by adjusting the motor speed.

The third wind tunnel was operated by a 3-hp axial fan in place of the afore-mentioned centrifugal fan.

The velocity distribution in the working section of the tunnels

[1] Numbers in brackets designate References at end of paper.

Contributed by the Heat Transfer Division and presented at the Annual Meeting, Atlantic City, N. J., November 29–December 4, 1959, of The American Society of Mechanical Engineers.

Note: Statements and opinions advanced in papers are to be understood as individual expressions of their authors and not those of the Society. Manuscript received at ASME Headquarters, August 13, 1959. Paper No. 59—A-123.

Table 1 Principal items of experiments and apparatus

Wind tunnel	Diam of jet, in.	Wind velocity, ft/sec	Diam of test pieces, in.	Re	Gr	Type of combined convection	Methods of measurement
First	2.4	0.2 ~ 1.2	0.0384 ~ 0.2482	3.5 ~ 110	1 ~ 1.85 × 10^3	cross parallel counter	transient
Second	10	0.7 ~ 6.0	0.381 0.878	123 ~ 2535	1.35 × 10^3 ~ 1.05 × 10^6	cross	steady
Third	10	33 ~ 115	0.878 2.36	5.9 × 10^3 ~ 1.44 × 10^5		cross	steady

Table 2 Data of some quantities on test pieces for transient method

Material and tolerance	Diam of test piece, in.	$\log_{10}\frac{t_1 - t_a}{t_2 - t_a}$	$\frac{uc}{A}$ Btu / ft² deg F	Corrections for heat loss-per cent
Carbon-chrome steel ± 5μ	0.0384	0.2	0.1382	3.5
	0.0620	0.2	0.2328	2.0
	0.0777	0.2	0.2927	0.9
	0.1172	0.1	0.4426	0.5
	0.1395	0.1	0.532	0.3
Brass ±15μ	0.1875	0.05	0.616	0
	0.2482	0.025	0.818	0

was observed to be uniform over more than 80 per cent of the diameter, on horizontal and vertical diametral lines, by utilizing anemometers.

Test Spheres for Transient Method. Seven test spheres different in size were used (see Table 2). The spheres were suspended at both sides by the temperature measuring chromel-alumel thermocouple wires and, for the larger spheres, by two diagonal wires as shown in Fig. 2. The thermocouple wires and junction, located at the center of the sphere, were electrically insulated by using alumina paste. The thermocouple wires are run through small glass tubes held in a yoke of larger ones as shown in the figure. The wires, of thermocouple-wire material shown at an angle of 30 deg from the horizon also served to experimentally determine the wire-conduction losses.

Care was taken to prevent alteration of the thermocouple response characteristics due to tension. The test spheres were highly finished in shape and surface polish. The thermocouple and support wires in the flow region of the sphere were rubbed down by an electrolytic-slide-polishing method [3] from 70μ to 20μ diameter, without any change of the characteristics of the thermocouple. This was done to prevent decreased sensitivity in the thermocouple circuit and to reduce the heat-conduction losses.

Test Spheres for Steady-State Method. Three test spheres were used (see Table 1). Fig. 3 shows the scheme for two smaller test spheres, partly simplified. A spherically shaped electrical heater is fitted tightly in hollow space, by using alumina paste, and the lead wires run through the glass and steel-pipe support sting as shown. An auxiliary heater, fixed between two glass tubes on the sting, supplies a counterheat flow to prevent conduction losses along the support. Heat balance was obtained by making the temperature difference between thermocouples 7 and 8 zero.

The sphere surface temperature was measured as seven points 1 to 7 shown in the figure. The thermocouples are led through drilled holes and along small grooves to exit on an insulating thread cover which is wrapped over the auxiliary heater. These were further wound with thread to keep them warm throughout. Care was taken in finishing the sphere shape and surface and in prevention of counterheat conduction through the thermocouple lead wires from the auxiliary heater. The ratio of the cross-sectional area of the supporting rod to the surface area of the test sphere is about 0.3 per cent. Deviation of temperature difference at any point on the sphere surface from the mean temperature difference was less than 0.1 per cent.

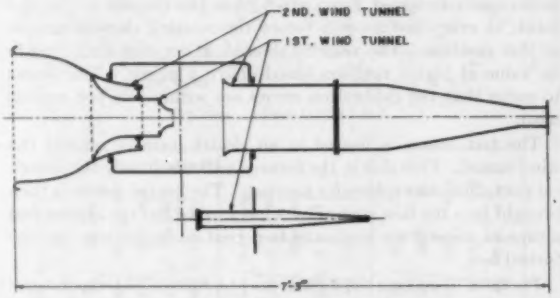

Fig. 1 Wind tunnels

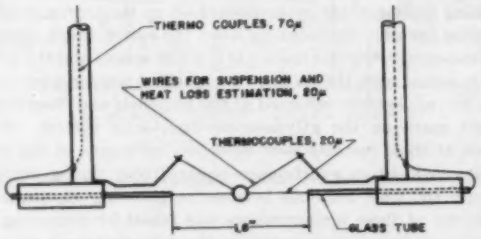

Fig. 2 Test spheres for transient method

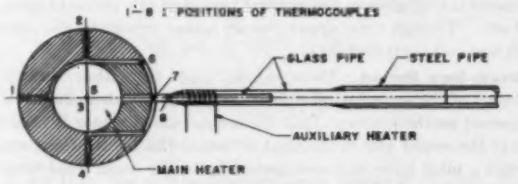

Fig. 3 Test spheres for steady-state method

The construction of the largest test sphere is substantially similar to the afore-mentioned except that a hollow spherical electrical heater was used.

Temperature measurement was made with 70μ-diameter copper-constantan thermocouples by using a potentiometer capable of 0.1 microvolt.

Experimental Procedure

Transient Method. Measurement and regulation of wind velocity was made by a first and second thermocouple anemometer. The first is set in the test position, without the test sphere, and comes into the same condition of heat transfer as the test sphere. The first anemometer, previously calibrated on the rotating arm, is thus used to calibrate the second anemometer which is fixed in position. The calibration was done in the circular doughnut-type chamber enclosed by a gauze in which the temperature sensing element of the anemometer is introduced through a circular slit opened at the bottom of the chamber. This reduced

the undesirable irregular motion of a wind drift caused by the arm.

One of the errors of the calibration is the estimation of the rotating velocity of air current. The measured velocity was below 10 per cent at the highest rotating velocity of the element and zero at lower velocities. Accordingly, even though the component velocity of air normal to the rotation direction was as much as 40 per cent of the measured value, error, due to regarding the measured value as the rotating air velocity, is 8 per cent and it results in an error below one per cent in the calibration of the anemometer. The induced air velocity was measured by the anemometer mounted 2-mm apart from the passage of the element, at every instant just before the rotating element arrives at that position. The velocity showed 20 per cent scattering in its value at higher rotation speed above 1 m/sec. This seems to mean that the calibration errors are within two per cent at most.

The test sphere is heated in an electric furnace outside the wind tunnel. Fine slits in the furnace wall admit only the spherical part of the test sphere for heating. The heated sphere is then brought into the flow stream by a mechanical linkage system and a time of about 3 sec is allowed to permit recovery from the disturbed flow.

Previous to making the measurements, successive temperatures $t_1, t_2, t_3 \ldots$ are specified in order that the $\ln (t_1 - t_a)/(t_2 - t_a)$ in equation (3) takes definite values (see Table 2) and the corresponding thermocouple potentials are set on the terminals of the potential circuit. By following down the switch which connects a galvanometer, the thermocouple of a test sphere and the terminals in series, with the cooling, the specified temperature conditions are successively obtained at the terminals and observed by a light mark on the galvanometer-lamp-scale system. Voice signals at these instants were recorded, by means of the relay circuit, on a 4-rpm synchronous-motor-driven timing drum to measure the time intervals between neighboring signals. The sensitivity of these measurements was raised by increasing the optical path length to 8 meters in the galvanometer-lamp-scale system. The error due to the transient operation of the galvanometer is negligible as the natural period of the galvanometer is 0.2 sec. Though these apparatus are rather primitive, the operation was quite satisfactory.

Steady-State Method. Measurement and regulation of wind velocity of the second wind tunnel are the same as described in the transient method, except that the second anemometer is located out of the center axis of the wind stream. But for the third wind tunnel a pitot tube was used according to the usual wind-tunnel test procedure. The test sphere was supported from the downstream side and the electrical currents are supplied to the main and auxiliary heaters by different batteries and slide-wire rheostats are used for control. The heat-transfer rate of the sphere is evaluated from both of the voltage drops at the heater and the standard resistor connected in series with the heater, measured with the afore-mentioned potentiometer. The auxiliary heater prevents a conduction error in the measured heat-transfer coefficient of about 30 per cent.

Materials and Properties

Emissivity. The emissivity of the brass spheres was measured at 0.24 by Nusselt's method [4]. This value was also used for the steel spheres as a 50 per cent error in this value would cause a heat-transfer coefficient error of less than two per cent.

Specific Heat. The specific heats, measured within two per cent error, are 0.092, 0.115, and 0.265 Btu/lb deg F for the brass, steel, and alumina-paste compound, respectively. Handbook values were used for other materials and the calculated values of wc/A are given in Table 2.

Heat-Conduction Losses in the Wires. The author tried to find the wire-conduction losses by comparing the rate of heat transfer on the test spheres with, and without, the diagonal support wires. Many tests were made on the two smallest spheres. For the smallest sphere the ratio of these losses to the total heat transfer was about 3.5 per cent at several velocities. Table 2 shows the values of the heat-loss correction used. These corrections for spheres larger than 0.0777-in. diameter were determined in proportion to a theoretical value (see Appendix). For test spheres larger than 0.1875-in. diameter this loss was negligible.

Physical Properties of Air. The heat-transfer data are expressed in terms of the Nusselt number hD/k_m, Reynolds number uD/ν_m, and the Grashof number $gD^3\Delta t/\nu_m^2 T_a$ where subscript m means the film temperature. The thermal conductivity and the kinematic viscosity were evaluated from the following equations

$$k = \frac{0.0167\,(1 + 1.94 \times 10^{-4}T)T^{3/2}}{T + 117} \text{ kcal/}m \text{ hr deg } C$$

$$\nu = 1.33323 \times 10^{-5} \frac{380}{380 + t}\left(\frac{273 + t}{273}\right)^{3/2}\frac{760}{p} \, m^2/\text{sec}$$

where p is the pressure in mm Hg.

Heat-Transfer Data

Some of the heat-transfer data for the three combinations of cross, counter and parallel flow, are shown in Figs. 4(a to d). The dashed lines show the natural convection equation (8) and the full lines the combined convection equations (13) to (16) given later in the paper. In Figs. 4(a and b) it is shown that the effect of natural convection is large, especially in the case of counterflow. The existence of regions is recognized in the figures where the heat-transfer coefficients are even less than for natural convection alone. In these regions, a variation in the falling rate of the sphere temperature was clearly seen in a shifting speed of the light mark on the lamp scale, indicating a nearly periodic variation of a high heat-transfer rate for a short time followed by a low rate for a long time. This behavior was remarkable for the larger spheres and accordingly it may be considered difficult to keep a thermal balance for counterflow at greater values of Grashof number. The same figures show also that natural convection effect for crossflow is smaller than that for parallel flow. In Fig. 4(d) it is shown that heat transfer was done by forced convection only, from the facts that the full lines were plotted from equation (5), and that discrepancies between the plotted points and the lines become larger for smaller air velocity or Reynolds number.

Part of the steady-state data are shown in Fig. 5.

The symbols Δ in Fig. 6 are the data which are considered to be uninfluenced by air turbulence; they will be reported later in detail, as mentioned in the introduction.

Forced Convection

Fig. 6 shows the heat-transfer results obtained in forced convection and reveals them to be markedly lower than Williams [5] at higher Reynolds number, in fair agreement with others [1, 6, 7] at medium values of Reynolds number, and to be in very good agreement with Allander [8] and the mass-transfer results of Frössling [9] by analogy, at low Reynolds numbers from 10 to 800, when the value of Prandtl number is taken as 0.715. These results based on properties evaluated at the film temperature are presented by the formulas

$$\text{Nu} = 2 + 0.493\,\text{Re}^{0.5} \qquad \text{for } 10 < \text{Re} < 1.8 \times 10^3 \qquad (5)$$

$$\text{Nu} = 2 + 0.300\,\text{Re}^{0.5054} \qquad \text{for } 1.8 \times 10^3 < \text{Re} < 1.5 \times 10^5 \qquad (6)$$

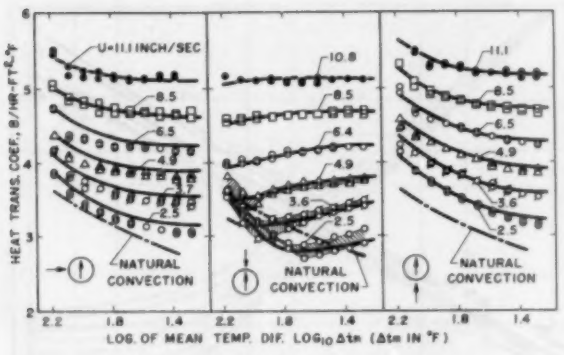

Fig. 4(a) (diam 0.2482 in.)

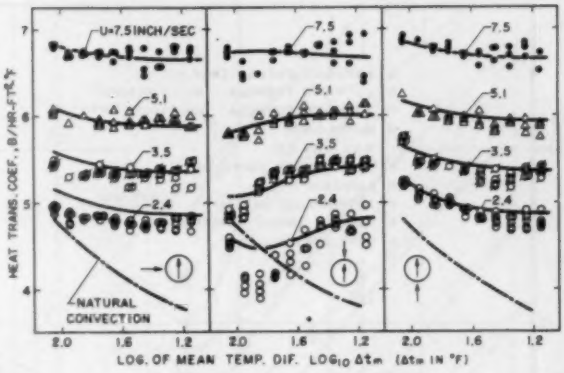

Fig. 4(b) (diam 0.1395 in.)

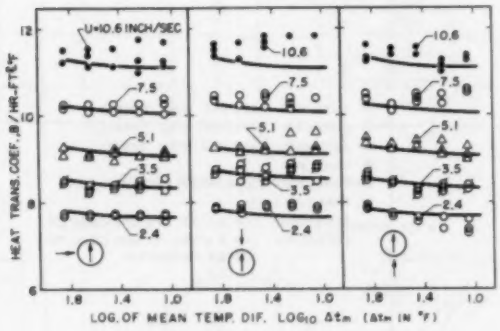

Fig. 4(c) (diam 0.0777 in.)

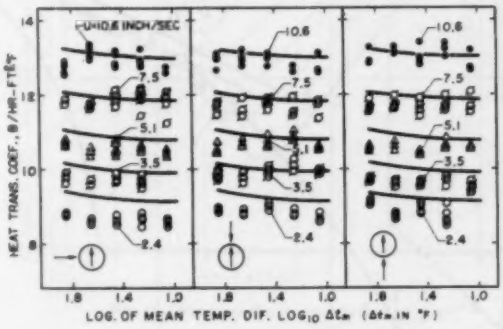

Fig. 4(d) (diam 0.0620 in.)

Fig. 4 Variation of heat-transfer coefficient h with temperature differences at different wind velocities. From left to right: Directions of forced convection and natural convection are cross, counter, and parallel, respectively.

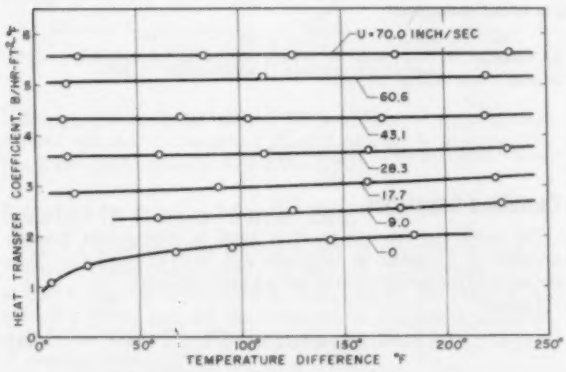

Fig. 5 Variation of heat-transfer coefficient h with temperature differences at different wind velocities (diam 0.878 in.) crossflow

For Reynolds number below 10 the Nusselt numbers are seen to begin falling gradually from equation (5) (B line), the difference being more than 10 per cent at Re = 3.5. This departure seems to be substantial and not due to experimental errors judging from an investigation of Figs. 4(*d*) and 7 or the accuracy of the experiments.

For this low Reynolds number range, theoretical solutions have been published by Kronig and Bruijsten [15] and the author [2] suming Stokes' flow. The former solution does not completely satisfy the boundary conditions. Another solution [16], obtained by assuming the velocity implied in the convection term of the energy equation as the uniform velocity u is expressed in the following form, which also satisfies Kronig's and Bruijsten's solution

$$\mathrm{Nu} = 2 + 0.5\ \mathrm{Pe} + 0(\mathrm{Pe}^2) \tag{7}$$

where

$$\mathrm{Pe} = \text{Péclet number} = \mathrm{Re\ Pr}$$

and 0 means order of magnitude.

Point D in Fig. 6 was obtained from equation (7), the third term omitted, by putting Pe = 0.1 and the arrows bounded by short horizontal bars show the variation in (Nu − 2) by assuming that the third term is one tenth of the second term. This point and the dotted line drawn through are based on the theory that the convection effect is overestimated. Points A and the arrows show the author's successive approximate solution and its one per cent error, respectively.

The upper limit of Reynolds number for the Stokes' solution is about 0.4 which gives calculated values of the drag coefficient that are 4 and 20 per cent lower than measured at Reynolds numbers of 1 and 3, respectively. If the theoretical solution underestimates the friction force then the theoretical Nusselt numbers will underestimate the heat-transfer coefficient. Accordingly, the curve which connects the valid portion of the theoretical points at Reynolds number near 0.4 and experimental data at Reynolds number near 3 is consistent with the foregoing. This curve presents rapid decrease of the increasing rate of (Nu − 2), which is Nusselt number dependent only on the convection current, with increase of Reynolds number, at Reynolds number between 2 and 10. But this seems to be consistent with the

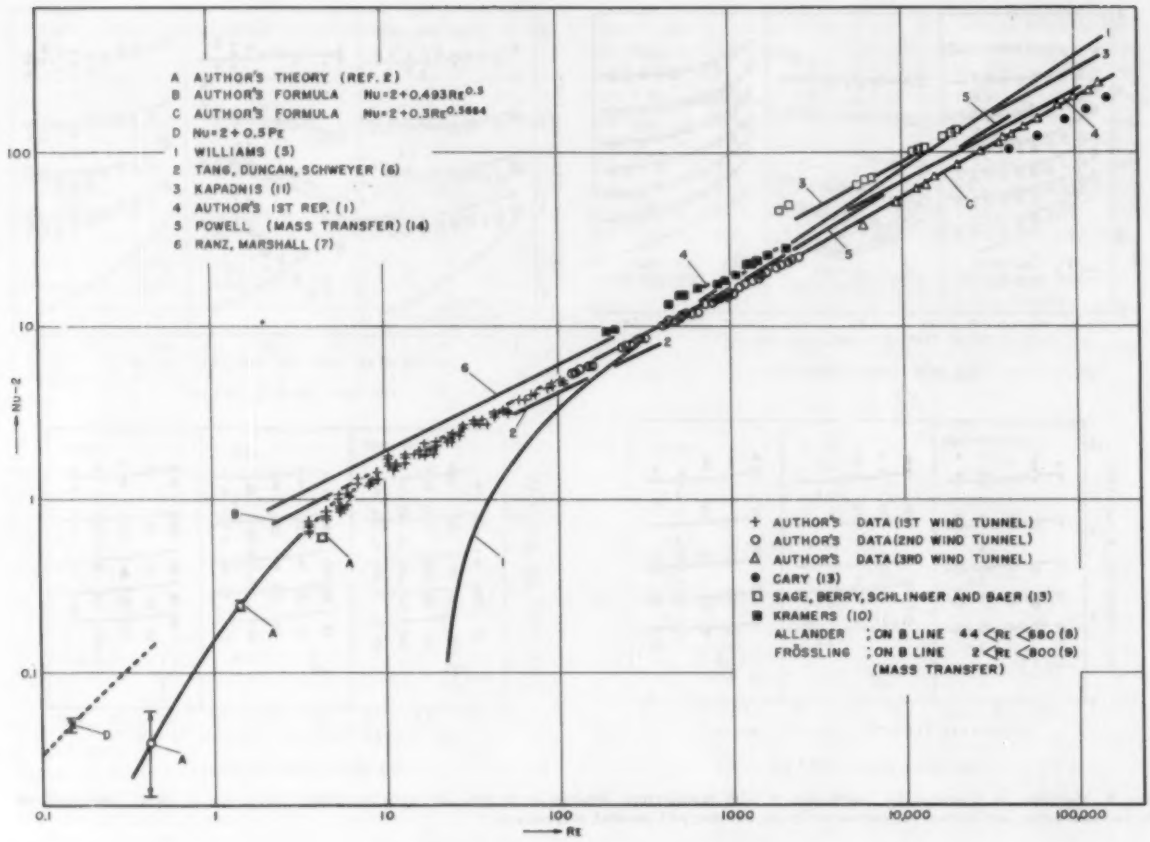

Fig. 6 Heat-transfer data in forced convection

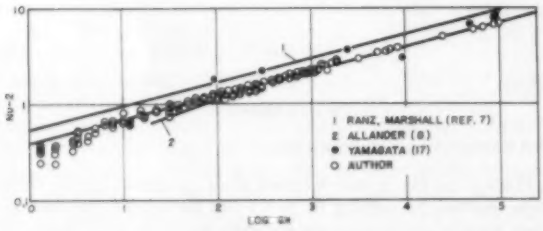

Fig. 7 Heat-transfer data in natural convection

experimental results by Nishi and Porter [17], that a vortex ring is formed at Reynolds number 8.15, for a sphere in an air flow, and the flow separation occurs, of course, below 8.15 and above 1, because it is clear that both the vortex and the dead space tend to prevent heat transfer.

Natural Convection

Natural-convection data by Yamagata [18] and the author are shown in Fig. 7 and compared with the empirical formulas of Allander [8] and Ranz and Marshall [7]. The line drawn through the plotted points is represented by

$$\mathrm{Nu} = 2 + 0.392\ \mathrm{Gr}^{0.25} \quad \text{for } 1 < \mathrm{Gr} < 10^5 \tag{8}$$

where properties are evaluated at the film temperature.

A tendency is seen for the plotted points to fall from this line at Grashof number near 1, which seems to be consistent with Mahony's equation [19]

$$\mathrm{Nu} = 2 + 0(\mathrm{Gr}^{0.5}) \quad \text{for} \quad \mathrm{Gr} \ll 1 \tag{9}$$

where 0 means order of magnitude.

Combined Convection

For combined convection, it is usual to express the Nusselt numbers in a relation of Reynolds and Grashof numbers. But the method followed in this paper is a little different.

Define:

$$\text{for forced convection } N_R = 0.493\ \mathrm{Re}^{0.5} \tag{10}$$

$$\text{for natural convection } N_G = 0.392\ \mathrm{Gr}^{0.25} \tag{11}$$

$$\text{for combined convection } N_K = \mathrm{Nu} - 2 \tag{12}$$

which defined numbers may be considered as Nusselt numbers dependent only on the convection current, apart from the molecular diffusion.

Fig. 8 shows the results for the case of crossflow in which the mean of the measured values of N_K are plotted versus N_R with the parameter N_G. The line drawn through the origin at an angle of 45 deg represents $N_K = N_R$ which accordingly shows the case of forced convection only. Further, the difference of the ordinates between that line and the curve of constant N_G, which is $N_K - N_R$, shows the increment of value in the Nusselt number due to N_G, i.e., natural convection.

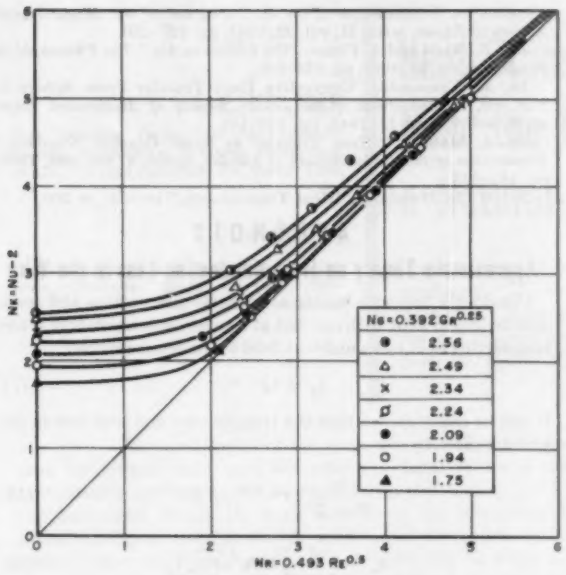

Fig. 8 Heat transfer in crossflow

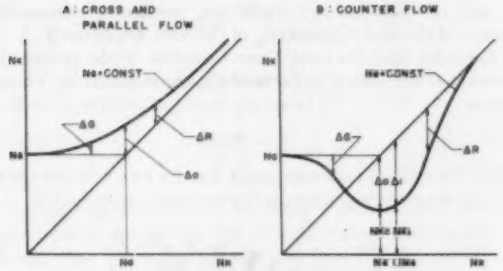

Fig. 9 Illustrations of heat-transfer formula

The procedures to be followed for prediction of the combined natural and forced-convection Nusselt number is illustrated in Fig. 9 and the formulas in the next section.

Procedure for Cross and Parallel Flows

Fig. 9(a) illustrates the application of the following procedure. There are three fundamental quantities, Δ_0 the increment of N_K at $N_R = N_G$, ΔR the increment in N_K due to the effect of N_G when $N_R > N_G$, and ΔG the increment in N_K due to the effect of N_R when $N_R < N_G$. The empirical formulas for the two cases of cross and parallel flow:

$$\begin{aligned} &\text{for } N_R > N_G,\ N_K = N_R + \Delta R \\ &\text{for } N_R < N_G,\ N_K = N_G + \Delta G \end{aligned} \tag{13}$$

where

$$\begin{aligned} \Delta R &= \Delta_0 \exp\,[-n\,(N_R - N_G)] \\ \Delta G &= \Delta_0 \exp\,[-m\,(N_G - N_R)] \\ \Delta_0 &= (N_K - N_R) \text{ at } N_R = N_G, \text{ as shown in Fig. 9}(a) \end{aligned} \tag{14}$$

Δ_0, n, and m are tabulated in Table 3.

Although this deduced equation mathematically shows $N_K > N_G$ at $N_R = 0$, its use may be allowed because the magnitude of ΔG is small there and the results agree satisfactorily with experiment. In the region $N_R < 1.7$ and within an error of 5 per cent,

$$\left.\begin{aligned} &N_K = N_R \text{ for } N_R > N_G \\ \text{and} \quad &N_K = N_G \text{ for } N_R < N_G \end{aligned}\right\} \tag{15}$$

and further, for the region $N_R > (3 \text{ or } 4) \times N_G$, the effect of natural convection seems to be quite negligible.

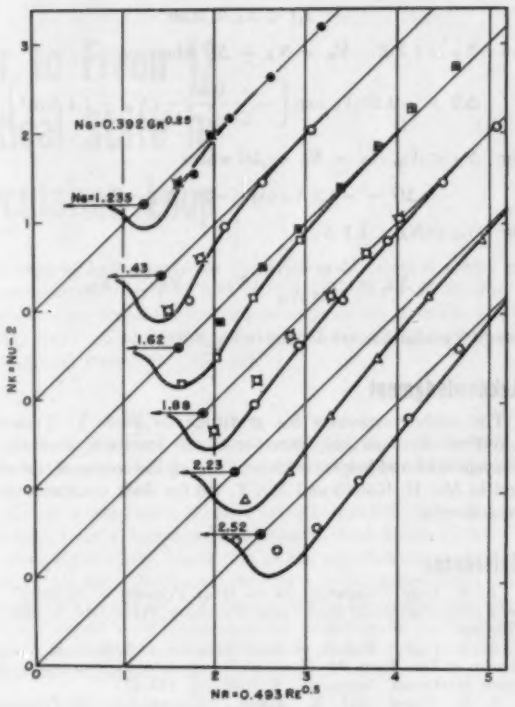

Fig. 10 Heat transfer in counterflow

Procedure for Counterflow

Fig. 10 shows the case for counterflow, where the origin is shifted for each value of the parameter N_G to avoid confusion of the figures. It is seen in the figure that minima occur near the point $N_R = N_G$ or where $Re = 0.632\sqrt{Gr}$. Further, it is seen, on comparing Figs. 8 and 10 or 4(a and c), that the counterflow values of Δ_0 are larger than those for cross and parallel flow at small Grashof numbers and conversely, they are the smaller values at large Grashof numbers. This seems to be consistent and expresses the experimental fact of difficulty in keeping a thermal balance with natural convection in counterflow at the larger values of Grashof numbers.

Fig. 9(b) illustrates the application of the following counterflow procedure for the region

Table 3 Values of Δ_0, n, and m

Case	Range	Δ_0	n	m
Crossflow	$7 > N_G > 2.56$	$\dfrac{0.257}{N_G}$	$\dfrac{0.693}{2 + 0.2\,N_G}$	$\dfrac{1 + 0.011\,N_G}{(1 + 0.1\,N_G)}$
	$N_G < 2.56$	$\dfrac{0.0154}{N_G^4}$	$18/N_G^4$	$47/N_G^4$
Parallel flow	$N_G < 2.56$	$\dfrac{0.0192}{N_G^4}$	$15/N_G^4$	$37/N_G^4$

$$1.1 < N_G < 2.56$$

for $N_R > 1.1\,N_G$, $N_K = N_R + \Delta R$ where

$$\Delta R = -0.27\,N_G \exp\left[-\frac{0.55}{(N_G - 1)}(N_R - 1.1\,N_G)^2\right]$$

for $N_R < N_G$, $N_K = N_G + \Delta G$ where

$$\Delta G = -0.2\,N_G \exp\left[-24\,(N_G - N_R)^2\right] \tag{16}$$

for $N_G < N_R < 1.1\,N_G$

$$N_K = \frac{N_R - N_G}{0.1\,N_G}(N_{K1} - N_{K0}) + N_{K0}$$

where N_{K1} and N_{K0} are defined in Fig. 9(*b*).

Acknowledgment

The author expresses his gratitude to Prof. Y. Tanasawa and Prof. F. Numachi, Director of the Institute for their encouragement and helpful criticisms during the course of the work, and to Mr. H. Kondō and Mr. T. Itō for their assistance in his experiments.

References

1 T. Yuge, "Experiments on Heat Transfer of Spheres," *Reports of the Institute of High Speed Mechanics*, Japan, vol. 5, 1955, pp. 175–183.

2 T. Yuge, "Theory of Heat Transfer of Spheres in Uniform Stream at Low Reynolds Numbers," *Reports of the Institute of High Speed Mechanics*, Japan, vol. 6, 1956, pp. 143–151.

3 K. Nagai and K. Mano, "Electrolytic-Slide-Polishing," *Science Reports of the Research Institute, Tōhoku University*, series B, vol. 1, 2, 1951, pp. 391–398.

4 W. Nusselt, "Die Wärmeübergang in der Verbrennungskraftmaschine," VDI Forschungheft 264, 1923.

5 W. H. McAdams, "Heat Transmission," McGraw-Hill Book Company, Inc., New York, N. Y., 1954, p. 265.

6 Y. Tang, J. Duncan, and H. Schweyer, "Heat and Momentum Transfer Between a Spherical Particle and Air Streams," NACA TN 2867, 1953.

7 W. E. Rana and W. R. Marshall, "Evaporation From Drops," *Chemical Engineering Progress*, vol. 48, 1952, pp. 141–146, pp. 173–180.

8 C. Allander, "Untersuchung des Adsorptionsvorganges in Adsorbentenschichten mit Linearer Adsorptionsisotherme," *Trans. Royal Institute of Technology*, Stockholm, no. 70, 1953.

9 N. Frössling, "Über die Verdunstung fallender Tropfen," *Beitrag Geophys.*, vol. 52, 1938, pp. 170–216.

10 H. Kramers, "Heat Transfer From Spheres to Flowing Media," *Physica*, vol. 12, 1946, pp. 61–80.

11 D. Kapadnis, "The Effect of Fluid Motion on Heat Transmission," *Indian Journal of Physics*, vol. 29, 1955, pp. 296–308.

12 D. H. Baer, W. G. Schlinger, V. J. Berry, and B. H. Sage, "Temperature Distribution in the Wake of a Heated Sphere," *Journal of Applied Mechanics*, vol. 20, TRANS. ASME, vol. 75, 1953, pp. 407–414.

13 J. R. Cary, "The Determination of Local Forced-Convection Coefficients for Spheres," TRANS. ASME, vol. 75, 1953, pp. 483–487.

14 F. H. Garner and R. W. Grafton, "Mass Transfer in Fluid Flow From a Solid Sphere," *Proceedings of the Royal Society of London*, series A, vol. 224, 1954, pp. 64–82.

15 R. Kronig and J. Bruijsten, "On the Theory of the Heat and Mass Transfer From a Sphere in a Flowing Medium at Low Values of Reynolds Number," *Applied Scientific Research*, vol. 2, 1951, pp. 439–446.

16 S. Ogiwara, "On the Evaporation of Fog and Cloud Particles (Studies on Evaporation—Part II)," *Journal of the Meteorological Society of Japan*, series II, vol. 22, 1944, pp. 127–150.

17 H. Nishi and A. Porter, "On Eddies in Air," *The Philosophical Magazine*, vol. 46, 1923, pp. 754–768.

18 K. Yamagata, "Convective Heat Transfer From Sphere in Still Air," *Transactions of the Japan Society of Mechanical Engineers*, vol. 9, Part II, 1943, pp. 132–138.

19 J. Mahony, "Heat Transfer at Small Grashof Numbers," *Proceedings of the Royal Society of London*, series A, vol. 238, 1956, pp. 412–423.

20 W. H. McAdams, "Heat Transmission," loc. cit., p. 268.

APPENDIX

Approximate Theory on Heat-Conduction Loss in the Wire

Consider a fine wire having a uniform cross section and semi-infinite length kept with one end at a constant temperature t_0 and transferring heat to an ambient fluid at the temperature

$$t_a = t_0 e^{-\tau x} \tag{17}$$[2]

It can be easily shown that the temperature and heat loss in the wire are given by

$$t = \frac{t_0}{\tau^2 - \beta^2}(\tau^2 e^{-\beta x} - \beta^2 e^{-\tau x}) \tag{18}$$

$$q_w = \frac{\tau}{\tau + \beta} t_0 \sqrt{hPk_wA_w} \tag{19}$$

where $\beta^2 = h\,P/k_w A_w$; x is measured along the wire; h, P, A_w, k_w are the heat-transfer coefficient, perimeter, cross-sectional area, and thermal conductivity of the wire, respectively.

Assuming that the local Nusselt number on the sphere at the position of the wire is equal to the mean value[2] [2, 9] τ may be put as

$$\tau = \mathrm{Nu}/D \tag{20}$$

Then the ratio of heat-conduction loss for two wires to the heat transfer from the test sphere is approximately expressed by

$$\frac{2q_w}{q_s} = \frac{\tau}{\tau + \beta}\sqrt{\frac{k_w}{k_a}}\,\frac{\sqrt{\mathrm{Nu}_w}}{\mathrm{Nu}_s}\,\frac{D_w}{D_s} \tag{21}$$

where the subscripts w, s, and a refer to the wire, sphere, and air, respectively.

If we assume [20] $k_w = 12.1$, $k_a = 0.0155$, and

$$\mathrm{Nu}_w = h_w D_w/k_a = 0.32 + 0.43\,\mathrm{Re}_w^{0.52} \tag{22}$$

then the foregoing equation (21) takes values nearly twice those determined by experiment. If the flow is like Stokes', it is clear that the foregoing calculation, in which the velocity was assumed to be uniform, will overestimate these conduction losses. Thus, from this solution, it is seen that the heat loss in the wires is almost accomplished in the thermal boundary layer of the test sphere which has a warming effect on the wires of $\tau/(\tau + \beta)$, about 0.5.

[2] This ambient fluid-exponential temperature distribution is arbitrarily selected as an approximation of the fluid temperature in the boundary layer of the sphere where the wires are attached. Note that in the boundary-layer region at the surface $x = 0$, $-k_a(\partial t_a/\partial x)_0 = k_a t_0 = h(t_0 - t_a) = h\,t_0(1 - e^{-\tau x})_{x=0} = h\,t_0$, so that $\tau = h/k_a = \mathrm{Nu}/D$.

Heat Transfer to Freon 12 Near the Critical State in a Natural-Circulation Loop

J. P. HOLMAN

Task Scientist, Fluid Mechanics Research Branch, Aeronautical Research Laboratory, WADC, Wright-Patterson Air Force Base, Ohio

J. H. BOGGS

Professor, Mechanical Engineering Department, Oklahoma State University, Stillwater, Okla. Assoc. Mem. ASME

An experimental investigation of heat transfer to Freon 12 in the critical region was conducted. A closed natural-circulation loop was used. Correlation of the data is presented. Separate equations are presented for reduced volumes less than one and for reduced volumes greater than one. The investigation covered a range of temperatures from 150 to 400 F and pressures from 500 to 950 psi.

INVESTIGATIONS of the phenomena of heat transfer near the critical state have indicated that large values of the heat-transfer coefficient may be expected in this region [1, 2].[1] Dickinson and Welch [1] have established the heat-transfer characteristics of water operating under forced convection in the critical and supercritical regions. They found that for temperatures below 660 F their data could be correlated by the conventional relation

$$\frac{hd}{k} = 0.023\left(\frac{\rho u d}{\mu}\right)^{0.8}\left(\frac{C_p\mu}{k}\right)^{0.4}$$

For surface temperatures above 800 F they found that their data could be correlated within 10 per cent by

$$\mathrm{St} = \frac{h}{C_p \rho u} = 0.00189$$

The authors were unable to obtain a correlation in terms of dimensionless groups for the critical region (650 to 800 F); instead, they presented plots of the heat-transfer coefficient h as a function of the surface temperature of the heat-transfer tube. In these plots the values of the heat-transfer coefficient become very large as the critical temperature is approached. The authors present data for pressures of 3500 and 4500 psia and for both these pressures the large increase of the heat-transfer coefficient is present although it is more pronounced for the 3500-psia points.

Doughty and Drake [2] have investigated free-convection heat transfer from a horizontal platinum wire to Freon 12 near the critical state. They found that in the superheated-vapor region away from the critical state their data could be correlated within 15 per cent by the curve recommended by McAdams [3]. In the critical region they found that the heat-transfer coefficients increase tenfold. Their results were presented as functions of reduced volume and reduced pressure defined by

$$\text{Reduced volume} = v/v_c$$

$$\text{Reduced pressure} = p/p_c$$

Within three per cent of the critical reduced volume they found that the heat-transfer film coefficient increases apparently without limit. This same increase occurs within a range of approximately one per cent of the critical reduced pressure.

Schmidt, Eckert, and Grigull [4] investigated the heat-transfer characteristics of ammonia operating near its critical state in a natural circulation loop. They defined an apparent thermal conductivity by

$$k_a = \frac{4q\,l}{\pi d^2 \Delta t_b} \tag{1}$$

and expressed this quantity in terms of dimensionless parameters related to the physical system. Their expressions were:

Laminar Flow,

$$k_a/k = 1/64(\mathrm{Gr}_b)(\mathrm{Pr})(y/d) \tag{2}$$

[1] Numbers in brackets designate References at end of paper.

Contributed by the Heat Transfer Division and presented at the Annual Meeting, Atlantic City, N. J., November 29–December 4, 1959, of THE AMERICAN SOCIETY OF MECHANICAL ENGINEERS.

NOTE: Statements and opinions advanced in papers are to be understood as individual expressions of their authors and not those of the Society. Manuscript received at ASME Headquarters, December 23, 1958. Paper No. 59—A-142.

Nomenclature

C_p = specific heat capacity at constant pressure, Btu/lb$_M$-deg F
d = a diameter, ft
g = gravitational constant, ft/hr^2
h = heat-transfer film coefficient, Btu/hr-ft^2-deg F
k = thermal conductivity, Btu/hr-ft-deg F
k_a = apparent thermal conductivity defined by equation (1), Btu/hr-ft-deg F
l = $^1/_2$ circumference of test loop, ft
l_t = length of test section, ft
p = pressure, consistent units
q = heat flow per unit time, Btu/hr
t = temperature, deg F
t_b = bulk temperature, deg F
t_w = surface temperature, deg F
u = velocity, consistent units
v = specific volume, ft^3/lb
y = vertical distance between center of test section and center of heat exchanger, ft
β = volume coefficient of expansion, 1/deg F
ρ = density, consistent units
μ = dynamic viscosity, lb/hr-ft

Dimensionless Group

Gr_b = Grashof number, $\dfrac{gd^3\beta_m\rho^2\Delta t_b}{\mu^2}$
Gr_f = $\dfrac{gd^3\beta_m\rho^2(t_w - t_b)_{\mathrm{avg}}}{\mu^2}$
Nu = Nusselt number, hd/k
Pr = Prandtl number, $C_p\mu/k$
Re = Reynolds number, $\rho u d/\mu$
St = Stanton number, $h/C_p u\rho$

Subscripts

b = bulk conditions
c = critical conditions
m = mean conditions
w = wall conditions

Turbulent Flow,

$$k_e/k = (\mathrm{Pr})(\mathrm{Gr}_b)^{1/3}(y/l)(0.316)^{-1/3}(l/d) \qquad (3)$$

These expressions show that the apparent thermal conductivity should become extremely large as the critical state is approached since both the specific-heat capacity and the volume coefficient of expansion become very large in the critical region. An experimental verification of this was given in reference [4]; however, the authors were not able to verify the exactitude of their analytical expressions due to a lack of adequate property data.

The experimental results of references [1] and [2] may be explained by a brief qualitative discussion of the critical state. According to reference [5] it is not clear whether one should speak of a critical state or a critical region. In the discussion in this paper the critical state will be considered as the point where the properties of the liquid and vapor phases of a substance have identical properties. This is the state where the surface tension of the meniscus separating the liquid and vapor phases vanishes.

In the regions having pressures lower than the critical value, boiling may take place. Boiling usually originates with the formation of small vapor bubbles on the heat-transfer surface. After these bubbles are formed they may interact with neighboring bubbles until they are eventually dissipated into the body of the fluid stream. The greater the surface tension the greater may be the size of the bubbles. The greater the size of the bubbles the less the freedom of movement of these bubbles; the less the freedom of movement, the smaller is the rate of energy or heat transfer.

As the critical point is approached the surface tension decreases. With this decrease in surface tension, smaller bubbles which disseminate very rapidly are formed on the heat-transfer surface. At the critical point the surface tension vanishes and hence a very large number of bubbles is formed which have a correspondingly rapid dissipation into the body of the fluid stream. Therefore very high heat-transfer rates may be expected in the immediate vicinity of the critical state.

If a large quantity of energy is removed by the fluid stream its caloric properties will be changed appreciably so that it would not be possible to operate exactly at the critical point. Therefore the heat-transfer rates near the critical state will depend, to a certain extent, on the total quantity of energy removed from the heat-transfer surface.

While the investigations just described have yielded valuable qualitative and quantitative information as to the heat-transfer trends to be expected in the vicinity of the critical state, it was felt that more information was needed regarding the quantitative behavior of a system operating in the critical region in terms of the significant physical parameters.

A natural-circulation loop similar to the apparatus of reference [4] was constructed using Freon 12, dichlorodifluoromethane, as the heat-transfer fluid. Freon 12 was chosen because of its relatively low critical temperature and pressure, nontoxic character, and the availability of data on its thermodynamic properties. A schematic of the test loop is shown in Fig. 1 and a photograph of the test setup is shown in Fig. 2. A photograph of the test section is given in Fig. 3. As shown, the fluid is heated in the test section and rises in the left side of the loop. Correspondingly, the fluid is cooled in the heat exchanger and falls in the right side of the loop. Hence a circulation is established because of the buoyancy forces due to the temperature difference on each side of the loop.

The test section and loop were constructed of AISI Type 304 stainless-steel tubing having a 0.500-in. OD and a 0.430-in. ID. The test section was heated by passing an electric current through the tube, and the power input was manually controlled with an induction voltage regulator on a General Electric testing transformer. Facilities were provided so that the temperature of the fluid at the entrance to the test section could be controlled manually through the water valves to the heat exchanger or by means of an electronic controller and a motorized valve. The pressure in the system was governed by the total mass of fluid in the system and the average fluid temperature. The total mass of fluid in the system was constant for each run.

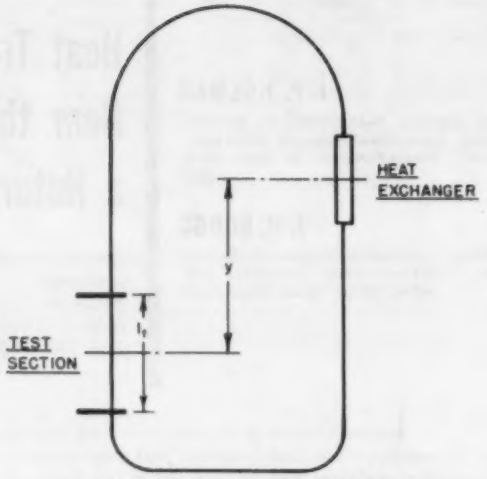

Fig. 1 Schematic of natural-circulation loop

The outside wall temperatures of the test section were obtained by measuring the outputs of No. 30 gage iron-constantan thermocouples which were spot-welded to the surface. The fluid bulk temperatures at inlet and exit to the test section were measured with a $^1/_{16}$-in-diameter thermocouple probe. The outputs of the tube-wall thermocouples were measured with a multipoint temperature recorder and the outputs of the bulk-temperature thermocouples were measured with a Rubicon precision potentiometer. The power input to the test section was measured with appropriate electrical instruments having an accuracy of one quarter of one per cent.

The flow rate of the fluid was measured by observing the differential pressure across a calibrated venturi. A venturi method of flow measurement was preferred because other methods would cause an appreciable pressure drop in the loop that would in turn directly affect the heat-transfer rate. The differential pressure across the venturi was measured with a Barton differential-pressure gage. The system pressure was measured with a Heise bourdon-tube pressure gage.

Thermodynamic properties of Freon 12 are given in reference [6]. The critical constants are:

$$t_c = 233.2 \text{ F}$$
$$p_c = 596.8 \text{ psia}$$
$$v_c = 0.02870 \text{ lb/ft}^3$$

Theory of the Thermal Syphon

Considering the forces acting on a fluid element, the driving pressure due to the buoyancy forces is

$$dp = g\rho\beta dt_y dl \qquad (4)$$

This pressure is balanced by the frictional resistance of the tube which may take one of two forms depending on the flow phenomena:

For laminar flow,

$$\Delta P_f = \frac{64\,\mu u l}{d^2} \qquad (5)$$

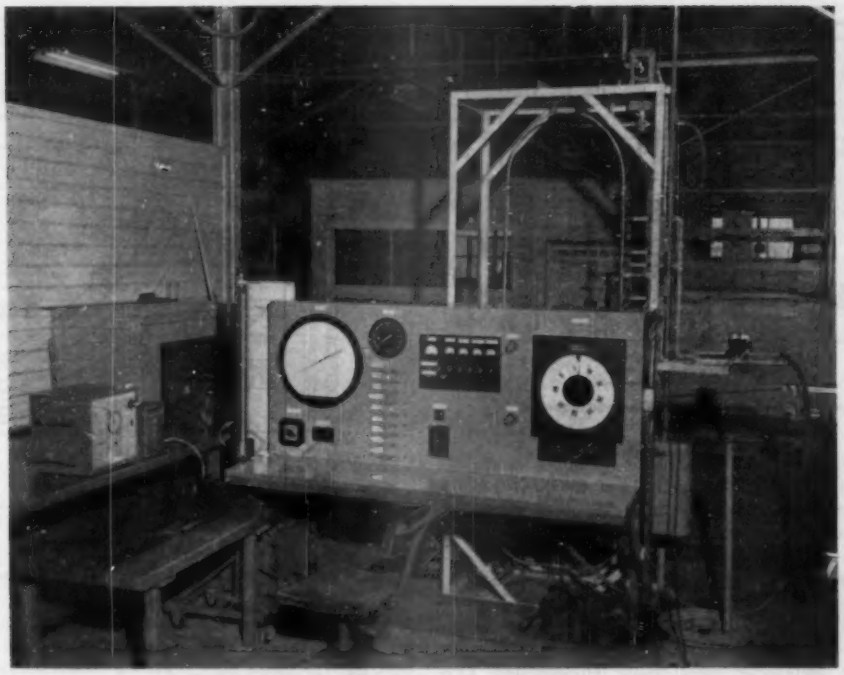

Fig. 2 Front view of test apparatus

For turbulent flow,

$$\Delta P_f = [0.316\,(\mathrm{Re})^{-1/4}]\,\frac{\rho u^2 l}{d} \tag{6}$$

This balance assumes that pressure changes due to changes in momentum are negligible and holds only for regions of operation where single-phase flow persists throughout the loop. The heat absorbed by a fluid element in the test section is given by

$$dq = \rho(\pi d^2/4)\,uC_p dt_b \tag{7}$$

One may define a heat-transfer coefficient in the conventional manner by

$$h_{avg} = \frac{q}{\pi d l_t (t_w - t_b)_{avg}} \tag{8}$$

After some algebraic manipulation the average heat-transfer coefficient for the heated section may be expressed by

$$h_{avg} = \frac{16\,\mu\,u^2 C_p}{y\,\beta_m d(t_w - t_b)_{avg}}\,(l/l_t) \tag{9}$$

for laminar flow and

$$h_{avg} = \frac{0.079\,(\mathrm{Re})^{-1/4}\,u^2\rho C_p}{y\,\beta_m\,(t_w - t_b)_{avg}}\,(l/l_t) \tag{10}$$

for turbulent flow.

The expressions for the heat-transfer coefficient may be reduced to dimensionless form by introducing the Nusselt, Reynolds, Prandtl, and Grashof numbers. Thus

$$\mathrm{Nu} = 16\,(\mathrm{Re})(\mathrm{Pr})(\mathrm{Gr}_f)^{-1}(l/l_t)(d/y) \tag{11}$$

for laminar flow and

$$\mathrm{Nu} = 0.079\,(\mathrm{Re})^{11/4}\,(\mathrm{Pr})(\mathrm{Gr}_f)^{-1}(l/l_t)(d/y) \tag{12}$$

for turbulent flow.

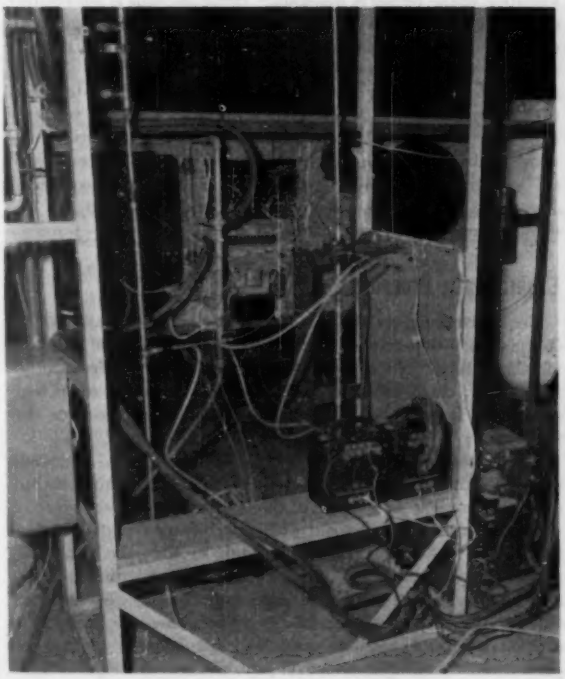

Fig. 3 Test section

While it is clear that the apparent thermal conductivity defined in reference [4] should become very large as the critical state is approached, the trend of the heat-transfer coefficient is not so apparent. Since the heat-transfer coefficient is a function of the ratio C_p/β_m and both the specific heat and the volume

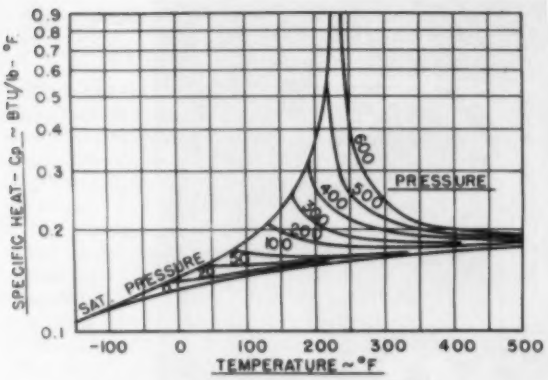

Fig. 4 Specific heat of superheated vapor Freon 12

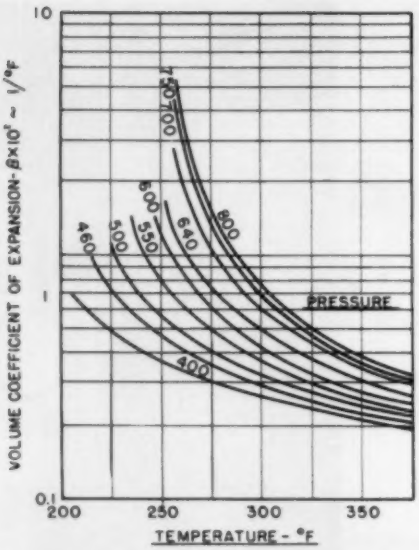

Fig. 5 Volume coefficient of expansion for superheated vapor Freon 12

coefficient of expansion become extremely large in the immediate vicinity of the critical point, an analysis of the heat-transfer behavior must involve a comparison of the rates of change of these two properties as the critical state is approached. The property data are not sufficiently accurate to make this comparison. Therefore, as in many cases, the problem reduces to one which must be solved by experimentation.

In equations (11) and (12) the thermal-syphon effect is described in terms of mean property values which are conveniently evaluated at the arithmetic mean bulk temperature. This evaluation assumes that the property values follow a linear variation in the region in question. Of course, this is not entirely correct, but in the region near the critical state the bulk-temperature difference for a given heat input, which is not too large, is small so that a linear relationship may be assumed. In the superheat region away from the critical state the bulk-temperature difference would be larger but in this region the property values are very nearly linear so that the assumption still seems valid. The assumption is certainly valid within the accuracy of the property data. The specific heat and volume coefficient of expansion for Freon 12 are plotted in Figs. 4 and 5. The values were obtained from reference [6].

Experimental Procedure

Before beginning the experiments the entire apparatus was charged to 900 psia with compressed air and allowed to stand for three days. No variations in pressure were observed other than those which could be attributed to changes in room temperature. It was therefore concluded that the apparatus was airtight.

The system was then evacuated by connecting it to a vacuum pump and the pump was allowed to run until an absolute pressure of 60 microns was established in the test setup.

The apparatus was charged with an arbitrary quantity of fluid by heating the Freon 12 supply tank so that the saturation pressure in the tank was greater than the saturation pressure corresponding to the temperature of the loop. The temperature of the loop was room temperature when no power was applied. For the room temperatures involved, the saturation pressure of Freon 12 is about 85 psia. It was usually sufficient to heat the supply tank to a point such that a pressure of 100 psia was established in the system. This insured that the system was charged entirely with liquid Freon 12.

After the system was charged, power was applied to the test section and a cooling-water flow was maintained to establish a particular test-section inlet temperature. Runs were made with a constant charge in the apparatus for several different inlet temperatures to the test section. The procedure was repeated for successively smaller charges by bleeding part of the Freon 12 back into the supply tank. For each constant charge in the loop, different power inputs were used with variations in the inlet temperature to the test section.

In the regions close to the critical state, fluctuations in pressure on the order of 20 to 30 psi were observed. Accompanying these fluctuations was an intense vibration of the test apparatus. When the rate of cooling water was increased so that the pressure in the apparatus was reduced, the fluctuations subsided; however, if the cooling-water flow rate was decreased or the power was increased the fluctuations became more severe and did not subside until the pressure had risen well above the critical value. In many instances the pressure fluctuations did not subside until a pressure of 750 to 800 psia had been attained.

The instability of operation in the vicinity of the critical point was attributed to the rapid change of properties in that region.

Reduction of Data

Since the analytical work yielded expressions based on an average value of the heat-transfer coefficient, the coefficient was evaluated from the experimental data by

$$h_{avg} = \frac{q}{\pi d\, l_f (t_w - t_b)_{avg}} \tag{13}$$

With the assumption of uniform heat generation, no axial heat flow, and a linear variation of electrical resistivity and thermal conductivity of the tube with temperature, the method of Kreith and Summerfield [7] was used to obtain the inside tube wall temperature from the measured outside wall temperature. An integrated average was taken to obtain $(t_w - t_b)_{avg}$.

No information was available on the thermal conductivity and viscosity of Freon 12 for the extended temperatures and pressures used in these tests. However, it was believed that estimated values of the thermal conductivity and viscosity could be used to verify the analytical work provided the estimates were consistent throughout the range of the tests. Consequently, the viscosity and thermal conductivity were calculated with the aid of the generalized correlations of references [8 and 9]. To use these generalized correlations it is necessary to have the variation

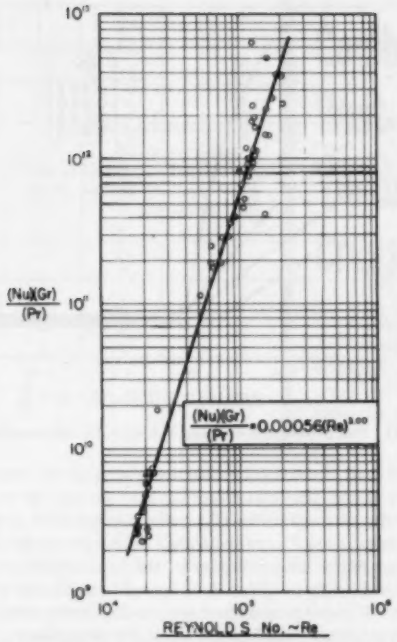

Fig. 6 Correlation of experimental data for $v_m/v_c < 1$

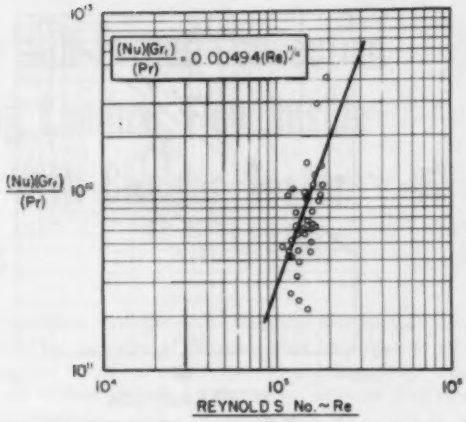

Fig. 7 Correlation of experimental data for $v_m/v_c > 1$

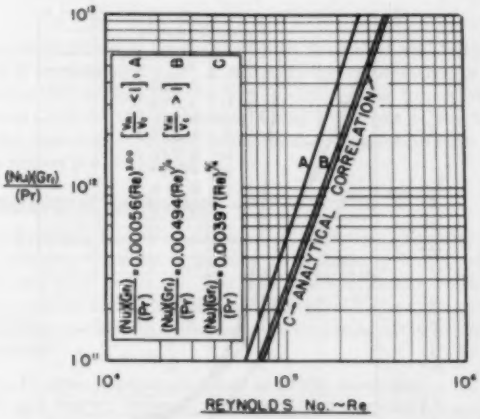

Fig. 8 Comparison of experimental correlations with analytical prediction

of the properties with temperature at one atmosphere pressure. The viscosity and thermal conductivity of Freon 12 at one atmosphere are given in references [10 and 11], respectively.

The accuracy of the generalized correlations is, of course, not known. Near the critical state they could be in error by as much as 100 per cent. However, the consistent estimates given by the generalized correlations are certainly better than nothing at all.

Test Results and Correlation of Data

A summary of the test results is given in Table 1. For all the tests the fluid was in turbulent flow; therefore one would expect the experimental data to follow the form of equation (12). Figs. 6, 7, and 8 show that this expectation is justified. The values of the constant factors in equation (12) are:

$$l = 109.3 \text{ in.}$$
$$l_1 = 25.25 \text{ in.}$$
$$d = 0.430 \text{ in.}$$
$$y = 37.0 \text{ in.}$$

For the regions $v_m/v_c < 1$ the correlation

$$\frac{\text{Nu Gr}_f}{\text{Pr}} = 0.00056\,(\text{Re})^2 \tag{14}$$

is obtained and for the regions where $v_m/v_c > 1$ the relation

$$\frac{\text{Nu Gr}_f}{\text{Pr}} = 0.00494\,(\text{Re})^{11/6} \tag{15}$$

is obtained. No data points are shown for pressures and temperatures where boiling could have occurred in the apparatus. Fig. 8 shows a comparison of these two expressions with the analytically predicted correlation. The two different correlations depending on the value of the reduced specific volume may be justified on the basis that the viscosity and thermal conductivity change abruptly across the critical region. It is believed that errors which may be present in the generalized correlations could easily account for the difference between the two correlations.

Table 1 Summary of test data (118 runs)

Test variable	Range of tests
Bulk temperature, t_b	150 to 400 deg F
Pressure, P	500 to 900 psia
Reynolds number, Re	15000 to 200000
Heat flux	10000 to 42000 Btu/hr-ft^2
Grashof number, Gr_f	$2.38 \times 10^{+7}$ to $3.2 \times 10^{+11}$ (approx)

For reference purposes Fig. 9 shows the inadequacy of the conventional forced-convection relationship

$$\text{Nu} = 0.023\,(\text{Re})^{0.8}(\text{Pr})^{0.4} \tag{16}$$

to predict the heat-transfer behavior of the natural-circulation system. In connection with this figure it is well to note that the natural-circulation loop is not a conventional forced-convection system since the flow rate is not independent of the heat-transfer rate as is normally the case.

Fig. 10 is a plot of selected values of the apparent thermal conductivities. The trends on the curves in the supercritical region agree with the trends presented by Schmidt, Eckert, and Grigull [4]. The boiling trend is shown for the subcritical pressures. Fig. 11 is a plot of selected values of the average heat-transfer coefficient. In this figure the influence of boiling at pressures below the critical value is very pronounced. For super-

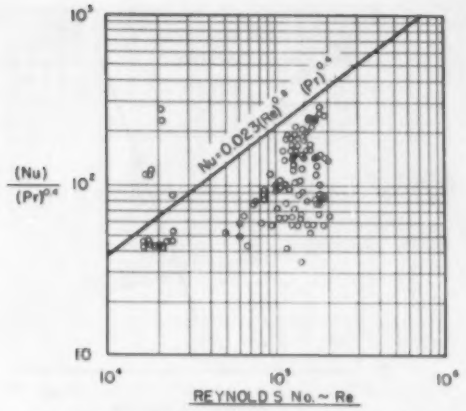

Fig. 9 Plot of experimental data showing inadequacy of conventional forced-convection relation to predict behavior of natural-circulation loop

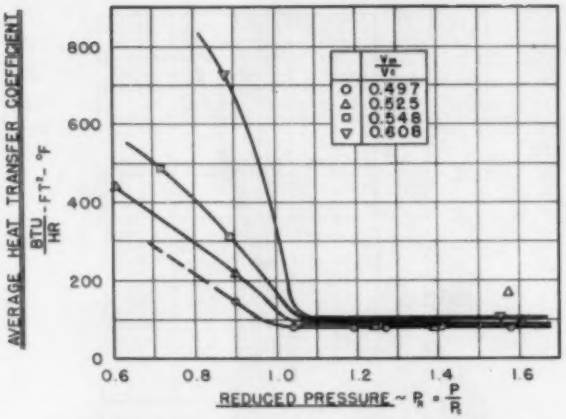

Fig. 11 Plot of selected average heat-transfer film coefficients

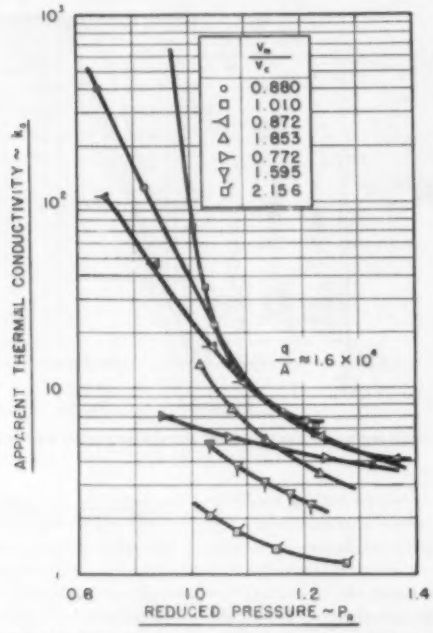

Fig. 10 Plot of selected apparent thermal conductivities

critical pressures the course of the heat-transfer coefficient curves is very nearly constant. Again, it is well to mention that Figs. 6, 7, and 8 do not include any data points for regions where boiling was encountered.

Perhaps the most important result of the experiments is, that for a natural-circulation loop, one does not experience any appreciable increase in the heat-transfer coefficient when operating near the critical state, provided boiling is not encountered. In connection with this result it may be presumed that the rates of change of the specific-heat capacity and the volume coefficient of expansion in the critical region are relatively equal. It is believed that the disagreement in the level of the experimental correlations and the analytical relation may be attributed to uncertainties of the property data in the critical region.

Conclusions

In consideration of the uncertainties involved in the fluid properties near the critical state, the results of the experimental data have shown that equation (12) may be used to predict the heat-transfer characteristics of a natural-circulation loop using a fluid operating near its critical state. The test results show that there is no appreciable increase in the heat-transfer coefficient in the critical region over that experienced in the superheat region. Although this result may at first seem to be a contradiction of the results of other investigators [1, 2], it has been shown that this disagreement is a logical consequence of the fact that the fluid-flow rate in a natural-circulation loop is dependent on the heat-transfer rate.

The trends of an apparent thermal conductivity defined by equation (1) are in agreement with the results of reference [4].

Acknowledgments

The authors wish to acknowledge the support of the Flight Propulsion Laboratory, General Electric Company, Cincinnati, Ohio, in the purchase of equipment for this project. They also wish to acknowledge the assistance of Prof. W. L. Sibbitt, formerly of Purdue University, who first suggested this problem.

References

1 N. L. Dickinson and C. P. Welch, "Heat Transfer to Supercritical Water," Trans. ASME, vol. 80, 1958, pp. 746–752.

2 D. L. Doughty and R. M. Drake, "Free Convection Heat Transfer From a Horizontal Right Cylinder to Freon 12 Near the Critical State," Trans. ASME, vol. 78, 1956, pp. 1843–1850.

3 W. H. McAdams, "Heat Transmission," McGraw-Hill Book Company, Inc., New York, N. Y., third edition, 1954, p. 176.

4 E. Schmidt, E. Eckert, and U. Grigull, "Heat Transfer by Liquids Near the Critical State," AAF Translation No. 527, Air Materiel Command, Wright Field, Dayton, Ohio.

5 "High Speed Aerodynamics and Jet Propulsion," vol. 1, "Thermodynamics and Physics of Matter," Princeton University Press, Princeton, N. J., 1955, pp. 419–500.

6 B. J. Eiseman, R. L. McHarness, and J. J. Martin, "The New Thermodynamic Properties of Freon 12," *Refrigerating Engineering*, vol. 63, 1955, pp. 31–44.

7 F. Kreith and M. Summerfield, "Heat Transfer to Water at High Flux Densities With and Without Surface Boiling," Trans. ASME, vol. 71, 1949, pp. 805–815.

8 E. W. Comings and R. S. Egly, "Viscosities of Gases and Vapors at High Pressures," *Industrial and Engineering Chemistry*, vol. 39, 1940, pp. 714–718.

9 E. W. Comings and M. F. Nathan, "Thermal Conductivity of Gases at High Pressures," *Industrial and Engineering Chemistry*, vol. 39, 1947, pp. 964–970.

10 A. F. Benning and W. H. Markwood, "Thermal Conductances and Heat Transmission Coefficients of Freon Refrigerants," Kinetic Chemicals Inc., Wilmington, Del., 1942.

11 J. M. Lenoir, "Thermal Conductivity of Gases at Atmospheric Pressure," University of Arkansas Experiment Station, Bulletin 18, August, 1953.

Combined Free and Forced-Convection Heat-Generating Laminar Flow Inside Vertical Pipes With Circular Sector Cross Sections[1]

PAU-CHANG LU[2]
Graduate Assistant,
Department of Mechanical Engineering,
Case Institute of Technology,
Cleveland, Ohio

Combined free and forced-convection, heat-generating laminar flow inside cylindrical pipes with elements parallel to the direction of the generating body force is solved by applying the finite Fourier sine transform and finite Hankel transforms when the cross sections of the pipes are circular sectors. A numerical example is provided to show the effects of various parameters.

THE FREE-CONVECTION effect in vertical pipe flow has recently become quite significant in a number of engineering applications. The modifier "vertical" here is employed to mean that the longitudinal dimension of the pipe is parallel to the direction of the generating body force, such as gravity or centrifugal force. In response to practical demands, a number of theoretical investigations have appeared in the literature: Ostrach [1, 2, 3, 4, 5][3] and Lietzke [6] have obtained solutions for parallel-plate channels in detail; Hallman [7] has presented results for circular pipes; and Han [8] has solved the problem for rectangular pipes by the classical Fourier method. This last problem in a more general form has been solved by means of the double-finite Fourier sine transform [9]. Results for circular annuli have been worked out in reference [9] as straightforward generalizations of those for circular pipes.

In this paper, only the problem with prescribed wall temperatures is considered. After a summarizing presentation of the governing equations and boundary conditions valid for any shape of cross sections, the problem is solved by means of the finite Fourier sine transform and finite Hankel transforms when the cross section is a circular sector.

Formulation of the Problem

The Governing Equations and Boundary Conditions. To formulate the problem, a general cylindrical co-ordinate system is established as shown in Fig. 1. The pipe wall is cylindrical with elements parallel to the direction of the generating body force. If, in addition to this characteristic, further assumptions are introduced that

(*a*) The flow is steady, laminar, and fully developed;
(*b*) the fluid is quasi-incompressible with constant c_p, c_v, μ, and k;
(*c*) the energy dissipation is negligible;
(*d*) $\partial T/\partial z$ = constant = A;

the equation of continuity, together with the fact that

$$w = w(x_1, x_2) \text{ only,} \tag{1}$$

gives

$$\rho \iint_S w d\sigma = \text{constant mass through-flow} = g; \tag{2}$$

[1] Based partly on a thesis submitted in partial fulfillment of the requirements for the degree of Master of Science at the Kansas State College.
[2] Formerly Graduate Research Assistant, Department of Mechanical Engineering, Kansas State College, Manhattan, Kan.
[3] Numbers in brackets designate References at end of paper.
Contributed by the Heat Transfer Division and presented at the Annual Meeting, Atlantic City, N. J., November 29–December 4, 1959, of THE AMERICAN SOCIETY OF MECHANICAL ENGINEERS.
NOTE: Statements and opinions advanced in papers are to be understood as individual expressions of their authors and not those of the Society. Manuscript received at ASME Headquarters, August 17, 1959. Paper No. 59—A-145.

Nomenclature

$A = \partial T/\partial z$
$B_\nu(\zeta) = J_\nu(\zeta)Y_\nu(R_1\xi_{\nu,m}) - Y_\nu(\zeta)J_\nu(R_1\xi_{\nu,m})$
$C = \left(\frac{\Pr}{c_p K T_{\Gamma_0}}\right)^{1/3} \frac{\Pi d^3}{\mu}$, dimensionless pressure-gradient parameter
$C_A = \left(\frac{\Pr d^3}{c_p K_A A}\right)^{1/3} \frac{\Pi}{\mu}$, dimensionless pressure-gradient parameter
C_m = constants
c_p, c_v = specific heat capacities at constant pressure and volume
d = hydraulic diameter of the pipe
$F = Qd^2/kT_{\Gamma_0}$, dimensionless heat-source term
$F_A = Qd/kA$, dimensionless heat-source term
f_s = body force per unit mass
$G = \frac{1}{K}\frac{\beta f_s}{k} g$, dimensionless mass through-flow
g = mass through-flow
$G_A = \frac{1}{K_A}\frac{\beta f_s}{k} g$, dimensionless mass through-flow
$\mathrm{Gr} = \frac{\rho^2 \beta f_s T_\Gamma d^3}{\mu^2}$, Grashof number
$\mathrm{Gr}_A = \frac{\rho^2 \beta f_s A d^4}{\mu^2}$, modified Grashof number
$J_\nu(\zeta)$ = Bessel function of first kind, νth order
$K = \gamma \mathrm{Ra}\left(\frac{\beta f_s d}{c_p}\right)$, dimensionless parameter
k = thermal conductivity
$K_A = \gamma \mathrm{Ra}_A\left(\frac{\beta f_s d}{c_p}\right)$, dimensionless parameter
m = 1, 2, 3, etc.

(*Continued on next page*)

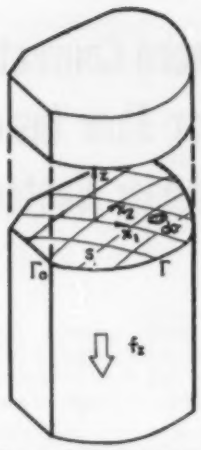

Fig. 1 Co-ordinate system

the Navier-Stokes' equations assume the form

$$\mu\nabla^2 w - (\rho - \rho_{\Gamma_0})f_z = \frac{dp}{dz} + \rho_{\Gamma_0} f_z \tag{3}$$

where ρ_{Γ_0} is ρ evaluated along an element Γ_0 of Γ; and the energy equation becomes

$$\rho c_v A w = Q + k\nabla^2\theta \tag{4}$$

Equation (3) can be further reduced to

$$\mu\nabla^2 w + \rho\beta f_z\theta = \Pi \tag{5}$$

for the following three cases [1]:

(*a*) Temperature differences in the whole region are small;
(*b*) the fluid is a liquid with $\rho\beta \doteq$ constant;
(*c*) the fluid is a perfect gas and the pressure differences in the region are small.

For each case suitable average values of ρ, β, and/or $\rho\beta$ are to be selected.

From equations (4) and (5) θ or w can be eliminated to yield, respectively,

$$\nabla^4 w + \frac{\rho^2\beta f_z c_v A}{\mu k} w = \frac{\rho\beta f_z}{\mu k} Q \tag{6}$$

and

$$\nabla^4\theta + \frac{\rho^2\beta f_z c_v A}{\mu k}\theta = \frac{\rho c_v A}{\mu k}\Pi - \frac{\nabla^2 Q}{k} \tag{7}$$

The two principal boundary conditions used are the nonslip condition at the wall,

$$w = 0 \text{ on } \Gamma \tag{8}$$

and the thermal condition at the wall,

$$\begin{aligned} \theta &= \theta_\Gamma \quad \text{on} \quad \Gamma \\ &= 0 \quad \text{on} \quad \Gamma_0 \end{aligned} \tag{9}$$

Using equations (4) and (5), respectively, conditions (8) and (9) may also be written as

$$\nabla^2\theta = -\frac{Q}{k} \text{ on } \Gamma \tag{10}$$

and

$$\left.\begin{aligned} \nabla^2 w &= \frac{1}{\mu}(\Pi - \rho\beta f_z\theta_\Gamma) \text{ on } \Gamma \\ &= \frac{\Pi}{\mu} \text{ on } \Gamma_0 \end{aligned}\right\} \tag{11}$$

With these boundary conditions w can be solved from equation (6); and then θ from equation (5). Or, θ may be found first from equation (7), and then w from equation (4). The pressure-gradient Π involved in the results can be expressed in terms of the known mass through-flow g, using equation (2).

When $A = 0$, equation (10) holds in the whole region because of equation (4); and hence becomes meaningless as a boundary condition. Here θ can be solved from equation (4) with the boundary condition (9), and then w can be found from equation (5) with the boundary condition (8). Or, w can be found from equation (6) with boundary conditions (8) and (11), and then θ from equation (5).

Nondimensionalization. In order to nondimensionalize the problem, the hydraulic diameter d of the pipe is used as the characteristic length. When $A \neq 0$, $(c_p K_A A d/\mathrm{Pr})^{1/2}$ and Ad are used as the characteristic velocity and temperature, respectively. When $A = 0$, $(c_p K T_{\Gamma_0}/\mathrm{Pr})^{1/2}$ and T_{Γ_0} are used. In this manner, the foregoing equations and conditions, grouped together for quick reference, are rewritten in dimensionless forms as follows:

(*a*) $A \neq 0$

$$G_A = \iint_S W_A d\bar{\sigma} \tag{12}$$

Nomenclature

n = 1, 2, 3, etc.
$\overline{\mathrm{Nu}}$ = average Nusselt number as defined in equation (29)
$\overline{\mathrm{Nu}_A}$ = average Nusselt number as defined in equation (28)
p = pressure
P_m = particular integral of a nonhomogeneous linear ordinary differential equation
Pr = $\mu c_p/k$, Prandtl number
Q = heat-source term, independent of z
q = normal wall heat flux, positive inward
R = r/d, dimensionless
r = two-dimensional radial co-ordinate
Ra = $\mathrm{Pr\ Gr}/\gamma$, Rayleigh number
Ra_A = $\mathrm{Pr\ Gr}_A/\gamma$, modified Rayleigh number
S = two-dimensional region investigated
s = length along a curve in S
T = absolute temperature
W = $\dfrac{w}{\left(\dfrac{c_p K T_{\Gamma_0}}{\mathrm{Pr}}\right)^{1/2}}$, dimensionless velocity
W_A = $\dfrac{w}{\left(\dfrac{c_p K_A A d}{\mathrm{Pr}}\right)^{1/2}}$, dimensionless velocity
w = axial velocity
X_m = as defined in equations (50), (51), (66), and (67)
x_1, x_2 = general curvilinear co-ordinates
$Y_\nu(\zeta)$ = Bessel function of second kind (Weber), νth order
z = axial co-ordinate
β = thermal coefficient of volumetric expansion
Γ = pipe wall. A reference element of it is denoted by Γ_0
γ = ratio of specific heat capacities
∇^2 = two-dimensional Laplacian
∇^4 = $\nabla^2\nabla^2$
$\eta_{\nu,m}$ = positive roots of $J_\nu(R_\lambda\eta_{\nu,m}) = 0$
θ = $T - T_{\Gamma_0}$
λ = r_λ/r_I, dimensionless
μ = dynamic viscosity
ν = $n\pi/\Phi$
$\xi_{\nu,m}$ = positive roots of $B_\nu(R_\lambda\xi_{\nu,m})' = 0$

(*Continued on next page*)

$$\begin{cases} \bar{\nabla}^4 W_A + \mathrm{Ra}_A W_A = F_A & (13) \\ W_A = 0 \text{ on } \Gamma & (14) \\ \left.\begin{aligned} \bar{\nabla}^2 W_A &= C_A - \tau_{A\Gamma} \text{ on } \Gamma \\ &= C_A \qquad \text{on } \Gamma_0 \end{aligned}\right\} & (15) \\ \bar{\nabla}^2 W_A + \tau_A = C_A & (16) \end{cases}$$

or

$$\begin{cases} \bar{\nabla}^4 \tau_A + \mathrm{Ra}_A \tau_A = \mathrm{Ra}_A C_A - \bar{\nabla}^2 F_A & (17) \\ \left.\begin{aligned} \tau_A &= \tau_{A\Gamma} \text{ on } \Gamma \\ &= 0 \quad \text{on } \Gamma_0 \end{aligned}\right\} & (18) \\ \bar{\nabla}^2 \tau_A = -F_A \text{ on } \Gamma & (19) \\ \mathrm{Ra}_A W_A = F_A + \bar{\nabla}^2 \tau_A & (20) \end{cases}$$

(*b*) $A = 0$

$$G = \iint_S W d\bar{\sigma} \qquad (21)$$

$$\begin{cases} \bar{\nabla}^2 \tau + F = 0 & (22) \\ \left.\begin{aligned} \tau &= \tau_\Gamma \text{ on } \Gamma \\ &= 0 \text{ on } \Gamma_0 \end{aligned}\right\} & (23) \\ \bar{\nabla}^2 W + \tau = C & (24) \\ W = 0 \text{ on } \Gamma & (25) \end{cases}$$

or

$$\begin{cases} \bar{\nabla}^4 W = F & (26) \\ W = 0 \text{ on } \Gamma & (25) \\ \left.\begin{aligned} \bar{\nabla}^2 W &= C - \tau_\Gamma \text{ on } \Gamma \\ &= C \qquad \text{on } \Gamma_0 \end{aligned}\right\} & (27) \\ \bar{\nabla}^2 W + \tau = C & (24) \end{cases}$$

Either of the two groups in each of the foregoing cases may be chosen as the working equations. The first groups are used in the present investigation.

Heat-Transfer Parameters. After the velocity and temperature distribution are known, the local heat fluxes and various heat-transfer parameters are easily obtainable. Specifically, average Nusselt numbers may be defined as

$$\overline{\mathrm{Nu}}_A = \frac{\oint_\Gamma q ds}{\oint_\Gamma d_e} \frac{d}{k} \Big/ Ad = \frac{\mathrm{Ra}_A G_A - \iint_S F_A d\bar{\sigma}}{\oint_\Gamma d\bar{s}} \qquad (28)$$

and

$$\overline{\mathrm{Nu}} = \frac{\oint_\Gamma q ds}{\oint_\Gamma d_e} \frac{d}{k} \Big/ T_{\Gamma_0} = -\frac{\iint_S F d\bar{\sigma}}{\oint_\Gamma d\bar{s}} \qquad (29)$$

which depend on known parameters only. Another often-used parameter is the mixed mean temperature

$$\theta_M = \iint_S \theta w d\sigma \Big/ \iint_S w d\sigma$$

which can be nondimensionalized as

$$\tau_{AM} = \iint_S \tau_A W_A d\bar{\sigma} / G_A \qquad (30)$$

$$\tau_M = \iint_S \tau W d\bar{\sigma} / G \qquad (31)$$

Analogy to Other Problems

An inspection of equations (13) and (17) shows that they both are analogous to the equation governing small deflections of a thin plate resting on an elastic foundation. If the boundary conditions happen to be analogous too, an exact similarity exists. When $A = 0$, equation (26) shows an analogy to the theory of thin plates not on elastic foundation.[4] The exact (velocity-to-temperature) analogy to pure forced-convection flow in this latter case is obvious.

Pipes of Circular Sector Cross Sections

Referring to Fig. 1, Γ in this case is composed of two radial lines, $\phi = 0$ and $\phi = \Phi$, and two circular arcs, $r = r_I$ and $r = r_\lambda = \lambda r_I$. Since the hydraulic diameter is

$$d = \frac{(\lambda^2 - 1)\Phi r_I}{\lambda - 1 + \frac{1}{2}(\lambda + 1)\Phi} \qquad (32)$$

the dimensionless radii are

[4] Several special cases have actually been solved by observing these analogies [9].

Nomenclature

$\Pi = \dfrac{dp}{dz} + \rho_{\Gamma_0} f_v$, pressure-gradient parameter
ρ = density
$\sum_m$ = summation over all $\eta_{r,m}$'s or $\xi_{r,m}$'s
σ = area in region S
$\tau = \theta / T_{\Gamma_0}$, dimensionless temperature difference
$\tau_A = \theta / Ad$, dimensionless temperature difference
Φ = angular measurement of a sector
ϕ = two-dimensional angular coordinate
$\Psi_B(\ )$ = finite Hankel transform defined by equation (47)
$\Psi_J(\ )$ = finite Hankel transform defined by equation (63)
$\Psi_S(\ )$ = finite Fourier sine tranform defined by equation (46)
$\Psi_{SB}(\ ) = \Psi_B[\Psi_S(\ )]$
$\Psi_{SJ}(\ ) = \Psi_J[\Psi_S(\ )]$

Subscripts

I = on inner wall of a ring sector
M = mixed mean value
m = 1, 2, 3, etc.
Γ = on Γ
Γ_0 = on Γ_0
λ = on outer wall of a circular sector
Φ = on wall $\phi = \Phi$
0 = on wall $\phi = 0$

Superscript

— dimensionless quantity, applied to s, ∇, and σ

$$R_I = \frac{1}{(\lambda+1)\Phi} + \frac{1}{2}\frac{1}{\lambda-1}$$
$$R_\lambda = \frac{\lambda}{(\lambda+1)\Phi} + \frac{1}{2}\frac{\lambda}{\lambda-1} \qquad (33)$$

For a full sector,
$$d = \frac{\Phi r_\lambda}{1+\Phi/2} \qquad (34)$$

and
$$R_I = 0$$
$$R_\lambda = \frac{1}{\Phi} + \frac{1}{2} \qquad (35)$$

When $\Phi = 2\pi$ the circular sector becomes an annulus or circle, plus one radial line. When Φ is small enough, the sector may be used to approximate a narrow isosceles trapezoid or triangle.

Choosing $(R_I, 0)$ as Γ_0, the following working equations are obtained:

(*a*) $A \neq 0$

$$G_A = \int_0^\Phi \int_{R_I}^{R_\lambda} W_A R\, dR\, d\phi \qquad (36)$$

$$\left(\frac{1}{R}\frac{\partial}{\partial R} R \frac{\partial}{\partial R} + \frac{1}{R^2}\frac{\partial^2}{\partial \phi^2}\right)^2 W_A + \mathrm{Ra}_A W_A = F_A \qquad (37)$$

$$W_A = 0 \text{ when } R = R_I,\quad R = R_\lambda,\quad \phi = 0 \text{ or } \phi = \Phi \qquad (38)$$

$$\left(\frac{1}{R}\frac{\partial}{\partial R} R \frac{\partial}{\partial R} + \frac{1}{R^2}\frac{\partial^2}{\partial \phi^2}\right) W_A = \begin{cases} C_A - \tau_{AI}(\phi) & \text{when } R = R_I \\ C_A - \tau_{A\lambda}(\phi) & \text{when } R = R_\lambda \\ C_A - \tau_{A0}(R) & \text{when } \phi = 0 \\ C_A - \tau_{A\Phi}(R) & \text{when } \phi = \Phi \end{cases} \qquad (39)$$

$$\left(\frac{1}{R}\frac{\partial}{\partial R} R \frac{\partial}{\partial R} + \frac{1}{R^2}\frac{\partial^2}{\partial \phi^2}\right) W_A + \tau_A = C_A \qquad (40)$$

(*b*) $A = 0$

$$G = \int_0^\Phi \int_{R_I}^{R_\lambda} WR\, dR\, d\phi \qquad (41)$$

$$\left(\frac{1}{R}\frac{\partial}{\partial R} R \frac{\partial}{\partial R} + \frac{1}{R^2}\frac{\partial^2}{\partial \phi^2}\right) \tau + F = 0 \qquad (42)$$

$$\tau = \begin{cases} \tau_I(\phi) & \text{when } R = R_I \\ \tau_\lambda(\phi) & \text{when } R = R_\lambda \\ \tau_0(R) & \text{when } \phi = 0 \\ \tau_\Phi(R) & \text{when } \phi = \Phi \end{cases} \qquad (43)$$

$$\left(\frac{1}{R}\frac{\partial}{\partial R} R \frac{\partial}{\partial R} + \frac{1}{R^2}\frac{\partial^2}{\partial \phi^2}\right) W + \tau = C \qquad (44)$$

$$W = 0 \text{ when } R = R_I,\quad R = R_\lambda,\quad \phi = 0 \text{ or } \phi = \Phi \qquad (45)$$

Solutions

Case I—Ring-Sector Cross Sections:

(*a*) $A \neq 0$

Applying successively the single Fourier sine transform[5]

$$\Psi_B(\ldots) = \int_0^\Phi (\ldots) \sin\frac{n\pi\phi}{\Phi}\, d\phi \qquad (46)$$

[5] Chapter 3 [10]; and Part B-V [11].

and the finite Hankel transform[5]

$$\Psi_{B}(\ldots) = \int_{R_I}^{R_\lambda} (\ldots) B_\nu(R\xi_{\nu,m}) R\, dR \qquad (47)$$

to equation (37) and boundary conditions (38) and (39), the velocity distribution is found to be[6]

$$W_A = \frac{\pi^2}{\Phi} \sum_{\substack{n=1 \\ (\nu)}}^{\infty} \sum_{m} \frac{\xi_{\nu,m}^2 J_\nu^2(R_\lambda \xi_{\nu,m}) \Psi_{SB}(W_A)}{J_\nu^2(R_I\xi_{\nu,m}) - J_\nu^2(R_\lambda\xi_{\nu,m})} B_\nu(R\xi_{\nu,m}) \sin\frac{n\pi\phi}{\Phi} \qquad (48)$$

where
$$\Psi_{SB}(W_A) = \frac{\Psi_{SB}(F_A) - X_1 - X_2}{\xi_{\nu,m}^4 + \mathrm{Ra}_A} \qquad (49)$$

and
$$X_1 = \Psi_B \left\langle \frac{\nu}{R^2} \left\{ [1-(-1)^n] C_A - \tau_{A0} + (-1)^n \tau_{A\Phi} \right\} \right\rangle \qquad (50)$$

$$X_2 = \frac{2}{\pi} \left\{ \frac{C_A[1-(-1)^n]}{\nu} \frac{J_\nu(R_I\xi_{\nu,m}) - J_\nu(R_\lambda\xi_{\nu,m})}{J_\nu(R_\lambda\xi_{\nu,m})} - \frac{J_\nu(R_I\xi_{\nu,m})}{J_\nu(R_\lambda\xi_{\nu,m})} \Psi_B(\tau_{A\lambda}) + \Psi_B(\tau_{AI}) \right\} \qquad (51)$$

The parenthesized ν under the summation sign is used to emphasize the fact that ν involves n.

Equation (40) then gives

$$\tau_A = C_A + \frac{\pi^2}{\Phi} \sum_{\substack{n=1 \\ (\nu)}}^{\infty} \sum_{m} \frac{\xi_{\nu,m}^4 J_\nu^2(R_\lambda\xi_{\nu,m}) \Psi_{SB}(W_A)}{J_\nu^2(R_I\xi_{\nu,m}) - J_\nu^2(R_\lambda\xi_{\nu,m})} B_\nu(R\xi_{\nu,m}) \times \sin\frac{n\pi\phi}{\Phi} \qquad (52)$$

The parameter C_A is related to G_A through equation (36). Thus,

$$G_A = 2\pi \sum_{\substack{n=1,3,5 \\ (\nu)}}^{\infty} \sum_{m} \frac{1}{n} \frac{\xi_{\nu,m}^2 J_\nu^2(R_\lambda\xi_{\nu,m}) \Psi_{SB}(W_A)}{J_\nu^2(R_I\xi_{\nu,m}) - J_\nu^2(R_\lambda\xi_{\nu,m})} \times \int_{R_I}^{R_\lambda} B_\nu(R\xi_{\nu,m}) R\, dR \qquad (53)$$

Once the velocity and temperature distributions are known, various heat-transfer parameters can be evaluated. For example,

$$\tau_{AM} = C_A + \frac{1}{G_A}\frac{\pi^2}{\Phi} \sum_{\substack{n=1 \\ (\nu)}}^{\infty} \sum_{m} \frac{\xi_{\nu,m}^4 J_\nu^2(R_\lambda\xi_{\nu,m}) [\Psi_{SB}(W_A)]^2}{J_\nu^2(R_I\xi_{\nu,m}) - J_\nu^2(R_\lambda\xi_{\nu,m})} \qquad (54)$$

where the orthogonality of B_ν has been observed. The determination of $\overline{\mathrm{Nu}}_A$ as defined in equation (28) offers no difficulty.

(*b*) $A = 0$

This is solved by employing the finite Fourier sine transform (46). The results are as follows:

$$\tau = \frac{2}{\Phi} \sum_{\substack{n=1 \\ (\nu)}}^{\infty} \Psi_B(\tau) \sin\frac{n\pi\phi}{\Phi} \qquad (55)$$

[6] W_A can also be obtained by applying only the finite Fourier sine transform. The result will involve ber_ν, bei_ν, ker_ν, and kei_ν-functions. The present form is chosen because of the extensive tabulation of J_ν and Y_ν now available. Also in the present way the difficult task of finding the particular integral and integration constants is avoided.

where

$$\Psi_S(\tau) = C_1 R^\nu + C_2 R^{-\nu} + P_1 \tag{56}$$

The integration constants C_1 and C_2 are to be determined from the boundary conditions

$$\begin{aligned} \Psi_S(\tau) &= \Psi_S(\tau_I) \quad \text{when} \quad R = R_I \\ &= \Psi_S(\tau_\lambda) \quad \text{when} \quad R = R_\lambda \end{aligned} \tag{57}$$

and the particular integral P_1 depends on the functional forms of τ_0, τ_Φ, and Q.[7]

When τ_0, τ_Φ, and Q are all constants,

$$\left.\begin{aligned} P_1 &= \frac{[1-(-1)^n]FR^2}{\nu(\nu^2-4)} + \frac{\tau_0 - (-1)^n\tau_\Phi}{\nu} \quad (\nu \neq 2) \\ &= -\frac{R^2 \ln R}{8} F[1-(-1)^n] \\ &\quad + \frac{\tau_0 - (-1)^n\tau_\Phi}{2} \quad (\nu = 2) \end{aligned}\right\} \tag{58}$$

The velocity distribution is given by

$$W = \frac{2}{\Phi} \sum_{\substack{n=1 \\ (\nu)}}^{\infty} \Psi_S(W) \sin \frac{n\pi\phi}{\Phi} \tag{59}$$

where

$$\Psi_S(W) = C_3 R^\nu + C_4 R^{-\nu} + P_2 \tag{60}$$

C_3 and C_4 are to be determined from the boundary conditions

$$\Psi_S(W) = 0 \qquad \text{when } R = R_I \text{ or } R_\lambda \tag{61}$$

The particular integral P_2 depends again on the functional forms of τ_0, τ_Φ, and Q. When they are constants,

$$\left.\begin{aligned} P_2 &= -\frac{C_1}{4(\nu+1)} R^{\nu+2} \\ &\quad - \frac{C_2}{4(\nu-1)} R^{-\nu+2} + \frac{F[1-(-1)^n]R^4}{\nu(\nu^2-4)(\nu^2-16)} \\ &\quad - \frac{\{[1-(-1)^n]C - \tau_0 + (-1)^n\tau_\Phi\}R^2}{\nu(\nu^2-4)} \\ &\qquad (\nu \neq 1, 2, \text{or } 4) \\ &= -\frac{C_1}{8} R^2 - \frac{C_2}{2} R \ln R + \frac{F[1-(-1)^n]R^4}{45} \\ &\quad + \frac{\{[1-(-1)^n]C - \tau_0 + (-1)^n\tau_\Phi\}R^2}{3} \quad (\nu = 1) \\ &= -\frac{C_1}{12} R^4 - \frac{C_2}{4} + \frac{F[1-(-1)^n]R^4 \ln R}{96} \\ &\quad + \frac{\{[1-(-1)^n]C - \tau_0 + (-1)^n\tau_\Phi\}R^2 \ln R}{8} \quad (\nu = 2) \\ &= -\frac{C_1}{20} R^5 - \frac{C_2}{12} R^{-2} - \frac{F[1-(-1)^n]R^4 \ln R}{384} \\ &\quad - \frac{\{[1-(-1)^n]C - \tau_0 + (-1)^n\tau_\Phi\}R^2}{48} \quad (\nu = 4) \end{aligned}\right\} \tag{62}$$

[7] The problem can always be solved, at least formally, by using the finite Hankel transform without the necessity of determining P_1, C_1, and C_2.

The determination of G and the heat-transfer parameters is rather straightforward. Instead of presenting the general forms, it would seem to be better practice to work out specific cases individually.

Case II—Full-Sector Cross Sections:

(*a*) $A \neq 0$

Applying successively the single finite Fourier sine transform (46) and the finite Hankel transform[5]

$$\Psi_J(\ldots) = \int_0^{R_\lambda} (\ldots) J_\nu(R\eta_{\nu,m}) R\, dR \tag{63}$$

to equation (37) and boundary conditions on $R = R_\lambda$, the velocity distribution is found to be

$$W_A = \frac{4}{\Phi R_\lambda^2} \sum_{\substack{n=1 \\ (\nu)}}^{\infty} \sum_{m}^{\infty} \Psi_{SJ}(W_A) \frac{J_\nu(R\eta_{\nu,m})}{J_{\nu+1}^2(R_\lambda\eta_{\nu,m})} \sin \frac{n\pi\phi}{\Phi} \tag{64}$$

where

$$\Psi_{SJ}(W_A) = \frac{\Psi_{SJ}(F_A) - X_3 - X_4}{\eta_{\nu,m}^4 + \mathrm{Ra}_A} \tag{65}$$

$$X_3 = \Psi_J\left(\frac{\nu}{R^2}\{[1-(-1)^n]C_A - \tau_{A0} + (-1)^n\tau_{A\Phi}\}\right) \tag{66}$$

$$X_4 = R_\lambda\eta_{\nu,m} J_{\nu+1}(R_\lambda\eta_{\nu,m}) \left\{\frac{C_A[1-(-1)^n]}{\nu} - \Psi_S(\tau_{A\lambda})\right\} \tag{67}$$

and

$$\tau_A = C_A + \frac{4}{\Phi R_\lambda^2} \sum_{\substack{n=1 \\ (\nu)}}^{\infty} \sum_{m} \frac{\eta_{\nu,m}^2 \Psi_{SJ}(W_A)}{J_{\nu+1}^2(R_\lambda\eta_{\nu,m})} J_\nu(R\eta_{\nu,m}) \times \sin \frac{n\pi\phi}{\Phi} \tag{68}$$

$$G_A = \frac{8}{\pi R_\lambda^2} \sum_{\substack{n=1,3,5 \\ (\nu)}}^{\infty} \sum_{m} \frac{1}{n} \frac{\Psi_{SJ}(W_A)}{J_{\nu+1}^2(R_\lambda\eta_{\nu,m})} \int_0^{R_\lambda} J_\nu(R\eta_{\nu,m}) R\, dR \tag{69}$$

Also

$$\tau_{AM} = C_A + \frac{1}{G_A} \frac{4}{\Phi R_\lambda^2} \sum_{\substack{n=1 \\ (\nu)}}^{\infty} \sum_{m} \frac{\eta_{\nu,m}^2 [\Psi_{SJ}(W_A)]^2}{J_{\nu+1}^2(R_\lambda\eta_{\nu,m})} \tag{70}$$

(*b*) $A = 0$

The results of Case I (*b*) apply here as well, except that, to have finite velocity and temperature at $R = 0$, C_3 and C_4 must be zero, while C_1 and C_2 are to be determined from

$$\left.\begin{aligned} \Psi_S(\tau) &= \Psi_S(\tau_\lambda) \\ \Psi_S(W) &= 0 \end{aligned}\right\} \quad \text{at} \quad R = R_\lambda \tag{71}$$

Numerical Example

To show the influences of various parameters, an example of intermediate difficulty is quoted in the following text.

The case chosen is that of a full sector with $\Phi = 60$ deg. The heat generation is uniform and the wall temperature is peripherally constant; A being nonzero. The average Nusselt number based on the characteristic temperature Ad is simply

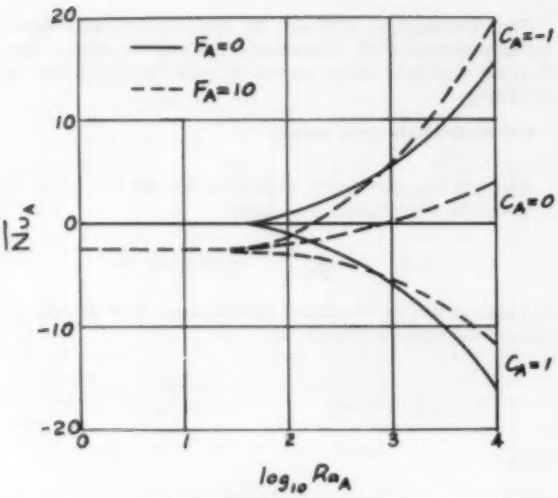

Fig. 2 Nusselt number for pipes of full-sector cross sections with $\Phi = 60$ deg

$$\overline{Nu}_A = 0.226 Ra_A G_A - 0.250 F_A \tag{72}$$

The relation between C_A and G_A turns out to be

$$\begin{aligned}
G_A &= 0.00193 F_A - 0.0388 C_A && \text{for } Ra_A = 1 \\
G_A &= 0.00188 F_A - 0.0379 C_A && \text{for } Ra_A = 10 \\
G_A &= 0.00182 F_A - 0.0368 C_A && \text{for } Ra_A = 100 \\
G_A &= 0.00121 F_A - 0.0250 C_A && \text{for } Ra_A = 1000 \\
G_A &= 0.000290 F_A - 0.00699 C_A && \text{for } Ra_A = 10000
\end{aligned} \tag{73}$$

A few curves calculated from the foregoing formulas are plotted to show the effects of C_A, F_A, and Ra_A (Fig. 2). Some remarks seem to be in order here. First of all, whether C_A or G_A should be used as the primary parameter is open to discussion. It is felt here that the value of C_A somewhat characterizes the type of the flow, while G_A generally does not (except that $G_A = 0$ may characterize the important case of an enclosed cavity). Second, when $C_A > 0$, large heat generation will reverse the direction of the flow and, eventually, the direction of the over-all heat transfer when Ra_A becomes high enough. The intersection of the curves for $F_A = 0$ and for $F_A = 10$ occurs because of the two effects of heat generation; namely, the direct effect and the effect through G_A. To calculate Nusselt numbers based on the mixed mean temperature, equation (54) must be used. For example, when $Ra_A = 10$ and $F_A = 0$,

$$\tau_{AM} = 0.0238 C_A$$

and the Nusselt number based on τ_{AM} is -3.59 for all values of C_A. Finally, the solutions break down for the following values of Ra_A: -369.7, -4245, -6410, -7086, -15440, -19710, and so on. The full significance of these critical Rayleigh numbers is not explored.

Final Remarks

From a mathematical viewpoint, the phenomenon of combined free and forced-convection heat-generating laminar flow inside vertical pipes is nothing but a two-dimensional boundary-value problem. When the boundary is a pair of parallel lines, the problem is solved in terms of elementary functions. When the boundary is a circle or two concentric circles, the problem is solved in terms of Bessel functions. For a rectangular or circular-sector boundary, the problem is solved in trigonometric series either by the classical Fourier method or by an equivalent method of integral transforms. It might be expected that solutions be constructable in terms of Mathieu functions when the boundary is an ellipse or two confocal ellipses.

Owing to the parameters chosen, the present results necessarily exclude the case of pure forced-convection flow. But, starting from the dimensional equations, the same technique is still applicable to this special case

Acknowledgments

The author wishes to thank Dr. Wilson Tripp, Dr. Jerzy R. Moszynski, and Dr. Simon Ostrach for enlightening discussions. Acknowledgments are also due to Prof. Linn Helander and Dr. Ralph G. Nevins, who helped in many ways.

References

1 S. Ostrach, "Laminar Natural-Convection Flow and Heat Transfer of Fluids With and Without Heat Sources in Channels With Constant Wall Temperatures," NACA TN 2863, 1952.

2 S. Ostrach, "Combined Natural-and Forced-Convection Laminar Flow and Heat Transfer of Fluids With and Without Heat Sources in Channels With Linearly Varying Wall Temperatures," NACA TN 3141, 1954.

3 S. Ostrach, "Unstable Convection in Vertical Channels With Heating From Below, Including Effects of Heat Sources and Friction Heating," NACA TN 3548, 1955.

4 S. Ostrach, "On the Flow, Heat Transfer, and Stability of Viscous Fluids Subject to Body Forces and Heated From Below in Vertical Channels," "50 Jahre Grenzschichtforschung," Friedr. Vieweg and Sohn, Braunschweig, Germany, 1955.

5 S. Ostrach, "Internal Viscous Flow With Body Forces," Boundary Layer Research, Springer Verlag, Berlin, Germany, 1958, pp. 185–208.

6 A. F. Lietzke, "Theoretical and Experimental Investigation of Heat Transfer by Laminar Natural Convection Between Parallel Plates," NACA Report 1223, 1955.

7 T. M. Hallman, "Combined Forced and Free-Laminar Heat Transfer in Vertical Tubes With Uniform Internal Heat Generation," TRANS. ASME, vol. 78, 1956, pp. 1831–1841.

8 L. S. Han, "Laminar Heat Transfer in Rectangular Channels," JOURNAL OF HEAT TRANSFER, TRANS. ASME, series C, vol. 81, 1959, pp. 121–128.

9 P. C. Lu, "A Theoretical Investigation of Combined Free and Forced-Convection Heat-Generating Laminar Flow Inside Vertical Pipes With Prescribed Wall Temperatures," MS thesis, Kansas State College, Manhattan, Kan., 1959.

10 I. N. Sneddon, "Fourier Transforms," McGraw-Hill Book Company, Inc., New York, N. Y., 1951.

11 I. N. Sneddon, "Functional Analysis," Encyclopedia of Physics, vol. 2, Springer Verlag, Berlin, Germany, 1955.

L. N. TAO
Associate Professor of Mechanics, Illinois Institute of Technology, Technology Center, Chicago, Ill.
Assoc. Mem. ASME

On Combined Free and Forced Convection in Channels

The heat-transfer problems of combined free and forced convection by a fully developed laminar flow in a vertical channel of constant axial wall temperature gradient with or without heat generations are approached by a new method. By introducing a complex function which is directly related to the velocity and temperature fields, the coupled momentum and energy equations are readily combinable to a Helmholtz wave equation in the complex domain. This greatly reduces the complexities of the problems. For illustrations, the cases of flows between parallel plates and in a rectangular channel are treated. It shows that this method is more direct and powerful than those of previous investigations.

Introduction

PROBLEMS OF HEAT TRANSFER in channels by means of free convection or combined free and forced convection have been the subject of investigations for many years. They are usually confined to the case of constant wall temperature. In recent years, due to some engineering applications in the fields of nuclear reactors, heat exchangers, and so forth, the problems have been extended to those with linearly varying wall temperature or constant wall temperature gradient.

Many recent analyses on combined free and forced convection with linearly varying wall temperature are focused on cases of fully developed flows. For flows in circular tubes with or without heat sources they have been treated by Ostroumov [1, 2],[1] Hamilton, et al. [3], Woodrow [4], and Hallman [5]; for flows between parallel plates by Ostroumov [1], Ostrach [6–9], and Wordsworth [10]; and for flows in rectangular channels by Han [11].

At first glance, this extension seems to be just a simple matter of changing the boundary condition of the temperature field. However, from the mathematical point of view this is not so simple as we expect even in the simple case of a fully developed laminar flow, since the basic equations of momentum and energy are no longer uncoupled as in those of the constant wall temperature problem. The energy equation is not independent of the velocity field. This means that in order to study these types of problems with linearly varying wall temperature it is necessary to find the solution of a fourth-order differential equation which is obtained by combining the momentum and energy equations. This is, of course, much more complicated than the cases of a set of uncoupled equations, such as those of combined free and forced convection with constant wall temperature and those of forced convection alone. In the first case the energy equation is independent of the velocity field, while in the latter the momentum equation is independent of the temperature field. All previous investigators seem to have used a fourth-order differential equation as their basic equation of the problem.

The purpose of this work is to suggest a new method by intro-

[1] Numbers in brackets designate References at end of paper.

Contributed by the Heat Transfer Division and presented at the Annual Meeting, Atlantic City, N. J., November 29–December 4, 1959, of THE AMERICAN SOCIETY OF MECHANICAL ENGINEERS.
NOTE: Statements and opinions advanced in papers are to be understood as individual expressions of their authors and not those of the Society. Manuscript received at ASME Headquarters, July 30, 1959. Paper No. 59—A-77.

Nomenclature

a, b = physical dimensions
a_n, b_n, c_n, d_n = parameters defined by Equations (45)
e_{mn}, f_{mn} = parameters defined by Equations (53)
g = gravitational acceleration
h = heat-transfer coefficient
k = thermal conductivity
l = reference length
p = pressure
q = heat-transfer rate
r_h = hydraulic radius
t = temperature
t_0 = reference temperature
t_w = wall temperature
u = dimensionless axial velocity $= u_3/u_m$
u_i = velocity components
u_m = mean axial velocity
x_i = physical co-ordinates
x, y = dimensionless co-ordinates $= (x_1/l, x_2/l)$
A = cross-sectional area
A_n, B_n, A_n', B_n' = integration constants
C_1 = axial wall temperature gradient
C_p = specific heat at constant pressure
E, F, G = functions defined by Equations (4) and (6)
Im( ) = imaginary part of a complex function
L_r, L_i = functions defined by Equations (44)
M_r, M_i = functions defined by Equations (50)
N_r, N_i = functions defined by Equations (52)
Nu = Nusselt number
Q = heat source intensity
Ra = Rayleigh number
Re( ) = real part of a complex function
T = temperature difference $= t - t_w$
T_m = mixed mean temperature difference
α = aspect ratio of a rectangular channel
β = coefficient of thermal expansion
ϵ = $(\mathrm{Ra})^{1/4}$
ζ_r, ζ_i = functions defined by Equations (25)
ξ_r, ξ_i = functions defined by Equations (29)
η_r, η_i = functions defined by Equations (32)
θ = dimensionless temperature difference $= kT/(\rho C_p C_1 u_m l^3)$
θ_m = dimensionless mixed mean temperature difference
κ = $\epsilon/\sqrt{2}$
λ_n, λ_n' = eigenvalues
μ = viscosity
ρ = density
ρ_w = density of fluid at the wall
ϕ = complex function $= u + i\epsilon^3\theta$
ψ = complex function $= \phi - G$

ducing a complex function whose real and imaginary parts are directly related to the velocity and temperature fields, respectively. In doing so, the coupled momentum and energy equations are readily combinable into a single second-order differential equation. To be more exact, for the heat-transfer problems of combined free and forced convection by a fully developed laminar flow in a vertical channel of constant axial wall temperature gradient with or without heat generations the governing equation is expressible in the form of a Helmholtz wave equation in the complex domain. Since the equation is a second-order one, it greatly reduces the complexities of the problem and is more accessible to many configurations which otherwise can not be easily solved by the usual mathematical techniques.

This new method is more direct and powerful. It gives the velocity and temperature fields simultaneously. The individual solutions of these two fields and other solutions require the splitting of some complex functions, which, in general, can be easily done by the use of some mathematical tables in the literature. Even in expressing the physical solutions in real functions from the original complex solutions, the present method is less complicated, particularly in cases where the cross section of the channel should be specified by two space variables, such as flows in rectangular channels.

The first part of this paper gives the mathematical formulation of the method. The heat-transfer coefficient and the Nusselt number are then derived in terms of this complex function. For illustrations, two previously investigated problems of flows between parallel plates and in a rectangular channel are treated in this paper by means of this complex function method. Finally, some discussions and conclusions of the method and its possible extensions are given in the last section of the paper.

Mathematical Formulation

Consider a steady laminar flow of a liquid in a vertical channel with heat sources under the influence of combined free and forced convection. The basic conservation equations [12] in Cartesian tensor notation are

$$\left.\begin{aligned} u_{i,i} &= 0 \\ \rho u_j u_{i,j} &= -p_{,i} + \mu u_{i,jj} + \rho g_i \beta (t - t_0) \\ \rho C_p u_i t_{,i} &= k t_{,ii} + Q \end{aligned}\right\} \tag{1}$$

Here we have taken that all fluid properties are constant except the density in formulating the buoyant effect. Let the axis of the channel be in the x_3-direction. Assume that the flow is fully developed, which implies a rectilinear motion [13], and that the axial wall temperature variation is linear. These conditions imply

$$\left.\begin{aligned} g_i &= (0, 0, g) \\ u_1 &= u_2 = 0, \quad u_{3,3} = 0 \\ t_{,3} &= C_1 \quad \text{or} \quad t = C_1 x_3 + t^*(x_1, x_2) \end{aligned}\right\} \tag{2}$$

The basic equations, Equations (1), are then

$$\left.\begin{aligned} \frac{\partial u_3}{\partial x_3} &= 0 \\ \frac{\partial^2 u_3}{\partial x_1^2} + \frac{\partial^2 u_3}{\partial x_2^2} + \frac{\rho g \beta T}{\mu} &= \frac{1}{\mu}\left(\frac{\partial p}{\partial x_3} + \rho_w g\right) \\ \frac{\partial^2 T}{\partial x_1^2} + \frac{\partial^2 T}{\partial x_2^2} - \frac{\rho C_p C_1}{k} u_3 &= -\frac{Q}{k} \end{aligned}\right\} \tag{3}$$

Using the following dimensionless quantities

$$\left.\begin{aligned} & x = x_1/l, \quad y = x_2/l \\ & u = u_3/u_m, \quad \theta = kT/(\rho C_p C_1 u_m l^2) \\ & E = \left(\frac{\partial p}{\partial x_3} + \rho_w g\right) l^3/\mu u_m, \quad F = Q/(\rho C_p C_1 u_m) \\ & \mathrm{Ra} = \rho^2 g C_p C_1 \beta l^4/k\mu \end{aligned}\right\} \tag{4}$$

Equations (3*b*, *c*) become

$$\left.\begin{aligned} \frac{\partial^2 u}{\partial x^2} + \frac{\partial^2 u}{\partial y^2} + \mathrm{Ra}\,\theta &= E \\ \frac{\partial^2 \theta}{\partial x^2} + \frac{\partial^2 \theta}{\partial y^2} - u &= -F \end{aligned}\right\} \tag{5}$$

Introducing two complex functions[2]

$$\phi = u + i\epsilon^2\theta, \qquad G = F + i\epsilon^{-2}E \tag{6}$$

where

$$\epsilon^4 = \mathrm{Ra}$$

Equations (5*a*, *b*) may be combined into a single equation,

$$\frac{\partial^2 \phi}{\partial x^2} + \frac{\partial^2 \phi}{\partial y^2} - i\epsilon^2\phi = -i\epsilon^2 G \tag{7}$$

This is an inhomogeneous Helmholtz wave equation. When $\nabla^2 G = 0$, where $\nabla^2 = (\ )_{xx} + (\ )_{yy}$, we introduce

$$\psi = \phi - G \tag{8}$$

Equation (7) is changed to a homogeneous Helmholtz wave equation (with inhomogeneous boundary conditions),

$$\frac{\partial^2 \psi}{\partial x^2} + \frac{\partial^2 \psi}{\partial y^2} - i\epsilon^2\psi = 0 \tag{9}$$

With appropriate boundary conditions, the solutions of this equation for some regular configurations may be found by various mathematical methods and techniques [14].

The velocity and temperature fields are clearly

$$u = \mathrm{Re}(\phi), \qquad \theta = \epsilon^{-2}\mathrm{Im}(\phi) \tag{10}$$

In the present problem of combined free and forced convection, the axial pressure gradient or the parameter E is a fixed quantity, which is definitely related to the mass flow and consequently to the axial temperature gradient and the heat source intensity. It may be determined from the following relation

$$\text{flow rate} = \int_A u_3 dx_1 dx_2 = u_m \int_A dx_1 dx_2 \tag{11}$$

or

$$\mathrm{Re}\left\{\int_A \phi dx dy\right\} = A/l^2 \tag{12}$$

To evaluate the heat-transfer coefficient or the Nusselt number, we first define a mixed mean temperature difference,

$$T_m = \frac{\int_A T u_3 dx_1 dx_2}{\int_A u_3 dx_1 dx_2} \tag{13}$$

In dimensionless form, it is

$$\theta_m = \frac{\int_A \theta u dx dy}{\int_A u dx dy} = \frac{l^2}{2\epsilon^2 A}\,\mathrm{Im}\left\{\int_A \phi^2 dx dy\right\} \tag{14}$$

[2] Here we assume that the Rayleigh number is positive. For nonpositive Ra, see the section of discussions of this paper.

This formula greatly reduces the mathematical manipulation used in previous investigations [5, 11], since we have avoided the lengthy multiplication of the functions u and θ.

The Nusselt number defined in the usual manner is

$$\mathrm{Nu} = \frac{hl}{k} = \frac{ql}{kT_m} \tag{15}$$

In dimensionless form, it is

$$\mathrm{Nu} = \frac{r_h}{l}\frac{1-F}{\theta_m} \tag{16}$$

where r_h is the hydraulic radius which is defined as the cross-sectional area divided by the circumference.

This formally completes the complex function method of the problem. In the subsequent sections the method is applied to the cases of flows between two parallel plates and in a rectangular channel.

Two Flat Plates

Consider the flow between two vertical parallel plates of width $2a$ with uniformly distributed heat sources throughout and linear axial temperature distribution at the walls. It is further specified that the wall temperature at the same horizontal level is equal.[3]

The governing equation and the boundary conditions are

$$\frac{d^2\phi}{dx^2} - i\epsilon^2\phi = -i\epsilon^2 G \tag{17}$$

and

$$\phi = 0 \quad \text{at} \quad x = \pm 1 \tag{18}$$

or

$$\frac{d^2\psi}{dx^2} - i\epsilon^2\psi = 0 \tag{19}$$

and

$$\psi = -G \quad \text{at} \quad x = \pm 1 \tag{20}$$

Here the reference length l is taken to be a.

The general solution of Equation (19) is

$$\psi = A_1 \cosh(i^{1/2}\epsilon x) + B_1 \sinh(i^{1/2}\epsilon x) \tag{21}$$

Using the boundary conditions (20), we obtain

$$\psi = -\frac{\cosh(i^{1/2}\epsilon x)}{\cosh(i^{1/2}\epsilon)} G \tag{22}$$

or

$$\phi = G\left[1 - \frac{\cosh(i^{1/2}\epsilon x)}{\cosh(i^{1/2}\epsilon)}\right] \tag{23}$$

To find the corresponding solutions of the velocity and temperature fields, we can easily split the function ϕ by the aid of some mathematical tables in the literature (see references listed in [15]). However, for the purpose of completeness and direct comparisons, all solutions of this paper are also given explicitly in terms of real functions. Then the velocity and temperature fields are, respectively,

$$\left.\begin{aligned} u &= \mathrm{Re}(\phi) = F\zeta_r - \epsilon^{-2}E\zeta_i \\ \theta &= \epsilon^{-2}\mathrm{Im}(\phi) = \epsilon^{-2}[\epsilon^{-2}E\zeta_r + F\zeta_i] \end{aligned}\right\} \tag{24}$$

where

$$\left.\begin{aligned} \zeta_r &= 1 - \frac{\cosh\kappa(1+x)\cos\kappa(1-x) + \cos\kappa(1+x)\cosh\kappa(1-x)}{\cosh 2\kappa + \cos 2\kappa} \\ \zeta_i &= \frac{\sinh\kappa(1+x)\sin\kappa(1-x) + \sin\kappa(1+x)\sinh\kappa(1-x)}{\cosh 2\kappa + \cos 2\kappa} \end{aligned}\right\} \tag{25}$$

with $\kappa = \epsilon/\sqrt{2}$

The parameter E or the pressure gradient may be found from

$$\mathrm{Re}\left\{\int_{-1}^{+1}\phi dx\right\} = 2 \tag{26}$$

By integration we obtain

$$\mathrm{Re}\left\{G\left[1 - \frac{\tanh(i^{1/2}\epsilon)}{i^{1/2}\epsilon}\right]\right\} = 1 \tag{27}$$

or

$$F\xi_r - \epsilon^{-2}E\xi_i = 1 \tag{28}$$

where

$$\left.\begin{aligned} \xi_r &= 1 - \frac{1}{2\kappa}\left[\frac{\sinh 2\kappa + \sin 2\kappa}{\cosh 2\kappa + \cos 2\kappa}\right] \\ \xi_i &= \frac{1}{2\kappa}\left[\frac{\sinh 2\kappa - \sin 2\kappa}{\cosh 2\kappa + \cos 2\kappa}\right] \end{aligned}\right\} \tag{29}$$

Therefore

$$E = \frac{\epsilon^2}{\xi_i}[F\xi_r - 1] \tag{30}$$

The mixed mean temperature difference is

$$\begin{aligned} \theta_m &= \frac{1}{4\epsilon^2}\mathrm{Im}\left\{\int_{-1}^{+1}\phi^2 dx\right\} \\ &= \frac{1}{4\epsilon^2}\mathrm{Im}\left\{G\left[3 - 3\frac{\tanh(i^{1/2}\epsilon)}{i^{1/2}\epsilon} - \tanh^2(i^{1/2}\epsilon)\right]\right\} \\ &= \frac{1}{4\epsilon^2}\left[\left(F^2 - \frac{E^2}{\epsilon^4}\right)\eta_i + \frac{2EF}{\epsilon^2}\eta_r\right] \end{aligned} \tag{31}$$

where

$$\left.\begin{aligned} \eta_r &= 3\xi_r - \frac{\sinh^2 2\kappa - \sin^2 2\kappa}{(\cosh 2\kappa + \cos 2\kappa)^2} \\ \eta_i &= 3\xi_i - \frac{\sinh 2\kappa \sin 2\kappa}{(\cosh 2\kappa + \cos 2\kappa)^2} \end{aligned}\right\} \tag{32}$$

Hence the Nusselt number of the problem is

$$\mathrm{Nu} = \frac{ha}{k} = \frac{2(1-F)}{\theta_m} \tag{33}$$

Rectangular Channels

Consider the flow in a rectangular channel of sides $2a$ and $2b$. The wall temperature distribution is taken to be constant at any peripheral section and linear in the axial direction. Let the reference length l be a and the aspect ratio b/a be α. Then we have

$$\frac{\partial^2\psi}{\partial x^2} + \frac{\partial^2\psi}{\partial y^2} - i\epsilon^2\psi = 0 \tag{34}$$

[3] Though we may have the case of two unequal wall temperatures at the same level, it does not change the main feature of the problem. The problem can be solved accordingly.

and boundary conditions

$$\psi = -G \quad \text{at} \quad x = \pm 1 \quad \text{and} \quad y = \pm\alpha \tag{35}$$

The solution of Equation (34) is

$$\psi = \sum_n [A_n \cosh(\lambda_n x) + B_n \sinh(\lambda_n x)] [A_n' \cos(\lambda_n' y) + B_n' \sin(\lambda_n' y)] \tag{36}$$

where λ_n and λ_n' are complex numbers which are related by

$$\lambda_n'^2 - \lambda_n^2 = i\epsilon^2 \tag{37}$$

To find the solution which satisfies the boundary conditions (35) we write

$$\psi = \psi_1 + \psi_2 \tag{38}$$

where ψ_1 satisfies

$$\left.\begin{aligned} \psi_1 &= -G \quad \text{at} \quad x = \pm 1 \\ \psi_1 &= 0 \quad \text{at} \quad y = \pm\alpha \end{aligned}\right\} \tag{39}$$

and ψ_2 satisfies

$$\left.\begin{aligned} \psi_2 &= 0 \quad \text{at} \quad x = \pm 1 \\ \psi_2 &= -G \quad \text{at} \quad y = \pm\alpha \end{aligned}\right\} \tag{40}$$

Then the solutions of ψ_1 and ψ_2 are, respectively,

$$\left.\begin{aligned} \psi_1 &= \sum_{1,3,5\ldots} A_n \cosh\left[\left(\frac{n^2\pi^2}{4\alpha^2} - i\epsilon^2\right)^{1/2} x\right] \cos\frac{n\pi y}{2\alpha} = \frac{4G}{\pi} \sum_{1,3,5\ldots} \frac{(-1)^{\frac{n+1}{2}}}{n} \frac{\cosh\left[\left(\frac{n^2\pi^2}{4\alpha^2} - i\epsilon^2\right)^{1/2} x\right]}{\cosh\left[\left(\frac{n^2\pi^2}{4\alpha^2} - i\epsilon^2\right)^{1/2}\right]} \cos\frac{n\pi y}{2\alpha} \\ \psi_2 &= \sum_{1,3,5\ldots} B_n \cosh\left[\left(\frac{n^2\pi^2}{4} - i\epsilon^2\right)^{1/2} y\right] \cos\frac{n\pi x}{2} = \frac{4G}{\pi} \sum_{1,3,5\ldots} \frac{(-1)^{\frac{n+1}{2}}}{n} \frac{\cosh\left[\left(\frac{n^2\pi^2}{4} - i\epsilon^2\right)^{1/2} y\right]}{\cosh\left[\left(\frac{n^2\pi^2}{4} - i\epsilon^2\right)^{1/2} \alpha\right]} \cos\frac{n\pi x}{2} \end{aligned}\right\} \tag{41}$$

Hence the solution of ϕ is

$$\phi = G\left\{1 + \frac{4}{\pi} \sum_{1,3,5\ldots} \frac{(-1)^{\frac{n+1}{2}}}{n} \left[\frac{\cosh\left[\left(\frac{n^2\pi^2}{4\alpha^2} - i\epsilon^2\right)^{1/2} x\right]}{\cosh\left[\left(\frac{n^2\pi^2}{4\alpha^2} - i\epsilon^2\right)^{1/2}\right]} \cos\frac{n\pi y}{2\alpha} + \frac{\cosh\left[\left(\frac{n^2\pi^2}{4} - i\epsilon^2\right)^{1/2} y\right]}{\cosh\left[\left(\frac{n^2\pi^2}{4} - i\epsilon^2\right)^{1/2} \alpha\right]} \cos\frac{n\pi x}{2}\right]\right\} \tag{42}$$

This shows that the velocity and temperature fields are

$$\left.\begin{aligned} u &= \mathrm{Re}(\phi) = FL_r - \epsilon^{-2} EL_i \\ \theta &= \epsilon^{-2}\,\mathrm{Im}(\phi) = \epsilon^{-2}[\epsilon^{-2} EL_r + FL_i] \end{aligned}\right\} \tag{43}$$

where

$$\left.\begin{aligned} L_r &= 1 + \frac{4}{\pi} \sum_{1,3,5\ldots} \frac{(-1)^{\frac{n+1}{2}}}{n} \left[\frac{\cosh a_n(1+x)\cos b_n(1-x) + \cosh a_n(1-x)\cos b_n(1+x)}{\cosh 2a_n + \cos 2b_n} \cos\frac{n\pi y}{2\alpha} \right. \\ &\qquad \left. + \frac{\cosh c_n(1+y/\alpha)\cos d_n(1-y/\alpha) + \cosh c_n(1-y/\alpha)\cos d_n(1+y/\alpha)}{\cosh 2c_n + \cos 2d_n} \cos\frac{n\pi x}{2}\right] \\ L_i &= \frac{4}{\pi} \sum_{1,3,5\ldots} \frac{(-1)^{\frac{n-1}{2}}}{n} \left[\frac{\sinh a_n(1+x)\sin b_n(1-x) + \sinh a_n(1-x)\sin b_n(1+x)}{\cosh 2a_n + \cos 2b_n} \cos\frac{n\pi y}{2\alpha} \right. \\ &\qquad \left. + \frac{\sinh c_n(1+y/\alpha)\sin d_n(1-y/\alpha) + \sinh c_n(1-y/\alpha)\sin d_n(1+y/\alpha)}{\cosh 2c_n + \cos 2d_n} \cos\frac{n\pi x}{2}\right] \end{aligned}\right\} \tag{44}$$

with

$$\left.\begin{aligned} a_n &= \frac{1}{2\sqrt{2}\,\alpha}\left[(n^4\pi^4 + 16\alpha^4\epsilon^4)^{1/2} + n^2\pi^2\right]^{1/2} \\ b_n &= -\frac{1}{2\sqrt{2}\,\alpha}\left[(n^4\pi^4 + 16\alpha^4\epsilon^4)^{1/2} - n^2\pi^2\right]^{1/2} \\ c_n &= \frac{\alpha}{2\sqrt{2}}\left[(n^4\pi^4 + 16\epsilon^4)^{1/2} + n^2\pi^2\right]^{1/2} \\ d_n &= -\frac{\alpha}{2\sqrt{2}}\left[(n^4\pi^4 + 16\epsilon^4)^{1/2} - n^2\pi^2\right]^{1/2} \end{aligned}\right\} \tag{45}$$

Equation (12) shows

$$\mathrm{Re}\left\{\int_{-\alpha}^{+\alpha}\int_{-1}^{+1} \phi\,dx\,dy\right\} = 4\alpha \tag{46}$$

or

$$\mathrm{Re}\left\{G\left[1 - \frac{8}{\pi^2} \sum_{1,3,5\ldots} \frac{1}{n^3}\left(\frac{\tanh(a_n + ib_n)}{a_n + ib_n} + \frac{\tanh(c_n + id_n)}{c_n + id_n}\right)\right]\right\} = 1 \tag{47}$$

We find

$$FM_r - \frac{E}{\epsilon^2} M_i = 1 \tag{48}$$

or the parameter E is

$$E = \frac{\epsilon^2}{M_i}[FM_r - 1] \tag{49}$$

where

$$M_r = 1 - \frac{8}{\pi^2} \sum_{1,3,5\ldots} \frac{1}{n^2} \left[\frac{1}{a_n^2 + b_n^2} \frac{a_n \sinh 2a_n + b_n \sin 2b_n}{\cosh 2a_n + \cos 2b_n} + \frac{1}{c_n^2 + d_n^2} \frac{c_n \sinh 2c_n + d_n \sin 2d_n}{\cosh 2c_n + \cos 2d_n} \right]$$

$$M_i = \frac{8}{\pi^2} \sum_{1,3,5\ldots} \frac{1}{n^2} \left[\frac{1}{a_n^2 + b_n^2} \frac{b_n \sinh 2a_n - a_n \sin 2b_n}{\cosh 2a_n + \cos 2b_n} + \frac{1}{c_n^2 + d_n^2} \frac{d_n \sinh 2c_n - c_n \sin 2d_n}{\cosh 2c_n + \cos 2d_n} \right] \tag{50}$$

The mixed mean temperature difference is evaluated from Equation (14),

$$\theta_m = \frac{1}{8\alpha\epsilon^2} \operatorname{Im} \left\{ \int_{-\alpha}^{+\alpha} \int_{-1}^{+1} \phi^2 dx dy \right\}$$

$$= \frac{1}{\epsilon^2} \operatorname{Im} \left\{ G^2 \left[\frac{1}{2} + \frac{2}{\pi^2} \sum_{1,3,5\ldots} \frac{1}{n^2} \left\{ [\operatorname{sech}^2 (a_n + ib_n) + \operatorname{sech}^2 (c_n + id_n)] - 3 \left[\frac{\tanh (a_n + ib_n)}{a_n + ib_n} + \frac{\tanh (c_n + id_n)}{c_n + id_n} \right] \right\} + \frac{4}{\alpha^2} \sum_{\substack{m,n \\ =1,3,5\ldots}} (e_{mn} + if_{mn}) \right] \right\}$$

$$= \frac{2EF}{\epsilon^2} N_r + \left(F^2 - \frac{E^2}{\epsilon^4} \right) N_i \tag{51}$$

where

$$N_r = \frac{1}{\epsilon^2} \left\{ \frac{3}{4} M_r - \frac{1}{4} + \frac{4}{\pi^2} \sum_{1,3,5\ldots} \frac{1}{n^2} \left[\frac{1 + \cosh 2a_n \cos 2b_n}{(\cosh 2a_n + \cos 2b_n)^2} + \frac{1 + \cosh 2c_n \cos 2d_n}{(\cosh 2c_n + \cos 2d_n)^2} \right] + \frac{4}{\alpha^2} \sum_{\substack{m,n \\ =1,3,5\ldots}} e_{mn} \right\}$$

$$N_i = \frac{1}{\epsilon^2} \left\{ \frac{3}{4} M_i + \frac{4}{\pi^2} \sum_{1,3,5\ldots} \frac{1}{n^2} \left[\frac{\sinh 2a_n \sin 2b_n}{(\cosh 2a_n + \cos 2b_n)^2} + \frac{\sinh 2c_n \sin 2d_n}{(\cosh 2c_n + \cos 2d_n)^2} \right] + \frac{4}{\alpha^2} \sum_{\substack{m,n \\ =1,3,5\ldots}} f_{mn} \right\} \tag{52}$$

and

$$e_{mn} = \frac{\left(m^2 + \frac{n^2}{\alpha^2} \right)^2 \frac{\pi^4}{16} - \epsilon^4}{\left[\left(m^2 + \frac{n^2}{\alpha^2} \right)^2 \frac{\pi^4}{16} + \epsilon^4 \right]^2}$$

$$f_{mn} = \frac{\left(m^2 + \frac{n^2}{\alpha^2} \right) \frac{\epsilon^2 \pi^2}{2}}{\left[\left(m^2 + \frac{n^2}{\alpha^2} \right)^2 \frac{\pi^4}{16} + \epsilon^4 \right]^2} \tag{53}$$

The Nusselt number, according to Equation (16), is

$$\mathrm{Nu} = \frac{ha}{k} = \frac{\alpha}{1 + \alpha} \frac{1 - F}{\theta_m} \tag{54}$$

Discussions and Conclusions

From the inspection of the basic equations we can easily see that the present set of equations is also applicable to the case of pure free convection with a linearly varying wall temperature. The only difference of the two problems is the magnitude of the axial pressure gradient or the parameter E. Discussions on this point are given in [9].

From Equation (6) we observe that the present method is only valid when the Rayleigh number is positive. For zero or negative Rayleigh number, the complex function ϕ is no longer meaningful since the velocity and temperature terms become indistinguishable. Mathematically, this may seem to be a shortcoming of the method. However, as we closely examine the problem, the mathematical requirement of positive Rayleigh number does agree with the physical conditions. First, let us look at the case of zero Rayleigh number. This means that either C_1 or β (or both) is zero. By examining Equations (3), we see that when $C_1 = 0$ this is a problem of constant wall temperature. The energy equation is independent of the velocity field. When $\beta = 0$ the buoyant term in the momentum equation disappears. This is identical to the pure forced convection problem. In either of these two cases, at least one of the basic equations involves only one dependent variable. Hence the equation is readily solvable. With one of the fields known, the other field, of course, is obtainable. Solutions in most problems of these cases are known.

In order to have a negative Rayleigh number, either C_1 or β is negative. In either of these two cases it implies that the density of the fluid is lighter at the bottom. They are equivalent to the problems of heating from below, which are connected to the phenomena of "Rayleigh instability" [16]. The flow characteristics are indeed different. Motions of columnar type or of cellular type may occur [9, 17, 18]. In these cases they certainly do not agree with the assumption of fully developed flows.

The present derivation does not include the frictional heating. It is well known that with frictional heating the energy equation becomes nonlinear. The equation may be solved by successive approximations, since the frictional heating term is usually small when compared with other terms. Then the present solution without frictional heating is still very useful. It represents the zeroth-order solution. In general, when the Rayleigh number is large, the effect due to the frictional heating is almost nil [7, 9].

As mentioned in the introduction, the present method is more direct and powerful. They can be readily seen from comparisons of two examples given in the paper. The governing equation of the present paper is a second-order one instead of the usual fourth-order equation. Also, we are able to obtain the solutions of the velocity and temperature fields simultaneously and express all solutions by circular and hyperbolic functions of complex arguments in less terms. Though we do have an extra step of splitting these complex functions in order to obtain all physical solutions, they, however, can be easily done by use of the mathematical tables of circular and hyperbolic functions of complex arguments [15]. The splitting of all the functions used, such as $\sin z$, $\cos z$, $\tan z$, $\sinh z$, $\cosh z$, $\tanh z$, $\sinh z/z$, and $\tanh z/z$, and so forth, are available in the literature.

Even when expressing all physical quantities in real functions, the present method is less complicated. This is particularly true when the cross section of the channel should be specified by two space variables. In the illustrative example of flows in rectangular channels, the present method gives the physical solutions in terms of some single series of elementary functions instead of the

double Fourier series [11]. It is a known fact that the Fourier series is usually a slowly convergent series.[4] In order to achieve the necessary accuracy of the numerical results, many terms of the series should be used. Computational work with double Fourier series is indeed quite lengthy. Also, the present approach gives the solution in a neater form.

At last, it should be mentioned that since the purpose of the paper is to suggest a new method of investigating the combined free and forced convection, no numerical results are given in this paper. Furthermore, the two examples given in this paper have been previously studied and the numerical results are available. Flows in other configurations are now in process and will be reported in the near future.

Acknowledgment

The author wishes to thank the Graduate School of Illinois Institute of Technology and the Esso Educational Foundation for a faculty research fellowship which made this investigation possible. Thanks also to Profs. S. P. Kezios and P. Chiarulli for their helpful suggestions and comments.

References

1 G. A. Ostroumov, "Svobodnaia Konvektsiia v Usloviiakh Vnutrennei Zadachi" (Free Convection Under the Conditions of the Internal Problem), State Publishing House, Technico-Theoretical Literature, Moscow, Leningrad, Russia, 1952; English translation, NACA TM 1407, 1958.

2 G. A. Ostroumov, "Matematicheskaya Teoria Ustanovivsheisya Teploperedachi v Krugloi Vertikalnoi Skvashine Pri Superpositsii Vynuzhdennoi i Svobodnoi Laminarnoi Konvektsii" (Mathematical Theory of the Steady Heat Transfer in a Circular Vertical Cavity With Superposition of Forced and Free Laminar Convection), *Zhurnal Tekhnicheskoi Fiziki*, vol. 20, no. 6, 1950, pp. 750–757.

3 D. C. Hamilton, H. F. Poppendiek, R. F. Redmond, and L. D. Palmer, "Free Convection in Fluids Having a Volume Heat Source," ORNL 1769 Engineering, Reactor Exp. Eng. Division, Oak Ridge National Laboratory, Oak Ridge, Tenn., Nov., 1954, Contract No. W-7405, eng. 26.

[4] Unless the Fourier coefficients are improved by some other mathematical means.

4 J. Woodrow, "Free Convection in Heat Generating Fluid (Laminar Flow)," AERE E/R 1267, Atomic Energy Research Establishment, Ministry of Supply, Harwell, Berks, England, Oct., 1953.

5 T. M. Hallman, "Combined Forced and Free-Laminar Heat Transfer in Vertical Tubes With Uniform Internal Heat Generation," TRANS. ASME, vol. 78, 1956, pp. 1831–1841.

6 S. Ostrach, "New Aspects of Natural-Convection Heat Transfer," TRANS. ASME, vol. 75, 1953, pp. 1287–1290.

7 S. Ostrach, "Combined Natural and Forced-Convection Laminar Flow and Heat Transfer of Fluids With and Without Heat Sources in Channels With Linearly Varying Wall Temperatures," NACA TN 3141, 1954.

8 S. Ostrach, "On the Flow, Heat Transfer, and Stability of Viscous Fluids Subject to Body Forces and Heated From Below in Vertical Channels," 50 Jahre Grenzschichtforschung, Verlag Friedr. Vieweg und Sohn, Braunschweig, Germany, 1955.

9 S. Ostrach, "Unstable Convection in Vertical Channels With Heating From Below Including Effects of Heat Sources and Frictional Heating," NACA TN 3458, 1955.

10 D. V. Wordsworth, "Laminar Free Convection Between Heat Producing Vertical Plates in a Liquid," AERE E/R 1270, Atomic Energy Research Establishment, Ministry of Supply, Harwell, Berks, England, Oct., 1953.

11 L. S. Han, "Laminar Heat Transfer in Rectangular Channels," JOURNAL OF HEAT TRANSFER, TRANS. ASME, series C, vol. 81, 1959, pp. 121–128.

12 L. Howarth, "Modern Developments in Fluid Dynamics—High Speed Flow," Oxford University Press, London, England, 1953, vol. II, pp. 757–853.

13 S. H. Maslen, "Transverse Velocities in Fully Developed Flows," *Quarterly of Applied Mathematics*, vol. 16, 1958, pp. 173–175.

14 P. M. Morse and H. Feshbach, "Methods of Theoretical Physics," McGraw-Hill Book Company, Inc., New York, N. Y., 1953, vol. II, pp. 1360–1582.

15 A. Fletcher, J. C. P. Miller, and L. Rosenhead, "Index of Mathematical Tables," McGraw-Hill Book Company, Inc., New York, N. Y., 1946, pp.186–188.

16 Lord Rayleigh, "On Convection Currents in a Horizontal Layer of Fluid When the Higher Temperature Is on the Upper Side," *Philosophical Magazine*, series 6, vol. 32, 1916, pp. 529–547.

17 K. Chandra, "Instability of Fluids Heated From Below," *Proceedings of Royal Society of London*, series A, vol. 164, 1938, pp. 231–242.

18 O. G. Sutton, "On the Stability of a Fluid Heated From Below," *Proceedings of Royal Society of London*, series A, vol. 204, 1950, pp. 297–309.

The Role of the Skin in Heat Transfer

A. M. STOLL

Physiologist, Special Technical Assistant to Director, Aviation Medical Acceleration Laboratory, U. S. Naval Air Development Center, Johnsville, Pa.

The author considers lines of fundamental research and the impact of human factors in the area of thermal exchange. Logically, this area of investigation may be divided into: (a) Heat exchange between man and his environment; and (b) internal energy balance between heat production and heat loss. Very little information has been compiled in an orderly fashion concerning the skin through which heat must flow in both directions to maintain man in his environment in a functional capacity. It is therefore the purpose of this paper to consider the human skin, its dimensions and properties with respect to its role in heat transfer, and the effects of its impairment or injury.

THE SKIN is readily recognized as the boundary layer of the body and is frequently considered as a thermal insulator or inert envelope containing a metabolically active source. Less often is it thought of in terms of its own thermal function although it is in itself a heat generator, absorber, transmitter, radiator, conductor, vaporizer, and detector. Very little is known about the physical dimensions of skin even though its importance is attested by the thriving community of dermatologists who devote their professional lives to the study of its health and welfare. Most of the data available date back to the 1800's and are of questionable accuracy largely due to the technical difficulties of assessing the dimensions of so irregular and heterogeneous a tissue. To appreciate some of these difficulties one need only consider the nature of the tissue as shown in Fig. 1. It is seen that the skin is comprised of two main portions—the epidermis and the dermis. The epidermis is subdivided into four layers, the stratum corneum, stratum lucidum, stratum granulosum, and stratum germinativum. One or two of these layers (viz., s. l. and s. gr.) may be absent in some areas of the body. The dermis is subdivided into two layers, subepithelial or papillary layer and the reticular layer, both of which are composed of connective tissue. All layers except the stratum corneum are living, growing tissue and therefore produce metabolic heat.

The thickness of the whole skin varies widely over the surface of the body. It may be more than 5 mm on the back and only 0.5 mm. on the eyelids. The usual thickness is 1 to 2 mm. The futility of attempting to strip the skin from the entire body evenly is so obvious as to discourage even the most dedicated anatomist. Therefore the physical dimensions determined for whole skin are for the most part calculated values although quite recently specific gravity has been determined directly [1].[1] Some of these are shown in Table 1. From these figures it is readily appreciated that, by weight as well as by surface area, skin is one of the largest organs of the body. It comprises about 6 per cent of the total body weight and exceeds the weight of the liver, the brain, the heart, and the kidneys put together.

Of greater interest in the present consideration are the thermal and optical properties which are even more difficult to measure and therefore are known only approximately. Some of these are shown in Table 2. Although these quantities are frequently referred to as "constants," it is obvious that they must be far more variable than constant since the medium itself is not only heterogeneous but of varying composition and thickness from place to place on the body surface. Furthermore, because of the presence of thermal and other sensory detectors in the skin, its thermal

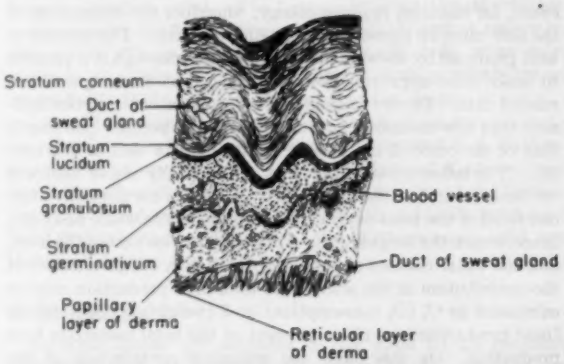

Fig. 1 Section of human skin showing all layers. (Adapted from photomicrograph by A. A. Maximow, Textbook of History, Maximow and Bloom, W. B. Saunders Company, Philadelphia, Pa., 1948.)

Table 1 Approximate values of the physical dimensions of whole skin for the "average man"

(70 kg in weight and 170 cm in height [1])

Dimension	Value
Weight	4 kg (8.8 lb)
Surface area	1.8 m^2 (20 sq ft)
Volume	3.6 l (3.7 qt)
Water content	70 to 75 per cent
Specific gravity	1.1
Thickness	0.5 to 5 mm (0.02 to 0.2 in.)

Table 2 Approximate values for thermal and optical properties of skin

Property	Value
Heat production	240 (?) kg cal/day
Conductance	9 to 30 kg cal/m^2 hr deg C
Thermal conductivity (k)	$(1.5 \pm 0.3) \times 10^{-3}$ cal/cm sec deg C at 23 to 25 deg C ambient
Diffusivity ($k/\rho c$)	7×10^{-4} cm^2/sec (surface layer 0.26-mm thick)
Thermal inertia ($k\rho c$)	90 to 400 $\times 10^{-3}$ cal^2/cm^4 sec deg C^2
Heat capacity (c)	~0.8 cal/gm
Emissivity (infrared)	~0.99
Reflectance (wave-length dependent)	Maximum 0.6 to 1.1 μ Minima <0.3 and >1.2 μ
Transmittance (wave-length dependent)	Maxima 1.2, 1.7, 2.2, 6, 11 μ Minima 0.5, 1.4, 1.9, 3, 7, 12 μ

[1] Numbers in brackets designate References at end of paper.

Contributed by the Heat Transfer Division and presented at the Annual Meeting, Atlantic City, N. J., November 29–December 4, 1959, of THE AMERICAN SOCIETY OF MECHANICAL ENGINEERS.

NOTE: Statements and opinions advanced in papers are to be understood as individual expressions of their authors and not those of the Society. Manuscript received at ASME Headquarters, August 13, 1959. Paper No. 59—A-138.

properties are influenced by an efficient feedback system operating through the cutaneous blood-flow system, as well as through a voluntary or cortical control whereby the entire organism is activated to remove itself from hazardous environments.

For example, local cooling causes a shutdown of blood flow to the skin to a minimum estimated at about 0.015 cc per min per sq cm [2]. Local heating brings about local vasodilatation, flooding the heated skin with blood at over 100 times the minimal rate, resulting in measured thermal conductivities as much as four times the value determined at normal room temperature. In addition, prolonged local heating brings about sweating, not only of the heated area but also of nonheated areas of the skin [3] indicating that remote as well as local effects may be produced by signals relayed from the skin detectors to the central nerve centers. More intense heating may stimulate pain receptors, resulting in reflex withdrawal of the limb or perhaps of the entire body.

Changes in skin temperature are accompanied by variations in heat production, as well as heat loss, in the skin. The secretion of sweat, for instance, requires energy; therefore the metabolism of the skin must be increased during such activity. The amount of heat produced by the skin itself is unknown although it is possible to make some approximation from its oxygen consumption and related data. *In vitro* measurements of oxygen consumption indicate that the metabolic rate of this tissue is perhaps one fourth that of the cerebral cortex and about one fifth that of the liver [4]. The latter is one of the most metabolically active tissues of the body which, in the dog, at least, accounts for approximately one third of the total oxygen consumption of the whole body [5]. Since in man the weight of the skin is about twice that of the liver, and the water content about equal [4], a very rough estimate of the contribution of the skin to the total heat production may be calculated as $^1/_3$ (O_2 consumption) $\times$ 2 (weight) $\times$ 33 per cent (heat production) = 12 + per cent of the total metabolic heat production. On this basis, the estimated contribution of the skin is about 240 kg cal per day for the "average man," a not insignificant amount.

The thermal conductivity of the whole skin is so much under the influence of blood flow that it proved desirable to deal with it in two parts; i.e., (*a*) the specific conductivity referring to the bloodless tissue, and (*b*) that caused by the flow of blood to the skin surface. Used in this sense thermal conductivity becomes obscured in the term conductance, Table 2 [2, 6], referring to the heat flux per unit gradient decrease in temperature through the skin and the underlying tissues of the body.

It becomes clear that to specify a firm value for thermal conductivity of skin in the usual engineering sense it would be necessary to separate the skin into homogeneous layers and measure each separately. Since this technique cannot be employed in the intact body, approximations have been made by other methods involving the measurement of the product of conductivity, heat capacity, and density as one entity, or by determining average diffusivity with respect to depth, and deriving from this the conductivity. The value noted in Table 2 is one recently given [7] for intact living skin. It was obtained by comparison of the product ($k\rho c$) of skin with that of a known substance (glass) and applies at normal room temperature (23 to 25 C). Other determinations [8, 9] have shown values of $k\rho c$ varying from 90 to 400 cal^2/cm^4 sec deg C^2 depending upon the physiological and physical conditions prevailing.

Heat capacity has been measured in excised pigskin [10] and because of the histological similarities between this and human skin, it has been assumed to be applicable to the latter as well. Since this value is fairly close to unity it has relatively little effect on the computations of thermal conductivity. However, as determinations of the latter become more dependable, direct determination of heat capacity in human skin should be made.

The importance of emissivity, reflectance, and transmittance of the skin has long been recognized. The fact that the skin emits heat very nearly like a black body, Table 2 [11], has permitted the development of various radiometric devices for the measurement of skin temperature. Reflectance and transmittance[2] are of particular importance in determining the extent and depth of heating of the skin exposed to energy of various wave lengths. Sources of such energy range from natural emitters such as the sun and the natural environment to artificial sources such as atomic flash, infrared and tungsten lamps, carbon arcs, furnaces, open fires, and myriad others. The determination of the effect on the skin of each of these types of energy constitutes a complicated study in itself since the optical properties vary with the degree of pigmentation of the skin, thickness of the layer, surface condition, and so on. One effect in common, however, is that prolonged or intense exposure results in death of the skin in whole or in part. If the entire skin surface is destroyed, even though deeper tissues are not, death of the individual is certain. Prevention of such deaths absorbs the interest of many physicians and surgeons and involves them in studies of heat transfer into the layers of the skin itself. These studies include evaluations of char depth, histological changes, metabolic processes, and the elaboration of substances by injured or thermally stimulated cells [12].

It develops, then, that the role of skin in heat transfer is manifold. It may be considered under certain circumstances to be a multiple-layer covering of a heat source through which heat passes at a measurable rate; a servomechanism for the regulation of this heat passage; an alarm system to detect and transmit signals indicating dangerous extremes of temperature; a living organ generating, dissipating, and modulating the flow of heat between the entire organism and its environment; and finally, an indispensable, vulnerable yet highly regenerative and adaptable thermal integument having remarkable ability to alter its properties, thus inhibiting heat loss in the cold and augmenting heat loss in the heat. In the field of thermal engineering its significance is reflected most obviously, perhaps, in the relative narrowness of the comfort zone. It is the skin rather than the body as a whole, which, by virtue of its wealth of sensory receptors, dictates the physical features of a comfortable environment. In this regard, it has been shown [13] that exposure to a thermal environment of 105/95 F (dry/wet bulb) results in impairment of performance dependent upon attention to cues (flashing lights), superimposed on a central task (tracking), even though the performance of the central task is unaffected. Thus modification of the sensory function of the skin offers one final possibility of broadening the thermal limits of man's field of operation. If it were possible to modulate sensations of heat and cold at the cortical or perceptual level, the limits of the comfort zone undoubtedly could be expanded considerably. Modulation at this level would not affect the thermoregulatory servosystem although it would narrow the individual's margin of safety by subduing the early warnings of impending danger. Later warnings such as giddiness, nausea, and increased heart rate would not be affected. Such modulation could not increase the absolute tolerance level of the body but it could reduce the mental and emotional discomfiture occasioned by long exposure to extreme, yet sublethal, environments. It is conceivable that in situations where weight is a critical factor, as in rocket ships for example, a significant reduction in heat-exchanger equipment might be effected by expansion of the comfort zone by even a small margin. In this way, performance of complicated tasks requiring judgment and precision on the part of the operator might be maintained over long periods of time at no added weight cost simply through elimination of the distraction and irritation afforded by an environment perceived as uncomfortable. In any event, modulation of this sensory system consti-

[2] The maxima and minima noted in Table 2 are rough average values obtained from a variety of sources too numerous to list. Many of these are to be found in issues of the *Journal of Applied Physiology*.

tutes an intriguing pharmaco-psychological problem in which the thermal senses are to be depressed selectively without interference with kinesthetic senses or motor function. Such an approach though somewhat risky, may well be the last resort in widening the thermal limits within which man may function effectively and constitutes, perhaps, the final aspect of the role of skin in heat transfer.

References

1 M. Feider and C. M. Bunche, "Physical Dimensions of the Skin," American Medical Association Archives of Dermatology and Syphilology, vol. 69, 1954, 563–569.

2 J. D. Hardy and G. F. Soderstrom, "Heat Loss From the Nude Body and Peripheral Blood Flow at Temperatures of 22° to 35°C," *Journal of Nutrition*, vol. 16, 1938, p. 493.

3 R. Seckendorf and W. Randall, "The Fractional Recruitment of Sweating During Heating of Limited Skin Areas," Federation Proceedings of Experimental Biology, vol. 18, 1959, p. 140.

4 W. S. Spector, editor, "Handbook of Biological Data," WADC TR 56–273, October, 1956, pp. 260 and 77.

5 S. E. Levy and A. Blalock, "Fractionation of the Output of the Heart and of the Oxygen Consumption of Normal Unanaesthetized Dogs," *American Journal of Physiology*, vol. 118, 1937, p. 368.

6 C. E. A. Winslow, L. P. Herrington, and A. P. Gagge, "Physiological Reactions of the Human Body to Varying Environmental Temperatures," *American Journal of Physiology*, vol. 120, 1937, p. 1.

7 A. J. H. Vendrik and J. J. Vos, "A Method for the Measurement of the Thermal Conductivity of Human Skin," *Journal of Applied Physiology*, vol. 11, 1957, pp. 211–215.

8 M. Lipkin and J. D. Hardy, "Measurement of Some Thermal Properties of Human Tissues," *Journal of Applied Physiology*, vol. 7, 1954, p. 212.

9 A. M. Stoll and L. C. Greene, "Relationship Between Pain and Tissue Damage Due to Thermal Radiation," *Journal of Applied Physiology*, vol. 14, 1959, pp. 373–382.

10 F. C. Henriques, Jr., and A. R. Moritz, "Studies of Thermal Injury I," *American Journal of Pathology*, vol. 23, 1947, pp. 531–549.

11 J. D. Hardy, "The Radiating Power of the Human Skin in the Infrared," *American Journal of Physiology*, vol. 127, 1939, pp. 454–462.

12 A. L. Lorincz and R. B. Stoughton, "Specific Metabolic Processes of Skin," *Physiological Reviews*, vol. 38, 1958, pp. 481–498.

13 A. E. Bursill, "The Restriction of Peripheral Vision During Exposure to Hot and Humid Conditions," *Quarterly Journal of Experimental Psychology*, vol. 10, 1958, pp. 113–129.

DISCUSSION

George Mixter, Jr.[3]

Suspended as I am between the heaven of pure physics, where all is known or knowable, and the hell of clinical medicine where nothing is known for sure, there is little I can add to this fine presentation.

The thermal and optical constants of skin as given are, I think, generally agreed upon by workers in the field. The "philosophy" of skin propounded in this paper is an admirable summing up by one well qualified to do so.

Without the help of my engineering and physicist friends at the Naval Materials Laboratory in Brooklyn, I should not presume to discuss the instrumentation of the 2-thermistor gradient amplifier you have just heard described, except to express delight that gradients of the order of thousandths of a degree may be measured with accuracy within such "semi-infinite solids".

It seems to me that papers given at this meeting are beginning to demarcate three major areas of biologic heat transfer, so far as its noxious effect on the organism is concerned. For brief exposures of less than 10 sec at high irradiances, the kpc of skin is relatively stable at around 10×10^{-4} cgs units. Here, damage to biologic systems (clinically called a flash burn) remains close to the surface and hinges upon the time-temperature tolerance of living cells. This is the field in which my colleagues and I are currently attempting to obtain accurate quantitative data.

As vertebrate feedback systems come into play, kpc begins to rise toward a 4 or 5-fold increase; in exposures to lower irradiances for moderate periods of time, as Dr. Webb has shown,[4] the limit of biologic tolerance is not cell death, but pain. Tolerance for transient exposures of this order of magnitude may well be altered by "modulation of the sensory system" as suggested by this author, although there is a narrow margin between the thermal requirements for intolerable pain and irreversible tissue damage, as she and Dr. Hardy have shown.

The third area of noxious thermal transfer involves even lower irradiances and longer times. Increased kpc–"thermal inertia"–of the skin results in suppression of the critical aspects of surface temperature, but at the expense of the whole organism, whose mean body mass temperature cannot be allowed to rise beyond a certain point. The balance between this absorption and protective feedbacks forms the subject of several papers in this series. These three areas are actually only gross subdivisions of a broad spectrum of thermal damage which are of interest alike to the physician, biologist, and engineer.

I should like again to congratulate Dr. Stoll, and to conclude by asking whether her thermistors are embedded in a diathermanous, or an opaque, medium. T. P. Davis of Rochester has treated the heat-flow situations involved in a masterful fashion (partially reported at the IRE meetings this fall in Philadelphia) but, thus far, the special case of the diathermanous solid has defied satisfactory analysis.

E. M. Sparrow[5]

Congratulations are extended to Dr. Stoll for an excellent exposition of the heat-transfer properties of skin as well as for the development of a highly accurate instrument for temperature measurement. In connection with the instrument, it may be worth while to pose a question which is frequently raised when engineering measurements are being made. Namely, is the disturbance of the temperature field due to the presence of the probe of sufficient magnitude to reduce the need for a highly precise instrument? Now, in the case of skin, it would appear that the usual physical disturbance of the temperature distribution would be augmented by physiological reactions. It would be appreciated if Dr. Stoll would comment on the magnitudes of these disturbances and, if possible, compare them with the accuracy of her instrument.

Alan H. Woodcock[6]

Dr. Stoll has certainly produced a fascinating paper on an organ of the human body about which surprisingly little is known. To the engineer it must be a very unsatisfactory engineering material since its properties are so extremely variable. Nevertheless, to the container engineer, it seems to be an ideal substance–one which is flexible, resilient, self-repairing, capable of increasing its thickness where abrasion is high. Added to this, the remarkable thermo-regulatory potentiality of living skin makes one wonder when compared to structures created by man.

One wonders at Dr. Stoll's suggestion of desensitizing the skin as a means of expanding the thermal comfort zone. In an environment which is oscillatory in its thermal regime, such as in

[3] MD, F.A.C.S., Associate Professor of Surgery, NYU-Postgraduate School of Medicine, NYC Consultant to Naval Materials Laboratory, Brooklyn, N. Y.

[4] Paul Webb, "Exposure to Aerodynamic-Heating Transients," ASME Paper No. 59—A-211.

[5] Professor of Mechanical Engineering, University of Minnesota, Minneapolis, Minn. Assoc. Mem. ASME.

[6] Chief, Biophysics Branch, Headquarters Quartermaster Research & Engineering Command, U. S. Army, Natick, Mass.

a satellite which is alternating between the shadow of the earth and sunlight, desensitizing the skin might have some value if the variations in temperature were great. However, in space travel, far from the earth, steady conditions can be expected and here tolerance of the human to abnormalities in deep body temperature would seem to be the governing factor.

Dr. Stoll is to be congratulated on an excellent paper containing a useful collection of pertinent data.

Author's Closure

The very kind comments of all the discussers are greatly appreciated and I shall endeavor to clarify the points raised.

The questions of Dr. Mixter and Professor Sparrow pertain to the oral presentation of data on a temperature-gradient measuring system under development for use in a skin simulator. The sensitive elements are thermistors and their calibration for the indication of absolute temperatures between 24 and 60 deg C, and of gradients of 0 to 2.5 deg C with an accuracy within 0.025 deg C, was described.

In answer to Dr. Mixter's very pertinent question, the thermistors are to be used in a diathermanous medium which is blackened on the surface to render it opaque and to conform to the manner in which irradiation of living skin is performed in measuring thermal pain and blister thresholds.

Professor Sparrow's point is also well taken. The amount of disturbance in the gradient occasioned by the introduction of the thermistors depends largely upon the discrepancy between the thermal conductivity of the thermistor material and that of the tissue (or simulated tissue). Neither that of the former nor the latter is known precisely at the present time. However, the thermistor elements under discussion are glass-covered ceramic beads and the thermal conductivity of these materials approximates 0.002 cal/cm sec deg C while that of the skin (0.0015 ± 0.0003, Table 2) appears to be not greatly different. The final answer to this question must await dynamic calibrations of the elements in situ. The calibration described was performed dynamically in water at levels between 24 and 50 deg C at which temperature the thermal conductivity of water is about 0.0014—0.0015 cgs unit, closely approximating that measured for skin and changing in the same direction with temperature. It was carried out primarily for the purpose of establishing the feasibility of using thermistors in this application since the resistance of both sensing elements changes with temperature. Such feasibility was established and it now remains to incorporate the gradient-measuring system in the simulated skin. As for the augmentation of thermal disturbances by physiological reactions, data on this point are entirely lacking, for such biological techniques as have been used have not separated the physical from the physiological events. It is hoped that the system described, after suitable calibration in inert materials, may be applied to the measurement of physiological effects.

As Dr. Woodcock suggests, the space vehicle intended for long-term occupancy may be expected to provide a constant environment where tolerance to abnormalities in deep body temperature would play the dominant role. However, in this situation one would anticipate a "shirt-sleeve environment" as postulated by J. E. Janssen in another of the Heat Transfer sessions (ASME Paper No. 59—A-207). The example cited in the present paper referred to the shorter term though relatively long-duration requirement for maintaining high-level performance in an environment normally perceived as uncomfortable, as for instance, that which might be experienced during rocket flight, or to come back to earth, any situation in which broadening of the thermal tolerance limits is required temporarily for purposes of performance maintenance.

In closing, I welcome this opportunity to thank the discussers once again for their kind remarks and critique; to point out, lest anyone be misled, that the title conferred on me in these discussions is entirely a courtesy accorded by my colleagues in the biological fields; and, finally, to thank the mentors of The American Society of Mechanical Engineers, particularly those of the Heat Transfer Section, for their invitation to participate in the activities of this splendid organization.

The Prediction of Human Thermal Tolerance When Using a Ventilating Garment With an Antiexposure Suit[1]

J. W. MC CUTCHAN
Associate Professor of Engineering,
University of California,
Los Angeles, Calif.
Mem. ASME

The physiological responses of human subjects have been investigated in the thermal environments ranging from 120 to 240 deg F while wearing the MA-2 ventilating garment, an MK-IV exposure suit, and other garments comprising 2.15 clo[2] of thermal resistance. The ventilating garment was given air inputs ranging from 2 to 14 cfm in volume, and from 50 to 90 F in temperature. The thermal responses of the subjects are shown graphically in terms of heat storage, heart rates, sweat rates, and composite indexes of these variables. The results of these experiments have been prepared in terms of an equation which is presented graphically as a nomograph. This nomograph predicts the cooling power of the MA-2 ventilating garment and is to be used in conjunction with the tolerance chart. The tolerance data, which were determined on steady exposures in a preheated chamber, are used to predict human tolerance for conditions where the air and wall temperatures are not constant.

In recent years requirements for air-crew clothing have become more exacting, partly because the occupants of today's high-speed aircraft must be prepared to perform under extremes of environmental temperature. In particular, they may be subjected to high temperatures in the cabin as a result of the ram air heating. Personnel also may be exposed to the cold encountered in a high-altitude bail-out or a forced landing over mountain, arctic, or air terrain. The cold environments require that the crew must wear about 3 or 4 clo[2] for protection. Additionally, an antiexposure suit is considered necessary for protection against loss of this insulation by wetting in the event of immersion in water after bail-out.

To have relative comfort and thermal balance while wearing 4 clo of clothing and an impermeable outer garment, a cabin temperature of about 30 F would be necessary. This would call for an impracticable amount of cabin cooling at high speeds. One solution is to limit the amount of air conditioning and expose the crew to a higher temperature which is still within human capacity to perform efficiently though not necessarily comfortably for short periods of time. However, this may entail many practical difficulties. For example, during the time the crew member wears the impermeable suit his sweat accumulation will have reduced the effective insulation value of his clothing. Therefore, if feasible, one should provide a "private climate" by means of air-conditioned clothing.

The use of ventilated clothing as a means of reducing heat or cold stress has been advocated by various persons over the past 50 years [1].[3] There are two ideas which should be emphasized as background for the present study; namely, economy of protection, and effectiveness of distribution of cooling in the suit:

(*a*) Ventilated clothing provides a mobile private climate for the wearer. In the industrial situation this is a substitute for either general space conditioning or local space cooling. In military aircraft where maximum power with minimum weight is critical to performance, any device which potentially favors this ratio immediately commands attention.

[1] This paper is the result of research sponsored by Wright Air Development Center (Aero Medical Laboratory) in co-operation with the University of California, Los Angeles, Cal.

[2] The unit of thermal resistance for clothing is the "clo"; one clo is equal to 0.88 deg F/(Btu/ft²hr), and expresses the insulation value of that quantity of clothing that will maintain comfortable thermal equilibrium in a man sitting at rest in an environment of: (*a*) 70 deg F air and wall temperature; (*b*) less than 50 per cent relative humidity; (*c*) and 20 ft/min air movement.

Contributed by the Heat Transfer Division and presented at the Annual Meeting, Atlantic City, N. J., November 29–December 4, 1959, of The American Society of Mechanical Engineers.

Note: Statements and opinions advanced in papers are to be understood as individual expressions of their authors and not those of the Society. Manuscript received at ASME Headquarters, August 13, 1959. Paper No. 59—A-114.

[3] Numbers in brackets designate References at end of paper.

Nomenclature

A_b = surface area of body, ft²
W_b = body weight, lb
W_c = mass air flow to chamber, lb/min
C_b = average unit heat capacity of human body, Btu/lb, deg F
C_p = unit heat capacity of air at constant pressure, Btu/lb deg F
HR = heart rate, beats per min
I = Craig index, dimensionless
p_a = water vapor pressure, atmospheric, in. Hg
p_s = water vapor pressure, suit ventilation (subscripts i and o, entering, leaving), in. Hg
q_c = convective heat transfer, Btu/ft²hr
q_e = evaporative heat transfer, Btu/ft² hr
q_m = metabolism, Btu/ft²hr
q_r = radiant heat transfer, Btu/ft² hr
q_R = respiratory heat transfer, Btu/ft² hr
q_s = body storage index, Btu/ft²hr
Δq_s = change in storage index due to ventilated suit, Btu/ft²hr
$q_{suit} = q_{(chart)} - \Delta q_s$, Btu/ft²hr
q_v = sensible heat transfer to air in ventilating garment, Btu/ft² hr
t_a = ambient air temperature, deg F

(*Continued on next page*)

(*b*) All previous models of ventilated clothing have featured some form of tubular-duct air distribution, often with inadequacies of distribution, or high pressure drop, or bulkiness of the ducts within the clothing. The MA-1 suit, designed by H. A. Mauch [2] and later the MA-2 suit, has a sandwich duct system with many ports for air distribution and a low pressure drop. It is designed for high cooling efficiency coupled with a garment construction of increased comfort and convenience. A picture of the MA-1 ventilating garment appeared in *Life Magazine* [3]. For demonstration purposes, *Life* used smoke in the ventilating air to give the reader a feel for the efficiency of the air-distribution system. Later, in *Mechanical Engineering* [4], a picture was published of the MA-2 ventilating garment, where the basic change was to extend the ventilating garment below the knees.

It is difficult to justify any extensive program of evaluation on any particular clothing assembly because these assemblies soon become obsolete. Nevertheless, the principle of the ventilating garment is so fundamental that it is the objective of this paper to provide a rational basis for the prediction of thermal tolerance when using an MA-2 ventilating garment with a modified MK-IV antiexposure suit.

The approach is to evaluate the environmental stress, without the ventilating garment, according to the procedures outlined by Craig L. Taylor [5]. This stress is measured by the "storage index" parameter and is expressed in Btu/ft²hr. The ventilating garment decreases this stress and the magnitude of this decrease in storage index is reflected in an increase in the subject's tolerance time.

Clothing Assembly

The clothing assembly including ventilating and outer garments has a mean effective clo of 2.15. Fig. 1 shows the assembly of clothing on the subject. The clothing for the trunk, arms, and legs remained the same throughout all experiments. This consisted of long woolen underwear, very light flying suit type K-1, experimental ventilating garment MA-1 and later MA-2, modified MK-IV antiexposure suit and liner.

It was planned to keep the same clothing for head, hands, and feet but we encountered distress in these areas at the 200 and 240 F environments and the clothing had to be modified. To prevent burning on the nose and ears, two Navy knit stocking caps were made into a hood which distributed the perspiration more uniformly and prevented burns. Leather gloves were worn over wool-knit gloves but when blisters resulted at the knuckles at 240 F we changed to wool-knit gloves up to 200 F and M1949 arctic mittens with A-11A wool inserts for the 200 and 240 F environments. The greatest discomfort resulted from hot feet. Even though the subjects wore heavy woolen stockings, the hot rubber boots of the MK-IV antiexposure suit were painful. The boots were removed from the suit and the subjects wore mukluks with woolen socks for the remainder of the experiments.

Environmental Conditions

The heat chamber consists of a one-man conditioned space equipped with controls for temperature, humidity, pressure (altitude), and air flow. In addition to these controls which are a part of the chamber, it was necessary to condition and control the air to the ventilated suit. Table 1 gives the control settings maintained in these experiments:

Table 1

PHYSICAL ENVIRONMENT

Variable	Settings
Air temperature, t_a	120, 160, 200, 240 F
Wall temperature, t_w	$t_w = t_a$
Mass, flow, W_a	6 lb per min
Barometric pressure, P	22.2 in. Hg (8000 ft alt)
Water vapor pressure, P_a	0.39 in. Hg

VENTILATED SUIT ENVIRONMENT

Ventilation, t_v	50, 70, 90 F
Ventilation air flow, V_v	2, 6, 10, 14 cfm[a]
Ventilation air humidity, $P_{a_{vg}}$	0.20 in. Hg

[a] The cfm values are those for a pressure of 22.2 in. Hg.

Since one of the objectives of this paper is to explain how the ventilating garment accomplishes its cooling effect, an attempt was made to measure the outlet dew point and temperature from the suit. The right-arm and right-leg outlet valves from the suit were manifolded together and this air was sampled by an electronic dew-point hygrometer. Since the chamber temperature was always above the ventilated-suit temperature no special provision was necessary for prevention of condensation in the air-sampling line.

Physiological Measurements

Skin temperatures were recorded on seven channels of a Brown automatic recording potentiometer, with an accuracy of ±0.5 deg F. A total of 15 thermocouples, in parallel, measure temperatures at seven major surface regions. The mean of these readings is reported. Deep body temperature is taken with a rectal thermocouple and recorded on a precision Leeds and Northrup potentiometer, accurate to ±0.1 deg F. Heart rate was indicated on an electrocardiotachometer.

Evaporative water loss was determined by the successive weighings on the seat scales. The accuracy of the scales in simulated water loss is ±5 gram. Another accounting for the evaporative loss was obtained from weighings before and after each run of the nude subject, of the subject fully clothed, and of the clothing separately. In order to partition the water lost through the ventilating garment, the dew point of the air out of the garment was periodically measured on a Chicago-type dew-point hygrometer.

Experimental Plan

The plan for these experiments is probably unique because they were done at two different times. Series 1 was planned and run in

Nomenclature

t_b = $^3/_4 t_r + {}^1/_4 t_s$, body temperature, deg F

t_g = garment surface temperature, deg F

$t_o = \dfrac{h_c t_a + h_r t_w}{h_r + h_c}$, operative temperature, deg F

t_{sr} = t_s at a vapor pressure of 0.8 in. Hg, deg F

t_r = rectal temperature, deg F

t_s = skin temperature, deg F

t_v = temperature of air entering ventilating garment (subscript *o*, leaving), deg F

t_w = wall temperature, deg F

V_v = ventilating air flow, ft³/min

W_g = water loss through ventilating garment, lb/ft²hr

W_R = respiratory water loss, lb/ft²hr

W_e = evaporative water loss, lb/ft² hr

W_{HHF} = evaporation loss from head, hands, and feet, lb/ft²hr

W_g = clothing moisture gain, lb/hr

W_n = nude weight loss, lb/hr

Δ = error term in heat balance, Btu/ft²hr

λ_e = heat of vaporization, Btu/lb

P = barometric pressure, in. Hg

θ = time, hr

ρ = weight density of air, lb/ft³

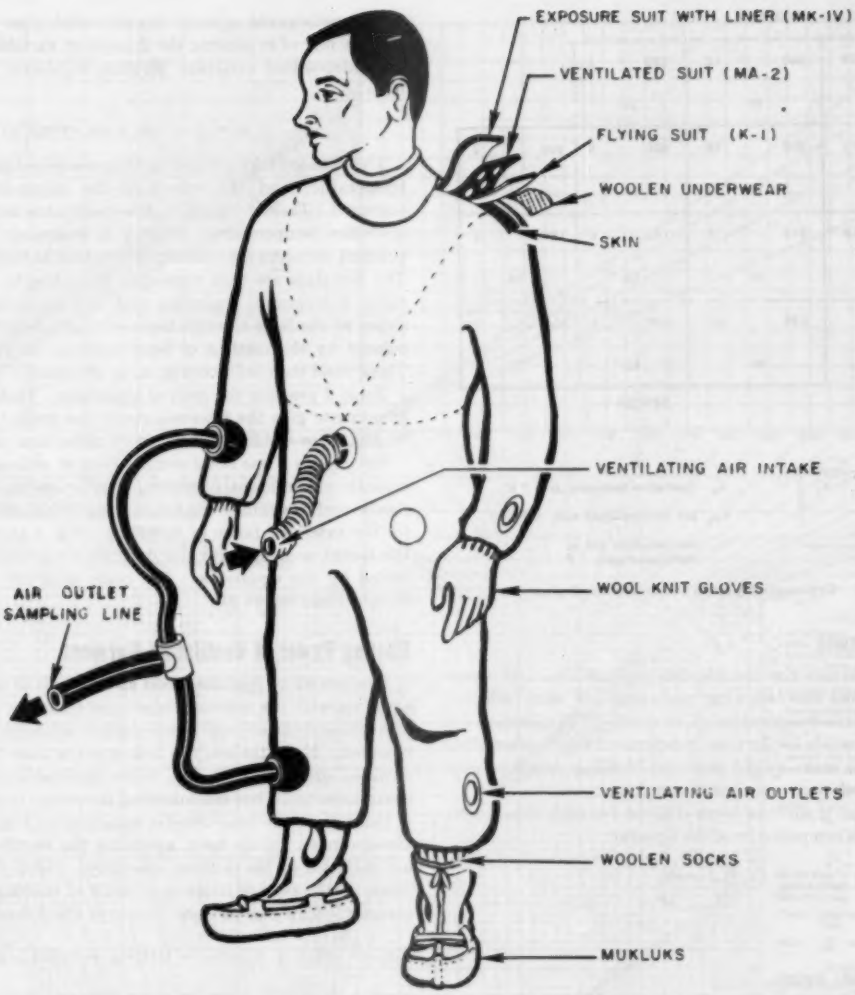

Fig. 1 Ventilated-suit assembly

1955. This experiment design was based upon the orthogonal square principle, which introduces economies of experiment time in a multivariant problem of this type. In series 1, two 3 × 3 orthogonal squares were planned, one for each subject. This made a total of 18 experiments, nine for each of the two subjects. The ranges of interest of the independent variables were operative temperature[4] 160 to 240 F, ventilating air 50 to 90 F, ventilating air rate 6 to 14 cfm. The extremes of these parameters and their mid-points were arranged as shown in the orthogonal square diagram, Fig. 2.

Series 2 was planned and run in 1958. Since the first series of experiments the questions most often asked concerned the effect of lower air flows and lower ambient temperatures. In this series it was planned to lower the ambient temperature range to 120 F; thus giving a temperature range from 120 to 240 F. The flow rate was lowered, giving a range from 2 to 14 cfm. The air temperatures to the ventilating garment remained the same, 50 to 90 F.

[4] Operative temperature is a weighted mean air and wall temperature; however, except where noted, $t_0 = t_a = t_w$.

Fig. 2 shows the plan for these experiments and illustrates how series 2 on the MA-2 ventilating garment augments the previous series on the MA-1 ventilating garment.

Transient Experiment

Fig. 3 is the time tolerance chart for thermal exposure that has previously been published [5] and is reproduced here for convenience. It should be kept in mind that all data on which this chart was based were taken in the so-called "steady state." Designers have criticized this chart as being too conservative. It is our belief that the data truly represent the tolerance for steady-state exposure and the criticism arises in our inability to apply this chart to the transient condition.

To gain some insight into this problem one additional experiment was planned and run at the 160 F chamber, 90 deg F air to ventilated suit at 2 cfm flow. This experiment was the same in every respect to the 160—90—2 experiment in the orthogonal square design except that the subject was placed in a cold chamber and zero time was marked when the heat was turned on.

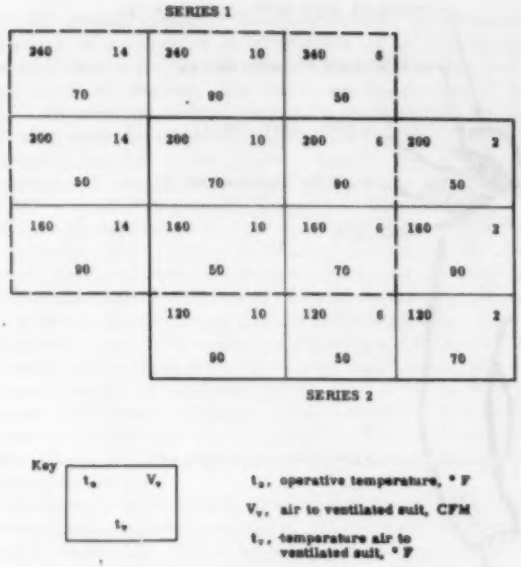

Fig. 2 Orthogonal square experimental design

Analysis of Results

In order to characterize the responses as a function of experimental conditions, the following measurements were selected: (*a*) Rectal and skin temperature at 45 min; (*b*) evaporative loss and body temperature as the time independent slopes after about 25 min; and (*c*) nude weight loss and clothing moisture gain, based on pre and post-experiment weighings.

Two additional quantities were derived for each experiment. Body storage was computed from the equation:

$$q_s = \frac{W_b C_b}{A_b} \frac{\Delta t_b}{\Delta \theta} \tag{1}$$

where

W_b = body weight, lb
C_b = body specific heat, Btu/lb, deg F
A_b = body surface area, sq ft
$\Delta t_b/\Delta\theta$ = time slope of body temperature, deg F/hr

A composite index of physiological effect known as the Craig index was computed for all experiments from the equation:

$$I = \frac{\mathrm{HR}_{\max}}{100} + \Delta t_r + \Delta W_n \tag{2}$$

where

$\mathrm{HR}_{\max}$ = maximum exposure heart rate, beats/min
Δt_r = rise in rectal temperature, deg C/hr
ΔW_n = nude weight loss, kg/hr

The orthogonal squares experimental plan provides a convenient way of expressing the dependent variables as functions of the independent variables, yielding regression equations of the form

$$y = c_1 + c_2 t_o + c_3 t_v + c_4 V_v \tag{3}$$

The data are first grouped in the preselected levels of operative temperature and the values of the dependent variable are averaged. These averages of three points are then plotted against operative temperature. With this treatment the other independent variables are considered constant at their average values. The raw data are then regrouped according to the levels of the other independent variables and the averages plotted. The slopes of the lines through these averages, which have been calculated by the method of least squares, are plotted in Fig. 4. These yield the coefficients c_2, c_3, c_4, of equation (3).

Table 2 presents the derived equations. Their standard errors of estimate give the intervals about the predicted values within which it is probable that two thirds of the data points will fall.

Since series 2 was not a complete set of orthogonal squares but actually an extension of series 1, the procedure was to compare results and to validate the application of the predictive equations for the extended range of variables. Fig. 4 shows the points of the recent analysis with the dash lines representing points predicted by the equations. The basic data are available in the Wright Field report [6].

Cooling Power of Ventilating Garment

The procedure just described and the use of the storage index equation with the tolerance chart are certainly the simplest and most valid if the objective is to predict tolerance in the U.C.L.A. chamber. Nevertheless, the feeling exists that the procedures as outlined graphically in Fig. 3 are applicable to other thermal environments. Thus the following procedure is proposed:

Using the basic heat-transfer equations or Fig. 3, calculate the storage index for the man, assuming the ventilating garment is not included in his clothing assembly. Next, calculate the decrease in the storage index as a result of wearing the ventilating garment. This can be done by use of the following equation:

$$\Delta q_s = -8.3 + 0.126 t_o - 0.037 t_v + 1.92 V_v, \text{ Btu/ft}^2\text{hr} \tag{11}$$

where t_o, t_v and V_v have the same units as before. This equation was derived from the slopes as previously described. Fig. 5 is a nomogram for this equation and can be used in conjunction with Fig. 3. The nomogram has the advantage over the equation in that the range of variables is emphasized and any extrapolations would have to be recognized as such.

The effective storage index is obtained from the following equation:

$$q_{s(\text{effective})} = q_{s(\text{chart})} - \Delta q_{s(\text{nomogram})} \tag{12}$$

Over-All Heat Balance

The system in question may be defined in two ways: (*a*) Only that portion of the body covered by the ventilating garment

Table 2 Predictive equations: Series I experiments

Variable	Equation	Std. error of estimate	Equation
Storage index, Btu/ft²hr	$q_s = -28.6 + 0.24t_o + 0.072t_v - 1.5V_v$	±4.28	(4)
Rectal temperature at 45 min, deg F	$t_r = 98.6 + 0.013t_o - 0.003t_v - 0.06V_v$	±0.30	(5)
Evaporative water loss, lb/ft², hr	$W_e = -0.035 + 4.3 \times 10^{-4}t_o + 1.03 \times 10^{-4}t_v + 9.02 \times 10^{-5}V_v$	±0.012	(6)
Nude weight loss, lb/hr	$\Delta W_n = -2.34 + 0.024t_o + 0.0095t_v - 0.093V_v$	±0.51	(7)
Clothing moisture gain, lb/hr	$\Delta W_g = -1.22 + 0.011t_o + 0.0035t_v - 0.060V_v$	±0.13	(8)
Maximum heart rate, beats/min	$\mathrm{HR}_{\max} = 75.2 + 0.29t_o - 0.05t_v - 0.67V_v$	±8.7	(9)
Craig index	$I = -2.03 + 0.029t_o + 0.008t_v - 0.14V_v$	±0.46	(10)

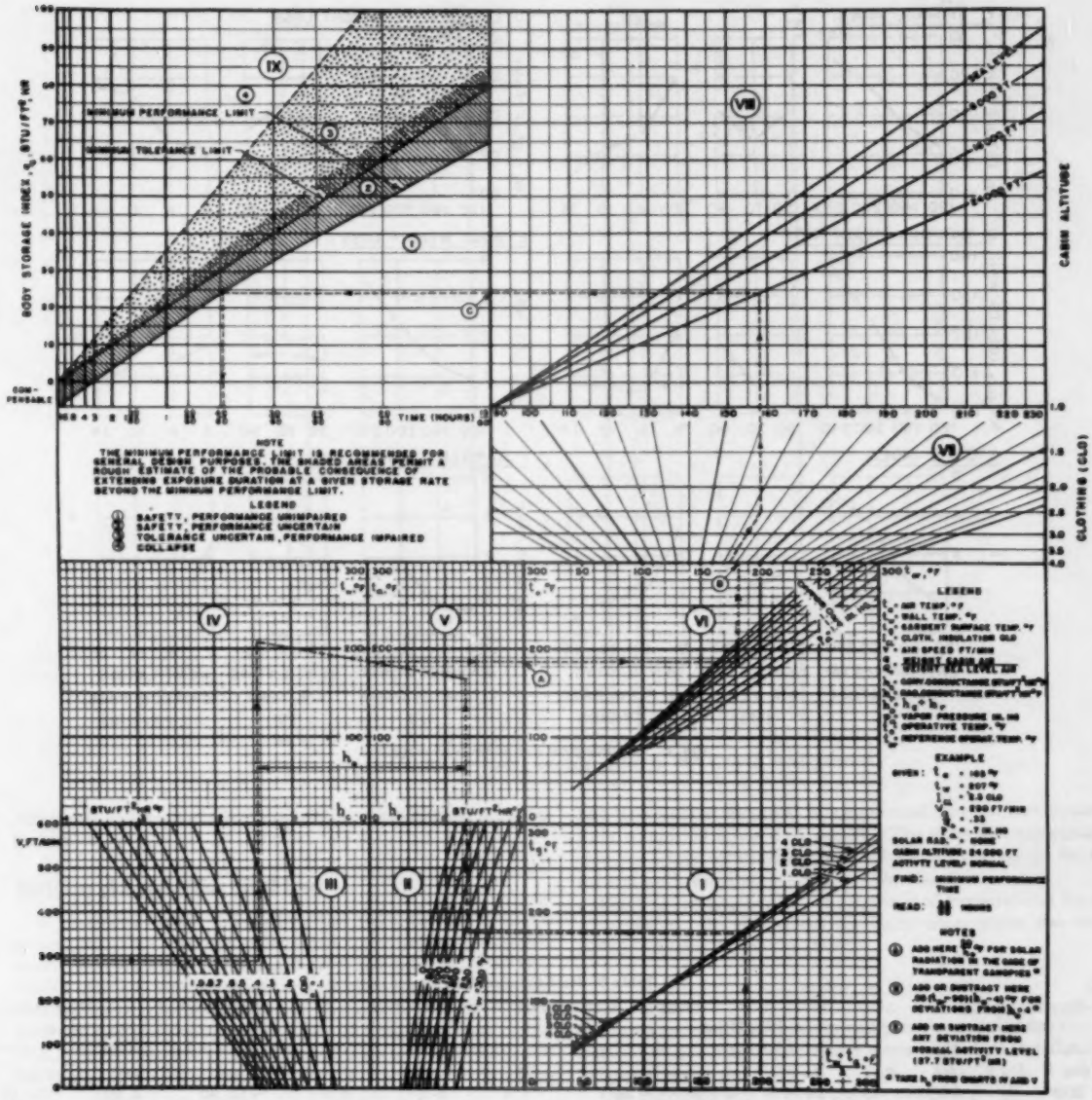

Fig. 3 Graphic computation of thermal tolerance

could be considered, or (*b*) the entire body of the subject. In order to make the data more readily comparable with previous work, it was decided to consider the entire body with its clothing assembly as our system.

The heat gains to the system are radiation, convection, and metabolism. The heat losses are due to evaporation and the convective change of the ventilating garment. The sum of those terms should equal the storage as expressed by the equation:

$$q_r + q_c + q_m - q_e - q_w = q_s \tag{13}$$

The various heat terms were obtained as follows: Radiation, convection, and metabolism were computed according to Blockley, et al. [7].

The evaporative loss W_e was multiplied by the latent heat of vaporization to give the heat lost by evaporation q_e:

$$q_e = W_e \lambda_e \tag{14}$$

The heat removed by the air through the ventilating suit q_w (neglecting evaporation since it is included in the foregoing) was computed from the following equation:

$$q_w = \frac{V \rho C_p}{A_b} (t_{wo} - t_{wi}) \tag{15}$$

Storage rate was determined from the slope of the body-temperature-time curve and equation (1). These computed quantities are given in Table 3. It is said that the first law of thermodynamics is merely a bookkeeping system on the forms of the energy so that our inability to make the over-all heat-balance check indicates that more research is necessary. Nevertheless, the magnitude of the error obtained by subtracting q_s from Σq is

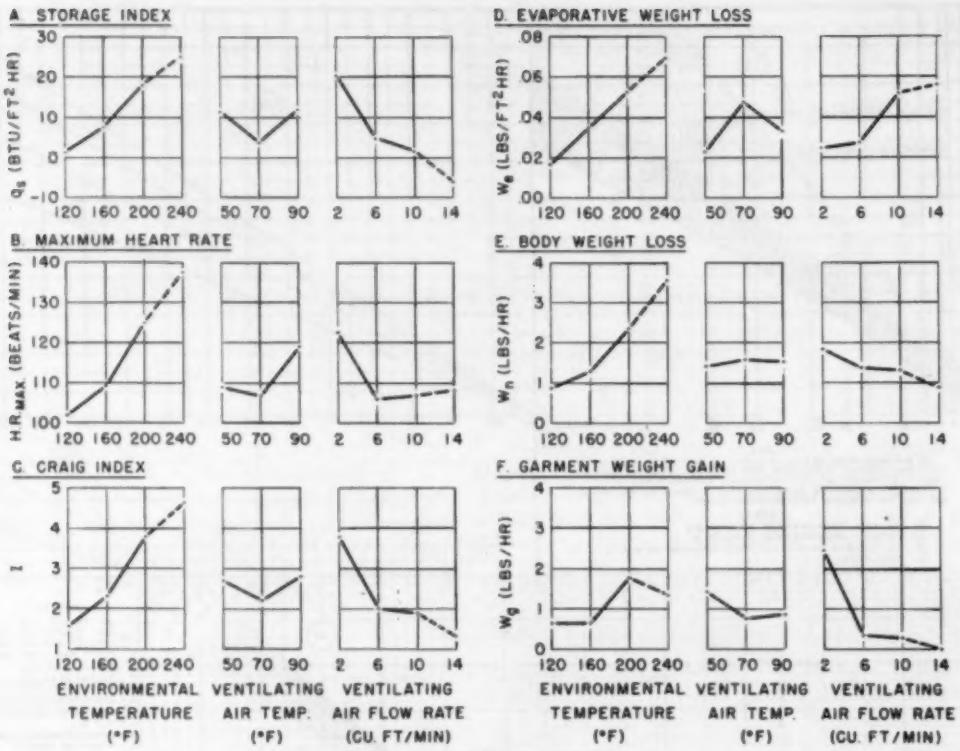

Fig. 4 Physiological and other responses

Table 3 Heat-balance data

Environmental conditions			Over-all heat balance (Btu/ft²hr)							Partition of evaporative loss $q_e = q_{ev} + q_R + q_{emax}$ (Btu/ft²hr)		
t_a, deg F	t_w, deg F	V_v, cfm	q_{r+c}	q_m	q_e	q_w	Σq	q_s	Δ	q_{ev}	q_R	q_{emax}
200	70	10	63	18.8	−49.3	−28.1	4.4	5.3	0.9	−13.40	−2.40	−33.48
200	90	6	63	20.1	−39.9	−17.3	25.9	12.7	13.2	−12.70	−2.53	−24.67
200	50	2	63	21.3	−26.1	−10.0	48.2	36.2	12.0	−5.82	−2.22	−18.06
160	50	10	38	18.5	−38.9	−34.0	−16.4	−1.5	−14.9	−7.00	−2.48	−29.42
160	70	6	38	19.1	−34.6	−16.8	5.7	2.5	3.2	−7.33	−2.48	−24.79
160	90	2	38	22.4	−34.3	−4.3	21.8	21.7	0.1	−3.67	−2.22	−28.41
120	90	10	12	18.7	−28.3	−9.8	−7.4	1.2	− 8.6	−1.75	−2.49	−24.06
120	50	6	12	18.7	−7.1	−15.8	7.8	−1.0	8.8	−3.29	−2.50	− 1.26
120	70	2	12	19.9	−15.2	−3.6	13.1	3.4	9.7	−2.04	−2.37	−10.80

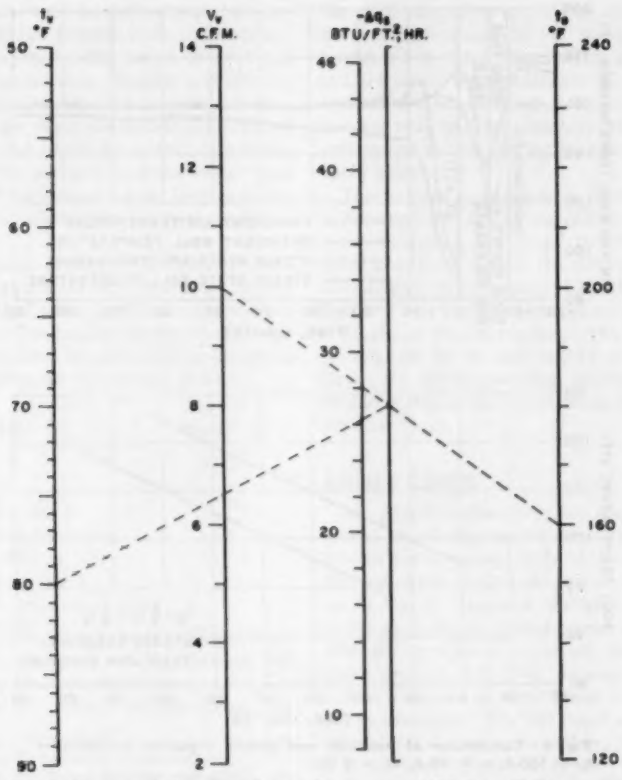

Fig. 5 Nomograph for computing cooling power of MA-2 ventilating garment

reasonable and lends confidence that the orders of magnitude are correct.

Partition of Evaporative Heat Loss

A persistent question regarding the ventilated clothing assembly is: "How much water is picked up by the air through the ventilated clothing?" Of course it is understood that, if the ventilated clothing kept the man in a comfort state, only the insensible loss would be removed by the ventilating air; and indeed for moderate temperature levels this was found to be the case. Nevertheless, the range of conditions under investigation did cause active sweating in many experiments and attempts were made to measure the amount.

We do not have reliable data for all experimental conditions listed in Table 3 but the values given represent our best judgment. The most significant point in this part of the study is to emphasize the importance of head, hands, and feet in the over-all tolerance problem.

Transient Experiment

In all experiments conducted in the UCLA Test Chamber, the attempt has been made to insure a constant thermal environment. The chamber is preheated above the test point so that, during the run, air and wall temperatures are essentially the same. It has come to our notice that this fact sometimes seems to have been overlooked with the resulting criticism that the published tolerance chart is too conservative.

This transient experiment was conducted in order to emphasize this condition on which the tolerance chart is based. The 160—90—2 condition was chosen because the thermal stress is high and the steady-state run at this same condition had been successfully completed a few days earlier. The same two experiments were as nearly identical as we could make them except for the air and wall-temperature history of the chamber.

Fig. 6 shows graphically the air and wall temperatures for the experiments. It also shows the body-temperature rise computed from the Burton equation:

$$t_s = {}^3/_4 t_r + {}^1/_4 t_a \qquad (16)$$

The experiments are directly comparable and explain why investigators get increased tolerance times when their test chamber is not preheated.

One suggested way of applying the steady exposure data of the tolerance chart to the transient case is to divide the exposure time into equal time increments, say 5 min. Next, compute the operative temperature for that period of time and, by use of the tolerance chart, arrive at the percentage of tolerance time equivalent to the subject's exposure. This procedure increases the predicted minimum tolerance time from 57 to 65 min. We note that this particular subject was in the chamber 65 and 75 min, respectively, which shows this individual has somewhat greater tolerance than the predicted minimum.

Conclusions

1 The predictive equation for the body-storage index for a man wearing the clothing assembly described has been checked for steady thermal exposure; that is, when the test chamber has been preheated:

$$q_s = -28.6 + 0.24t_a + 0.072t_r - 1.5V_v \pm 4.28 \qquad (4)$$

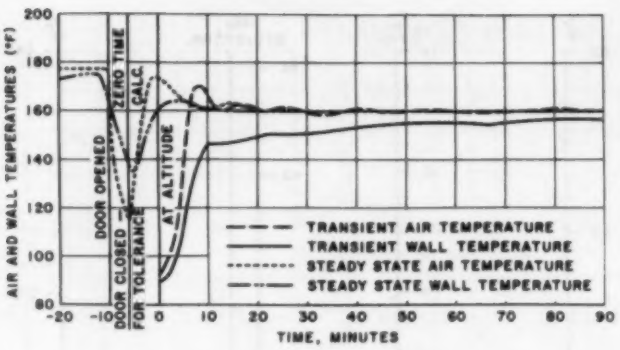

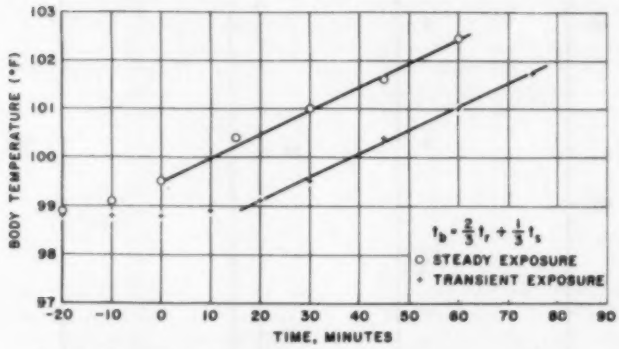

Fig. 6 Comparison of transient and steady exposure conditions— t_b = 160 F, t_c = 90 F, V_c = 2 cfm

range

$$t_b = 120 - 240 \text{ F}$$

$$t_c = 50 - 90 \text{ F}$$

$$V_c = 2 - 14 \text{ cfm}$$

This equation is used in conjunction with the time-tolerance chart.

2 A recommended procedure, for predicting the effect of environments other than the ones studied, is to use the existing tolerance chart in conjunction with the following predictive equation:

$$\Delta q_s = -8.3 + 0.126t_b - 0.037t_c + 1.92V_c \qquad (11)$$

This predictive equation is also presented in graphic form. From these charts, the effective storage index can be computed.

$$q_{s(\text{effective})} = q_{s(\text{tolerance chart})} - \Delta q_{s(\text{nomograph})} \qquad (12)$$

3 A conservative method for applying the steady exposure data to a transient condition is suggested. This method is based on the division of exposure time into 5-min intervals and a computation is made for the percentage of tolerance time used.

4 The importance of the head, hands, and feet in the over-all tolerance picture is emphasized. The partition of the water-loss quantities indicates that more data should be collected on this specific problem.

References

1 E. S. Fetcher, S. E. Rappaport, and J. F. Hall, Jr., "The Biophysical Requirements for Ventilated Clothing," U. S. Air Force Technical Report No. 5702, Aero Medical Laboratory, Wright-Patterson Air Force Base, Dayton, Ohio, 1948.

2 H. A. Mauch, J. F. Hall, and F. K. Klemm, "A Ventilating System for Clothing," WADC Technical Report 55-152, Aero Medical Laboratory, Wright-Patterson Air Force Base, Dayton, Ohio, 1955.

3 Ralph Morse, "Jet Age Man," *Life Magazine*, December 6, 1954, pp. 141–153.

4 Paul Webb, Abstract of "Ventilated Clothing as a Protection Against Heat Exposure," *Mechanical Engineering*, vol. 28, 1956, p. 558.

5 C. L. Taylor, "Description and Prediction of Human Response to Aircraft Thermal Environments," TRANS. ASME, vol. 79, 1957, pp. 1024–1028.

6 D. C. Skilling, J. W. Mc Cutchan, and C. L. Taylor, "A Quantitative Investigation of the MA-1 Ventilating Garment When Used With a Modified MK-IV Anti-Exposure Suit," WADC TR 56-209, Wright-Patterson Air Force Base, Dayton, Ohio, December, 1956.

7 W. V. Blockley, F. W. Mc Cutchan, and C. L. Taylor, "Prediction of Human Tolerance for Heat in Aircraft: A Design Guide," WADC Technical Report 53-346, Wright-Patterson Air Force Base, Dayton, Ohio. 1954.

DISCUSSION

H. A. Mauch[5]

The author states in the introduction to his paper that, "It is difficult to justify any extensive program of evaluation on any particular clothing assembly because these assemblies soon become obsolete. Nevertheless, the principle of the ventilating garment is so fundamental that it is the objective of this paper to provide a rational basis for the prediction of thermal tolerance when using an MA-2 ventilating garment with a modified MK-IV antiexposure suit."

It may be of interest to note that the principle of this ventilating garment[6] is indeed being used or under consideration for a

[5] Mauch Laboratories, Inc., Dayton, Ohio.

[6] U. S. Patents No. 2791168, 2897741, and foreign patents. Licensee: Aeroplastics, Inc., Bridgeport, Conn.

number of industrial applications such as environmental protective coveralls, ventilating inserts for hospital beds, car seats and seat covers, hair drying hoods, etc. This makes the author's paper a particularly timely contribution. Ideally, a predictive formula to be used for design purposes in such cases should, however, include additional variables which the author did not need in the specific case he investigated for the Air Force. In particular, the effective clo value of the assembly and the water vapor pressure of the ventilating air may vary.[7] Also, instead of the 8000-ft altitude in the author's experiments, sea level conditions will usually apply.

Since the empirical investigation of the influences of five variables would necessitate a large number of experiments, we derived a predictive formula by a method which combined the empirical and the analytical approach. This method is described in Appendix C of the WADC Report listed by the author as Reference [2]. The formula thus derived yields the Storage Index:

$$q_s = 0.45 \frac{t_o - 95}{i_{clo} + 0.7} - \frac{V_v}{100}(136 - t_v - p_v) \qquad \text{Btu/ft}^2\text{, hr}$$

in which:

t_o = operative temperature, deg F
i_{clo} = mean effective clothing insulation
V_v = ventilating air flow, ft³/min
t_v = temperature of vent air, deg F
p_v = water vapor pressure, vent air, mm Hg

The results obtained by applying this formula to the author's experiments, with $i_{clo} = 2.15$ and $p_v = 5$ mm Hg, correlate well with the results obtained using the author's equation (4).[8]

The formula also illustrates the experimental experience that the ventilating effect approaches zero, when the sum of t_v plus p_v (in mm Hg) equals 136, or, to mention the two possible extremes, when either saturated air at 95 F or completely dry air at 136 F is used for ventilation.

Another interesting rule of thumb suggested by the formula is the fact that one can (roughly) trade one degree F of the temperature of the ventilating air against one mm Hg of its water vapor pressure.

The formula is based on a metabolic rate of 20 Btu/ft², hr which applies to the sitting resting position of a subject. If, in a practical case, the actual metabolic rate deviates from this value in either direction, the difference must be added to or subtraced from the q_s predicted by the formula, before one enters Section IX of Fig. 3 of the author's paper.

Finally, a word of caution. The author's predictive equations (9) and (10) for the max heart rate and the Craig Index, respectively, are, strictly speaking, only valid for test durations as used by the author in his experiments and do not apply to arbitrary exposure times.

Author's Closure

Mr. Mauch's discussion has emphasized some of the specific limitations of these experiments and this is appreciated. Even though it is an extrapolation of these data it is suggested that the thermal effects of altitude and clothing can be taken care of by use of Fig. 3. However, variation in the water vapor pressure of the air to the ventilated garment is best accounted for by Mr. Mauch's equation as all of our data were taken at a constant vapor pressure of 0.20-in. mercury.

Another point of clarification concerns the time duration of the experiments. The 120 deg F and 160 deg F exposures were scheduled for two hr, the 200 deg F for one hr, and the 240 deg F for 45 min. Experiments were terminated before these times only when the subject's heart rate reached 140 beats per min or when the rectal temperature rose to 102 deg F.

[7] Variations of the water vapor pressure of the environmental air can be neglected, if this air is not to be used for ventilation.

[8] Experience shows that, for moderate altitude variations, the test results do not change significantly, if the *volume* flow of the ventilating air is maintained.

Journal of HEAT TRANSFER — Technical Briefs

This section consists of contributions of 750 words or less (about 2½ double-spaced typewritten pages, including figures). Technical Briefs will be reviewed and approved by the specific division's reviewing committee prior to publication. After approval such contributions will be published as soon as possible, normally in the next issue of the Journal.

Heat Transfer by Laminar Flow From a Rotating Cone

C. L. TIEN[1]

THE EXACT SOLUTION for the laminar flow of an incompressible viscous fluid over a rotating disk was first considered by von Karman [1][2] and later was integrated numerically by Cochran [2]. The heat transfer from such a rotating disk has been studied by Millsaps and Pohlhausen [3] and Sparrow and Gregg [4]. Recently, Wu [5] has pointed out that the solution for the flow field can be used for the incompressible laminar boundary layer induced on the surface of a rotating cone. Their results are restricted to cases of small rotation, small temperature differences, and constant fluid properties. The effects of compressibility and property variations, which would be important for cases of large rotation and large temperature differences, were examined by Ostrach and Thornton [6]. The present analysis is to indicate that the heat-transfer results for a rotating disk can be also used for a rotating cone under boundary-layer approximations. This implies that the cone angle should be sufficiently large so that the boundary-layer character exists.

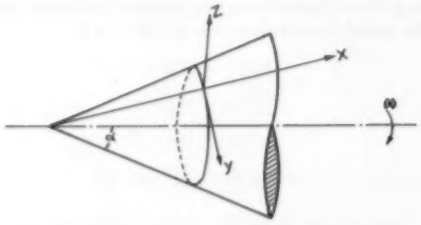

Fig. 1 Co-ordinate system of a rotating cone

Incompressible Case

Let (x, y, z) be a rectangular curvilinear fixed co-ordinate system as shown in Fig. 1. Let the x-axis be measured along a meridional section, the y-axis along a circular cross section, and z-axis perpendicular to both x and y. Let u, v, and w be the velocity components along x, y, and z, respectively. Since the angular speed of the cone is assumed to be constant, the physical problem is axially symmetric. The governing equations under boundary-layer approximations are as follows:

Continuity:
$$\frac{\partial u}{\partial x} + \frac{u}{x} + \frac{\partial w}{\partial z} = 0$$

Momentum:
$$u\frac{\partial u}{\partial x} + w\frac{\partial u}{\partial z} - \frac{v^2}{x} = \nu\left(\frac{\partial^2 u}{\partial z^2}\right)$$

$$u\frac{\partial v}{\partial x} + \frac{uv}{x} + w\frac{\partial v}{\partial z} = \nu\left(\frac{\partial^2 v}{\partial z^2}\right)$$

Energy:
$$u\frac{\partial t}{\partial x} + w\frac{\partial t}{\partial z} = \left(\frac{k}{\rho C_p}\right)\left(\frac{\partial^2 t}{\partial z^2}\right) + \left(\frac{\nu}{C_p}\right)\left[\left(\frac{\partial v}{\partial z}\right)^2 + \left(\frac{\partial u}{\partial z}\right)^2\right]$$

with boundary conditions:

$u(x, y, o) = 0$, $\quad u(x, y, \infty) = 0$,

$v(x, y, o) = \omega x \sin\alpha$, $\quad v(x, y, \infty) = 0$,

$w(x, y, o) = 0$,

$t(x, y, o) = t_w$ $\quad t(x, y, \infty) = t_\infty$

The partial differential system can be reduced to a set of ordinary nonlinear differential equations in dimensionless form by introducing the following transformations:

$$u = (\omega x \sin\alpha) F(\eta),$$
$$v = (\omega x \sin\alpha) G(\eta),$$
$$w = (\nu\omega \sin\alpha)^{1/2} H(\eta),$$
$$t = \left(\frac{\nu\omega}{C_p}\right)[X^2 S(\eta) + Q(\eta) + T_\infty]$$

where
$$\eta = z\left(\frac{\omega \sin\alpha}{\nu}\right)^{1/2}$$

and
$$X = \left(\frac{\omega}{\nu}\right)^{1/2} x \sin\alpha$$

The equations after the above transformations are

$$H' + 2F = 0 \tag{1}$$

$$F'' - HF' = F^2 - G^2 \tag{2}$$

$$G'' - HG' - 2FG = 0 \tag{3}$$

$$S'' - (\mathrm{Pr})\,HS' + (\mathrm{Pr})\,H'S = -(\mathrm{Pr})(F'^2 + G'^2) \tag{4}$$

$$Q'' - (\mathrm{Pr})\,HQ' = 0 \tag{5}$$

with the boundary conditions becoming

$F(0) = 0$ $\quad F(\infty) = 0$

$G(0) = 1$ $\quad G(\infty) = 0$

$H(0) = 0$

$S(0) = 0$ $\quad S(\infty) = 0$

$Q(0) = T_w - T_\infty$ $\quad Q(\infty) = 0$

The first three equations (1), (2), and (3) with the corresponding boundary conditions were integrated numerically by Cochran [2]. The last two equations (4) and (5) were integrated by Millsaps and Pohlhausen [3] for a range of Prandtl numbers from 0.5 to 10. If dissipation effect is neglected, Equation (4) disappears and Sparrow and Gregg [4] recalculated the results for

[1] Department of Mechanical Engineering, University of California, Berkeley, Calif.

[2] Numbers in brackets designate References at end of paper.

Contributed by the Heat Transfer Division of THE AMERICAN SOCIETY OF MECHANICAL ENGINEERS. Manuscript received at ASME Headquarters, October 9, 1959.

fluids of all Prandtl numbers. Similar heat-transfer results can be obtained from [4] for the present case of a rotating cone. For a given fluid, the variation of the heat-transfer coefficient with angular velocity is given by

$$h \sim \omega^{1/2}$$

For the limiting situations of very low and very high Prandtl numbers, the following asymptotic expressions for the heat transfer can be obtained as

$$h\left(\frac{\nu}{\omega \sin \alpha}\right)^{1/2}/k = 0.88447 \text{ Pr} \qquad \text{Pr} \to 0$$

and

$$h\left(\frac{\nu}{\omega \sin \alpha}\right)^{1/2}/k = 0.62048\,(\text{Pr})^{1/2} \qquad \text{Pr} \to \infty$$

For a nonisothermal rotating cone with a variation of surface temperature in the following manner

$$t_w - t_\infty = Ax^m,$$

the energy equation with boundary-layer approximations and negligible dissipation effect becomes after the transformation

$$Q'' - (\text{Pr})\, HQ' - mFQ = 0.$$

The numerical solution to the above equation and the heat-transfer results have been obtained and discussed by Hartnett [7] for a Prandtl number of 0.72 (for air) and values of m ranging from 0 to 10.

Compressible Case

It was shown [6] that the viscous dissipation is negligible for the compressible flows in which a relatively highly heated or cooled disk is rotating with a moderate velocity. With negligible dissipation effect the governing equations under boundary-layer approximations in the rectangular curvilinear co-ordinates for an axially symmetric compressible viscous flow are as follows:

Continuity: $$\frac{1}{x}\frac{\partial}{\partial x}(\rho x u) + \frac{\partial}{\partial z}(\rho w) = 0$$

Momentum: $$\rho\left(u\frac{\partial u}{\partial x} + w\frac{\partial u}{\partial z} - \frac{v^2}{x}\right) = \frac{\partial}{\partial z}\left[\mu\left(\frac{\partial u}{\partial z}\right)\right]$$

$$\rho\left(u\frac{\partial v}{\partial x} + w\frac{\partial v}{\partial z} + \frac{uv}{x}\right) = \frac{\partial}{\partial z}\left[\mu\left(\frac{\partial v}{\partial z}\right)\right]$$

Energy: $$\rho C_p\left(u\frac{\partial t}{\partial x} + w\frac{\partial t}{\partial z}\right) = \frac{\partial}{\partial z}\left(k\frac{\partial t}{\partial z}\right)$$

The boundary conditions for the present case are the same as those in the incompressible case.

Assuming linear variations of viscosity and conductivity with temperature [6], we have

$$\mu = C\mu_\infty/\bar{\rho}, \qquad k = CC_p\mu_\infty/\text{Pr}\,\bar{\rho}$$

where C is constant, $\bar{\rho} = \rho/\rho_\infty$ and subscript ∞ denotes quantities at undisturbed region. With the following transformations:

$$u = (\omega x \sin\alpha)\, F(\eta),$$
$$v = (\omega x \sin\alpha)\, G(\eta),$$
$$w = (C\nu_\infty\, \omega x \sin\alpha)^{1/2} H(\eta)/\bar{\rho},$$
$$t = Q(\eta)(t_w - t_\infty) + t_\infty,$$
$$\eta = C^{-1/2}\int_0^z \left(\frac{\nu_\infty}{\omega \sin\alpha}\right)^{1/2}\bar{\rho}\,dz,$$

the governing equations for the flow and temperature fields become the same as those in the incompressible case of negligible dissipation effect. Thus the solutions to the compressible case can be obtained from the solutions for the incompressible case. It is seen from the transformation that the effect of compressibility is to distort the co-ordinate and velocity component normal to the cone surface.

For the heat-transfer results, it can be shown that for Pr = 0.72 and $C = 1$ (implying small temperature differences),

$$h\left(\frac{\nu_\infty}{\omega \sin\alpha}\right)^{1/2}/k_\infty = 0.329$$

References

1 Th. von Karman, "Über Laminare und Turbulent Reibung," *Zeitschrift für Angewandte Mathematik und Mechanik*, vol. 1, 1921, p. 233.

2 W. G. Cochran, "The Flow Due to a Rotating Disc," Proceedings, Cambridge Philosophical Society, vol. 30, 1934, p. 365.

3 K. Millsaps and K. Pohlhausen, "Heat Transfer by Laminar Flow From a Rotating Plate," *Journal of Aeronautical Science*, vol. 19, 1952, p. 120.

4 E. M. Sparrow and J. L. Gregg, "Heat Transfer From a Rotating Disk to Fluids of Any Prandtl Number," JOURNAL OF HEAT TRANSFER, TRANS. ASME, series C, vol. 81, 1959, p. 249.

5 C. S. Wu, "The Three Dimensional Incompressible Laminar Boundary Layer on a Spinning Cone," Applied Scientific Research, sec. A, vol. 8, 1959, p. 140.

6 S. Ostrach and P. R. Thornton, "Compressible Laminar Flow and Heat Transfer About a Rotating Isothermal Disk," NACA TN 4320, August, 1958.

7 J. P. Hartnett, "Heat Transfer From a Nonisothermal Disk," *Journal of Applied Mechanics*, TRANS. ASME, series E, vol. 26, 1959, p. 672.

Apparent Emissivity and Heat Transfer in a Long Cylindrical Hole

E. M. SPARROW[1] AND L. U. ALBERS[2]

Introduction

THE RADIANT INTERCHANGE within a long cylindrical hole was first analyzed by Buckley [1][3] in 1927. A completely independent study was made by Eckert (refs. [2, 3]) in 1935. The formulation of the problem was carried out along similar lines by both investigators, and it was found that the radiation process was governed by an integral equation. Solutions, however, were obtained by completely different methods, both of which were approximate. Fair agreement between the results is found to exist for high and moderate values of the surface emissivity. For low emissivities, significant discrepancies occur.

Both calculation procedures are potentially of great utility in a variety of problems in radiant heat transfer, but neither has yet been verified. The present investigation is part of a study to discover and evaluate approximate techniques for solving radiation problems. The purpose of this note is to report on accurate numerical solutions for the long cylindrical hole, and with this information, to test the accuracy of the previous approximate solutions. Heat-transfer results are presented and discussed.

The physical system under consideration is shown schemati-

[1] Formerly, NASA Lewis Research Center. At present, Professor of Mechanical Engineering, University of Minnesota, Minneapolis, Minn. Assoc. Mem. ASME.

[2] NASA, Lewis Research Center, Cleveland, Ohio.

[3] Numbers in brackets designate References at end of paper.

Contributed by the Heat Transfer Division of THE AMERICAN SOCIETY OF MECHANICAL ENGINEERS. Manuscript received at ASME Headquarters, March 7, 1960.

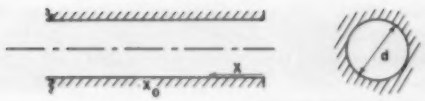

Fig. 1 Semi-infinite cylindrical cavity

cally in Fig. 1. The mouth of the cylindrical hole is taken as the origin of co-ordinates, $x = 0$. The hole extends to an indefinite length in the positive x-direction. The cylindrical wall has graybody emissivity ϵ, reflectivity $\rho = 1 - \epsilon$, and is isothermal along its entire length. Radiation from the outside environment is not included in the analysis; but, since the problem is linear, this can be computed independently and then added to the results discussed here. The hole is filled with a nonparticipating gas or else, a vacuum.

Analysis

Attention is directed to some typical location x_0 on the wall. The radiation flux leaving x_0 is composed of two parts: Emitted energy and reflected energy. The emission per unit time and area is given by the usual expression $\epsilon\sigma T^4$. To describe the reflection, we introduce the symbol $H(x_0)$ to denote the energy incident on x_0 per unit time and area. Thus the amount ρH is reflected. Then using $B(x_0)$ to represent the combined radiant flux leaving x_0, we have

$$B(x_0) = \epsilon\sigma T^4 + \rho H(x_0) \quad \text{or} \quad \frac{B(x_0)}{\sigma T^4} = \epsilon + \frac{\rho H(x_0)}{\sigma T^4} \tag{1}$$

The last form of this equation compares the energy leaving the surface to the emission of a black body. Introducing the apparent emissivity ϵ_a

$$\epsilon_a = B/\sigma T^4 \tag{2}$$

there is obtained

$$\epsilon_a(x_0) = \epsilon + \frac{\rho H(x_0)}{\sigma T^4} \tag{3}$$

Since the incident energy is always positive, it is clear that the apparent emissivity will always exceed the actual emissivity. A knowledge of the apparent emissivity is of first importance in interpreting pyrometry data. In order to use Equation (3) it is necessary to know the incident energy $H(x_0)$. It is easy to see that the energy incident at x_0 is related to the energy which leaves all other locations along the wall. The expression for $H(x_0)$ is derived in the references and need not be repeated here. Utilizing those findings, Equation (3) may be written as

$$\epsilon_a(X_0) = \epsilon + (1 - \epsilon)\int_0^\infty \epsilon_a(X) \left\{1 - |X - X_0| \frac{2(X - X_0)^2 + 3}{2[(X - X_0)^2 + 1]^{3/2}}\right\} dX \tag{4}$$

where

$$X = x/d,\ X_0 = x_0/d$$

This is an integral equation since the unknown variable ϵ_a appears under the integral sign as well as in other parts of the equation. The quantity in braces is called the kernel of the integral equation.

The approximation procedure used by Buckley in solving this equation is as follows: First, he approximated the kernel by fitting it with an expression composed of a sum of n exponential terms. Then using a theorem due to Whittaker (ref. [1], p. 758), he reasoned that the solution for ϵ_a should have the form of a sum of n exponentials, plus a constant term. The proposed solution contains certain unknown constants, which are found by substituting back into the integral Equation (4). Buckley applied this method for $\epsilon = 0.1$, 0.25, 0.5, and 0.75 using both one and two term expressions for the kernel, with increasingly closer agreement between the results as ϵ increased. For $\epsilon = 0.9$, calculations were carried out only for the one term exponential kernel. A very different approximation method was used by Eckert. He started by supposing that the variation of ϵ_a with X could be represented by a broken curve composed of n straight line segments. The constants in the linear equations were selected by satisfying the integral equation at n locations. Then he used this broken line expression as a first approximation in an iteration scheme, introducing it into the right side of Equation (4). When the integration is carried out, it is clear that a new (and presumably improved) expression for ϵ_a becomes available. Eckert terminated the iteration at this point, although in principle it might be continued. He applied this procedure for $\epsilon = 0.1$, 0.3, 0.5, 0.7, and 0.9 using for all cases a starting curve consisting of three straight lines.

In the present investigation, accurate solutions of the governing integral Equation (4) have been obtained by numerical means in conjunction with an electronic digital computer. The procedure was one of iteration, with the necessary numerical integrations being carried out by Simpson's rule.[4] Of course, in any numerical scheme, the range of integration cannot extend to infinity. So, in handling the integral in Equation (4), cognizance was taken of the fact that ϵ_a approaches unity for large values of x and in this range, the integration was carried out analytically.[5] Numerical solutions were obtained for ϵ values of 0.1, 0.25, 0.5, 0.75, and 0.9. The results thus obtained will be discussed below.

Results

The variation of the apparent emissivity with position, as

[4] At $X = X_0$, the integrand has a discontinuous derivative. To avoid integration errors, a trapezoidal formula was used on either side of the discontinuity whenever the discontinuity was at an even numbered point.

[5] When $\epsilon_a = 1$, the integral from some location X_1 to infinity is: $[(X_1 - X_0)^2 + 1]^{1/2} - 0.5\ [(X_1 - X_0)^2 + 1]^{-1/2} - (X_1 - X_0)$.

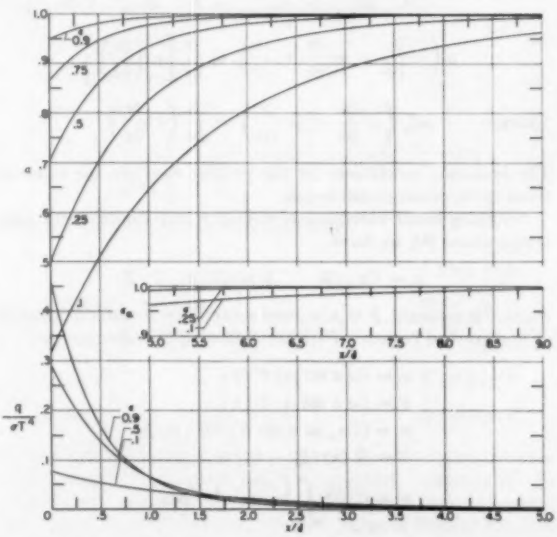

Fig. 2 Apparent emissivity and local heat transfer in a long cylindrical hole

found from the numerical solutions of Equation (4), is shown in the upper part of Fig. 2. For any given ϵ value, it is seen that the apparent emissivity approaches unity as x increases. In other words, for sufficiently large x, the energy leaving the surface is equal to the black body emission σT^4, regardless of the ϵ value.[6] The higher the emissivity ϵ of the surface, the shorter the length required to achieve the black body condition $\epsilon_a = 1$. For any given ϵ, the apparent emissivity is a minimum at the mouth of the hole, since it is here that the incident energy (and hence the reflected energy) is least. The numerical value of ϵ_a at the mouth of the tube is found to be $\sqrt{\epsilon}$, and this corroborates the analytical finding of Buckley.

Now, we turn to the comparison of the previous solutions with the more exact results of the present investigation. For each ϵ value, the maximum deviation of the prior results from the current ones is given in Table 1. The greatest deviations occur for $\epsilon = 0.1$, and a slightly more detailed presentation for this case is made in Table 2. In constructing the tables, it was necessary to read Eckert's results from a graph, while Buckley's solutions were available in analytical form.

Table 1 Maximum deviation of ϵ_a from present results

$\epsilon \rightarrow$	0.9	0.75	0.5	0.25	0.1
Buckley	−0.0013	0.0024	0.0064	0.014	0.026
Eckert	−0.015		−0.015		−0.18

Table 2 ϵ_a results for $\epsilon = 0.1$

$x/d \rightarrow$	0	1	2	3	4	5
Present	0.316	0.646	0.807	0.891	0.937	0.963
Buckley	0.316	0.659	0.831	0.917	0.958	0.980
Eckert	0.34	0.54	0.63	0.77	0.84	0.89

From the tables, it is readily seen that Buckley's results are of good accuracy over the entire range of ϵ values, with the best accuracy found at the higher ϵ. Eckert's results are also of acceptable accuracy for high and moderate ϵ values; but at low ϵ, marked deviations are evident. However, this does not mean that Eckert's procedure is fundamentally inferior to that of Buckley. Rather, it means that a somewhat finer approximation is needed when Eckert's procedure is applied to low ϵ values. For instance, instead of truncating the procedure after one iteration, a second one might be carried out. Alternately, instead of starting with a broken line curve of three segments, a four-segment curve might be used.

It is apparent from these comparisons that both calculation procedures hold great promise as powerful tools in solving radiation problems. It is also indicated that in applications, especially in the low ϵ range, results should be checked by repeating the procedure to a finer approximation.

Once the results for the apparent emissivity ϵ_a are known, the heat transfer is readily computed. The net local heat transfer q per unit area is the difference between emitted energy and the absorbed incident energy at any position x, i.e.,

$$q = \epsilon\sigma T^4 - \alpha H \tag{5}$$

Noting that $\epsilon = \alpha$ for a graybody and utilizing Equation (3), it follows that

$$\frac{q}{\sigma T^4} = \frac{\epsilon}{1-\epsilon}(1 - \epsilon_a) \tag{6}$$

So, q is obtained from ϵ_a by a simple arithmetic operation. Utilizing the ϵ_a results from the upper part of Fig. 2, heat-transfer results have been computed and are plotted on the lower part of the figure. To avoid obscuring the results, the curves for $\epsilon = 0.25$ and 0.75 have been omitted. From the figure, it is seen that near the mouth of the hole, there is a higher local heat transfer associated with the high emissivity surfaces. The opposite is true in the interior of the hole.

Finally, the total heat Q which is transferred out to the surroundings is obtained by integrating the local values. Results calculated in this way are listed in Table 3

Table 3 Over-all heat-transfer results

$\epsilon \rightarrow$	0.9	0.75	0.5	0.25	0.1
$\frac{Q}{\frac{\pi}{4}d^2\sigma T^4}$	0.959	0.914	0.831	0.677	0.495

The tabulation gives the ratio of the energy radiated from the hole relative to the black body emission from a disk just equal to the hole cross section. So, this represents an *average* apparent emissivity for the hole as seen by an observer outside the hole.

References

1 H. Buckley, "On the Radiation From the Inside of a Circular Cylinder," *Philosophical Magazine*, vol. 4, no. 23, 1927, pp. 753–762.

2 E. R. G. Eckert, "Das Strahlungsverhaltnis von Flächen mit Einbuchtungen und von zylindrischen Bohrungen," *Archiv fur Wärmewirtschaft und Dampfkesselwesen*, vol. 16, 1935, pp. 135–138.

3 E. R. G. Eckert and R. Drake, "Heat and Mass Transfer," McGraw-Hill Book Company, Inc., New York, N. Y., 1959.

[6] This is identical to what occurs in an isothermal enclosure under thermal equilibrium conditions.

On the Variable-Density Single-Fluid Model for Two-Phase Flow[1]

NOVAK ZUBER[2]

Introduction

TWO-PHASE FLOW bears a similarity to nonisothermal single phase shear flow in that the velocity field is characterized not only by the Reynolds modulus, but it depends also upon the density gradients in the fluid as well as upon the direction of flow, i.e., whether the flow is co-gravity or counter-gravity. In a recent paper Bankoff [1][3] proposed a model for turbulent, co-current flow of liquid and gas or vapor through a pipe or channel, which assumes the fluid to be of a single phase whose density is a function of radial position. Because visual observations of the bubble flow regime indicate that, in the counter-gravity flow, the vapor phase tends to be concentrated near the center of the vertical pipe Bankoff observed that his model should describe this flow regime. The purpose of this note is to see to what extent this may be true.

Assuming that the radial void fraction and the velocity are given by power-law distributions, Bankoff derived the following equation for the ratio of the mean velocities of vapor and liquid[4] u''/u', in terms of the mean local void fraction α,

$$\frac{u''}{u'} = \frac{1-\alpha}{K-\alpha} \tag{1}$$

[1] This work was performed as a part of an investigation of boiling water reactor stability, sponsored by the Reactor Safety Branch, U. S. AEC under contract No. AT (04-3)-165.

[2] Research Laboratory Ramo-Wooldridge Corp., Los Angeles, Calif.

[3] Numbers in brackets designate References at end of paper.

[4] This ratio is often referred to as the "slip velocity ratio."

Contributed by the Heat Transfer Division of THE AMERICAN SOCIETY OF MECHANICAL ENGINEERS. Manuscript received at ASME Headquarters, December 11, 1959.

The flow parameter K is determined by the exponents of the velocity and of the void distribution; it is therefore a function of at least pressure, quality, and mass flow rate. Because of insufficient experimental information the value of K was not directly predicted by Bankoff. However, he was able to show, analytically, that for circular pipes the effective range of variation of K is from about 0.5 to 1.0. For an assumed value of $K = 0.89$ good agreement was reported with Martinelli-Nelson correlation for steam-water void fractions and frictional pressure drops over a range of pressure from 100 to 2500 psia and void fractions from 0 to 0.80–0.85.

It will be shown in this note that Equation (1) is in agreement with experimental data reported by Russian researchers [2, 3, 4, 5, 6]. It will be seen also that the range of variation of the flow parameter K ($0.5 \leq K \leq 1$) predicted by Bankoff is in excellent agreement with the values determined from these experiments. Because Russian experiments were performed over a wide pressure range (3 atm to 200 atm), it is possible to determine the values of the flow parameter K as a function of pressure and, at a *given pressure*, to determine the range of void fraction α, for which the flow can be described adequately by the variable density model.

The Bubble Flow Regime

In shear flow the largest velocity gradients occur in the vicinity of the solid surface. A bubble located in this region is acted upon by the lift due to the Bernoulli effect and by the lift due to the Magnus effect,[5] both acting in the direction perpendicular to the surface of the duct. In counter-gravity flow these two forces act in the same direction, whereas in co-gravity flow they oppose each other. Consequently, in counter-gravity flow the bubble will migrate toward the center of the duct, whereas in co-gravity flow it will seek a location off center. Similar considerations apply to a bubble population; in this case, as analyzed by Bankoff, because of random contacts between bubbles there is also a driving force which tends to produce bubble diffusion toward regions of lower bubble concentration. In steady-state these forces balance each other at every point and determine the vapor distribution across the pipe. The nonuniform vapor distribution across a pipe is clearly indicated by the experimental results reported by Petrick [7] and by Wallis and Griffith [8].

Through the buoyancy bubbles affect the flow conditions and thereby affect the velocity distribution in the liquid. The effects of the vapor distribution and of the velocity distribution are interdependent, consequently, the velocity profile in counter-gravity two-phase flow is more pronounced than in single phase flow. Because the vapor phase is concentrated in the high velocity region it will be transported at a faster rate than it would otherwise be were the distribution uniform across the duct. Thus the *mean* velocity of the vapor u^v will be larger than the *mean* velocity of the liquid u', although at any point the liquid and the vapor move at the same rate.[6]

An analysis of experimental data which considers one-dimensional effects only is based, necessarily, on the mean values. It is seen how this approach leads to the conclusion of the existence of a slip velocity ($u^v - u' > 0$), and how it introduces the concept of a slip velocity ratio larger than one, i.e., of $u^v/u' > 1$.

Comparison of the Variable Density Model With Experimental Results

Because of the nonuniform radial distribution of the vapor phase the mean vapor volume fraction α, which is determined by static measurements (for example, by x-ray) is not equal to the vapor volumetric flow concentration which is defined by

$$\beta = \frac{V^v}{V^v + V'} = \frac{u_0{}^v}{u_0{}^v + u_0{}'} \tag{2}$$

The value of β can be determined by metering the two phases separately before mixing. The deviation of the ratio α/β from unity is a measure of the nonuniform vapor concentration. To form this ratio we use the definitions of the linear and superficial velocities

$$u^v = \frac{u_0{}^v}{\alpha} = \frac{V^v}{A^v} \tag{3}$$

$$u' = \frac{u_0{}'}{1 - \alpha} = \frac{V'}{A'} \tag{4}$$

Substituting Equations (3) and (4) into Equation (2) it follows that

$$\frac{\alpha}{\beta} = \frac{(1 - \alpha)u' + u^v\alpha}{u^v} \tag{5}$$

Because the values of u' and u^v are not measured it is advantageous to define a coefficient C given by

$$C = \frac{(1 - \alpha)u' + \alpha u^v}{u^v} \tag{6}$$

Equation (5) then becomes

$$\frac{\alpha}{\beta} = C \tag{7}$$

It follows from Equations (7) and (6) that when the slip velocity ratio u^v/u' equals unity then $C = 1$ and $\alpha = \beta$. Thus the deviation of C from unity, i.e., the inequality between the vapor volume fraction α and the vapor volumetric flow concentration β, is an indication of the concentration of the vapor phase in the high velocity region and therefore of the two-dimensional character of the flow. Because both α and β can be determined separately, Equation (7) was used by Russian researchers to investigate the character of two-phase flow.

Russian experiments were performed with air-water and steam-water mixtures in forced flow through circular ducts. The vapor and the liquid were mixed before entering the test section. For air-water mixtures flowing through vertical and horizontal pipes the void fraction α was determined by weighing. It was reported that, up to a value of $\beta = 0.9$, the relation between α and β was given by

$$\frac{\alpha}{\beta} = 0.833 \tag{8}$$

For steam-water mixtures, α was determined from pressure drop measurements and correlations for two-phase flow. Data from references [2, 3, 4, 5] are shown in Fig. 1, which is reproduced from these reports.

Kholodovski [6] used Equation (6) to correlate all Russian data for steam-water mixtures; the correlation is claimed to be valid for two-phase flow of air and water as well as for liquid metals. The coefficient C depends upon liquid properties, pressure, and mass flow rate. The effect of flow velocity appears as a multiplying factor in Equation (7), thus

$$C(u_0{}' + u_0{}^v)^{0.019} = \frac{u_0{}' + u_0{}^v}{u^v} = \frac{\alpha}{\beta} \tag{9}$$

[5] A circulation is induced by the nonuniform shear acting on the bubble.

[6] This statement is correct provided that the bubble velocity relative to the liquid at rest is neglected. For water at 1 atmosphere this relative velocity is of the order of 25 cm/sec.

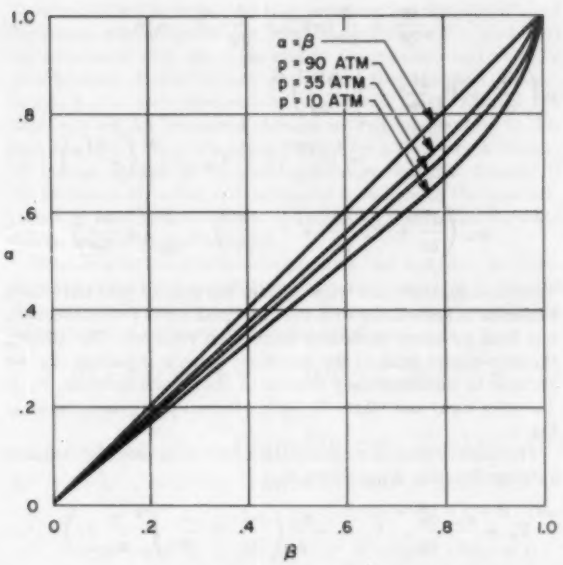

Fig. 1 The experimentally determined relation between α and β as functions of pressure for water in forced-circulation. (This figure is reproduced from the papers by Armand, Refs. [2], [3], [4], [5].)

The values of C for a vapor-water mixture as function of pressure are given in Table 1, which is reproduced from Reference [6].

Table 1

Pressure, kg/cm²	C	Pressure, kg/cm²	C
3	0.793	65	0.799
5	0.790	81	0.808
7	0.786	110	0.827
9	0.784	115	0.830
10	0.783	140	0.850
20	0.783	145	0.856
30	0.785	180	0.904
40	0.788	185	0.911
60	0.796	200	0.938
		210	0.975

The units for the velocity are meters/second. It can be seen from Equation (9) that the effect of flow velocity is small; consequently, as a first approximation, the coefficient C can be taken as a parameter which depends upon pressure only. It can be seen from Fig. 1 that, at a given pressure over a large range, α can be linearly related to β; thus, in this range, the coefficient C is constant. The limits of this range are discussed and correlated in Reference [6].

In order to compare the variable density model with experimental results we shall relate Equations (1) and (6). Solving for the slip velocity ratio it follows from Equation (6) that

$$\frac{u''}{u'} = \frac{1-\alpha}{C-\alpha} \tag{10}$$

If we identify the coefficient C with the flow parameter K, Equation (10) becomes identical with Equation (1) derived analytically by Bankoff. Moreover, the range of variation of K ($0.5 \leq K \leq 1.0$) predicted by Bankoff is in good agreement with Equation (8) and with the values shown in Fig. 1 and in Table 1. It is also in good agreement with the values reported by Kholodovski [6] for a vapor-mercury system in the pressure range from 2.5 kg/cm² to 15 kg/cm².

Discussion

In order to evaluate the performance of a boiling system it is necessary to predict the vapor volume fraction α. In an analysis of experimental data there is a choice of several variables which can be used to express the dependence of α, upon the characteristics of the system and experimental conditions. One of these variables which has been found useful is the slip velocity ratio

$$\frac{u''}{u'} = \frac{x}{1-x}\,\frac{1-\alpha}{\alpha}\,\frac{\rho'}{\rho''} \tag{11}$$

The results of Russian investigations indicate that, at a given pressure over a considerable range of β, the value of the coefficient C, i.e., the value of K, remains constant. In this range, Equation (1) shows that the slip velocity ratio is a function of one variable only, i.e., of α, instead of two, i.e., of the quality and of the vapor volume fraction as indicated by Equation (11). This fact introduces considerable simplifications in an analysis of a two-phase flow system. We note also that the slip velocity ratio is increasing monotonically with α.

It is important to observe that Russian experiments were performed with circular pipes (diameters ranging from 2.5 cm to 7.6 cm) and water circulation velocities ranging from 0.1 m/sec to 1.6 m/sec. In view of the simplification which Equation (1) introduces into the analysis of a two-phase flow system an investigation with rectangular channels appears desirable.

Nomenclature

A = cross-sectional area of the duct, ft²
A' = cross-sectional area occupied by the liquid, ft²
A'' = cross-sectional area occupied by the vapor, ft²
u' = mean velocity of the liquid, ft/hr
u'' = mean velocity of the vapor, ft/hr
u_0' = V'/A = superficial velocity of the liquid, ft/hr
u_0'' = V''/A = superficial velocity of the vapor, ft/hr
V' = volumetric flow rate of the liquid, ft³/hr
V'' = volumetric flow rate of the vapor, ft³/hr
$x = \dfrac{\rho''V''}{\rho'V' + \rho''V''}$ = quality
$\alpha = \dfrac{A''}{A' + A''}$ = vapor volume fraction
$\beta = \dfrac{V''}{V' + V''}$ = volumetric flow concentration
K = flow parameter
C = flow coefficient
ρ' = density of the liquid, lb/ft³
ρ'' = density of the vapor, lb/ft³

References

1 S. G. Bankoff, "A Variable Density Single-Fluid Model for Two-Phase Flow With Particular Reference to Steam-Water Flow," ASME-AIChE Heat Transfer Conference, Storrs, Conn., 1959, Paper No. 59—HT-7.

2 A. A. Armand, "The Resistance in Two-Phase Flow Through Horizontal Pipes," *Izvest. Vsesou. Teplotek. Inst.*, no. 1, 1946, pp. 16–23, AERE Lib/Trans. 828.

3 A. A. Armand and G. G. Treschev, "Investigation of the Resistance During the Movement of Vapor-Water Mixtures in Heated Pipes at High Pressure," *Izvest. Vsesou. Teplotek. Inst.*, no. 4, 1947, pp. 1–5, AERE Lib/Trans. 816.

4 A. A. Armand and E. I. Nevstrueva, "Investigation of the Mechanism of Two-Phase Flow in Vertical Pipes," *Izvest. Vsesou. Teplotek. Inst.*, no. 2, 1950.

5 A. A. Armand, "Investigation of the Mechanism of Two-Phase Flow in Vertical Pipes," article in the book entitled, "Hydrodynamics and Heat Transfer With Boiling," edited by M. A. Styrikovich, Acad. Nauk. SSSR., Moscow, 1954.

6 G. E. Kholodovski, "New Method for Correlating Experimental Data for the Flow of a Steam-Water Mixtures in Vertical Pipes," *Teploenergetika*, vol. 4, no. 7, 1957, pp. 68–72.

7 M. Petrick, "Two-Phase Air-Water Flow Phenomena," Argonne Nat. Lab. Rept., ANL5787, March, 1958.

8 Wallis and P. Griffith, "Liquid and Gas Distributions in Two-Phase Boiling Analogy," M.I.T. Tech. Rept. No. 13, December, 1958.

Nearly Quasi-Steady Free Convection Heat Transfer in Gases

E. M. SPARROW[1] **and J. L. GREGG**[2]

Introduction

In free convection problems where the surface temperature varies with *time*, heat-transfer computations are often carried out under the assumption that quasi-steady conditions prevail. That is, it is supposed that at each and every instant there exists an instantaneous steady state and, as a consequence, the steady heat-transfer relationships may be applied instantaneously. The tremendous practical simplification embodied in the quasi-steady assumption is that it avoids the exceedingly difficult problem of solving for the details of the unsteady velocity and temperature fields.

However, there is always a difference between the actual instantaneous heat transfer and the quasi-steady value. The extent of the deviation depends both on the rapidity of the changes in surface temperature and on the response characteristics of the fluid. The aim of this analysis is to determine the first-order deviations from the quasi-steady condition and to find a criterion to distinguish when the heat transfer is essentially quasi-steady. The system chosen for study is a vertical plate suspended in a gas (Prandtl number = 0.72) as pictured in Fig. 1. The surface temperature T_w is spatially uniform, but is permitted to take on arbitrary, but continuously differentiable, variations with time.

The rather sparce previous analytical work on unsteady free convection has been primarily focused on the special problem of a sudden step change in surface temperature or heat flux, for example, reference [1].[3] A very recent paper [6] which appeared after the completion of the present study discusses the particular temperature variations which give rise to similar boundary layer solutions.

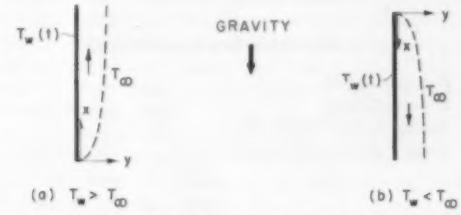

Fig. 1 Physical model and co-ordinates

Analysis

The unsteady free convection problem is governed by the basic conservation principles—mass, momentum, and energy. The boundary layer form of these laws for buoyancy-induced flow of a perfect gas ($p = \rho RT$) over a vertical plate is

$$\frac{\partial \rho}{\partial t} + \frac{\partial}{\partial x}(\rho V_x) + \frac{\partial}{\partial y}(\rho V_y) = 0 \tag{1}$$

$$\rho\left(\frac{\partial V_x}{\partial t} + V_x\frac{\partial V_x}{\partial x} + V_y\frac{\partial V_x}{\partial y}\right) = \pm\frac{g\rho}{T_\infty}(T - T_\infty) + \frac{\partial}{\partial y}\left(\mu\frac{\partial V_x}{\partial y}\right) \tag{2}$$[4]

$$\rho c_p\left(\frac{\partial T}{\partial t} + V_x\frac{\partial T}{\partial x} + V_y\frac{\partial T}{\partial y}\right) = \frac{\partial}{\partial y}\left(k\frac{\partial T}{\partial y}\right) \tag{3}$$

Viscous dissipation and work against the gravity field have been neglected in accordance with the usual practice in free convection, but fluid property variations have been retained. By affixing the plus-minus signs to the buoyancy force in equation (2), we are able to simultaneously treat both the situations where $T_w > T_\infty$ (plus sign) and where $T_w < T_\infty$ (minus sign), as pictured in Fig. 1.

The conservation of mass equation may be satisfied by defining a stream function ψ as follows [3]

$$V_x = \frac{\rho_\infty}{\rho}\frac{\partial \psi}{\partial y}, \quad V_y = -\frac{\rho_\infty}{\rho}\left(\frac{\partial \psi}{\partial x} + \frac{\partial}{\partial t}\int_0^y \frac{\rho}{\rho_\infty}\,dy\right) \tag{1a}$$

Then by replacing V_x and V_y in favor of ψ and introducing the following new variables

$$\theta = (T - T_\infty)/(T_w - T_\infty), \quad Y = \int_0^y (\rho/\rho_\infty)dy \tag{4a}$$

equations (2) and (3) become

$$\frac{\partial^2\psi}{\partial Y\partial t} + \frac{\partial \psi}{\partial Y}\frac{\partial^2\psi}{\partial Y\partial x} - \frac{\partial \psi}{\partial x}\frac{\partial^2\psi}{\partial Y^2} = \frac{g}{T_\infty}(\Delta T)\theta + \nu_\infty\frac{\partial^3\psi}{\partial Y^3} \tag{2a}$$

$$\frac{\partial \theta}{\partial t} + \theta\frac{\dot{\Delta T}}{\Delta T} + \frac{\partial \psi}{\partial Y}\frac{\partial \theta}{\partial x} - \frac{\partial \psi}{\partial x}\frac{\partial \theta}{\partial Y} = \frac{\nu_\infty}{\mathrm{Pr}}\frac{\partial^2\theta}{\partial Y^2} \tag{3a}$$

where

$$\Delta T \equiv |T_w - T_\infty|, \quad \dot{\Delta T} = d(\Delta T)/dt, \quad \ddot{\Delta T} = d^2(\Delta T)/dt^2 \tag{4b}$$

In the derivation of equations (2a) and (3a), the gas properties have been represented by: $\rho\mu$ = const; ρk = const; c_p = const.

As has already been noted, our goal is to investigate the deviations of the actual instantaneous heat transfer from the quasi-steady value. With this in mind, it is natural to seek solutions for the temperature and velocity distributions in the form of a series expansion about the quasi-steady state. So, the stream function ψ and the dimensionless temperature θ are written in the form

$$\psi = [64g(\Delta T)\nu_\infty{}^2x^3/T_\infty]^{1/4}\{F(\eta) + \lambda_0 f_0(\eta) + \lambda_1 f_1(\eta) + \ldots\} \tag{5a}$$

$$\theta = \Theta(\eta) + \lambda_0\theta_0(\eta) + \lambda_1\theta_1(\eta) + \ldots \tag{5b}$$

where

$$\eta = (Y/x^{1/4})[g(\Delta T)/4\nu_\infty{}^2T_\infty]^{1/4} \tag{6a}$$

while the expansion parameters $\lambda_0, \lambda_1, \ldots$ are defined by

$$\lambda_0 = \frac{\dot{\Delta T}}{\Delta T}\left[\frac{xT_\infty}{g(\Delta T)}\right]^{1/4}, \quad \lambda_1 = \frac{\ddot{\Delta T}}{\Delta T}\left[\frac{xT_\infty}{g(\Delta T)}\right], \ldots \tag{6b}$$

[1] At present, Professor of Mechanical Engineering at the University of Minnesota. Formerly, NASA, Lewis Research Center, Cleveland, Ohio. Assoc. Mem. ASME.

[2] NASA, Lewis Research Center, Cleveland, Ohio. Assoc. Mem. ASME.

[3] Numbers in brackets designate References at end of paper.

Contributed by the Heat Transfer Division of The American Society of Mechanical Engineers. Manuscript received at ASME Headquarters, April 21, 1960.

[4] It has been shown in reference [2] that, for a perfect gas, the buoyancy force $g(\rho_\infty - \rho)$ reduces identically to $\frac{g\rho}{T_\infty}(T - T_\infty)$.

The variable η may be immediately recognized as the Schmidt and Beckmann similarity variable, while the functions $F(\eta)$ and $\Theta(\eta)$ are associated with the quasi-steady temperature and velocity distributions. It can be easily shown that the expansion parameters $\lambda_0, \lambda_1, \ldots$ each represent the ratio of two times; namely, the time required for impressed changes in wall temperature to diffuse across the boundary layer divided by a time which characterizes the rapidity of the wall temperature changes. Clearly, if the boundary layer responds promptly to impressed changes (i.e., relatively small diffusion times and small λ values), then the state will be essentially quasi-steady.

Returning to the differential equations (2*a*) and (3*a*), we introduce the series for ψ and θ, grouping terms according to whether they are multiplied by $\lambda_0, \lambda_1 \ldots$. From this, there results the following set of ordinary differential equations:

$$\Theta'' + 3(\mathrm{Pr})F\Theta' = 0 \qquad \Theta(0) = 1, \quad \Theta(\infty) = 0 \quad (7a)$$

$$F''' + 3FF'' - 2(F')^2 + \Theta = 0$$
$$F(0) = F'(0) = 0, \quad F'(\infty) = 0 \quad (7b)$$

$$\theta_0'' + \mathrm{Pr}(3F\theta_0' - 2F'\theta_0) - \mathrm{Pr}(2\Theta + 0.5\eta\Theta' - 5f_0\Theta') = 0$$
$$\theta_0(0) = \theta_0(\infty) = 0 \quad (8a)$$

$$f_0''' + 3Ff_0'' - 6F'f_0' + 5F''f_0 - (F' + 0.5\eta F'' - \theta_0) = 0$$
$$f_0(0) = f_0'(0) = f_0'(\infty) = 0 \quad (8b)$$

where we now truncate the series after the λ_0 terms. Inspection of the differential equations shows that the functions $\Theta, \theta_0, \ldots$ and $F, f_0, \ldots$ must be computed in sequence, i.e., θ_0 cannot be computed without a prior knowledge of Θ. This circumstance requires that we restrict ourselves to time-dependent wall temperatures for which the λ_n form a rapidly decreasing sequence with increasing n and further, that λ_0 be small relative to unity. The boundary conditions on equations (7) and (8) were determined from the physical conditions that $V_x = V_y = 0$ and $T = T_w$ at $y = 0$ and that $V_x \to 0$ and $T \to T_\infty$ as $y \to \infty$.

Equations (7*a*) and (7*b*) may be recognized as coinciding with the governing equations for the steady-state free-convection problem. A solution for Pr = 0.72 (gases) has been obtained by Ostrach [4], but it was necessary to re-solve to greater accuracy for present purposes. Then, using this solution as input data, equations (8*a*) and (8*b*) were also solved for Pr = 0.72. The important numerical results to be used in the heat-transfer computations are:

$$\Theta'(0) = -0.5046, \qquad \theta_0'(0) = -0.7721 \quad (9)$$

A graph of the functions Θ, θ_0, and F', f_0', respectively associated with the temperature and velocity profiles, is given in Fig. 2.

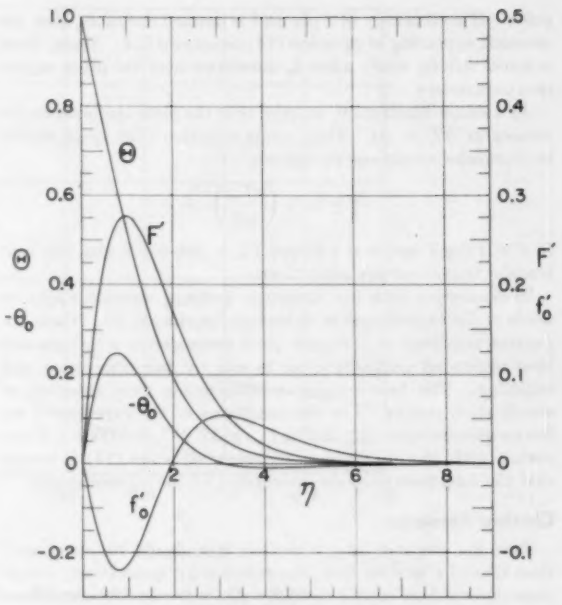

Fig. 2 The functions Θ, θ_0, F', and f_0'

Heat-Transfer Results

Local and Over-All Heat Transfer. The instantaneous *local* heat flux at the plate surface, q_{inst}, may be calculated by application of Fourier's law: $q = -(k\,\partial T/\partial y)_{y=0}$. After introducing the series expansion (5*b*) for θ and taking account of the definition (6*a*) of η, the expression for q becomes

$$q_{\mathrm{inst}} = -\frac{k_\infty(\Delta T)}{x^{1/4}}\left[\frac{g(\Delta T)}{4\nu_\infty{}^2 T_\infty}\right]^{1/4}[\Theta'(0) + \lambda_0\theta_0'(0) + \ldots] \quad (10)$$

where $\Theta'(0)$, $\theta_0'(0)$ are abbreviations for $(d\Theta/d\eta)_{\eta=0}, \ldots$

The quasi-steady heat transfer q_{qs} is given by

$$q_{qs} = -\frac{k_\infty(\Delta T)}{x^{1/4}}\left[\frac{g(\Delta T)}{4\nu_\infty{}^2 T_\infty}\right]^{1/4}\Theta'(0) \quad (11)$$

Then the important relationship between the instantaneous and quasi-steady heat transfer is found by combining equations (10) and (11)

$$\frac{q_{\mathrm{inst}}}{q_{qs}} = 1 + 1.530\,\frac{\dot{\Delta T}}{\Delta T}\left[\frac{xT_\infty}{g(\Delta T)}\right]^{1/3} + \ldots, \quad \mathrm{Pr} = 0.72 \quad (12)$$

where we have evaluated λ_0 from equation (6*b*), and the numerical values of $\Theta'(0)$ and $\theta_0'(0)$ appropriate to Pr = 0.72 have been used. Since ΔT as defined here is always positive [see equation (4*b*)], it follows that the instantaneous heat transfer exceeds the quasi-steady value when $|T_w - T_\infty|$ increases with time ($\dot{\Delta T} > 0$) and is less than quasi-steady when this temperature difference decreases with time. Of course, this remark is strictly true only when the previously noted restrictions on λ_n are fulfilled.

An alternate form of the results may be obtained by introducing local heat-transfer coefficients as follows: $h_{\mathrm{inst}} \equiv q_{\mathrm{inst}}/\Delta T$, $h_{qs} \equiv q_{qs}/\Delta T$. Then equation (12) may be rephrased as

$$\frac{h_{\mathrm{inst}}}{h_{qs}} = 1 + 1.530\,\frac{\dot{\Delta T}}{\Delta T}\left[\frac{xT_\infty}{g(\Delta T)}\right]^{1/3} + \ldots, \quad \mathrm{Pr} = 0.72 \quad (12a)$$

Finally, if consideration is given to the over-all heat transfer $Q = \int_0^L q\,dx$, it is found that

$$\frac{Q_{\mathrm{inst}}}{Q_{qs}} = 1 + 0.918\,\frac{\dot{\Delta T}}{\Delta T}\left[\frac{LT_\infty}{g(\Delta T)}\right]^{1/3} + \ldots, \quad \mathrm{Pr} = 0.72 \quad (13)$$

Criterion for Quasi-Steady Heat Transfer. We now proceed to derive a criterion for distinguishing the conditions under which the quasi-steady relationships may be applied with sufficient accuracy in unsteady heat-transfer computations. Suppose that an accuracy of 5 per cent is considered sufficient for the local heat transfer for many applications. Then, from equation (12), we find that when

$$\frac{\dot{\Delta T}}{\Delta T}\left[\frac{xT_\infty}{g(\Delta T)}\right]^{1/3} \leq 0.033 \quad (14)$$

the state can be considered as quasi-steady for heat-transfer pur-

poses. If an accuracy of 2 per cent is deemed desirable, then the constant appearing in equation (14) becomes 0.013. Again, these remarks strictly apply when λ_0 dominates over the other expansion parameters.

As a simple illustration, suppose that the plate temperature increases as $\Delta T = At$. Then, using equation (14), quasi-steady heat-transfer conditions prevail when

$$t \geq 9.75 \left(\frac{xT_\infty}{gA}\right)^{1/3}$$

If $A = 1$ deg F/sec, $x = 1$ ft, and $T_\infty = 560$ deg F abs, the heat transfer is quasi-steady after 25 sec.

In connection with our analytical findings, mention might be made of the experiments of Eckert and Soehngen [5]. Their apparatus consisted of a copper plate preheated in a furnace and then suspended vertically in air to cool by free convection and radiation. The heat-transfer measurements were reported as steady-state results. For the conditions of the experiment, we have computed that $(\dot{\Delta}T/\Delta T)[xT_\infty/g(\Delta T)]^{1/3} \approx 0.0003$. Comparing with the quasi-steady criterion, equation (14), it is seen that the data were properly interpreted by the experimenters.

Closing Remarks

Since the response of a turbulent flow should be more rapid than that of a laminar flow, the criterion for quasi-steady conditions derived here should certainly also serve for turbulent flow.

References

1 Robert Siegel, "Transient Free Convection From a Vertical Flat Plate," TRANS. ASME, vol. 80, 1958, pp. 347–359.

2 E. M. Sparrow and J. L. Gregg, "The Variable Fluid Property Problem in Free Convection," TRANS. ASME, vol. 80, 1958, pp. 879–886.

3 Franklin K. Moore, "Unsteady Laminar Boundary-Layer Flow," NACA TN 2471, 1951.

4 Simon Ostrach, "An Analysis of Laminar Free-Convection Flow and Heat Transfer About a Flat Plate Parallel to the Direction of the Generating Body Force," NACA TR 1111, 1953.

5 E. R. G. Eckert and E. E. Soehngen, "Studies on Heat Transfer in Laminar Free Convection With the Zehnder-Mach Interferometer," Technical Report 5747, WADC, 1948.

6 K-T Yang, "Possible Similarity Solutions for Laminar Free Convection on Vertical Plates and Cylinders," *Journal of Applied Mechanics*, vol. 27, TRANS. ASME, series E, vol. 82, 1960, p. 230.

The Effect of Mass Transfer on Free Convection[1]

R. EICHHORN[2]

Consideration is given to the constant property laminar boundary layer equations with free convection and mass transfer. It is shown that similar solutions are possible for blowing rate distributions varying as the distance from the leading edge raised to the power $(n - 1)/4$ where n is the exponent in a power law surface temperature distribution. Solutions to the equations in the form of skin friction and heat-transfer parameters, and velocity and temperature profiles are presented for the constant wall temperature case for a fluid with $Pr = 0.73$. The cases considered range from strong suction to strong blowing.

Mass transfer has a pronounced effect on the heat transfer but only a slight effect on the skin friction. In light of the solutions presented, these effects are shown to be physically rational.

[1] Publication from the Heat Transfer Laboratory, University of Minnesota. This investigation was carried out under the auspices of the Air Research and Development Command, Air Force Contract No. AF(600)-1226.

[2] Assistant Professor, Princeton University, Princeton, N. J.

Contributed by the Heat Transfer Division of THE AMERICAN SOCIETY OF MECHANICAL ENGINEERS. Manuscript received at ASME Headquarters, May 3, 1960.

Introduction

RECENT literature displays much interest in the possibility of reducing heat transfer to high-speed aircraft and missiles with mass transfer or ablation cooling. Also the problem of mass transfer has been of perennial interest to the chemical engineer.

To obtain an estimate of the effect of buoyancy forces on a flow with mass transfer, we present here the results of numerical solutions of the boundary layer equations for a fluid with constant properties and Pr = 0.73 in free convection flow and for several values of the blowing parameter ranging from strong suction to strong blowing. The case treated corresponds to a vertical flat plate with uniform wall temperature.

Analysis

We consider a vertical flat plate as sketched in Fig. 1 from whose surface is ejected a fluid having the same physical properties as the quiescent ambient fluid but having a different temperature. Motion within the boundary layer will be assumed to result from buoyancy forces due to temperature differences. Under these conditions the mass diffusion equation does not enter.

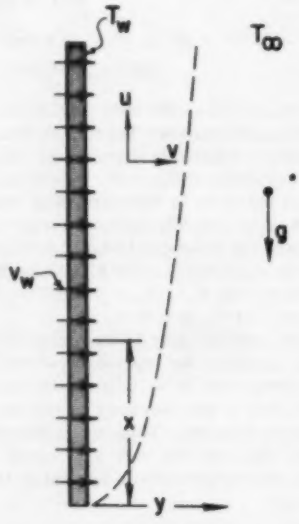

Fig. 1 Co-ordinate system

The only difference between the problem considered here and the usual free convection problem enters through the boundary conditions. For this reason and for the sake of brevity we will not present the derivation of the equations here. A rather complete treatment is given in reference [1].[3] Taking the equations of motion in the Prandtl boundary layer form and performing the usual operations leading to similar solutions gives the equations

$$f''' + (n + 3)ff'' - 2(n + 1)f'^2 + \theta = 0 \qquad (1)$$

$$\theta'' - \Pr[4nf' - (n + 3)f\theta'] = 0 \qquad (2)$$

where f and θ are the dimensionless stream function and temperature, respectively, both functions of η defined by

$$\eta = \frac{y}{x}\left(\frac{\mathrm{Gr}}{4}\right)^{1/4} \qquad (3)$$

Primes in Equations (1) and (2) denote differentiation with re-

[3] Numbers in brackets designate References at end of paper.

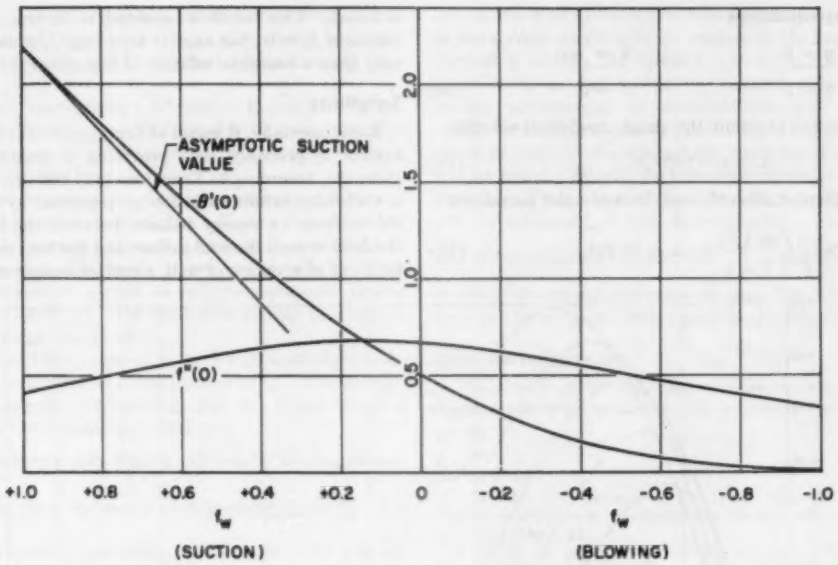

Fig. 2 Heat transfer and skin friction results, uniform wall temperature, Pr = 0.73

spect to η and the term n is determined by the wall-temperature distribution, given by

$$T_w - T_\infty = Bx^n \tag{4}$$

The Grashof number in Equation (3) is given by

$$\mathrm{Gr} = \frac{g\beta x^3(T_w - T_\infty)}{\nu^2} \tag{5}$$

where g is the acceleration due to gravity, β is the coefficient of thermal expansion, ν is the kinematic viscosity, and x is the distance measured from the lower end of the plate. The distance normal to the plate is denoted by y.

The velocities in the x and y-directions and the temperature distribution are given by the equations

$$u = \frac{4\nu}{x}\left(\frac{\mathrm{Gr}}{4}\right)^{1/2} f', \tag{6}$$

$$v = -\frac{\nu}{x}\left(\frac{\mathrm{Gr}}{4}\right)^{1/4}[(n+3)f + (n-1)f'\eta], \tag{7}$$

$$\frac{T - T_\infty}{T_w - T_\infty} = \theta, \tag{8}$$

respectively.

The boundary conditions in the physical system are:

$y = 0$	$y \to \infty$
$T = T_w(x)$	$T \to T_\infty$
$u = 0$	$u \to 0$
$v = v_w(x)$	

(9)

In the transformed system these boundary conditions become

$\eta = 0$	$\eta \to \infty$
$f = f_w$ (a constant)	$f' \to 0$
$f' = 0$	$\theta \to 0$
$\theta = 1$	

(10)

In Equations (10), the boundary condition $f = f_w$ (a constant) was applied to preserve the x independency of Equations (1), (2), and (7), as necessary for similar solutions. The specific form of the required blowing distribution then results from Equation (7) as

$$v_w(x) = -\frac{\nu}{x}\left(\frac{\mathrm{Gr}}{4}\right)^{1/4}(n+3)f_w \tag{11}$$

From Equation (11), we see that $v_w(x)$ is dependent on x in the power law fashion

$$v_w \propto x^{\frac{n-1}{4}} \tag{12}$$

In forced convection the blowing rate distribution is also of power law form, but there the particular power depends on the pressure gradient and not on the wall-temperature variation [3]. From Equation (12) a uniform wall-temperature plate requires a blowing distribution $v_w \propto x^{-1/4}$, which is infinite at the leading edge. This is in the nature of similar solutions, however, and it is generally felt that such inadequacies can be tolerated and the methods will still give accurate results sufficiently far from the leading edge.

The heat transfer and skin friction, as usual, are readily interpreted in terms of boundary conditions on θ and f as

$$\mathrm{Nu}\Big/\left(\frac{\mathrm{Gr}}{4}\right)^{1/4} = -\theta'(0) \tag{13}$$

and

$$\frac{\tau}{4\rho\left(\frac{\nu}{x}\right)^2\left(\frac{\mathrm{Gr}}{4}\right)^{1/4}} = f''(0) \tag{14}$$

As seen from Equation (11), the case of suction corresponds to $f_w > 0$ and the case of blowing to $f_w < 0$. For very large suction rates the velocity u becomes small compared to v so that the momentum equation drops out (convection in the x-direction is no longer important) and the energy equation reduces to

$$\theta'' + (n+3)\,\mathrm{Pr} f_w\theta' = 0 \tag{15}$$

with the boundary conditions

$$\eta = 0 \qquad \eta \to \infty$$
$$\theta = 1 \qquad \theta \to 0 \tag{16}$$

Equations (15) and (16) admit the simple analytical solution

$$\theta = e^{-(n+3)\mathrm{Pr} f_w \eta} \tag{17}$$

from which by differentiation the wall heat-transfer parameter

$$\mathrm{Nu} \Big/ \left(\frac{\mathrm{Gr}}{4}\right)^{1/4} = (n+3)\,\mathrm{Pr} f_w \tag{18}$$

is found. This result is expected to be true for large positive values of f_w only, but exactly how large f_w must be can be found only from a complete solution of Equations (1) and (2).

Solutions

Experimentally, it would at first appear that the most tractable system is probably that providing a constant blowing rate. However, according to Equations (12) and (4), this case requires a wall-temperature variation proportional to x and, as can be shown from an energy balance between the heat conducted in the fluid toward the wall surface and the heat convected with the fluid out of a section of wall, a coolant temperature variation also

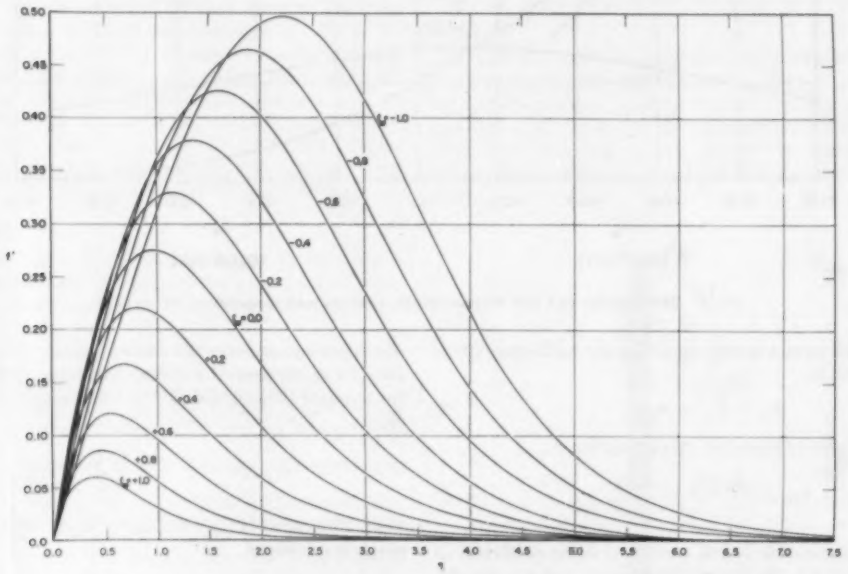

Fig. 3 Velocity profiles, uniform wall temperature, Pr = 0.73

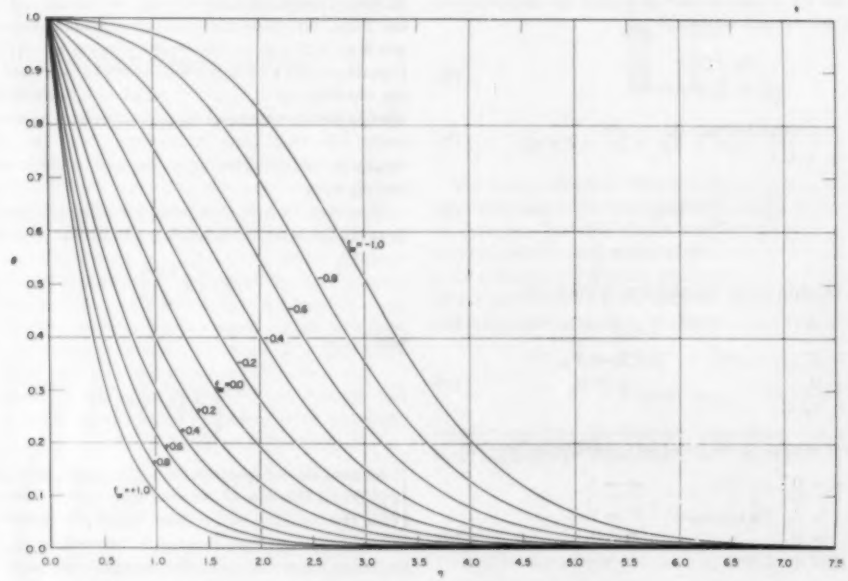

Fig. 4 Temperature profiles, uniform wall temperature, Pr = 0.73

proportional to x. Therefore it was decided arbitrarily to consider the constant wall temperature case ($n = 0$) for which the energy balance requires a locally constant coolant supply temperature.

The information desired from a solution of Equations (1), (2), and (10) is essentially $f'(\eta)$, $\theta(\eta)$, $f''(0)$, and $\theta'(0)$ giving the complete velocity and temperature profiles and the skin friction and heat-transfer parameters.

Solutions to the equations for constant wall temperature and $Pr = 0.73$ were obtained numerically on a Univac Scientific 1103 digital computer for several values of f_w ranging from strong suction to strong blowing. The method used was essentially one of successive approximation applied to integral equations derived from Equations (1) and (2). The method is similar to that described in [2], although less detailed.

Values of $f''(0)$ and $\theta'(0)$ correct to three significant figures are shown in Table 1 as a function of the parameter f_w. The same information is graphically portrayed in Fig. 2. The interesting conclusions to be noted from these data are:

1 The skin friction is only slightly affected by the mass transfer.

2 The effect of mass transfer is most pronounced on the heat transfer.

3 The heat transfer is essentially zero at $f_w = -1.0$ and approaches closely the asymptotic suction value [equation (18) with $n = 0$] for $f_w > +1.0$.

Table 1 Skin friction and heat-transfer parameters

f_w	$f''(0)$	$-\theta'(0)$
+1.0	0.409	2.192
0.9	0.446	1.994
0.8	0.488	1.798
0.7	0.530	1.606
0.6	0.573	1.420
0.5	0.611	1.241
0.4	0.644	1.072
0.3	0.668	0.912
0.2	0.681	0.764
0.1	0.684	0.629
0.0	0.674	0.507
−0.1	0.654	0.399
−0.2	0.627	0.305
−0.4	0.557	0.162
−0.6	0.476	0.0725
−0.8	0.399	0.0264
−1.0	0.336	0.00748

The velocity and temperature profiles for selected values of f_w are presented in Figs. 3 and 4. Physical reasons for the behavior of the skin friction and heat-transfer coefficients shown in Fig. 2 are easily deduced from Figs. 3 and 4. As stronger blowing is provided ($f_w < 0$), the heated fluid is pushed farther from the wall where the buoyancy forces can act to accelerate the flow with less influence of viscosity due to the presence of the wall. This effect acts to increase the shear by increasing the maximum velocity within the boundary layer. On the other hand, the position of the maximum velocity point is moved farther from the wall which effect acts to decrease the wall shear. The latter effect predominates slightly resulting in a small decrease in the wall shear for increasing blowing rates. For suction the same principles are in operation but acting in the reverse direction, viz., the maximum velocity decreases but at the same time moves closer to the wall as increasing suction is applied. Because of this complicated interaction the point of maximum shear interestingly occurs at a slightly positive value of f_w (suction).

The behavior of the heat-transfer parameter is much as one would expect: For blowing, the exuding gas forms a buffer layer against which heat must travel by conduction resulting in a drop in the heat-transfer coefficient. For suction, the opposite effect occurs, the fluid at the ambient temperature being brought closer to the surface resulting in an increase in the heat transfer. With increasing suction the upward velocity in the boundary layer contributes less and less to the transfer of heat with the heat transfer approaching the asymptotic suction value as a result.

The value of f_w at which the full equation [Equation (2)] reduces sensibly to the asymptotic equation [Equation (15)] can now be found. Adopting a 5 per cent difference as a criterion, one finds from Table 1 that the heat transfer is predicted by Equation (18) for values of $f_w > 0.68$, approximately. From equation (11), this criterion can be restated as $\left|\frac{v_w x}{\nu}\right| > 1.44\ \mathrm{Gr}^{1/4}$, for the range in which the asymptotic relations hold. Of course, no similar criteria can be advanced with regard to the skin friction.

Acknowledgment

The author gratefully acknowledges the efforts of Mr. W. M. Minkowycz who obtained the numerical solutions presented herein.

References

1 E. M. Sparrow and J. L. Gregg, "Similar Solutions for Free Convection From a Nonisothermal Vertical Plate," TRANS. ASME, vol. 80, 1958, p. 379.

2 E. R. G. Eckert, P. J. Schneider, A. A. Hayday, and R. M. Larson, "Mass Transfer Cooling of a Laminar Boundary Layer by Injection of a Light-Weight Foreign Gas," *Jet Propulsion*, vol. 28, 1958, p. 34.

3 J. P. Hartnett and E. R. G. Eckert, "Mass-Transfer Cooling in a Laminar Boundary Layer With Constant Fluid Properties," TRANS. ASME, vol. 79, 1957 p. 247.

An Interferometric Method of Studying Boundary Layer Oscillations

J. P. HOLMAN,[1] H. E. GARTRELL,[2] AND E. E. SOEHNGEN[3]

BOUNDARY layer oscillations and their effects on transition may be studied by imposing a controlled disturbance on the boundary layer flow and then observing the oscillations due to this disturbance. A method for conducting such studies in free convection boundary layers is described in this note. A thin wire, 0.001 in. in diameter, is placed in the boundary layer near the leading edge of a heated vertical plate. The wire is then pulsed with an electrical signal which heats it periodically according to the pulse frequency in the external circuit. This periodic heating generates oscillations in the boundary layer. A typical boundary layer wave resulting from the pulses is shown in Fig. 1 as viewed with an interferometer.

The boundary layer waves may be observed with motion-picture photography to examine the nature of the oscillations in detail. The wave parameters which are of interest are (a) wave amplitude; (b) wave length; (c) wave speed; and (d) wave energy. The amplitude may be measured as

$$a = (y_{max} - y_{min})/2 \qquad (1)$$

where y_{max} is the distance from the wall to the maximum point in a particular isotherm and y_{min} is the distance from the wall to the

[1] Associate Professor, Mechanical Engineering Department, Southern Methodist University, Dallas, Texas.

[2] Air Technical Intelligence, Wright-Patterson Air Force Base, Ohio.

[3] Fluid Dynamics Research Branch, Aeronautical Research Laboratory, Wright-Patterson Air Force Base, Ohio.

Contributed by the Heat Transfer Division of THE AMERICAN SOCIETY OF MECHANICAL ENGINEERS. Manuscript received at ASME Headquarters, April 21, 1960.

Fig. 1 Typical free convection boundary layer wave

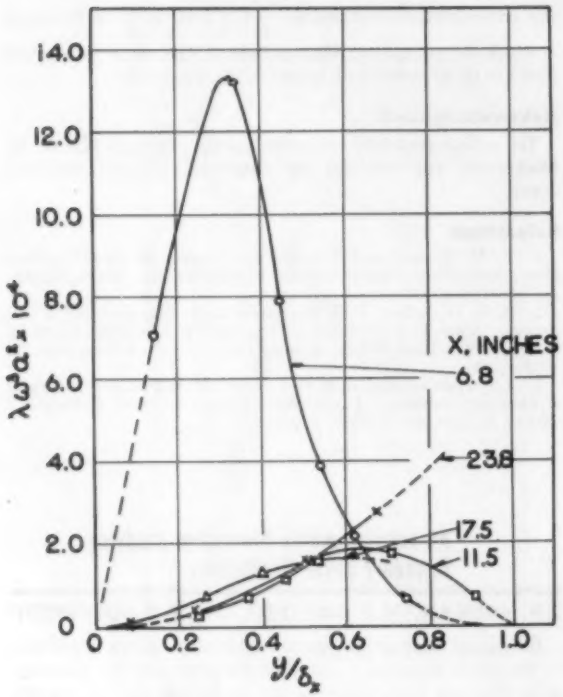

Fig. 2 Wave energy parameter, 1.5 cps pulse frequency, 0.078 sec pulse duration

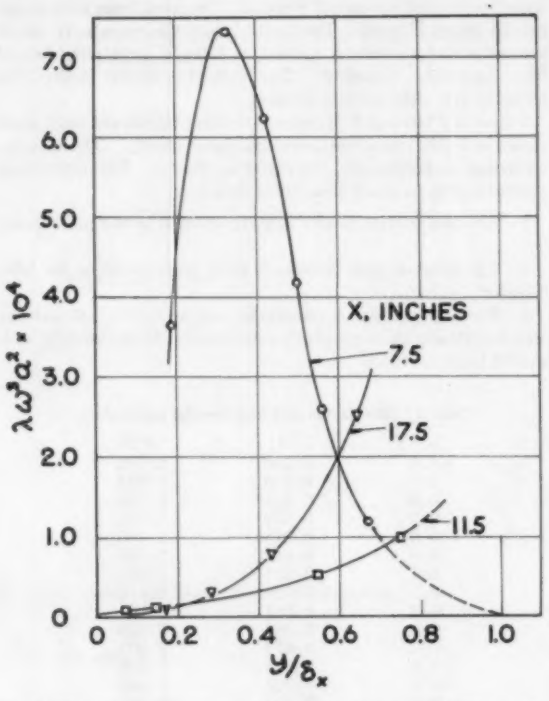

Fig. 3 Wave energy parameter, 1.0 cps pulse frequency, 0.078 sec pulse duration

minimum point in the isotherm. The amplitude is thus determined for each isotherm and its variation through the boundary layer may be studied.

The wave length may be measured by measuring the distance between the maximum points in each isotherm. The wave speed is calculated by following the movement of the wave through several frames of the motion picture record. The boundary layer frequency may be defined as

$$\omega = c/\lambda \tag{2}$$

where c is the observed wave speed and λ is the observed wave length. Detailed results of the variation of these quantities are given in reference [1].[4]

The wave energy may be determined in an analogy to a one-dimensional sound wave. Then the intensity of the wave, or the energy flux per unit area, per unit time, is given by

$$E_w = {}^1/_2\rho c\omega^2 a^2 \tag{3}$$

Noting that the pressure in the boundary layer is constant and that the temperature variation is probably of the same order as the experimental error in determining the wave parameters, the grouping which may be chosen to represent the wave energy is

$$\lambda\omega^3 a^2 \tag{4}$$

Thus, in the crude analogy, the wave energy varies with the cube of the frequency and the square of the amplitude. Some values of the wave energy parameter are shown in Figs. 2 and 3. δ_x is the steady-state boundary layer thickness. For the results shown in these figures the pulse wire was located at a distance of six inches from the leading edge of the plate. A discussion of these results and some other measurements is given in reference [1]. Motion pictures of the boundary layer oscillations are available from the authors.

[4] Numbers in brackets designate References at end of paper.

References

1 J. P. Holman, H. E. Gartrell, and E. E. Soehngen, "A Study of Free Convection Boundary Layer Oscillations and Their Effects on Heat Transfer," WADD Technical Report 59-3, Wright-Patterson Air Force Base, Ohio, November, 1959.

2 E. R. G. Eckert and E. E. Soehngen, "Studies on Heat Transfer in Laminar Free Convection With the Zehnder-Mach Interferometer," Air Force Technical Report 5747, Dayton, Ohio, 1948.

3 E. R. G. Eckert and E. E. Soehngen, "Interferometric Studies on the Stability and Transition to Turbulence of a Free Convection Boundary Layer," Proceedings, General Discussion on Heat Transfer, I.Mech.E., London, England, 1951.

Journal of HEAT TRANSFER

Information for Authors

• Manuscripts should be submitted in final form to the Editor. Each manuscript must be accompanied by a statement that it has not been published elsewhere nor has it been submitted for publication elsewhere. A paper which would occupy more than 8 pages of the Journal may be returned to the author for abridgment.

• The author should state his business connection, the title of his position, and his mailing address. A short abstract (50 to 100 words) should be included on the first page immediately preceding the introductory paragraph of the paper.

Three copies of the manuscript are required. One of these must be a carefully prepared printer's copy, typed in double spacing, on one side of the page only, with wide margins, on $8^1/_2$ by 11-in. opaque white paper. Mimeographed manuscripts, if prepared with exceptional care, can be accepted provided they are completely edited.

• As far as possible, all mathematical expressions should be typewritten. Greek letters and other symbols not available on the typewriter should be carefully inserted in ink. Care should be taken to distinguish between capital and lowercase letter, between zero (0) and the letter (*O*), between the numeral (1) and the letter (*l*), etc. A letter representing a vector cannot be printed with an arrow above or below it. The letter should be underscored with a single wavy line, wherever it appears in the text, to designate boldface type.

• A list of symbols carefully marked for the use of the editor (thus: κ, Greek l.c. kappa), if it has not been included in the body of the paper, should accompany the manuscript on a separate page.

• Before preparing a manuscript the author should study printed articles in the Journal, with special attention to the form and style of mathematical expressions, tables, footnotes, references, and abstract. Numbers that identify mathematical expressions should be enclosed in parentheses. Numbers that identify references at the end of the paper should be enclosed in brackets. Care should be taken to arrange all tables and mathematical expressions in such a way that they will fit into a single column when set in type. Equations that might extend beyond the width of one column (fractions that should not be broken or long expressions enclosed in parentheses) should be rephrased to go on two or more lines within column width. Fractional powers are preferred to root signs and should always be used in more elaborate formulas. The solidus should be used instead of the horizontal line for fractions wherever possible.

• A normal paper should not exceed 8 pages in the Journal. It is about 8000 words or 20 double-spaced typewritten pages exclusive of drawings. A Technical Brief should not exceed 750 words or about one page in the Journal inclusive of drawings.

• Originals and two copies of figures must accompany the manuscript. Line drawings should not be larger than $8^1/_2 \times 11$ in. and should be planned for reduction to column width. Lettering should be large enough to be clearly legible when the illustration is reduced. The originals of line drawings must be in India ink on white or pale blue tracing paper or tracing cloth. Photographs of equipment or test specimens must be glossy prints and should be used sparingly. Captions for figures should be typed double-spaced and included as the last page of the manuscript. The figure number and author's name should be written in the margin or on the back of each illustration.

• Titles of papers should be brief.

• Authors can obtain copies of the ASME Manual MS-4, "An ASME Paper," from the Editor and are urged to do so before drafting their papers in final form.

• Papers published in Journals of the Transactions of the ASME must be presented at a Meeting, either in person or by title.

• An author is entitled to 25 preprints free of charge (in the case of two authors, 15 each; three or more authors, 10 each). Larger quantities of preprints or reprints can be ordered from Editorial Department, The American Society of Mechanical Engineers, 29 West 39th Street, New York 18, N. Y. Quotations will be sent on request.

Please address all communications to:

Editor, ASME,

29 West 39th Street,

New York 18, N. Y.

ASME Publications Committee